Correlated electrons in high-temperature superconductors

Elbio Dagotto

Department of Physics, National High Magnetic Field Laboratory, and MARTECH, Florida State University, Tallahassee, Florida 32306

Theoretical ideas and experimental results concerning high-temperature superconductors are reviewed. Special emphasis is given to calculations performed with the help of computers applied to models of strongly correlated electrons proposed to describe the two-dimensional CuO_2 planes. The review also includes results using several analytical techniques. The one- and three-band Hubbard models and the t-J model are discussed, and their behavior compared against experiments when available. The author found, among the conclusions of the review, that some experimentally observed unusual properties of the cuprates have a natural explanation through Hubbard-like models. In particular, abnormal features like the mid-infrared band of the optical conductivity $\sigma(\omega)$, the new states observed in the gap in photoemission experiments, the behavior of the spin correlations with doping, and the presence of phase separation in the copper oxide superconductors may be explained, at least in part, by these models. Finally, the existence of superconductivity in Hubbard-like models is analyzed. Some aspects of the recently proposed ideas to describe the cuprates as having a $d_{x^2-y^2}$ superconducting condensate at low temperatures are discussed. Numerical results favor this scenario over others. It is concluded that computational techniques provide a useful, unbiased tool for studying the difficult regime where electrons are strongly interacting, and that considerable progress can be achieved by comparing numerical results against analytical predictions for the properties of these models. Future directions of the active field of computational studies of correlated electrons are briefly discussed.

CONTENTS

I. INTRODUCTION AND EXPERIMENTAL RESULTS

More than seven years ago, J. G. Bednorz and K. A. Müller (1986) announced the discovery of superconductivity in a ceramic copper oxide material at a temperature of about 30 K. These compounds are poor conductors, and thus their result was unexpected and cautiously considered. However, the confirmation of these experiments by Takagi *et al.* (1987) generated a frenetic race for the preparation of materials with even higher critical temperatures. Dozens of "high-T_c" compounds have been discovered in the last few years, and currently a mercury-based material has the highest confirmed critical temperature of about 133 K (Schilling *et al.*, 1993). Since 77 K is the boiling temperature of nitrogen, it is quite possible that new technologies may emerge from

 0034-6861/94/66(3)/763(78)/$12.80 ©1994 The American Physical Society

the field of high T_c, like SQUID (superconducting quantum interference device) magnetometers and Josephson integrated circuits (Simon, 1991), although exciting, early promises of levitating trains seem unlikely. The critical current densities are still not high enough for most technological applications, but progress is very rapid on this front (Larbalestier, 1991).

Although the initial frenzy has subsided, the field still remains very active and large, and it is rapidly evolving. On the experimental side, results are being consolidated, mainly due to a considerable improvement in the quality of the samples compared with those used in the early studies of the high-T_c materials. In particular, high-quality single crystals are currently available. Considerable work is being carried out at temperatures above T_c, since it is believed that the unusual normal-state properties of these materials may contain the key features for understanding their superconductivity. Much work has been devoted to some unexpected properties of the cuprates, like the linear behavior of the d.c. resistivity with temperature, a Hall coefficient that is temperature dependent, the presence of short coherence lengths, and the energy dependence of the relaxation rate $1/\tau$. These unusual properties suggest that the normal state cannot be described by a Fermi liquid, an issue currently under much discussion. Actually, we know that organic superconductors, heavy fermion superconductors, Nb_3Sn, and other materials are not well described by the BCS model (Bardeen, Cooper, and Schrieffer, 1957). However, the BCS or pairing *theory* is a broader concept and describes fermions in which an effective attractive interaction produces a condensate, with large overlaps between pairs. The source of the attraction is not crucial for this theory to hold, and thus BCS ideas are not at all excluded as a possible explanation of the behavior of the new superconductors.

The search for new materials has been mainly empirical, since no predictive theory is currently known for the high-T_c compounds. The fact is that no one knows why the cuprates behave as they do. However, several theories have been proposed to describe them. One- and three-band Hubbard models, as well as the *t-J* model, are believed to represent the gross features of the electronic behavior of the new materials. Unfortunately, most of the available experimental data are not accurate enough to convincingly confirm or rule out most of the theories. Antiferromagnetism, defects, phonons, and the strong anisotropy of the materials complicate the interpretation of the results, and they seem to conspire to hide the key properties of the normal state. It is possible that theories that combine the pairing ideas with the presence of strong antiferromagnetic correlations may properly describe the high-T_c superconductors. In this family, consider, for example, the spin-bag theories (Schrieffer, Wen, and Zhang, 1988, 1989; Kampf and Schrieffer, 1990; Levin *et al.*, 1992), antiferromagnetic Fermi-liquid theories (Millis, Monien, and Pines, 1990), and also the recently developed $d_{x^2-y^2}$ theories that have attracted considerable attention (Bickers, Scalapino, and White, 1989; Monthoux, Balatsky, and Pines, 1991). The interchange of magnons may produce the attractive force needed to pair the charge carriers (Miyake, Schmitt-Rink, and Varma, 1986; Scalapino, Loh, and Hirsch, 1986; Bickers, Scalapino, and Scalettar, 1987; Monthoux and Pines, 1993). Note that spin bags are very different from Landau quasiparticles, since the overlap Z between bare and dressed holes is very small [$Z \sim 0.1$, according to some calculations (Dagotto and Schrieffer, 1991)]. This effect produces considerable deviations from the standard Fermi-liquid results, but these excitations still correspond to those of a Fermi liquid. Among the Fermi-liquid-based theories should be included also the Van Hove singularity scenario (Markiewicz, 1991; Newns, Pattnaik, and Tsuei, 1991; Pattnaik *et al.*, 1992; and references therein), the so-called hole mechanisms (Hirsch and Marsiglio, 1989), the nested Fermi liquid (Virosztek and Ruvalds, 1990), and the recently proposed antiferromagnetic van Hove scenario (Dagotto, Nazarenko, Moreo, 1994).

Some other theorists strongly believe that the BCS theory cannot work in these new superconductors (Anderson, 1990b). Instead, scenarios in which the elementary excitations in the new materials are spinons (zero charge, spin-$\frac{1}{2}$) and holons (charge e, spin 0) have been proposed. As a toy model, the one-dimensional Hubbard model has been widely discussed (Anderson, 1990a). However, it remains to be shown that one- and two-dimensional models have a similar qualitative behavior. Other non-Fermi-liquid theories that have attracted considerable attention are anyon superconductivity (Laughlin, 1988a, 1988b; Chen *et al.*, 1989; Wen, Wilczek, and Zee, 1989), the marginal Fermi-liquid theories (Varma *et al.*, 1989), gauge theories (Nagaosa and Lee, 1990), and several others. Clearly, we are still a long way from developing a *predictive* theory to describe the new materials. We all expect that a triumphant theory should indicate the direction for developing new superconductors with even higher critical temperatures.

It is interesting to remember that before 1986 some theorists believed that condensed-matter physics was a mature field. Actually, few researches were trying to find high-temperature superconductors at that time. The discovery of the new superconductors has shown the weaknesses of our area of research. After several years of intense theoretical studies, it is clear that we still do not have the proper skills and tools to deal with strongly correlated electrons. The main problem is that real calculations are not easy. Most of the models proposed for the new superconductors contain interactions that are strong, and thus perturbative calculations of bubble and ladder diagrams are questionable.[1] Other approximations are self-consistent (mainly mean-field-like), but it is

[1]Nevertheless, there are other analytical methods that seem to be able to handle strong correlations. See, for example, Fulde (1991) and Fulde and Unger (1993).

difficult to judge how close to the actual properties of the model these results are. It is interesting to observe that theories that start with the same Hamiltonian may arrive at completely different descriptions of their properties. The subject is so complicated that we need as much help as possible. The discovery of the new superconductors has clearly shown the need for new, well-controlled approaches to the field of correlated electrons.

In an attempt to close the gap between a model, as defined by its Hamiltonian, and, for example, the actual properties of its ground state, a large number of theorists have turned to the use of computers. High-T_c physics has strongly motivated theorists to work on correlated electrons; but it may be claimed that, from a theorist's point of view, the particular model or material is not as crucial as the development of the tools to handle them. Computational results can contribute to the acceptance or rejection of mean-field-based theories, and can also indicate directions in which new approaches should be developed. Much progress has been made in this direction, with numerical calculations routinely being viewed as impartial referees that may eventually select the proper analytic description of a given model. Actually, the cross-fertilization between computational and analytical work in the area of correlated electrons is quickly growing.

As an additional motivation for carrying out computational work in the context of high-T_c superconductors, note that the new cuprate compounds differ markedly from the more conventional superconductors by having a very small coherence length ξ. This length is usually associated with the average size of a Cooper pair. For conventional superconductors, $\xi \sim 500$ Å to 10 000 Å; thus the size of the pair is larger than the average distance between pairs. This particular feature allows a mean-field BCS-like treatment of the problem to be accurate and reliable. However, the new superconductors have $\xi \sim 12$ Å to 15 Å, and thus standard mean-field approximations are clearly questionable. These results were obtained mainly via H_{c2} (all high-T_c materials are type-II superconductors). The cuprates are in the "clean" limit, since the electron mean free path (~ 150 Å) is much larger than ξ [for more details, see Welp *et al.* (1989); Batlogg (1990), p. 66; Batlogg (1991), p. 48; Burns (1992)]. The coherence length in the c direction is only 2 to 5 Å, i.e., even smaller than the interplane distance, while ξ in-plane is only ~ 3 to 4 lattice spacings (since the distance between Cu ions in the plane is 3.8 Å). Such small Cooper pair sizes indicate that studies on finite two-dimensional clusters, like those reported in this review, may be relevant in describing the physics of the cuprates.

The field of high-T_c superconductors has generated several thousand publications. It would be quite difficult to describe this field even if we restrict the description to theoretical aspects. In this review, we shall concentrate on the more modest goal of describing the progress achieved in the study of models of correlated electrons using computational techniques. However, several analytical techniques will also be described and their results discussed. The review should be considered as a "progress report" in which we have attempted to focus on some basic aspects of this rapidly evolving field. Another goal of the review is to provide a simple overview of the experimental situation in high-T_c materials, summarizing the basic agreements and discrepancies between theory and experiment. For additional literature, the reader should consult other review articles or books, like those by Fukuyama, Maekawa, and Malozemoff (1989); Burns (1992); and Maekawa and Sato (1991). For previous short reviews on theoretical work related to the subject of this paper, see Dagotto (1991); Fukuyama (1991); Fulde and Horsch (1993); Lu, Zhao-Bin, and Yan-Min (1993); and references therein. A recent review article on Monte Carlo results that is complementary to the present one was presented by W. von der Linden (1992). In his review, more models are analyzed than in the present paper, but with less emphasis on the comparison between theory and experiment as done here. It is also worth keeping in mind that the vast literature related to this subject cannot be mentioned in a single review article. We used our own judgment and prejudices to select the subjects that we considered more relevant, and apologize beforehand for any omission.

This review is organized as follows. In Sec. I, a brief summary of the properties of some high-T_c superconductors is given. Models that describe the behavior of electrons in these materials are presented. In Sec. II, the most important algorithms for studying correlated electrons are described. Results for the particular cases of half-filling and a few holes doped into an antiferromagnet are discussed in Sec. III. A rough comparison of the numerical results with experiments are discussed in Sec. IV. Several observables—like the optical conductivity $\sigma(\omega)$, photoemission spectra $N(\omega)$, magnetic susceptibilities, and others—are considered and contrasted, with theoretical predictions coming mainly from numerical studies. It is concluded that some "anomalous" properties of the cuprates are not so unexpected once the electronic models of correlated electrons are properly analyzed with powerful unbiased tools like computational techniques. Regarding the final goal of finding superconductivity in these models, we believe that $d_{x^2-y^2}$ is the most likely channel where such a condensate may exist when holes are immersed in an antiferromagnetic background. Conclusions are presented in Sec. V.

A. Structure and phase diagram of the cuprates

This section provides a short overview of the lattice structure and phase diagram of the most widely studied high-T_c compounds (a superconducting compound is said to belong to the family of high-T_c superconductors *if* it has CuO_2 planes). In general, the high-T_c materials are basically tetragonal, and all of them have one or more

CuO_2 planes in their structure, which are separated by layers of other atoms (Ba, O, La, . . .). Most researchers in this field strongly believe that superconductivity is related to processes occurring in the CuO_2 planes, with the other layers simply providing the carriers (and thus they are called charge reservoirs). All high-T_c materials have such charge reservoirs. In the CuO_2 planes, each copper ion is strongly bounded to four oxygen ions separated by a distance of approximately 1.9 Å. The critical T_c seems to depend on the number of CuO_2 planes that are within a short distance of each other in the structure. For example, $Tl_2Ca_2Ba_2Cu_3O_{10}$, which has a relatively large T_c of 125 K, has three adjacent CuO_2 planes. The fact that T_c increases with the number of layers has led to some theoretical proposals linking the number of CuO_2 planes with the critical temperature.

Another property common to these materials is the presence of antiferromagnetic order at low temperatures in the undoped regime, i.e., when no free carriers exist in the planes. Upon doping, the long-range spin order is destroyed, and the superconducting phase appears. However, this does not mean that spin correlations are unimportant for superconductivity. Even without strict long-range order, the spin-correlation length can be large in the superconducting phase, producing a local arrangement of magnetic moments that at short distances differs very little from that observed below the Néel temperature in the insulating regimes. Actually, several ideas have been discussed in the literature relating antiferromagnetism and superconductivity. For example, the interchange of magnons instead of phonons may be a possible mechanism of pairing in these materials, as will be discussed in Sec. IV.E.

Material	T_c (K)
$Hg_Ba_2Ca_2Cu_3O_{8+\delta}$	133
$Tl_2Ca_2Ba_2Cu_3O_{10}$	125
$YBa_2Cu_3O_7$	92
$Bi_2Sr_2CaCu_2O_8$	89
$La_{1.85}Sr_{0.15}CuO_4$	39
$Nd_{1.85}Ce_{0.15}CuO_4$	24
$RbCs_2C_{60}$	33
Nb_3Ge	23.2
Nb	9.25
Pb	7.20
UPt_3	0.54

A large number of compounds with the characteristic CuO_2 planes have been synthesized. This is not too surprising, since it is possible to modify the number of planes per unit cell and the atoms separating the nearby planes, as well as the structure, composition, and size of the charge reservoir, producing a huge number of combinations. In the table, we present a short list of the most widely studied compounds in this field, with their critical temperatures T_c (for a more complete list, see Burns, 1992 and Harshman and Mills, 1992). For comparison we also show the critical temperature of some "old" superconductors like Nb, Pb, and Nb_3Ge. The latter had the highest critical temperature known before 1986 (see Testardi, Wernick, and Roger, 1974). The T_c of a superconducting heavy fermion material (UPt_3) and a fullerene are also given.

In the remainder of this section, we discuss the structure and phase diagram of some particular high-T_c compounds in more detail.

1. $La_{2-x}Sr_xCuO_4$

This compound was among the first high-temperature superconductors discovered. It crystallizes in a body-centered-tetragonal structure (bct), which has been known for several years from studies on K_2NiF_4. It is usually called the **T** structure, and it is shown in Fig. 1 (to visualize the bct lattice, simply concentrate only on the Cu atoms of the figure). In $La_{2-x}Sr_xCuO_4$, the CuO_2 planes are ~ 6.6 Å apart, separated by two LaO planes which form the charge reservoir that captures electrons from the conducting planes upon doping. The atomic configurations of the elements forming this compound are Cu:[Ar]$(3d)^{10}(4s)$; La:[Xe]$(5d)(6s)^2$; O:[He]$(2s)^2(2p)^4$; and Sr:[Kr]$(5s)^2$. In the crystal, oxygen is in a O^{2-} valence state that completes the p shell. Lanthanum loses three electrons and becomes La^{3+}, which is in a stable closed-shell configuration. To conserve charge neutrality, the copper atoms must be in a Cu^{2+} state, which is obtained by losing the $(4s)$ electron (weakly bounded to the atom) and also one d electron. This creates a *hole* in the d shell, and thus Cu^{2+} has a net spin of $\frac{1}{2}$ in the crystal. Each copper atom in the conducting planes has an oxygen (belonging to the charge reservoir) above and below in the **c** direction. These are the so-called apical O atoms or just O_z. Then, in this compound, the copper ions are surrounded by octahedra of

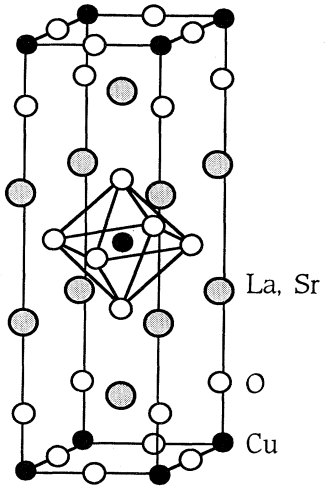

FIG. 1. Crystal structure of $La_{2-x}Sr_xCuO_4$ (**T** phase). Taken from Almasan and Maple (1991).

oxygens (shown in Fig. 1) as in a perovskite structure (Ashcroft and Mermin, 1976, p. 557). However, the distance Cu—O_z is ~ 2.4 Å, which is considerably larger than the distance Cu—O in the planes (~ 1.9 Å). Then, the Cu—O_z bond is much weaker than the in-plane Cu—O bond, and thus considering the Cu atoms as immersed in perfect octahedra of oxygens is somewhat misleading. The dominant bonds are those on the plane, and the importance of the apical oxygens is somewhat questionable. We shall see below that many of the high-T_c materials have apical oxygens. Their distance to coppers in the conducting planes is remarkably similar in different compounds, being always about 2.4 Å.

Upon doping, La^{3+} are randomly replaced by Sr^{2+}, and thus fewer electrons are donated to the CuO_2 planes. It will be shown later that these electrons come from oxygen ions, changing their configuration from O^{2-} to O^{-} (and thus creating one *hole* in their p shell). Metallic behavior has already been observed for very small doping concentrations, $x \geq 0.04$. The sign of the Hall coefficient shows that, indeed, the carriers are holes, as expected. The actual phase diagram of this material is shown in Fig. 2, according to results obtained by Keimer *et al.* (1992) and Birgeneau (1990). Near half-filling, antiferromagnetic order is clearly observed, which theoretical studies have shown; it is well described by a simple Heisenberg antiferromagnetic Hamiltonian representing the interactions between the spin-$\frac{1}{2}$ holes located on the copper atoms (Chakravarty, 1990). [However, some authors disagree. See, for example, Kaplan, Mahanti, and Chang (1992) and Mahanti, Kaplan, Chang, and Harrison (1993).] Experimentally, Aeppli *et al.* (1989) and Hayden, Aeppli, Osborn, *et al.* (1991) showed that spin-wave theory with only first neighbor interactions accounts for the spin dynamics of La_2CuO_4. A small residual interaction between planes leads to a finite Néel critical temperature of about 300 K. The spin-glass phase of Fig. 2 was considered by Harshman *et al.* (1988). For Sr dopings between $x \sim 0.05$ and ~ 0.30, a superconducting phase is found at low temperatures. The maximum value of T_c is observed at the "optimal" doping $x \sim 0.15$. A structural phase transition was also found in this compound, as shown in Fig. 2. At high temperature the structure is tetragonal, but at lower temperatures the copper atoms and the six oxygens surrounding them slightly deviate from their positions, forming an orthorhombic structure [Burns (1992), p. 94]. This small distortion is usually neglected in most theoretical studies of this compound. (For a description of the rest of the phase diagram shown in Fig. 2, consult the original references by Keimer *et al.*, 1992 and Birgeneau, 1990. This phase diagram was also discussed by Torrance *et al.*, 1989.)

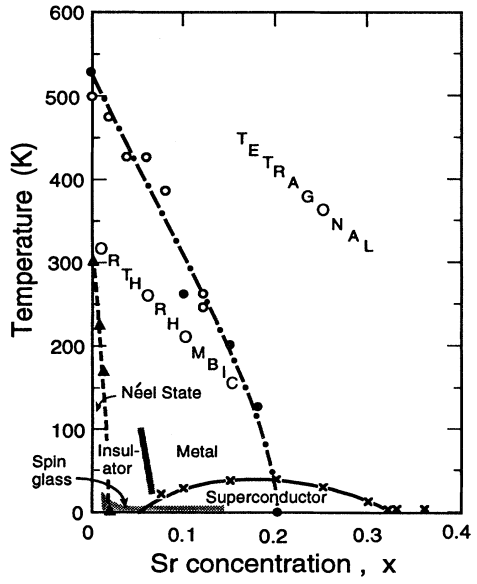

FIG. 2. Phase diagram of $La_{2-x}Sr_xCuO_4$ (from Keimer *et al.*, 1992).

2. $YBa_2Cu_3O_{6+x}$

Superconductivity in this material (which is sometimes called YBCO) was discovered in early 1987 (Wu *et al.*, 1987), soon after the lanthanum compound was reported by Bednorz and Müller. The (primitive tetragonal) structure of this compound is shown in Fig. 3, and it is clearly more complicated than the structure of $La_{2-x}Sr_xCuO_4$. In YBCO, there are *two* CuO_2 planes per unit cell approximately ~ 3.2 Å apart, separated by yttrium ions. The figure shows that these pairs of CuO_2 planes are themselves separated by layers of atoms containing bari-

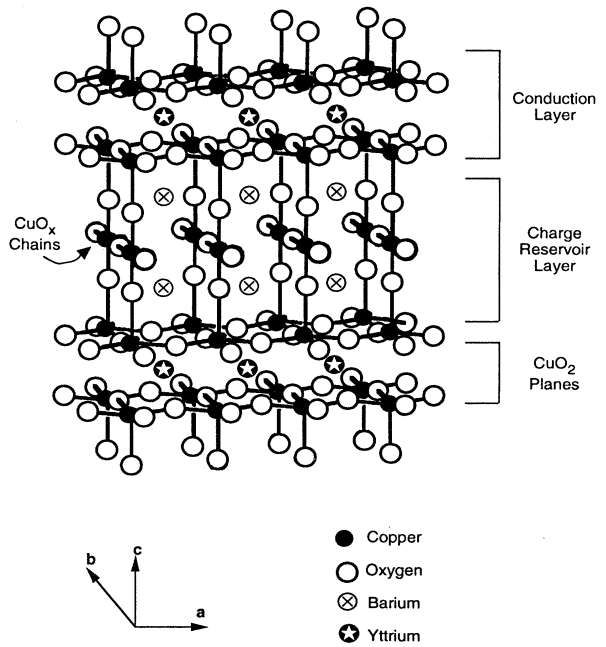

FIG. 3. Crystal structure of $YBa_2Cu_3O_{6+x}$ (taken from Jorgensen, 1991).

um, oxygen, and copper, which form the charge reservoir. As for the lanthanum compound, the number of carriers in the conduction planes is controlled by the amount of charge transferred between the conduction layer and the charge reservoir. The distance between the pairs of conducting planes is ~ 8.2 Å.

The atomic configurations of Y and Ba are $[Kr](5s)^2(4d)$ and $[Xe](6s)^2$, respectively, while those of Cu and O have been described before for the lanthanum compound. In the crystal, yttrium is in the valence state Y^{3+}, while barium is in Ba^{2+}. Copper on the planes is Cu^{2+}, and oxygen is O^{2-}. Note that in this compound there are Cu atoms in the charge reservoir, contrary to what occurs in $La_{2-x}Sr_xCuO_4$. In combination with oxygen atoms, they form one-dimensional structures along the **b** direction (shown in Fig. 3) which are called the Cu-O chains. Since not all cuprate superconductors have chains, it is believed that this structure does not play a key role in the superconducting mechanism. However, their presence affects other measurable properties of the material, such as the optical conductivity, as will be discussed in Sec. IV.B. The distance Cu—O in the chains is ~ 1.9 Å, as it is in the planes. The chains are well defined for $YBa_2Cu_3O_7$, but at other oxygen concentrations they have defects. Actually, at the minimum oxygen concentration ($x=0$), no Cu—O chains exist.

How can we control the amount of doping in the planes? This is achieved by modifying the chemistry of the charge reservoir. In this material, the number of carriers depends on the oxygen content in the formula $YBa_2Cu_3O_{6+x}$. In the case $x=1$, the oxygen atoms are structurally ordered and form the Cu—O chains shown in Fig. 3; when x is reduced, oxygen atoms are taken from the chains. Adding oxygen to the compound is believed to be equivalent to adding holes to the planes. However, this scenario is still not fully supported by measurements of the sign of the Hall coefficient, since this quantity is appreciably temperature dependent for this compound. The possibility of having holes on the chains, rather than only in the planes, complicates this issue even further. In this review we shall not discuss these subtle details further, and we shall assume that increasing the oxygen content is equivalent to adding holes to the conducting planes (for more details see Burns, 1992 and references therein).

In Fig. 4, the phase diagram of $YBa_2Cu_3O_{6+x}$ is shown. The range of defect concentrations (oxygen excess) in this compound is large, allowing the properties to change from insulating to superconducting. For x close to 0, an antiferromagnetic phase is observed with a Néel temperature over 500 K. This spin order is caused by the spin-$\frac{1}{2}$ holes in the d shell of the in-plane coppers, as in other compounds (the copper of the chains is not magnetic). At $x_c \sim 0.3$ ($\delta_c \sim 0.7$ in the notation of the figure), antiferromagnetic long-range order disappears and the superconducting phase starts developing. The "optimal" composition (i.e., the one that gives the largest T_c) is slightly below $x \sim 1$ ($\delta \sim 0.0$). Unfortunately, it is not possible to explore whether T_c can be increased further by adding oxygen beyond $x=1$, since they have already completed the Cu—O chain structure at this composition. A structural phase transition occurs in this material near $x_c \sim 0.3$ from a tetragonal to an orthorhombic phase, similar to that found for $La_{2-x}Sr_xCuO_4$. In this structural transition, the conduction planes CuO_2 are only slightly affected.

3. $Nd_{2-x}Ce_xCuO_4$

The structure of this compound is body-centered tetragonal (shown in Fig. 5), like that of $La_{2-x}Sr_xCuO_4$. The difference between the two lies in the position of the oxygen atoms of the charge reservoir. The structure corresponding to $Nd_{2-x}Ce_xCuO_4$ is usually called **T′** structure. It is interesting to note that the **T** structure can

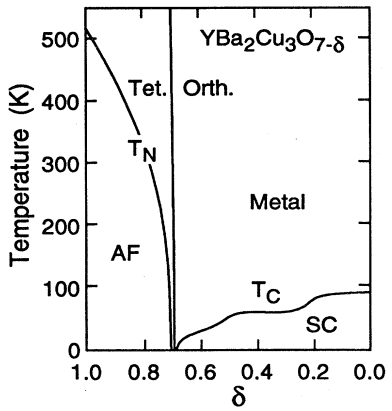

FIG. 4. Phase diagram of $YBa_2Cu_3O_{6+x}$ (taken from Burns, 1992; Koike *et al.*, 1989).

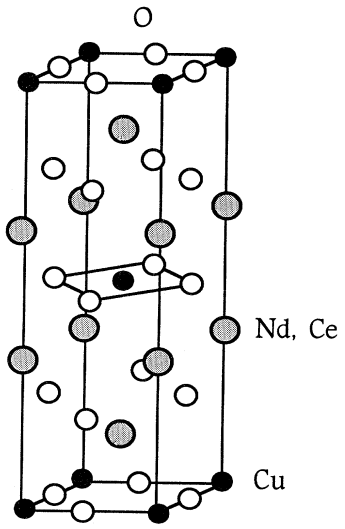

FIG. 5. Crystal structure of $Nd_{2-x}Ce_xCuO_4$ (**T′** phase). Taken from Almasan and Maple (1991).

only be easily hole doped, while the T′ structure can be easily electron doped, the reason for this asymmetry being unknown. The atomic configurations of the elements forming the compound are Nd:[Xe]$(4f)^4(6s)^2$ and Ce:[Xe]$(4f)(5d)(6s)^2$, while Cu and O have been described before. In the crystal, copper becomes Cu^{2+}, oxygen is O^{2-}, and neodymium is in a state Nd^{3+}. After doping, i.e., when a Nd ion is replaced by Ce^{4+}, the CuO_2 planes get an excess of electrons. This is confirmed by the experimentally observed sign of the Hall coefficient. It is believed that an added electron occupies a hole in the d shell of copper, producing a $S=0$ closed-shell configuration.

The phase diagram of this material is compared in Fig. 6 with a hole-doped compound. The similarities between the two diagrams are remarkable. Both present an antiferromagnetic phase with a similar Néel temperature (although for electron-doped materials, the antiferromagnetic phase is more stable upon doping, since $x>0.12$ is necessary to destroy the spin long-range order). When x is increased further, a superconducting phase appears close to antiferromagnetism in both cases, with an "optimal" composition close to $x=0.15$. The electron-doped phase diagram clearly illustrates that superconductivity is a relatively "small" effect compared with antiferromagnetism; and thus in theoretical studies it is important to isolate the proper degrees of freedom and energy scales of the pairing mechanism responsible for superconductivity, from those causing the bulk magnetic properties. Otherwise, the existence of this phase can be hidden in calculations that are dominated by other larger scales related to the insulating state.

The family of high-T_c superconductors is very large. A more complete list of superconducting materials and their critical temperatures can be found in a recent review article (Harshman and Mills, 1992). In particular, it is worth mentioning the layered copper oxide superconductors that include bismuth and thallium in the charge reservoir layers. These are more complex compounds, with the general formulas $Bi_mSr_2Ca_{n-1}Cu_nO_{2n+m+2}$ and $Tl_mBa_2Ca_{n-1}Cu_nO_{2n+m+2}$ (where m and n are integers), and are typically identified by the shorthand notation Bi (or Tl) $m2(n-1)n$, e.g., Bi2212. In particular, Tl2223 has one of the highest confirmed critical temperatures, $T_c\sim 125$ K, of the high-T_c family. [Recent results (Putilin *et al.*, 1993; Schilling *et al.*, 1993) suggest the presence of superconductivity at 133 K in some copper oxides that include Hg.] It contains *three* CuO_2 planes per unit cell, which are separated by Ca atoms ~ 3.2 Å apart, which is very similar to the distance between planes in $YBa_2Cu_3O_{6+x}$. The sets of three planes are ~ 11.6 Å apart. Details about the structure of these materials can be found in a review article by Jorgensen (1991; see also Burns, 1992).

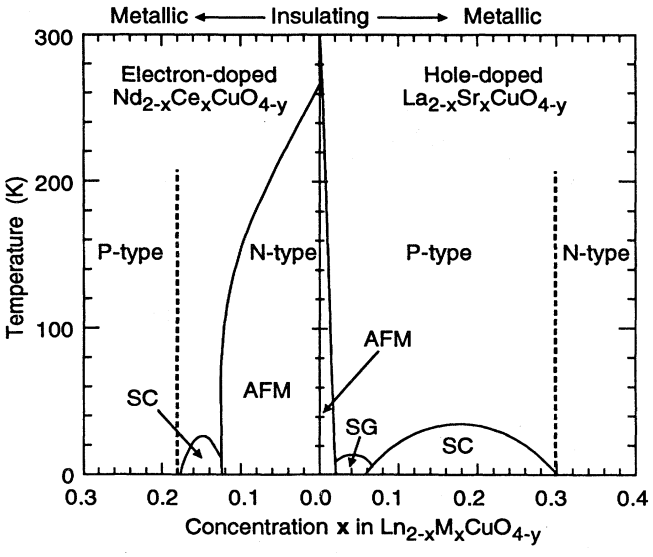

FIG. 6. Phase diagram of $Nd_{2-x}Ce_xCuO_4$ and $La_{2-x}Sr_xCuO_4$ (together for better comparison). Taken from Almasan and Maple (1991).

B. Normal-state properties

It is widely believed that understanding the normal-state properties of the high-T_c cuprates will also shed light on the superconducting mechanism. The basis for this expectation resides in the unusual normal-state properties of these materials. For example, strong anisotropies are observed, mainly caused by the two-dimensional nature of the problem, and magnetic phases exist close to the superconducting regions. In addition, there are properties of the cuprates that have raised the possibility of observing deviations from a Fermi-liquid description of the normal state. For example, we know that in a canonical Fermi-liquid metal the magnetic susceptibility and the Hall coefficient are temperature independent, the resistivity grows like T^2 at low temperatures, and the NMR relaxation is proportional to temperature $(1/T_1\sim T)$. These behaviors have *not* been observed in the cuprates, although a Fermi-liquid description is still not ruled out (see, for example, Levin *et al.*, 1992).

In this section, we briefly describe the normal-state property of the cuprates that is more frequently mentioned as indicative of an unusual normal state, namely, the experimentally observed linear dependence of the resistivity ρ with temperature (for a short review, see Batlogg, 1990, 1991). In conventional low-temperature (T) superconductors, it has been experimentally observed that $\rho\approx a+bT^5$, at low T (but larger than T_c). This temperature dependence arises from the scattering of electrons with phonons. At higher temperatures, a linear behavior is expected, and the interpolation between the two regimes is given by the Grüneisen-Bloch formula (Burns, 1992). The residual resistivity a at $T=0$ is caused by scattering with magnetic impurities, point or line defects, other electrons, etc. Several metals, such as Cu, Al, Ni, and Na, obey this behavior accurately (Burns, 1992, Chap. 4). However, the behavior of ρ observed in the high-T_c superconductors is different. Single crystal

measurements of ρ in the CuO_2 planes carried out for several different compounds have shown an approximate linear behavior over the measured temperature range. In Fig. 7, results for the in-plane resistivity ρ_{ab} are shown for $La_{1.85}Sr_{0.15}CuO_4$, $YBa_2Cu_3O_7$, Bi2201, and Bi2212 compounds (the average between the a and b crystal directions, i.e., ρ_{ab}, is measured for multidomain or *twinned* crystals, although the preparation of untwinned crystals is possible). For comparison, note that copper at room temperature has a resistivity of 1.7 $\mu\Omega$ cm, while the resistivity of carbon is 1500 $\mu\Omega$ cm. Thus ρ_{ab} of the cuprates at room temperature is more similar to that of carbon than copper! The linear behavior is clear, and the slopes of the curves are very similar for the various compounds, suggesting a common scattering mechanism for carrier transport in the CuO_2 planes. The results for Bi2201 are particularly interesting, since the linear behavior is observed in this material even at low temperatures close to $T_c = 7$ K, in a wide range of temperatures from 7 K to 700 K.

It is important to note that in those materials where the composition can be changed easily by chemical doping, the linear behavior $\rho \sim T$ is observed *only* in a narrow carrier-concentration window near the "optimal" compositions, i.e., those corresponding to the highest critical temperatures (Batlogg *et al.*, 1992; Takagi *et al.*, 1992). This detail is not sufficiently remarked upon in the literature. To illustrate this result, ρ_{ab} measured in single crystals of $La_{2-x}Sr_xCuO_4$ for several compositions are shown in Fig. 8(a). Contrary to the linear dependence at $x = 0.15$, under- and overdoped samples follow a different power-law behavior over a wide range. Then, the temperature dependence of the resistivity is more involved than what theorists usually believe. In addition, the electron-doped compounds do *not* show a linear behavior of the resistivity with temperature, but rather a quadratic dependence $\rho \sim T^2$ (see Hidaka and Suzuki, 1989; Tsuei, Gupta, and Koren, 1989). The T^2 dependence is consistent with electron-electron scattering in a Fermi liquid, and thus a lack of universality seems to exist between hole- and electron-doped materials. This is another issue not sufficiently remarked upon in the literature. The behavior of the resistivity with temperature is not the only "anomalous" property of the normal state of the high-T_c superconductors. Puzzling results have been observed in the optical conductivity $\sigma(\omega)$, Raman scattering, measurements of the Hall coefficient

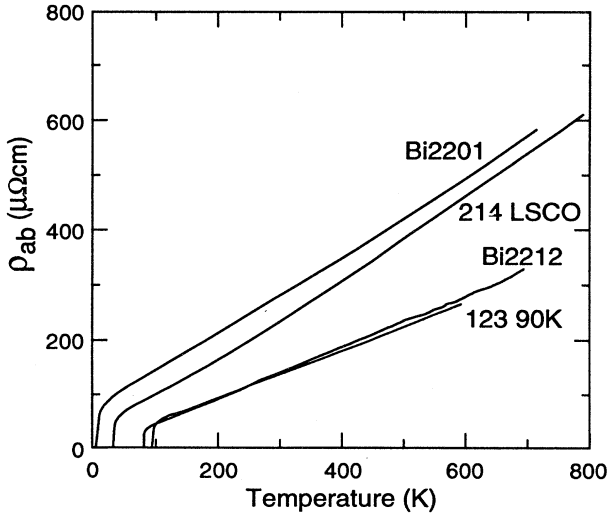

FIG. 7. Temperature dependence of the in-plane resistivity ρ_{ab} measured on crystals of various cuprate superconductors. 123 90*K* denotes YBCO at the optimal composition $x = 1$, while 214 LSCO corresponds to $La_{2-x}Sr_xCuO_4$ with $x = 0.15$ (from Batlogg *et al.*, 1992).

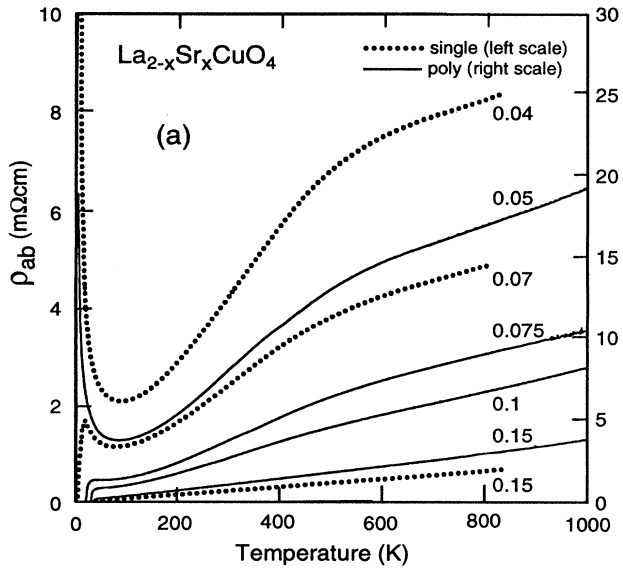

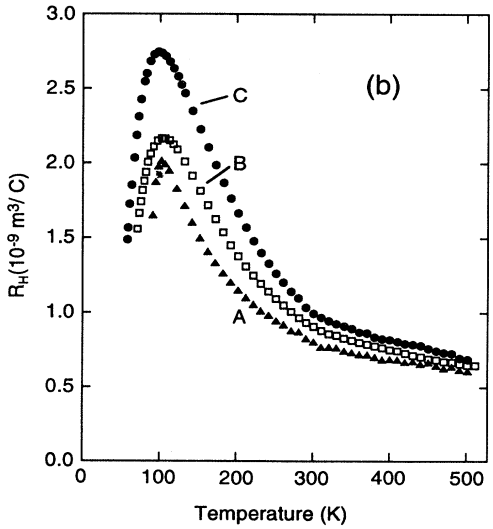

FIG. 8. (a) In-plane resistivity ρ_{ab} as a function of temperature for several compositions of $La_{2-x}Sr_xCuO_4$ (from Takagi *et al.*, 1992); (b) Hall coefficient R_H as a function of temperature for YBCO (Harris, Yan, and Ong, 1992). Sample A has $T_c = 91$ K; sample B, $T_c = 74$ K; and sample C, $T_c = 60$ K.

($R_H \sim T^{-1}$ in YBCO compounds), and several others. Many of them will be discussed in the following sections. As an example, in Fig. 8(b), experimental results for R_H in YBCO at different oxygen concentrations are shown (Harris, Yan, and Ong, 1992). While in simple models of weakly interacting electrons it is expected that R_H would be approximately constant, the experimental results for the cuprates show a strong $1/T$ temperature dependence. Finally, the presence of a "spin-gap" in YBCO is another normal-state property that deserves considerable attention. For example, in the 60-K compounds of the YBCO family, the spin-gap is observed at about 150 K and seems to dominate the normal-state physics of the underdoped materials. Ito, Takenaka, and Uchida (1993) and Bucher *et al.* (1993) have recently measured the in-plane resistivity and Hall coefficient for YBCO, concluding that the charge transport in the CuO_2 planes is determined by spin scattering.

C. Electronic models

1. Three-band model

After analyzing in some detail the structure and phase diagram of the high-T_c superconductors, the next step is to write a Hamiltonian to describe the behavior of electrons in these materials. Due to the complexity of their structure, it is important to make some simplifying assumptions. To begin with, it is reasonable to construct a Hamiltonian restricted to electrons moving on the CuO_2 planes. The very strong Cu—O bonds on the planes justifies this assumption. Of course, some features of the phase diagram can only be explained by adding a coupling between the planes (like the existence of a finite Néel critical temperature), but it is expected that those fine details can be studied *after* the physics of the planes is understood. Even under these assumptions, the planar CuO_2 problem is still very difficult to analyze. The copper ions Cu^{2+} have nine electrons in the five d orbitals, while O^{2-} has the three p orbitals occupied. However, this complicated problem can be further simplified. All copper ions in the high-T_c materials are surrounded by oxygens. As explained in Sec. I.A.1, in $La_{2-x}Sr_xCuO_4$, a CuO_6 structure is formed around each Cu^{2+}, which corresponds to an elongated octahedron. For other compounds, like $YBa_2Cu_3O_{6+x}$, the copper has five oxygens in its vicinity, while in the electron-doped material $Nd_{2-x}Ce_xCuO_4$, four oxygens form a square around the copper ion (see Figs. 1, 3, 5). In all these geometries, the degeneracy between the d orbitals produced by the rotational invariance of isolated ions is removed by the lattice structure. After some calculations, it can be shown that the copper and oxygen orbitals separate, as schematically shown in Fig. 9. The state with the highest energy has mainly $d_{x^2-y^2}$ character, and it carries the missing electron (i.e., the hole) that gives the ion its spin $\frac{1}{2}$. Thus in the absence of doping (i.e., with one hole per unit cell on the plane), the material is well described by a model of mostly localized spin-$\frac{1}{2}$ states that give to these materials their antiferromagnetic character. The other orbitals at lower energies are occupied, and as a first approximation they will be neglected in the construction of the Hamiltonian.

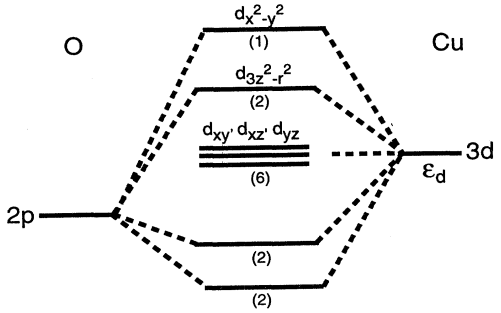

FIG. 9. Bonding between a Cu^{2+} and two O^{2-} ions. Only the d electrons of Cu and the p_x and p_y orbitals of the oxygens are considered. The numbers in parentheses indicate the occupations of the different levels in the undoped compound (from Fulde, 1991).

What occurs upon doping? As an example, let us consider $La_{2-x}Sr_xCuO_4$, where an additional electron is removed from the CuO_2 plane by the substitution of a La atom by a Sr atom. The energy levels shown in Fig. 9 may suggest that we simply have to take out another electron from the $d_{x^2-y^2}$ orbital to describe the physics of the doped compounds. However, in this picture the strong Coulombic repulsion between holes in the same orbital is not taken into account. Actually neglecting interactions, one would have expected La_2CuO_4 to be metallic with a half-filled conduction band. However, the material is an insulator with antiferromagnetic properties showing that correlations are very strong. Double occupancy of the same orbital must be energetically unfavored by the Coulombic interactions. Based on this line of reasoning, it is possible to construct a Hamiltonian for electrons in the copper oxide planes (see Emery, 1987; Littlewood, Varma, and Abrahams, 1987; Varma, Schmitt-Rink, and Abrahams, 1987; Emery and Reiter, 1988a). Using the *hole* notation, where the vacuum is defined as all the orbitals shown in Fig. 9 occupied, the Hamiltonian is

$$H = -t_{pd} \sum_{\langle ij \rangle} p_j^\dagger (d_i + \text{H.c.}) - t_{pp} \sum_{\langle jj' \rangle} p_j^\dagger (p_{j'} + \text{H.c.})$$
$$+ \epsilon_d \sum_i n_i^d + \epsilon_p \sum_j n_j^p + U_d \sum_i n_{i\uparrow}^d n_{i\downarrow}^d$$
$$+ U_p \sum_j n_{j\uparrow}^p n_{j\downarrow}^p + U_{dp} \sum_{\langle ij \rangle} n_i^d n_j^p \,. \qquad (1.1)$$

p_j are fermionic operators that destroy holes at the oxygen ions labeled j, while d_i corresponds to annihilation operators at the copper ions i. $\langle ij \rangle$ refers to pairs of

nearest neighbors i (copper) and j (oxygen) sites. The hopping terms correspond to the hybridization between nearest neighbors Cu and O atoms, and are roughly proportional to the overlap between orbitals. For completeness, a direct O-O hopping term is also included with amplitude t_{pp}. These hopping terms allow the movement of the electrons on the lattice, providing their kinetic energy. U_d and U_p are positive constants that represent the repulsion between holes when they are at the same d and p orbitals, respectively. U_{pd} has a similar meaning; i.e., it corresponds to the Coulombic repulsion when two holes occupy adjacent Cu—O. In principle, interactions at larger distances should also be included in the Hamiltonian, but they are presumed to be screened by the finite density of electrons (unfortunately, the actual screening correlation length is difficult to calculate to support this assumption). The on-site energies ϵ_d and ϵ_p represent the difference in energy between the occupied orbitals of oxygen and copper. In the strong-coupling limit, and with one particle per unit cell, this model reduces to the spin Heisenberg model with a superexchange antiferromagnetic coupling (Emery and Reiter, 1988a; Fulde, 1991).

Hamiltonian (1.1) shows that for $\Delta \doteq \epsilon_p - \epsilon_d > 0$, the first hole added to the system will energetically prefer to occupy the d orbital of the copper ions. As explained before, this is indeed the observed situation in the "undoped" materials which have one hole per unit cell. When another hole is added to this unit cell, and working in the regime where U_d is larger than Δ, the new hole will mainly occupy oxygen orbitals. This is in agreement with electron-energy-loss spectroscopy (EELS) experiments (Nücker *et al.*, 1987). From a band-structure calculation (Hybertsen *et al.*, 1989), we can estimate the actual values of the parameters in Hamiltonian (1.1). In eV's they are

$\epsilon_p - \epsilon_d$	t_{pd}	t_{pp}	U_d	U_p	U_{pd}
3.6	1.3	0.65	10.5	4	1.2

showing that indeed we are in the strong-coupling regime. For a comparison between predictions for these parameters obtained by different groups, see Mila (1988).

2. One-band models

The three-band model has several parameters, and it is still somewhat complicated. It would be desirable to reduce it to an even simpler model. Zhang and Rice (1988) made progress in this direction by the following argument. Consider one copper ion surrounded by four oxygens. A hole at the oxygen can be in a symmetric or antisymmetric state with respect to the central hole at the copper ion. These states can be combined with the Cu hole to form spin singlet or triplet states. To second order in perturbation theory about the atomic limit, Zhang and Rice showed that the spin singlet state has the lowest energy, and assumed that it is possible to work in this singlet subspace without changing the "physics" of the problem. Then, the hole originally located at the oxygen has been replaced by a spin singlet state centered at the copper. This is equivalent to removing one Cu spin-$\frac{1}{2}$ from the square lattice of copper spins, and thus the effective model corresponds to spins and holes (absence of the spin) on a two-dimensional square lattice. The oxygen ions are no longer explicitly present in the effective model. After some calculations, Zhang and Rice concluded that the effective Hamiltonian describing the physics of the three-band model is the so-called t-J model (which was previously introduced by Anderson, 1987), defined as

$$H = J \sum_{\langle ij \rangle} \left[\mathbf{S}_i \cdot \mathbf{S}_j - \frac{1}{4} n_i n_j \right] - t \sum_{\langle ij \rangle \sigma} [c_{i\sigma}^{\dagger}(1-n_{i-\sigma})(1-n_{j-\sigma})c_{j\sigma} + \text{H.c.}] , \tag{1.2}$$

where $\mathbf{S}_i$ are spin-$\frac{1}{2}$ operators at the sites i of a two-dimensional square lattice, and J is the antiferromagnetic coupling between nearest neighbors sites $\langle ij \rangle$. The hopping term allows the movement of electrons without causing a change in their spin, and explicitly *excludes* double occupancy due to the presence of the projector operators $(1-n_{i-\sigma})$. Then, this model has only three possible states per site, i.e., an electron with spin up or down, or a hole. The rest of the notation is standard.

It is important to remark that the reduction of the three-band model to the t-J model is still controversial. Emery and Reiter (1988b) have argued that the resulting quasiparticles of the three-band model have both charge and spin, in contrast to the Cu-O singlets that form the effective one-band t-J model. Their result was based on the study of the exact solution in a ferromagnetic background, and their conclusion was that the t-J model is incomplete for representing the low-energy physics of the three-band model. Zhang and Rice (1990) and Emery and Reiter (1990) continued their exchange of ideas on this subject, and the issue is still unresolved [although Chen, Schüttler, and Fedro (1990) and Schüttler and Fedro (1992) have presented fairly convincing evidence that the reduction to a one-band model is possible]. Other authors have also contributed to the discussion (see, for example, Eskes and Sawatzky, 1988; Mila, 1988; Stechel and Jennison, 1988; Zaanen and Oles, 1988; Ramsak and Prelovšek, 1989; Schüttler and Fedro, 1989; and Belinicher and Chernyshev, 1993). Most of the results shown in the rest of this review are for one-band models; thus we shall *assume* that the reduction from the original three-band Hamiltonian to a one-band is possible, although certainly more work is needed to clarify this point.

In addition to the t-J and three-band Cu-O models, theorists have been extensively studying, since the early days of high-T_c superconductivity, the two-dimensional

one-band Hubbard model (Hubbard, 1963), mainly in the strong-coupling limit. This model is defined as

$$H=-t\sum_{\langle ij\rangle,\sigma}(c_{i\sigma}^{\dagger}c_{j\sigma}+c_{j\sigma}^{\dagger}c_{i\sigma})+U\sum_{i}(n_{i\uparrow}-\tfrac{1}{2})(n_{i\downarrow}-\tfrac{1}{2}) , \tag{1.3}$$

where, as usual, $c_{i\sigma}^{\dagger}$ is a fermionic operator that creates an electron at site i of a square lattice with spin σ. U is the on-site repulsive interaction, and t the hopping amplitude. Although we know that the actual materials present a band structure with three dominant bands (as shown in Fig. 10), the one-band Hubbard model tries to mimic the presence of the charge-transfer gap Δ by means of an *effective* value of the Coulomb repulsion $U_{\rm eff}$, and thus it presents only two bands (see Zaanen, Sawatzky, and Allen, 1985). The "oxygen" band becomes the lower Hubbard band of this model. Note also that in the strong-coupling limit, it can be shown that the Hubbard model reduces to the *t-J* model, Eq. (1.2), with the addition of terms involving three sites. These terms have not received much attention and are usually excluded from the numerical studies described in the rest of the review. Their importance is unclear. Also note that the term $-\frac{1}{4}n_i n_j$ appears spontaneously in the strong-coupling expansion of the Hubbard model. Again, its actual importance compared with the rest of the terms is not obvious.

Why is this Hamiltonian so much studied? The dimensionality of the problem is easy to understand, since the model attempts to describe electrons in the CuO_2 planes. The restriction of working in strong coupling can also be understood easily. For example, at half-filling this model reduces to the Heisenberg model when the on-site Coulomb interaction is large, and we know that the Heisenberg model describes well the spin dynamics of the undoped cuprates. However, the particular form of the Hamiltonian, where the oxygens are not considered and the interactions are restricted to an on-site term, is more difficult to justify. The reader may find enlightening the article by Anderson and Schrieffer (1991) where this issue is discussed. There are also interesting calculations on finite clusters by Hybertsen *et al.* (1990) and Bacci, Gagliano, Martin, and Annett (1991), where it was shown that the one-band Hubbard model (supplemented with a small next-nearest-neighbor hopping term t') can reproduce the low-energy spectrum of the three-band model. Hybertsen *et al.* found that this is achieved by taking the Hubbard model parameters as $U=5.4$ eV, $t=0.43$ eV, and $t'=-0.07$ eV, i.e., $U/t\sim 12$. These authors also found that the *t-t'-J* model with $J=0.128$ eV, and the same value of t and t' as for the one-band Hubbard model, also reproduces well the spectra of the more complicated three-band Hamiltonian.

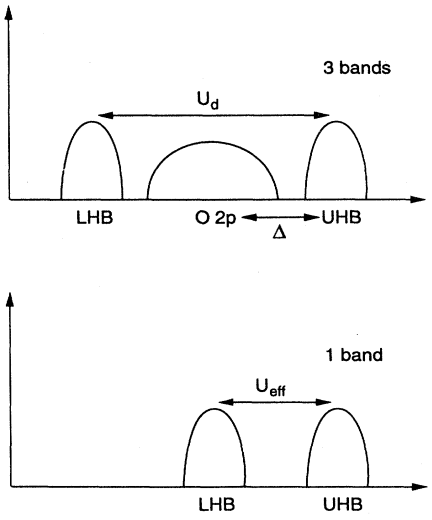

FIG. 10. Schematic band structure of the CuO_2 planes. U_d is the Coulombic repulsion at the copper ions, while Δ is the difference in energy between copper and oxygen orbitals. The lower part of the figure represents the one-band Hubbard model that simulates the charge-transfer gap by a Hubbard gap using an effective $U_{\rm eff}$.

Of course, this is only a test of the short-distance properties of the models, and not of their long-range behavior. Thus, in this author's opinion, there is no *a priori* clear justification for the enormous effort undertaken by hundreds of theorists in studying this very particular model (certainly including the author!). However, as we shall see below, several normal-state properties of the model qualitatively mimic those of the real materials; thus an *a posteriori* justification for its use can be claimed. Unfortunately, thus far there is no conclusive evidence of superconductivity in the one-band Hubbard model, although it is not clear whether that is a failure of the one-band approximation or of the tools used to search for a superconducting state (more details are given in Sec. IV.E.1 and Appendix C). As with any simple model of a complicated material, we can only justify its introduction after its low-energy properties are known with some accuracy. This is precisely the goal of most of the computational work described in the rest of the review.

II. ALGORITHMS

The study of models of strongly correlated electrons is a difficult problem. There are no well-controlled analytical techniques to analyze them in two dimensions. Mean-field and variational approximations are self-consistent, but it is difficult to judge if they actually describe properties of the ground state of the system or of an excited state. As explained in the introduction, these difficulties have led numerous groups to study these models using computational techniques. In some sense the situation is similar to that of particle physics in the 1970's when it became clear that an understanding of strongly correlated quarks in quantum chromodynamics (QCD) would be difficult to achieve by the standard one-loop bubble summation. In those days, the field of lattice

gauge theory was developed (for a review, see Kogut, 1979, 1983), and currently its predictions for the hadron spectrum of QCD have reached a reasonable level of accuracy. At present, we may be facing similar developments in condensed matter, since it is clear that considerable progress can be made with the help of computers in the study of correlated electrons.

Many techniques are currently being used to study numerically the models of correlated electrons presented in Sec. I.C. However, the vast majority of the papers in the literature can be grouped into those where exact diagonalization (or Lanczos) techniques were used, and those produced with quantum Monte Carlo methods. Both algorithms will be reviewed in this section. A large number of physical results obtained with these techniques will be discussed in the rest of the review.

A. Lanczos technique

1. Method

The basic idea of the Lanczos method is that a special basis can be constructed where the Hamiltonian has a tridiagonal representation. This is carried out iteratively as shown below. First, it is necessary to select an arbitrary vector $|\phi_0\rangle$ in the Hilbert space of the model being studied. If the Lanczos method (Lanczos, 1950; Pettifor and Weaire, 1985) is used to obtain the ground-state energy of the model, then it is necessary that the overlap between the actual ground state $|\psi_0\rangle$ and the initial state $|\phi_0\rangle$ be nonzero. If no *a priori* information about the ground state is known, this requirement is usually easily satisfied by selecting an initial state with *randomly* chosen coefficients in the working basis that is being used. If some other information about the ground state is known, like its total momentum and spin, then it is convenient to initiate the iterations with a state already belonging to the subspace having those quantum numbers (and still with random coefficients within this subspace).

After $|\phi_0\rangle$ is selected, we can define a new vector by applying the Hamiltonian $\hat{H}$ to the initial state. Subtracting the projection over $|\phi_0\rangle$, we obtain

$$|\phi_1\rangle=\hat{H}|\phi_0\rangle-\frac{\langle\phi_0|\hat{H}|\phi_0\rangle}{\langle\phi_0|\phi_0\rangle}|\phi_0\rangle\ , \tag{2.1}$$

which satisfies $\langle\phi_0|\phi_1\rangle=0$. Now we can construct a new state that is orthogonal to the previous two as

$$|\phi_2\rangle=\hat{H}|\phi_1\rangle-\frac{\langle\phi_1|\hat{H}|\phi_1\rangle}{\langle\phi_1|\phi_1\rangle}|\phi_1\rangle-\frac{\langle\phi_1|\phi_1\rangle}{\langle\phi_0|\phi_0\rangle}|\phi_0\rangle\ . \tag{2.2}$$

It can be easily checked that $\langle\phi_0|\phi_2\rangle=\langle\phi_1|\phi_2\rangle=0$. The procedure can be generalized by defining an orthogonal basis recursively as

$$|\phi_{n+1}\rangle=\hat{H}|\phi_n\rangle-a_n|\phi_n\rangle-b_n^2|\phi_{n-1}\rangle\ , \tag{2.3}$$

where $n=0,1,2,\ldots$, and the coefficients are given by

$$a_n=\frac{\langle\phi_n|\hat{H}|\phi_n\rangle}{\langle\phi_n|\phi_n\rangle},\quad b_n^2=\frac{\langle\phi_n|\phi_n\rangle}{\langle\phi_{n-1}|\phi_{n-1}\rangle}\ , \tag{2.4}$$

supplemented by $b_0=0, |\phi_{-1}\rangle=0$. In this basis, it can be shown that the Hamiltonian matrix becomes

$$H=\begin{bmatrix} a_0 & b_1 & 0 & 0 & \cdots \\ b_1 & a_1 & b_2 & 0 & \cdots \\ 0 & b_2 & a_2 & b_3 & \cdots \\ 0 & 0 & b_3 & a_3 & \cdots \\ \vdots & \vdots & \vdots & \vdots & \end{bmatrix}; \tag{2.5}$$

i.e., it is tridiagonal, as expected. Once in this form the matrix can be diagonalized easily using standard library subroutines. However, to diagonalize completely the model being studied on a finite cluster, a number of iterations equal to the size of the Hilbert space (or of the subspace under consideration) are needed. In practice, this would demand a considerable amount of CPU time. However, one of the advantages of this technique is that accurate enough information about the ground state of the problem can be obtained after a small number of iterations (typically of the order of ~ 100 or less). Thus the method is suitable for the analysis of low-temperature properties of the models of correlated electrons described in Sec. I.C.

To understand the rapid convergence to the ground state which is obtained using this algorithm, it is convenient to consider a variation of this technique known as the modified Lanczos method (Dagotto and Moreo, 1985; Gagliano *et al.*, 1986). In this method, the diagonalization proceeds using "2×2 steps"; i.e., first the Hamiltonian in the basis $|\phi_0\rangle$ and $|\phi_1\rangle$ (defined before) is diagonalized. The lowest energy state is always a better approximation to the actual ground state than $|\phi_0\rangle$. This new, improved state can be used as the initial state of another 2×2 iteration, and the procedure is repeated as many times as needed until enough accuracy has been reached. It is then clear that the modified Lanczos method, or the original Lanczos, can be described as a systematic way to improve a given variational state that is used to represent the ground state of the system (Dagotto and Moreo, 1985; Heeb and Rice, 1993); thus it is not surprising that ground-state properties can be obtained accurately well before the rest of the matrix eigenvalues are evaluated.

In spite of these advantages, memory limitations impose severe restrictions on the size of the clusters that can be studied with this method. To understand this point, note that although the lowest energy state can be written in the $\{|\phi_n\rangle\}$ basis as $|\psi_0\rangle=\sum_m c_m|\phi_m\rangle$, this expression is of no practical use unless $|\phi_m\rangle$ itself is expressed in a convenient basis to which the Hamiltonian can be easily applied. For example, in spin-$\frac{1}{2}$ models it is convenient to work in the basis where S_z is defined at every site, schematically represented as $|n\rangle=|\uparrow\downarrow\uparrow\cdots\rangle$.

For the models described in Sec. I.C, the size of this type of basis set grows exponentially with the system size. For example, the dimension of the Hilbert space of a Hubbard model (four states per site) on an N-site cluster is, in principle, 4^N, which for $N=16$ corresponds to $\sim 4.3\times 10^9$ states. Such a memory requirement is beyond the reach of present-day computers. In practice, this problem can be considerably alleviated by the use of symmetries of the Hamiltonian that reduce the matrix to a block-form. The most obvious symmetry is the number of particles in the problem which is usually conserved, at least for fermionic problems. The total projection of the spin S^z_{total} may also be a good quantum number. For translational invariant problems, the total momentum $\mathbf{p}$ of the system is also conserved, introducing a reduction of $1/N$ in the number of states (this does not hold for models with open boundary conditions or explicit disorder). In addition, several Hamiltonians have other symmetries, like spin inversion. On a square lattice, rotations of $\pi/2$ about a given site, and reflections with respect to the lattice axes, are good quantum numbers (although care must be taken in their implementation, since some of these operations are combinations of others and thus not independent). Upon introduction of these symmetries, the linear size of the largest block that is necessary to diagonalize for a Hubbard model on the 4×4 square cluster is $\sim 1\,350\,000$ at half-filling and zero momentum (Fano, Ortolani, and Semeria, 1990; Fano, Ortolani, and Parola, 1992. In these papers, interesting group theory tricks have been used to make the study of this cluster possible in an efficient way. See also Dagotto, Moreo, Ortolani, Poilblanc, and Riera, 1992). It is then clear that the use of symmetries is very important in performing Lanczos calculations on large enough clusters. Currently, the one-band Hubbard model can be studied on clusters only slightly larger than the 4×4 lattice, at least near half-filling, while at low electronic densities larger systems can be dealt with. The three-band Hubbard model can be analyzed on the cluster Cu_4O_8 (2×2 cells), but not much bigger. The t-J model has been studied on clusters of up to 26 sites at low hole density (see Sec. III.B), and perhaps lattices of 32 sites will be reachable soon. Note that this model reaches a maximum in the dimension of its Hilbert space at an intermediate hole density. At this point, it is also convenient to clarify that it has become commonplace in the Lanczos literature to diagonalize not only clusters with $M\times M$ sites, but also other square clusters that completely cover the two-dimensional square lattice, which have axes forming a nonzero angle with the lattice axes. Examples can be found in Oitmaa and Betts (1978). Some of the "magic number" of sites that admit such a covering of the bulk lattice with "tilted" squares are $N=8,10,16,18,20,26,32,\ldots$. The general rule is $N=n^2+m^2$, where the positive integers n,m are both even or odd. For example, $10=1^1+3^2$, $20=2^2+4^2$, $50=5^2+5^2$, etc. (for more details see Appendix A).

How can we obtain explicitly the actual ground state of the problem? Each element $|\phi_n\rangle$ of the basis is represented by a large set of coefficients, when it is itself expanded in the basis selected to carry out the problem (like the S^z basis). Thus, in practice, it is not convenient to store each one of the $|\phi_m\rangle$ vectors individually, since such a procedure would demand a memory requirement equal to the size of the Hilbert space multiplied by the number of Lanczos steps (typically ~ 100). However, there is a simple solution to this problem, and it consists of running the Lanczos subroutine *twice*. In the first run, the coefficients c_m are obtained, and in the second the vectors $|\phi_m\rangle$ are systematically reconstructed one by one and stored in the vector $|\psi_0\rangle$. Another procedure to get the ground state is to use the modified Lanczos method described before. In the 2×2 steps, the ground state is always explicitly at hand. While this technique converges more slowly to the ground state than the standard Lanczos method, the latter needs to be run twice to get the ground state explicitly. Thus in some cases it is easier to use the modified Lanczos approach, which is somewhat simpler to program. An even more pedestrian technique is the power method, which consists of applying the Hamiltonian n-times to the initial state until all excited states are filtered out and only the ground state remains. This procedure is the slowest in speed of convergence, but in simple problems is enough and easy to program.

To end this section about the Lanczos method, we shall describe a recent attempt to increase the size of the clusters that this technique can reach. The idea is that, for some particular cases, it may occur that the wave function of the ground state, expanded in some working basis that is selected for the problem (schematically $|\psi_0\rangle=\sum_m c_m|m\rangle$), may contain states with very small weight c_m. Then, it could be possible to neglect those states in the basis and still get accurate enough results for the ground-state properties. These types of ideas (that we call the truncation method) have been recently used in quantum chemistry by Wenzel and Wilson (1992) and, in the context of correlated electrons, by Riera and Dagotto (1993a, 1993b; see also Knowles and Handy, 1989; Kovarik, 1990; De Raedt and von der Linden, 1992; De Raedt and Frick, 1993; Prelovšek and Zotos, 1993; and references therein). For the particular case of the t-J_z model, the approach works very well, and clusters of 50 sites can be easily studied keeping only a few hundred thousand states in the basis (which is a negligible percentage of the total basis set size). Physical results obtained with this approach will be described elsewhere in this review. However, when the method is applied to the t-J model, its convergence to the ground-state energy becomes slow (logarithmic) when the size of the basis is increased (Prelovšek and Zotos, 1993). To describe properly the strong quantum fluctuations of the spin background, most of the S^z basis is needed. Then, the truncation technique is very accurate for particular Hamiltonians, while for others it only provides a rough estimation of the ground-state properties. This approach should be

seriously considered every time a new problem that needs computational work appears. In particular, it seems suitable for problems with gaps in the spectrum (like a spin-gap).

2. Dynamical properties

One of the most appealing features of the Lanczos method is that it allows the calculation of *dynamical* properties of a given Hamiltonian (Mori, 1965a, 1965b; Haydock, Heine, and Kelly, 1972; Gagliano and Balseiro, 1987). As shown below, the quantum Monte Carlo technique is, unfortunately, not suitable for extracting this information, since the simulations are carried out in imaginary time. Currently the Lanczos approach is the only reliable technique for evaluating dynamical responses in a controlled way (of course, with the restriction of working on small clusters). Here, we shall set up the main formalism. In general, we are interested in calculating quantities such as

$$I(\omega)=-\frac{1}{\pi}\mathrm{Im}[\langle\psi_0|\hat{O}^\dagger\frac{1}{\omega+E_0+i\epsilon-\hat{H}}\hat{O}|\psi_0\rangle]\ , \qquad (2.6)$$

where $\hat{O}$ is the operator that we are analyzing (which depends on the actual experimental setup under consideration), $|\psi_0\rangle$ is the ground state of the Hamiltonian $\hat{H}$ whose ground-state energy is E_0, ω is the frequency, and ϵ is a small (real) number introduced in the calculation to shift the poles of the Green's function into the complex plane. Introducing a complete basis, $\sum_n|\psi_n\rangle\langle\psi_n|=1$, and using the well-known identity

$$\frac{1}{x+i\epsilon}=P\left[\frac{1}{x}\right]-i\pi\delta(x)\ ,$$

valid when $\epsilon\to 0$ (where x is real, and P denotes the principal part), we arrive at

$$I(\omega)=\sum_n|\langle\psi_n|\hat{O}|\psi_0\rangle|^2\delta(\omega-(E_n-E_0))\ , \qquad (2.7)$$

which is another way to express the spectral decomposition of a given operator. $|\psi_n\rangle$ can be selected as eigenvectors of the Hamiltonian with eigenvalues E_n. In practice, the δ functions are smeared by a finite ϵ; i.e., they are replaced by Lorentzians according to

$$\delta(x)\to\frac{1}{\pi}\frac{\epsilon}{x^2+\epsilon^2}\ .$$

In order to evaluate numerically Eq. (2.7), it is convenient to write the Hamiltonian matrix in a special basis. As before, we shall apply the Lanczos method to write $\hat{H}$ in a tridiagonal form; but, instead of starting the iterations with a random state, we choose

$$|\phi_0\rangle=\frac{\hat{O}|\psi_0\rangle}{\sqrt{\langle\psi_0|\hat{O}^\dagger\hat{O}|\psi_0\rangle}} \qquad (2.8)$$

as the initial configuration for reasons that will become clear soon. Following Fulde (1991), consider the matrix $(z-\hat{H})$ and the identity $(z-\hat{H})(z-\hat{H})^{-1}=I$, where $z=\omega+E_0+i\epsilon$. Decomposed in the basis $|\phi_n\rangle$ defined in Eq. (2.3), with $|\phi_0\rangle$ as given by Eq. (2.8), we arrive at $\sum_n(z-\hat{H})_{mn}(z-\hat{H})^{-1}_{np}=\delta_{mp}$. For the special case $p=0$, we obtain $\sum_n(z-\hat{H})_{mn}x_n=\delta_{m0}$, where $x_n=(z-\hat{H})^{-1}_{n0}$. This represents a system of equations for the unknown x_0. The particular case of $n=0$ corresponds to

$$\langle\phi_0|\frac{1}{z-\hat{H}}|\phi_0\rangle\ ,$$

which is the quantity we want to study. We need, then, to solve this linear system of equations.

For this purpose we use Cramer's rule, i.e.,

$$x_0=\frac{\det B_0}{\det(z-\hat{H})}\ ,$$

where the matrices in the $\{|\phi_n\rangle\}$ basis are given by

$$z-\hat{H}=\begin{bmatrix} z-a_0 & -b_1 & 0 & 0 & \cdots \\ -b_1 & z-a_1 & -b_2 & 0 & \cdots \\ 0 & -b_2 & z-a_2 & -b_3 & \cdots \\ 0 & 0 & -b_3 & z-a_3 & \cdots \\ \vdots & \vdots & \vdots & \vdots & \end{bmatrix} \qquad (2.9)$$

and

$$B_0=\begin{bmatrix} 1 & -b_1 & 0 & 0 & \cdots \\ 0 & z-a_1 & -b_2 & 0 & \cdots \\ 0 & -b_2 & z-a_2 & -b_3 & \cdots \\ 0 & 0 & -b_3 & z-a_3 & \cdots \\ \vdots & \vdots & \vdots & \vdots & \end{bmatrix}\ , \qquad (2.10)$$

where the coefficients a_n, b_n were defined earlier when the Lanczos method was introduced. The determinants of these matrices are expanded as $\det(z-\hat{H})=(z-a_0)\det D_1-b_1^2\det D_2$ and $\det B_0=\det D_1$, where, in general, the matrix D_n is obtained from Eq. (2.9) by removing the first n rows and columns. Then, it can be easily shown that

$$x_0=\frac{1}{z-a_0-b_1^2\dfrac{\det D_2}{\det D_1}}\ . \qquad (2.11)$$

The ratio of determinants on the right-hand side of Eq. (2.11) can also be expanded as

$$\frac{\det D_2}{\det D_1}=\frac{1}{z-a_1-b_2^2\dfrac{\det D_3}{\det D_2}}\ , \qquad (2.12)$$

and the procedure can be repeated until a full continued fraction is constructed. Recalling the definition of the spectral intensity $I(\omega)$, we can show that

$$I(\omega)=-\frac{1}{\pi}\mathrm{Im}\left[\frac{\langle\psi_0|\hat{O}^\dagger\hat{O}|\psi_0\rangle}{z-a_0-\dfrac{b_1^2}{z-a_1-\dfrac{b_2^2}{z-a_2-\cdots}}}\right], \tag{2.13}$$

which establishes the relation between Eq. (2.6) and a continued fraction expansion. Recalling that $z=\omega+E_0+i\epsilon$ and knowing the ground-state energy of the system, we can, for any value of the frequency ω and the width ϵ, obtain the spectral function. From the eigenvalues of the Hamiltonian in the special Lanczos basis obtained by iterating with the initial state Eq. (2.8), we can get very accurately the positions of the poles in the spectral function.

In practice, the best way to proceed in order to get the dynamical response of a finite cluster is in two steps. First, run the Lanczos subroutine using Eq. (2.8) as the initial state. It is clear that, with this procedure, we are testing the subspace of the Hilbert space in which we are interested, and thus all the states found in the Lanczos step will contribute to the spectral function (there will be as many poles as iterations carried out, assuming that this number is smaller than the total size of the subspace being explored). Secondly, in order to find the intensity of each pole, it is useful to recall that any energy *eigenvector* $|\psi_n\rangle$ of the tridiagonal representation of the Hamiltonian can be written as $|\psi_n\rangle=\sum_m c_m^n|\phi_m\rangle$, where $|\phi_m\rangle$ are the orthonormalized vectors defined in the Lanczos procedure, with $|\phi_0\rangle$ given by Eq. (2.8). Then, it can be easily shown that

$$|\langle\psi_n|\hat{O}|\psi_0\rangle|^2=|c_0^n|^2\langle\psi_0|\hat{O}^\dagger\hat{O}|\psi_0\rangle\ , \tag{2.14}$$

and thus the intensity can be written in terms of the first component of each eigenvector obtained when the tridiagonal Hamiltonian matrix is diagonalized. In summary, the whole process simply amounts to a Lanczos run with a very particular initial state. To test the convergence of the procedure, it is generally enough to plot the spectral function with a particular ϵ, and to test by eye how the results evolve with the number of iterations. Other more sophisticated methods to terminate the iterations can be implemented (Pettifor and Weaire, 1985; Viswanath and Müller, 1990, 1991).

Sometimes it is necessary to calculate moments of the distribution $I(\omega)$. This can be done very easily. For example, the integral over frequency of the spectral function gives

$$\int_0^\infty d\omega\, I(\omega)=\sum_n|\langle\psi_n|\hat{O}|\psi_0\rangle|^2=\langle\psi_0|\hat{O}^\dagger\hat{O}|\psi_0\rangle\ , \tag{2.15}$$

where we have assumed that the eigenvectors of the Hamiltonian are normalized to 1, i.e., $\sum_n|c_0^n|^2=1$. Equation (2.15) is a generic expression for some of the sum rules frequently mentioned in the literature for various operators $\hat{O}$ (as will be shown in later examples). If higher moments of the distribution are needed, the following relation holds,

$$\int_0^\infty d\omega\,\omega^p I(\omega)=\langle\psi_0|\hat{O}^\dagger\hat{O}|\psi_0\rangle\sum_n|c_0^n|^2(E_n-E_0)^p\ , \tag{2.16}$$

where all the necessary information to calculate it was obtained earlier when the spectral function was evaluated (poles and intensities).

B. Quantum Monte Carlo technique

The Monte Carlo method is well known in the context of statistical mechanics and condensed-matter physics (for a recent review see Binder and Heermann, 1992). here, we shall briefly describe an application of this general algorithm to the quantum-mechanical many-body problem of interacting electrons on a lattice, working in the grand-canonical ensemble. The basic idea of this approach was presented some time ago by Blankenbecler, Scalapino, and Sugar (1981). Suppose we want to evaluate the expectation value of a physical observable $\hat{O}$, at some finite temperature $T=1/\beta$. If $\hat{H}$ is the Hamiltonian of the model, this expectation value is defined as

$$\langle\hat{O}\rangle=\frac{\mathrm{Tr}(\hat{O}e^{-\beta\hat{H}})}{\mathrm{Tr}(e^{-\beta\hat{H}})}\ , \tag{2.17}$$

where the notation is the standard. From now on, let us concentrate on the particular case of the one-band Hubbard model, which was defined in Eq. (1.3). The Hamiltonian of this model, with the addition of a chemical potential, can be naturally separated into two terms as

$$\begin{aligned}\hat{K}&=-t\sum_{\langle ij\rangle,\sigma}(c_{i\sigma}^\dagger c_{j\sigma}+c_{j\sigma}^\dagger c_{i\sigma})-\mu\sum_i(n_{i\uparrow}+n_{i\downarrow})\ ,\\ \hat{V}&=U\sum_i(n_{i\uparrow}-\tfrac{1}{2})(n_{i\downarrow}-\tfrac{1}{2})\ .\end{aligned} \tag{2.18}$$

Discretizing the inverse temperature interval as $\beta=\Delta\tau L$, where $\Delta\tau$ is a small number and L is the total number of time slices, we can apply the well-known Trotter's formula to rewrite the partition function as

$$Z=\mathrm{Tr}(e^{-\Delta\tau L\hat{H}})\sim\mathrm{Tr}(e^{-\Delta\tau\hat{V}}e^{-\Delta\tau\hat{K}})^L\ , \tag{2.19}$$

where a systematic error of order $(\Delta\tau)^2$ has been introduced, since $[\hat{K},\hat{V}]\neq 0$. In order to integrate out the fermionic fields, the interaction term $\hat{V}$ has to be made quadratic in the fermionic creation and annihilation operators by introducing a decoupling Hubbard-Stratonovich transformation. At this stage, we can select from a wide variety of possibilities to carry out this decoupling, i.e., we can choose continuous or discrete, real or complex fields, belonging to different groups. In particular, and for illustration purposes, here we use a simple transformation using a discrete spinlike field (Hirsch, 1985),

$$e^{-\Delta\tau U(n_{i\uparrow}-1/2)(n_{i\downarrow}-1/2)}=\frac{e^{-\Delta\tau U/4}}{2}\sum_{s_{i,l}=\pm1}e^{-\Delta\tau s_{i,l}\lambda(n_{i\uparrow}-n_{i\downarrow})}\ , \tag{2.20}$$

which is carried out at each lattice site i and for each temperature (or imaginary-time) slice l. The constant λ is defined through the relation $\cosh(\Delta\tau\lambda)=\exp(\Delta\tau U/2)$. Transformation (2.20) reduces the four-fermion self-interaction of the Hubbard model to a quadratic term in the fermions coupled to the new spinlike field $s_{i,l}$. Thus in this formalism the interactions between electrons are mediated by the spin field. Now we can carry out the integration of the fermions. While this is conceptually straightforward and, for a finite lattice of $N\times N$ sites, gives determinants of well-defined matrices, arriving at the actual form of these matrices is somewhat involved and beyond the scope of this review. We shall simply present the result of the integration (more details can be found in Gubernatis *et al.*, 1985 and White, Scalapino, Sugar, Loh, *et al.*, 1989). The partition function can be exactly written as

$$Z=\sum_{\{s_{i,l}=\pm 1\}} \det M^{+}(s)\det M^{-}(s)\ , \tag{2.21}$$

where

$$M^{\sigma}=I+B_L^{\sigma}B_{L-1}^{\sigma}\cdots B_1^{\sigma} \tag{2.22}$$

and

$$B_l^{\pm}=e^{\mp\Delta\tau\nu(l)}e^{-\Delta\tau K}\ . \tag{2.23}$$

I is the unit matrix, $\nu(l)_{ij}=\delta_{ij}s_{i,l}$, and K is the matrix representation of the operator $\hat{K}$. Usually the physical observable $\hat{O}$ can be expressed in terms of Green's functions for the electrons moving in the spin field. Then, expressions similar to Eqs. (2.21)–(2.23) can be derived for Eq. (2.17). Once the partition function is written only in terms of the spin fields, we can use standard Monte Carlo techniques (such as Metropolis or heat bath methods) to perform a simulation of the complicated sums over $s_{i,l}$ that remain to be done. The probability distribution of a given spin configuration is given, in principle, by $(1/Z)\det M^{+}\det M^{-}$ (unless it becomes negative; see the next section).

A simple modification of the Blankenbecler, Scalapino, and Sugar algorithm allows the calculation of ground-state properties in the canonical ensemble, i.e., with a fixed number of electrons. This approach is called Projector Monte Carlo. Consider the ground state $|\psi_0\rangle$ of a system, and denote by $|\phi_0\rangle$ a trial state with a nonzero overlap with the actual ground state. The expectation value of a physical observable $\hat{O}$ can be exactly written as

$$\frac{\langle\psi_0|\hat{O}|\psi_0\rangle}{\langle\psi_0|\psi_0\rangle}=\lim_{\lambda,\lambda'\to\infty}\frac{\langle\phi_0|e^{-\lambda'\hat{H}}\hat{O}e^{-\lambda\hat{H}}|\psi_0\rangle}{\langle\phi_0|e^{-(\lambda'+\lambda)\hat{H}}|\psi_0\rangle}\ . \tag{2.24}$$

The steps necessary to simulate Eq. (2.24) using the Monte Carlo method are very similar to those discussed in deriving Eq. (2.21). First, $\lambda+\lambda'$ is discretized in a finite number of slices; then the Trotter approximation, as well as the Hubbard-Stratonovich decoupling, are used. Fermions are integrated out, and all observables are finally expressed in terms of the spin fields, which are treated using a Metropolis algorithm (for details see White, Scalapino, Sugar, Loh, *et al.*, 1989 and Imada and Hatsugai, 1989). Results obtained using these techniques, as well as other modifications of these methods, will be discussed in several sections of the present review. Finally, it is interesting to notice that there are numerical methods of the Monte Carlo family that are closely related to mean-field approximations to Hubbard-like models. These are the variational Monte Carlo methods, where the Monte Carlo algorithm is used to evaluate expectation values for a variational wave function (which typically satisfies the local constraint of no double occupancy if the large U/t limit is analyzed). As in any other variational approach, the results are sensitive to short-distance correlations, and it is not clear if they are a good test of the long-range-order properties of the system. However, interesting investigations of antiferromagnetism and superconductivity have already been carried out with this technique (Gros, 1988, 1989; Yokoyama and Shiba, 1988; G. J. Chen *et al.*, 1990).

C. Sign problems

For the one-band Hubbard model, the quantum Monte Carlo simulations described earlier can be carried out at half-filling with no difficulty, since the product $\det M^{+}\det M^{-}$ is positive [it can be shown that $\det M^{+}=A\times\det M^{-}$ for any configuration of the Hubbard-Stratonovich spin fields, where A is a positive number (Hirsch, 1985)]. Results at half-filling will be discussed in Sec. III.A. However, in the case of an arbitrary density $\langle n\rangle\neq 1$, this is no longer true for the repulsive Hubbard model (other models like the attractive Hubbard model do not have this problem, and they can be simulated at all densities). Then, the "probability" of a given spin configuration is no longer positive definite. In this situation, to obtain results using this technique, it is convenient to separate the product of the determinants into its absolute value and its sign, i.e., $\det M^{+}\det M^{-}=\mathrm{sgn}\times|\det M^{+}\det M^{-}|$ for each spin configuration. Using this trick, the expectation value of any operator $\hat{O}$ can be written as

$$\langle\hat{O}\rangle=\frac{\langle\langle\hat{O}\ \mathrm{sgn}\rangle\rangle}{\langle\langle\mathrm{sgn}\rangle\rangle}\ , \tag{2.25}$$

where $\langle\langle\cdots\rangle\rangle$ denotes an expectation value obtained using a probability proportional to $|\det M^{+}\det M^{-}|$. Similar tricks can be applied to cases where the determinant becomes complex as it occurs in problems of lattice gauge theory in the context of particle physics (Barbour *et al.*, 1986). Although Eq. (2.25) is an exact identity, in practice the denominator can become very small if the number of spin configurations with positive and negative determinants is similar. Unfortunately, this is the case for the Hubbard model in some regime of couplings and densities, and at low temperatures. For example, in Fig. 11, $\langle\langle\mathrm{sgn}\rangle\rangle$ is shown as a function of the density $\langle n\rangle$,

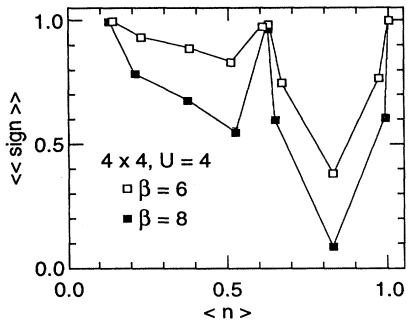

FIG. 11. Mean value of the sign as a function of the density for the one-band Hubbard model on a 4×4 cluster at $U/t=4$. Results for two temperatures are shown (from White, Scalapino, Sugar, Loh *et al.*, 1989).

working at $U/t=4$ and two temperatures, on a 4×4 cluster (from White, Scalapino, Sugar, Loh *et al.*, 1989). The qualitative behavior is clear, i.e., the sign is decreasing rapidly when the temperature is reduced, especially at densities close to half-filling. Similar trends have been observed for larger clusters and couplings. Actually, it has been shown that $\langle\langle \text{sgn} \rangle\rangle$ converges exponentially to zero as the temperature decreases (Hamann and Fahy, 1990; Loh *et al.*, 1990). This effect imposes severe constraints on the temperatures that can be reached using Monte Carlo techniques in simulations of the Hubbard model away from half-filling. This is the well-known "sign problem."

How does this complication affect the accuracy of the results? In Fig. 12, the expectation value of the energy $E=\langle \hat{H} \rangle$ for the Hubbard model is plotted as a function of temperature T, on a 4×4 cluster working at $U/t=4$ and density $\langle n \rangle=0.875$ (from Moreo, 1993b), using the same number of Monte Carlo sweeps at all temperatures.

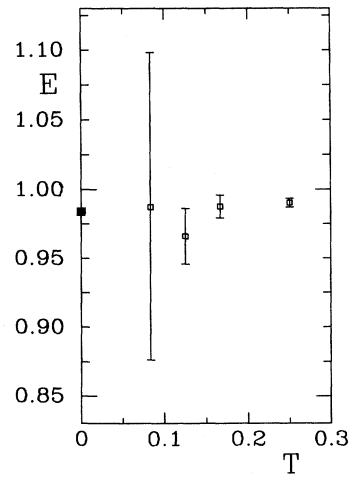

FIG. 12. Quantum Monte Carlo mean value of the energy E for the one-band Hubbard model as a function of temperature T, on a 4×4 cluster working at $U/t=4$ and density $\langle n \rangle=0.875$ (from Moreo, 1993a). The square at $T=0$ is obtained with exact diagonalization techniques.

note the rapid increase of the error bars as the temperature decreases. For comparison, the exact result at zero temperature for the case of two holes on a 4×4 cluster is also shown (Dagotto, Moreo, Ortolani, Poilblanc, and Riera, 1992). It would have been somewhat difficult to accurately obtain this zero-temperature energy from the Monte Carlo data alone. Of course, increasing considerably the number of sweeps in Fig. 12 and reducing $\Delta\tau$ will obtain better results; thus this figure serves simply as a rough illustration of the trends in the sign problem. Actually, with some effort, the energy of the ground state can be obtained with small error bars even away from half-filling (remember also that the Monte Carlo results need additional corrections to take into account the systematic $\Delta\tau$ errors). However, results for other quantities like spin-spin correlations show a similar qualitative behavior, but typically with larger error bars than in the case of the energy; and it is difficult to improve these results even with long Monte Carlo runs.

The study of the sign problem, and the possibility of finding a cure for it, is a very important subject in the context of simulations of correlated electrons. Some time ago, considerable excitement was generated by a paper by Sorella *et al.* (1988, 1989) in which it was claimed that using a projector Monte Carlo algorithm, and an appropriate trial wave function $|\phi_0\rangle$, would result in the mean value of the sign converging to a nonzero constant as $\beta\rightarrow\infty$. In such a case, it was argued, some physical quantities could be calculated simply by neglecting the signs of the determinants. Unfortunately, these conclusions were somewhat premature, as discussed later by Loh *et al.* (1990) and Sorella (1991), who showed that the expectation value of the sign actually decreases exponentially with β. Then, neglecting the signs of the determinants leads to an uncontrolled approximation. Loh *et al.* (1990) showed that some physical quantities related to superconducting correlations present a *qualitatively* different behavior with and without the signs included in the averages.

It is also important to clarify that the sign problem is caused not only by the signs that appear due to fermionic anticommutations. For example, consider the case of the spin-$\frac{1}{2}$ Heisenberg model with nearest- and next-nearest-neighbor interactions, which can be simulated using random-walk Monte Carlo methods (Barnes, 1991; see also Dagotto, 1991). In this technique, matrix elements of the interactions are used as probability in the Monte Carlo algorithm. Unfortunately, it is not possible to write these matrix elements in a positive-definite way for an arbitrary value of the couplings in the Hamiltonian. Then, the sign problem is a widely extended plague that affects several areas of quantum simulations, not only strongly correlated electrons. The study of the sign problem continues attracting considerable attention. Some recent attempts to fight the problem can be found in Assaad and De Forcrand, 1990; Batrouni and Scalettar, 1990; Dagotto, Moreo, Sugar, and Toussaint, 1990; Hamann and Fahy, 1990; Fahy and Hamann, 1991;

Furukawa and Imada, 1991a; Zhang and Kalos, 1991; Muramatsu, Zumbach, and Zotos, 1993; Vekic and White, 1993; and references therein.

Finally, we shall briefly describe a recently proposed technique for alleviating the sign problem. The method is based on the possibility that the operators used to describe, for example, hole excitations in Hubbard and t-J models are "poor," in the sense that they are bad approximations to the actual "dressed" quasiparticle operators that create real holes in these models. Having proper quasiparticle operators alleviates the sign problem, since in projector or Green's-function Monte Carlo methods an initial state is selected upon which $e^{-\Delta\tau\hat{H}}$ acts repeatedly until convergence is reached ($\Delta\tau$ being a small number); thus if the initial Ansatz is very good, the sign problem may destroy the statistics only after a good convergence is observed (at least in the ground-state energy). A method to systematically construct better operators was discussed by Dagotto and Schrieffer (1991), Boninsegni and Manousakis (1991), and Furukawa and Imada (1991b), and implemented by Boninsegni and Manousakis (1991, 1993) and Furukawa and Imada (1991b), with good results for the cases of one and two holes in the t-J model, and the weak-coupling Hubbard model [Monte Carlo results for one hole were also obtained by Barnes and Kovarik (1993)]. In this technique, the information gathered using Lanczos methods is very useful for guiding the construction of the variational states.

We should also like to mention a class of numerical work that is closely allied with traditional diagrammatic calculations and so takes a rather different approach than the Monte Carlo and exact diagonalization methods on which we shall focus. Pioneered by Bickers, Scalapino, and White (1989) and further developed by Serene and Hess (1991), these techniques rely on a numerical solution of self-consistent equations for the one- and two-particle interacting electron Green's functions and interaction vertices. These approaches are able to study the competition between particle-hole and particle-particle instabilities and to estimate transition temperatures. Unfortunately, an adequate treatment of this technique is beyond the scope of this review.

III. CORRELATED ELECTRONS AT LOW HOLE DOPING

A. Results at half-filling

As explained before, in the one-band Hubbard model at half-filling $\langle n \rangle = 1$, particle-hole symmetry arguments can be used (Hirsch, 1985) to show that $\det M^+ = A \times \det M^-$ ($A > 0$) for any configuration of the Hubbard-Stratonovich spin field in the quantum Monte Carlo [see Eq. (2.21)]. Then, the product of determinants cannot be negative, and a simulation in which the probability of the spin configuration $\{s_{il}\}$ is proportional to $\det M^+ \det M^-$ can proceed without problems. For this particular density, strong numerical evidence suggests that the ground state has long-range spin order for any nonzero value of the coupling. For example, in the strong-coupling limit $U/t \gg 1$, the Hubbard model is equivalent to the spin-$\frac{1}{2}$ Heisenberg model defined by the Hamiltonian

$$H = J \sum_{\langle ij \rangle} (\mathbf{S}_i \cdot \mathbf{S}_j - \tfrac{1}{4}) , \tag{3.1}$$

where $J = 4t^2/U$, and the rest of the notation is standard. This model has been extensively studied using several different analytical and numerical methods. According to these results, the ground state has antiferromagnetic long-range order at zero temperature (for details see Oitmaa and Betts, 1978; Reger and Young, 1988; Chakravarty, 1990; Barnes, 1991; Manousakis, 1991; and references therein). Exotic scenarios like those described by the resonant valence bond (RVB) states or flux phases do not seem to be realized in this model [at least from the point of view of computational studies; the flux phases do not seem stable in the t-J model either (Bonesteel and Wilkins, 1991; Dagotto, Moreo, Ortolani, Poilblanc, and Riera, 1992), and thus they will not be addressed in this review]. Even with the inclusion of next-nearest-neighbor spin-spin interactions, no indications of such states have been found numerically (Dagotto, 1991; Poilblanc *et al.*, 1991; and references therein).

At small and intermediate coupling U/t in the one-band Hubbard model, quantum Monte Carlo (QMC) simulations and Lanczos results suggest that antiferromagnetic spin order is still present in the ground state, even though double occupancy is allowed. Among the first studies to show these results were those of Hirsch and Tang (1989) and White, Scalapino, Sugar, Loh, *et al.* (1989). The actual value of the local moment decreases from $\frac{1}{2}$ as the coupling is reduced. This state is usually called spin-density wave (SDW) and is analytically connected to the Néel-like ground state at large U/t. As a recent example of these types of studies, and also to show a case in which Lanczos and QMC techniques give results in excellent agreement, we show in Fig. 13 the exact spin-spin correlation function defined as $C(r) = C(i-j) = \frac{1}{4}(-1)^{i_x+i_y+j_x+j_y} \langle (n_{i\uparrow} - n_{i\downarrow})(n_{j\uparrow} - n_{j\downarrow}) \rangle$ in the ground state of the Hubbard model as a function of distance on a 4×4 cluster and at $U/t = 4$ (we used the notation $i = (i_x, i_y)$, and the sign was introduced to make the correlations positive if staggered order exists). This result was obtained with the Lanczos technique (Fano, Ortolani, and Parola, 1992). The X point corresponds to a site (2,0) lattice spacings from the origin, while M is (2,2) from the origin. Indications of long-range order are clear in this figure. For comparison, we also include in Fig. 13 results obtained using quantum Monte Carlo techniques applied to the same cluster. It is interesting to note the convergence of the QMC results to the Lanczos results as the temperature is reduced. Even working at high temperatures, it would have been possible to infer the tendency towards spin long-range order from the re-

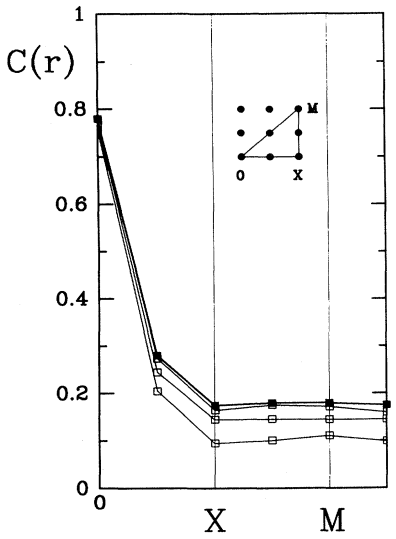

FIG. 13. Spin-spin correlation $C(r)$, defined in the text, corresponding to the one-band Hubbard model for different values of the distance r on a 4×4 cluster, at $U/t=4$. The solid squares are exact results at zero temperature obtained using the Lanczos technique (Fano, Ortolani, and Parola, 1992). The open squares are results obtained with the quantum Monte Carlo approach (Moreo, 1993a) at different temperatures (starting from below $\beta=4$, 6, and 12).

sults of this small cluster. This effect may be caused by the rapid growth of the spin-correlation length ξ, when the temperature is decreased, since in the regime where ξ is larger than the lattice size, the results are qualitatively similar to those at zero temperature. This example shows that convergence to zero-temperature results for a *finite* cluster can be reached at relatively high temperatures, depending on the physics of the problem.

In Fig. 14(a), results for the spin-spin correlations on larger clusters obtained using QMC are shown (Moreo, 1993b). The presence of spin long-range order is clear in these studies, and the finite-size effects are very small. Temperature effects do not alter significantly the qualitative behavior of the correlations. Figure 14(b) shows an alternative method to search for long-range order. $S(\pi,\pi)$ is the structure factor at momentum $\mathbf{Q}=(\pi,\pi)$, which corresponds to the sum of the correlation $C(i-j)$ over all distances. If there is long-range order, this quantity has to increase and diverge with the size of the cluster. Such an effect is clearly observed in Fig. 14(b) at $U/t=4$, showing the presence of antiferromagnetic spin order in this model. Actually, spin-wave theory makes specific predictions for the finite-size corrections to $S(\pi,\pi)$. Corrections of these forms have been observed by quantum Monte Carlo and Lanczos methods, clearly showing that the lattice is ordered in the thermodynamic limit. For what value of U/t does long-range order exist? Hirsch and Tang (1989) showed numerically that spin-density-wave order exists even for U/t as small as 2, and it is widely believed that the ground state is ordered for all nonzero values of U/t.

These results obtained at half-filling can be described intuitively by a mean-field approximation to the one-band Hubbard model (Schrieffer, Wen, and Zhang, 1989). These types of approximations are self-consistent, and it is difficult to judge their accuracy unless contrasted against results obtained using unbiased techniques, like the numerical methods described in this section. For the particular case of half-filling, the agreement between numerics and mean-field results is very good, and thus the analytic approximation seems to have captured the important physics of the problem. Let us write the number operator at a given site i as $n_{i\sigma}=\langle n_{i\sigma}\rangle+(n_{i\sigma}-\langle n_{i\sigma}\rangle)$, where $\langle n_{i\sigma}\rangle$ is the expectation value in the ground state, and the second term will be assumed to be "small." Within this approximation, the on-site Coulombic interaction becomes

$$n_{i\uparrow}n_{i\downarrow}\approx-\langle n_{i\uparrow}\rangle\langle n_{i\downarrow}\rangle+n_{i\uparrow}\langle n_{i\downarrow}\rangle+n_{i\downarrow}\langle n_{i\uparrow}\rangle\ . \quad (3.2)$$

As an ansatz for the mean value of the number operators, we select a SDW state; i.e., we choose

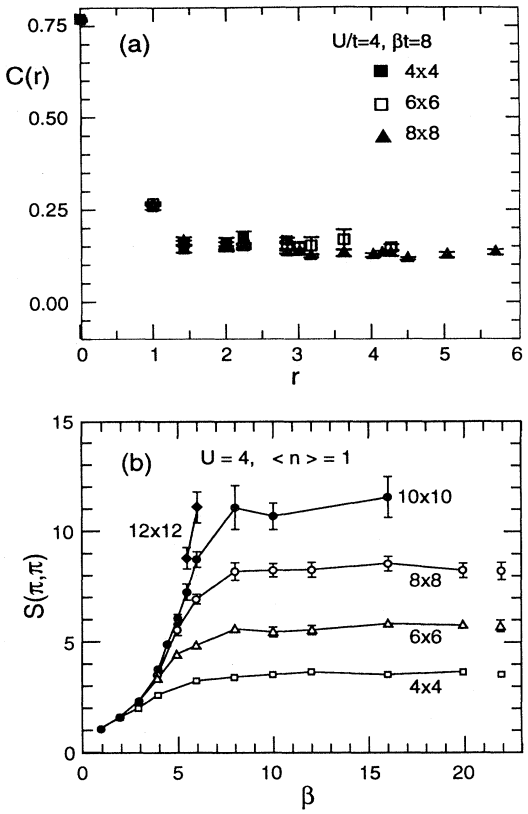

FIG. 14. (a) Spin-spin correlation $C(r)$ for the one-band Hubbard model at half-filling using quantum Monte Carlo techniques at $U/t=4$, $\beta=8/t$, and several cluster sizes (from Moreo, 1993b; see also Moreo, 1992b); (b) antiferromagnetic structure factor $S(\pi,\pi)$ as a function of β (inverse temperature) for a variety of lattice sizes. These results were obtained with a quantum Monte Carlo algorithm (White, Scalapino, Sugar, Loh, *et al.*, 1989).

$\langle n_{i\uparrow}\rangle = \frac{1}{2}[1+S(-1)^{|i|}]$ and $\langle n_{i\downarrow}\rangle = \frac{1}{2}[1-S(-1)^{|i|}]$, where S is a variational parameter to be fixed by minimization of the mean-field energy, and $|i| = i_x + i_y$, where $i=(i_x,i_y)$. In the limit $U/t=0$, the parameter S vanishes, and we correctly reproduce the result that, at any site, $\langle n_{i\uparrow}\rangle = \langle n_{i\downarrow}\rangle = \frac{1}{2}$ if the particles are noninteracting. At large U/t, S converges to 1 and the Ansatz becomes a spin staggered Néel state. This state is a good qualitative approximation to the ground state of the Heisenberg model (which is the effective model at large Coulombic repulsion and half-filling), although spin fluctuations are not included. Then, both the limits of large and small U/t are properly described by the mean-field state. To obtain results at intermediate values of the coupling, we have to solve the mean-field Hamiltonian, which is now quadratic in the fermionic fields. After some algebra and working in momentum space using $c_{i\sigma} = (1/\sqrt{N})\sum_{\mathbf{p}} e^{-i\mathbf{p}\cdot i} c_{\mathbf{p}\sigma}$, we arrive at the Hamiltonian

$$H_{MF} = \sum_{\mathbf{p}\sigma} \epsilon_{\mathbf{p}} c^{\dagger}_{\mathbf{p}\sigma} c_{\mathbf{p}\sigma} - \frac{U}{2}\sum_{\mathbf{p}} S[c^{\dagger}_{\mathbf{p}+\mathbf{Q}\uparrow} c_{\mathbf{p}\uparrow} - c^{\dagger}_{\mathbf{p}+\mathbf{Q}\downarrow} c_{\mathbf{p}\downarrow}] + \frac{U}{4} S^2 N \ , \tag{3.3}$$

where $\epsilon_{\mathbf{p}} = -2t(\cos p_x + \cos p_y)$, $\mathbf{Q}=(\pi,\pi)$, and the chemical potential μ is zero at half-filling if the Coulombic interaction is written in a particle-hole symmetric form as in Eq. (1.3). Note that in the mean-field Hamiltonian (3.3) the spin index is diagonal, and the operators with momentum $\mathbf{p}$ only interact with those of momentum $\mathbf{p}+\mathbf{Q}$ (since $\mathbf{p}+2\mathbf{Q}=\mathbf{p}$). Thus the diagonalization of H_{MF} amounts to solving just a 2×2 matrix problem for each spin and momentum (restricted to only half the Brillouin zone). The eigenvectors can be easily obtained following steps very similar to those used in textbooks to study the BCS model (i.e., attractive Hubbard model). They are given by

$$\begin{aligned} \gamma^{(+)}_{\mathbf{p}\uparrow} &= u_{\mathbf{p}} c_{\mathbf{p}\uparrow} - v_{\mathbf{p}} c_{\mathbf{p}+\mathbf{Q}\uparrow} \ , \\ \gamma^{(+)}_{\mathbf{p}\downarrow} &= u_{\mathbf{p}} c_{\mathbf{p}\downarrow} + v_{\mathbf{p}} c_{\mathbf{p}+\mathbf{Q}\downarrow} \ , \\ \gamma^{(-)}_{\mathbf{p}\uparrow} &= v_{\mathbf{p}} c_{\mathbf{p}\uparrow} + u_{\mathbf{p}} c_{\mathbf{p}+\mathbf{Q}\uparrow} \ , \\ \gamma^{(-)}_{\mathbf{p}\downarrow} &= v_{\mathbf{p}} c_{\mathbf{p}\downarrow} - u_{\mathbf{p}} c_{\mathbf{p}+\mathbf{Q}\downarrow} \ , \end{aligned} \tag{3.4}$$

where the upper index indicates that there are two eigenvectors per spin and momentum $\mathbf{p}$ in the reduced Brillouin zone. $\gamma^{(+)}_{\mathbf{p}\sigma}$ has eigenvalue $\lambda_{\mathbf{p}} = E_{\mathbf{p}}$, while for $\gamma^{(-)}_{\mathbf{p}\sigma}$ it is $\lambda_{\mathbf{p}} = -E_{\mathbf{p}}$, where $E_{\mathbf{p}} = \sqrt{\epsilon^2_{\mathbf{p}} + \Delta^2_{\mathrm{SDW}}}$, and the spin-density-wave gap is given by $\Delta^2_{\mathrm{SDW}} = U^2 S^2/4$. The functions used in the definition of the eigenvectors are

$$u^2_{\mathbf{p}} = \frac{1}{2}\left[1+\frac{\epsilon_{\mathbf{p}}}{E_{\mathbf{p}}}\right], \quad v^2_{\mathbf{p}} = \frac{1}{2}\left[1-\frac{\epsilon_{\mathbf{p}}}{E_{\mathbf{p}}}\right] . \tag{3.5}$$

The self-consistent equation for the mean-field parameter S is

$$\frac{1}{U} = \frac{1}{N}\sum_{|\mathbf{p}|\le|\mathbf{p}_F|} \frac{1}{\sqrt{\epsilon^2_{\mathbf{p}} + \Delta^2_{\mathrm{SDW}}}} \ , \tag{3.6}$$

where the sum over momenta is restricted to half the Brillouin zone ($\mathbf{p}_F$ is the momentum at the noninteracting Fermi surface and at half-filling). In this mean-field approximation, the ground state is obtained by populating all the "quasiparticle" states with negative energy, as shown in Fig. 15(a); i.e.,

$$|\phi_{\mathrm{MF}}\rangle = \Pi_{|\mathbf{p}|\le|\mathbf{p}_F|} (\gamma^{(-)}_{\mathbf{p}\uparrow})^{\dagger} (\gamma^{(-)}_{\mathbf{p}\downarrow})^{\dagger} |0\rangle \ , \tag{3.7}$$

where $|0\rangle$ is the empty state. Solving gap equation (3.6), we obtain the result shown in Fig. 15(b). The gap is finite for all nonzero values of U/t. At large coupling, it grows proportional to U/t, while in the very weak coupling region $U/t<1$, it follows an exponential behavior $\Delta_{\mathrm{SDW}} \sim e^{-\pi/\sqrt{U}}$. Then, in this approximation, spin-density-wave order exists for *all* values of the coupling, in qualitative agreement with the numerical studies (for additional details, see Schrieffer, Wen, and Zhang, 1989). Note that in two-dimensional problems, the Mermin-Wagner theorem prevents the existence of long-range order at finite temperature if the spontaneously broken symmetry is continuous. Actually, the spin-correlation length becomes infinite only at zero temperature. In the actual cuprate superconductors, a small residual interaction in the c direction (i.e., between CuO_2 planes) induces a *finite* critical Néel temperature, as was shown in the phase diagrams of several compounds (Figs. 2, 4, 6). Spin long-range order has been found numerically not only in the one-band Hubbard model but also in the three-band case (Scalettar, 1989; Dopf, Muramatsu, and Hanke, 1990; Scalettar *et al.*, 1991). Calculations similar to those described here but made explicitly for the YBCO material have been reported by Furukawa and Imada (1992).

It is believed that the "physics" of the half-filled limit

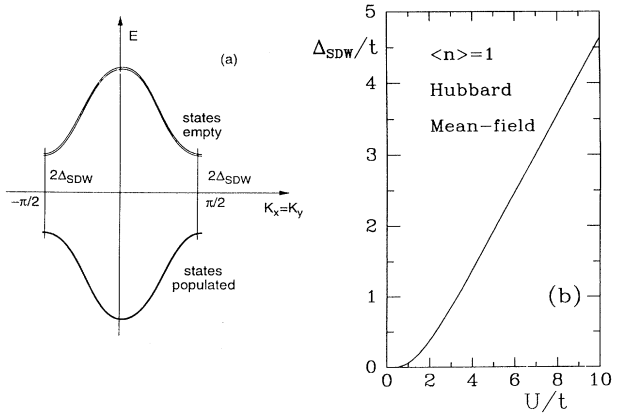

FIG. 15. (a) Spectrum of quasiparticles in the mean-field approximation used to describe the SDW state at half-filling (see Schrieffer, Wen, and Zhang, 1988). The lower band of negative energy states is populated, while the upper band is empty. (b) Mean-field SDW gap as a function of the coupling U/t (provided by A. Nazarenko, 1993, unpublished).

is mostly understood in models of correlated electrons with repulsive interactions. Then, the bulk of this review is devoted to the more challenging and interesting, but considerably less understood, situation where carriers are added to the planes.

B. Properties of holes in antiferromagnets

In this section we describe the present status of studies of a few holes in an antiferromagnetic background. These studies were carried out mainly using numerical methods, but also with the help of some rough analytical techniques, as shown below. The models we shall use are the t-J and Hubbard models. In the early days of these studies, it was suggested that the effect of doping could be mimicked by adding frustration to the spin-$\frac{1}{2}$ Heisenberg model (Inui, Doniach, and Gabay, 1988). This issue was studied by Nori, Gagliano, and Bacci (1992); Bacci, Gagliano, and Nori (1991); and Nori and Zimanyi (1991). These authors found that the effects of doping and frustration are quite different in models of correlated electrons. Therefore, the original proposal mapping doping to frustration has been discarded. Our investigations here will be carried out directly using Hubbard-like models.

1. String picture

To gain some intuition on the behavior of holes doped into an antiferromagnet, we shall start with the study of just one hole. In spite of its apparent simplicity, this problem is highly nontrivial, and a considerable effort has been devoted to its analysis. The physics of a hole arises from a competition between the superexchange energy lost near the hole and its kinetic energy. It is reasonable to expect that the antiferromagnetic order parameter will reduce its magnitude near the hole, increasing the mobility of the carrier inside such a spin bag (Kampf and Schrieffer, 1990). In the regime of strong coupling, where double occupancy is suppressed, an interesting picture emerges. Consider a hole added to an antiferromagnet at a given site. As this initial state evolves in time, the hole can move some distance l away from its original position by the action of the hopping term. However, in such excursions the spins along the path of the hole are incorrectly aligned with respect to the Néel background, as shown in Fig. 16. Then, if the hole is moved a distance l from the origin, the energy spent is proportional to l; thus over the hole acts an effective "confining" linear potential that tends to localize it. Such a confinement is not strict. For example, complicated paths have been found that avoid the problem of having an energy that grows with l and thus give mobility to the hole (Trugman, 1988); but, in general, the effects of this so-called string linear potential strongly influence the physics of holes in antiferromagnets.

More formally, let us consider the problem of one hole

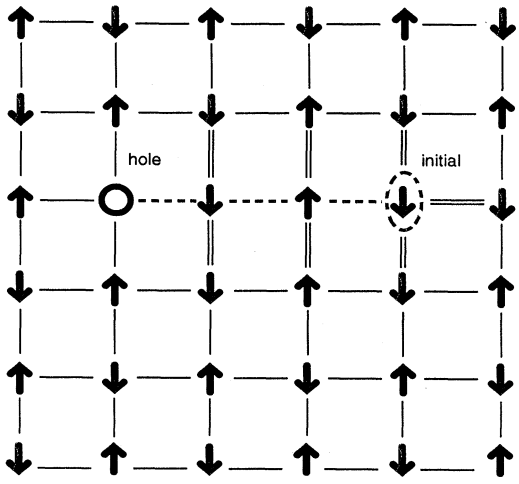

FIG. 16. Example of a hole moving in a Néel background to illustrate the concept of strings: "initial" denotes the site where the hole is initially injected; the circle is the hole in its actual position after the hopping term acts 3 times; and the dashed line is the path followed by the hole. The double lines indicate links that are "ferromagnetic," i.e., where magnetic energy is paid. The number of ferromagnetic links grows like the length of the path.

moving in a staggered spin background (Shraiman and Siggia, 1988a, and references therein; see also Brinkman and Rice, 1970; Eder, Becker, and Stephan, 1990; Prelovšek, Sega, and Bonča, 1990; and Eder, 1992). To simplify the problem, we take into account only the Ising part of the spin interaction, i.e., we consider the so-called t-J_z Hamiltonian defined as

$$H = J_z \sum_{\langle ij \rangle} S_i^z S_j^z - t \sum_{\langle ij \rangle, \sigma} (\bar{c}_{i\sigma}^{\dagger} \bar{c}_{j\sigma} + \bar{c}_{j\sigma}^{\dagger} \bar{c}_{i\sigma}) , \tag{3.8}$$

where no transverse spin fluctuations are included, and $\bar{c}_{j\sigma}^{\dagger} = c_{j\sigma}(1 - n_{j-\sigma})$. The rest of the notation was already introduced in the definition of the t-J model [Eq. (1.2)]. The ground state in the absence of holes is a perfect Néel state with energy $E_{0h} = -\frac{1}{4} J_z 2N$, where $2N$ is the number of links of a two-dimensional square lattice with N sites. The state obtained by removing one arbitrary spin from the cluster will be denoted as $|0\rangle$. This state is like a strong of zero length; i.e., all the links, but the four around the hole, are antiferromagnetic. Applying $H' = H - E_{0h}$ (with $t = 1$) on $|0\rangle$, we obtain

$$H'|0\rangle = J_z|0\rangle - 2|1\rangle . \tag{3.9}$$

The first term appears due to the four antiferromagnetic links that were missing once the hole was created. The new state $|1\rangle$ is defined as $|1\rangle = \frac{1}{2} \sum_{\tau_1} |\tau_1\rangle$, where $\{\tau_1\}$ denote unit vectors in the directions $\pm\mathbf{x}, \pm\mathbf{y}$. The state $|\tau_1\rangle$ represents a "string" of length 1, which has been created from the state without strings by moving the hole one lattice spacing in the direction τ_1. In general, we can define states $|\tau_1, \tau_2, \tau_3, \ldots, \tau_l\rangle$, which are obtained after l

applications of the hopping term starting from the no string state $|0\rangle$. The hole position is obtained by adding as vectors $\tau_1+\tau_2+\cdots+\tau_l$. Now, let us apply the Hamiltonian to $|1\rangle$. The result is

$$H'|1\rangle=\frac{5}{2}J_z|1\rangle-2|0\rangle-\sqrt{3}|2\rangle \ . \tag{3.10}$$

The diagonal term arises from a simple calculation of the energy of a state with a string of length 1 (there are four missing links surrounding the hole, plus three links that have become ferromagnetic due to the movement of the hole one lattice spacing). The second term corresponds to moving the hole back to the origin. The new state in the third term is defined as

$$|2\rangle=\frac{1}{2\sqrt{3}}\sum_{\tau_1,\tau_2\neq-\tau_1}|\tau_1,\tau_2\rangle \ ,$$

where the sum represents the 12 states that can be obtained by moving a hole two lattice spacings from the origin ($2\sqrt{3}$ is its normalization).

These ideas can be generalized to l applications of the hopping term by defining an orthonormal "string" basis as

$$|l\rangle=\frac{\sqrt{3}}{2}(h^\dagger)^l|0\rangle \ , \tag{3.11}$$

where the operator $h^\dagger$, acting over a state with a hole at a given position, creates *three* new states where the hole has moved one more lattice spacing (at least for l larger than one lattice spacing; Shraiman and Siggia, 1988a). More formally,

$$h^\dagger|\tau_1\tau_2\cdots\tau_l\rangle=\frac{1}{\sqrt{3}}\sum_{\tau_{l+1}\neq-\tau_l}|\tau_1\tau_2\cdots\tau_l\tau_{l+1}\rangle \ ,$$

where $\sqrt{3}$ is the normalization of the three newly created states. On the other hand, the application of h retraces the path of the hole in one lattice spacing. It can be shown that the hopping term in the original Hamiltonian is equal to $\sqrt{3}(h+h^\dagger)$, and that $hh^\dagger=1$. Then,

$$H'=J_z(\tfrac{3}{2}+l)|l\rangle-\sqrt{3}(|l-1\rangle+|l+1\rangle) \ , \tag{3.12}$$

which is valid for $l\geq 2$ (note that some paths are neglected in this approximation; i.e., we are implicitly working on a Bethe lattice). This problem can be solved numerically with great accuracy. According to Shraiman and Siggia (1988a), the ground-state energy of H' is $e_{1h}=-2\sqrt{3}+2.74J_z^{2/3}$, which is very similar to the result obtained numerically in the fully interacting problem on finite clusters, as we shall show in Sec. III.B.2. Equation (3.12) corresponds to a discretized version of the problem of a Schrödinger particle in a linear potential, which in the continuum limit becomes

$$H'|l\rangle=\left[-a^2\sqrt{3}t\frac{d^2}{dl^2}+J_z\frac{l}{a}\right]|l\rangle \ , \tag{3.13}$$

where a is the lattice spacing, and a constant energy term has been omitted; to derive Eq. (3.13), it is useful to formally expand in powers of the lattice spacing, which is achieved using

$$|l+1\rangle=|l\rangle+a\frac{d}{dl}|l\rangle+a^2\frac{d^2}{dl}|l\rangle+\cdots \ .$$

This problem can be solved exactly, and the result is expressed in terms of Airy function eigenvalues. Actually, through the change of variables $l/a=(J_z/t)^{-1/3}x$ (x is dimensionless), the coupling dependence can be extracted explicitly, and Eq. (3.13) can be written as

$$H'|l\rangle=t(J_z/t)^{2/3}\left[-\sqrt{3}\frac{d^2}{dx^2}+x\right]|l\rangle \ . \tag{3.14}$$

This result clearly shows that the energy levels of a hole in a Néel background without spin fluctuations behaves as $(J_z/t)^{2/3}$. This characteristic dependence is not restricted to the t-J_z model; it is also found (below) in numerical studies of the t-J model that take into account all the hole paths, and the transverse spin fluctuations. Thus the string description of holes in antiferromagnets seems to have captured many of the important features of this complicated problem.

Finally, by dimensional analysis we can estimate the characteristic "size" of the hole ground-state wave function in real space. Suppose this wave function decays at large distances as $\exp(-l^2/L^2)$, where L is the typical scale we are looking for (the results below are independent of the actual functional form of the wave function). Changing variables in the exponent as before, we obtain $(l/L)^2=[(ax)/L]^2(t/J_z)^{2/3}$. In the dimensionless variable x, the size of the wave function is also a dimensionless number b, and thus we conclude that $(a/L)^2(t/J_z)^{2/3}=b^{-2}$, which implies $L/a\sim(t/J_z)^{1/3}$. Thus the hole is able to explore a larger lattice when J_z is reduced, which is reasonable, since the attractive potential is weaker. This also tells us that finite cluster calculations will have stronger finite-size effects as the superexchange coupling is reduced.

2. Energy and momentum of a hole

Let us now consider numerical results for the actual t-J model in two dimensions, obtained without the approximations employed in the string picture. The energy of one hole in the t-J model, e_{1h}, measured with respect to the energy of the undoped system, is shown in Fig. 17. This result was obtained using a 4×4 cluster and exact diagonalization techniques in the subspace of one hole. In the same figure, we also show the energy of one hole in the t-J_z model [defined in Eq. (3.8)] on an 8×8 cluster (Barnes *et al.*, 1989). For this particular case in which the transverse spin fluctuations are switched off, and if only one hole is studied, it can be shown, using the guided random-walk approach developed by Barnes and

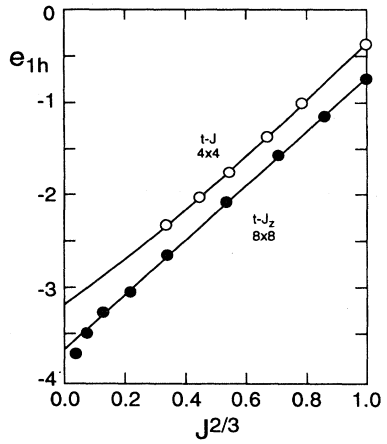

FIG. 17. Energy of one hole with respect to the undoped system e_{1h}, as a function of the coupling J at $t=1$. Results are shown for the t-J model on a 4×4 cluster (from Dagotto *et al.*, 1990b), and for the t-J_z model on a 8×8 cluster (from Barnes *et al.*, 1989).

Daniell (1988), that there are no sign problems. Thus the study of one hole in the t-J_z model can be carried out on relatively large clusters.[2] Figure 17 implies that the energy of one hole is proportional to $J_z^{2/3}$ with high accuracy. Actually, the best Monte Carlo fit $e_{1h}/t = -3.66+2.96(J_z/t)^{0.655}$ is in excellent agreement with the string picture explained previously. More recently, the most accurate results available for the one hole energy in the t-J_z model have been obtained with the "truncation" Lanczos algorithm described in Sec. II.A (Dagotto and Riera, 1993). The reported result is $e_{1h}=-3.620+2.924(J_z/t)^{0.666}$, obtained using clusters with up to 50 sites and five-digit-accuracy ground-state energies. The string picture is clearly very robust for the t-J_z model.

However, in the t-J model it is not obvious that the string picture should work. In principle, the spin fluctuations could "cut" the strings, restoring the Néel spin order. For some time it was assumed that this formalism was not suitable for the more realistic t-J model. However, numerical results on small clusters showed that the ground-state energy of one hole in the interval $0.2\le J/t\le 1.0$ could be fit very accurately as $e_{1h}/t=-3.17+2.83(J/t)^{0.73}$, which had an exponent close to the $\frac{2}{3}$ power law. It is possible that in some region of parameter space, the string typical time scale could be much faster than that of the spin fluctuations, and thus the strings could not be easily erased (for a discussion see Dagotto, Joynt, *et al.*, 1990 and Dagotto, Moreo, Joynt, *et al.*, 1990). In other words, the hole might "emit" a string and retrace it back in a time proportional to $1/t$, while the Heisenberg term would need a $1/J$ time to cut the string. Similar conclusions can be obtained by studying excited states of the hole through the dynamical spectral function, as shown in Sec. III.B.4. Then, the string picture seems to work even in the presence of spin fluctuations.

It is interesting to note that for the t-J model the momentum of the hole ground state seems to be $\mathbf{p}=(\pi/2,\pi/2)$. The evidence for this result comes from a combination of spin-wave, variational, and numerical methods carried out by several different groups (Schmitt-Rink, Varma, and Ruckenstein, 1988; Shraiman and Siggia, 1988a; Trugman, 1988; Dagotto, Moreo, and Barnes, 1989; Sachdev, 1989; Poilblanc, Schulz, and Ziman, 1992; and references therein). These results are not surprising, since, in the one-band Hubbard model at $U/t=0$, the Fermi surface is defined by the equation $\cos p_x+\cos p_y=0$; thus $\mathbf{p}=(\pi/2,\pi/2)$ belongs to this surface. In addition, we expect a smooth connection between weak and strong coupling for one hole. Although for a nonzero coupling there is no symmetry argument requiring that all points on the original Fermi surface remain degenerate, it is reasonable to expect that it is one of those points that will be emptied upon doping of a hole. For the t-J model the selected momentum seems to be $\mathbf{p}=(\pi/2,\pi/2)$. However, note that the states with momentum $\mathbf{p}=(0,\pi),(\pi,0)$ are very close in energy (as discussed below); thus small perturbations (like a t' hopping at a distance of two lattice spacings) may change the hole momentum (see Gagliano, Bacci, and Dagotto, 1990). The study of this near degeneracy deserves more attention. Actually, recent analysis by Dagotto, Nazarenko, and Boninsegni (1994) has shown that the small energy difference between $\mathbf{p}=(0,\pi)$ and $(\pi/2,\pi/2)$ may explain the anomalous behavior of the Hall coefficient in the cuprates, as well as the presence of a large Fermi surface.

For the particular case of one hole in an antiferromagnet, an analytical approach has been developed that gives results in good agreement with the exact diagonalization predictions. The basic idea was introduced by Schmitt-Rink, Varma, and Ruckenstein (1988) and is based on (i) the analysis of the Heisenberg term of the t-J Hamiltonian using the Holstein-Primakoff transformation and the $1/S$ expansion; and on (ii) the replacement of the fermionic operators by the composition of spin-wave and spinless hole operators. The approach was used by Kane, Lee, and Read (1989) in the "dominant pole approximation" to study the single-particle Green's function of one hole, assuming that the weight beyond the first pole was incoherent. This additional approximation may be questionable, since the arguments based on the string picture suggest the presence of sharp peaks at finite frequencies related to the excited states of a particle moving in a linear confining potential. More recently, Marsiglio *et al.* (1991), Martinez and Horsch (1991), and Liu and

[2]Unfortunately, the occurrence of any finite transverse coupling or the addition of more holes induces matrix elements that can become negative. Thus this Monte Carlo approach cannot be applied to more realistic cases without finding sign problems.

Manousakis (1991) have studied the self-consistent Born approximation to this reformulated problem (see also Mattis, Dzierzawa, and Zotos, 1990 and Mattis and Chen, 1991). This is equivalent to the rainbow approximation for the holon propagator, where the spinon lines are noncrossing. A remarkable agreement with the exact diagonalization results was found for small J/t. The inclusion of vertex corrections does not change the zero-order results appreciably for the t-J model at small J/t (Liu and Manousakis, 1991; Martinez and Horsch, 1991). Unfortunately, an extension of this approach to a finite density of holes is difficult.

What is the shape of the hole ground-state wave function in real space? Hartree-Fock calculations in the context of the spin-bag approach suggest that the hole ground state has a cigarlike shape (Su, 1988), elongated along a diagonal of the lattice (see also Lorenzana *et al.*, 1993). This result was also numerically observed using Lanczos techniques (Dagotto, Moreo, and Barnes, 1989), showing that this peculiar shape is a consequence of the finite momentum $\mathbf{p}=(\pi/2,\pi/2)$ along the lattice diagonal. The size of this "spin polaron" is proportional to $1/J^{1/3}$ (Barnes *et al.*, 1989), in agreement with the string picture, and thus it increases as J/t decreases. This explains the observed feature that finite-size effects become more severe on finite clusters as the superexchange is reduced. Inside the spin polaron the antiferromagnetic order parameter is depleted, but there is no evidence that the spins are ferromagnetically aligned [unless a very small regime of J/t is reached where the Nagaoka "phase" is realized (Nagaoka, 1966; Dagotto, Moreo, and Barnes, 1989)]. At reasonable values of J/t, this is not a ferromagnetic polaron. Note also that there are no conceptual differences between holes in strong coupling trapped in a "string" potential created by the antiferromagnetic background, and the spin-bag excitations introduced by Schrieffer, Wen, and Zhang (1988) in a spin-density-wave background. In strong coupling the effective confining potential is mostly linear, while in weak coupling it may have some other form; but one evolves smoothly into the other with a change in the coupling U/t.

3. Dispersion relation of a hole

It is instructive to calculate the dispersion relation of one hole in an antiferromagnetic background. Its total bandwidth W provides information about the renormalization effects caused by the spin waves that are created and absorbed while the hole propagates (although, in a semilocalized spin polaron problem like this one, the language of spin waves is somewhat misleading). Moreover, if the normal state is *assumed* to be formed by a gas of noninteracting (but spin-wave-renormalized) holes, then some observables can be calculated (Trugman, 1990a; Dagotto, Nazarenko, and Boninsegni, 1994) and compared with experiments, once the dispersion relation is known. In addition, the specific $\mathbf{p}$ dependence of the energy provides information about anisotropies in the system. In Fig. 18(a), early results for the dispersion relation of one hole are shown. They were obtained numerically on a 4×4 cluster by fixing the momentum $\mathbf{p}$ in the initial state used in the Lanczos approach (the subsequent iterations preserve the quantum numbers of the original state). W is defined as the difference between the energy of the state with the minimum energy [typically corresponding to momentum $\mathbf{p}=(\pi/2,\pi/2)$] and of the state with the highest energy, which seems to correspond to $\mathbf{p}=(0,0)$ in Fig. 18(a) [which becomes degenerate with $\mathbf{p}=(\pi,\pi)$ in an antiferromagnetic background]. W can also be obtained from the position of the first pole in the hole spectral functions. It can be observed that the total width is considerably smaller than the bandwidth of a free electron which is $W=8t$, and decreases as the coupling J/t decreases. The bandwidth W seems proportional to J/t, at least for small J/t (Dagotto, Joynt, *et al.*, 1990). This result is in agreement with other calculations by Kane, Lee, and Read (1989), Prelovšek, Sega, and Bonča (1990), and Trugman (1990b) [it is also interesting to note that studies for the three-band model at strong coupling reveal a dispersion relation similar to that found for one-band models (Ding, Lang, and Goddard, 1992)]. According to the string picture discussed in

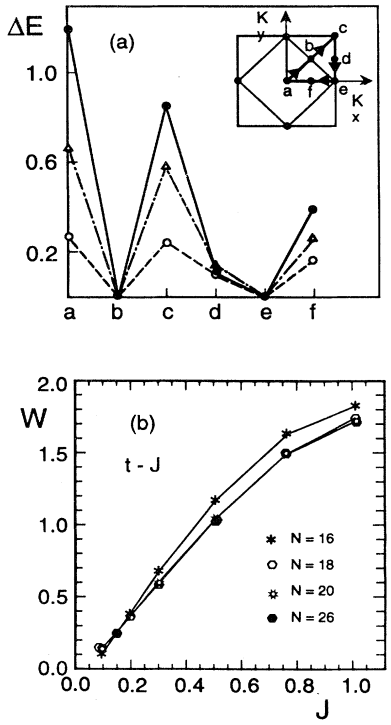

FIG. 18. Energy of a hole with momentum $\mathbf{p}$ with respect to the one-hole ground-state energy (ΔE), for several values of the coupling J/t. The open circles correspond to $J/t=0.2$, the triangles to $J/t=0.4$, and the solid circles to $J/t=1.0$ (from Dagotto, Joynt, Moreo, Bacci, and Gagliano, 1990). (b) Bandwidth W of the t-J model as a function of J (with $t=1$) for different cluster sizes (from Poilblanc, Ziman, *et al.*, 1993).

Sec.III.B.1, a hole needs a considerable energy to move in the background of antiferromagnetically aligned spins. Due to this effect, the hole acquires a large effective mass m^*, which is reflected in a bandwidth smaller than its bare value (the proper definition of the effective mass involves the dispersion-relation energy vs momentum only near the bottom of the band, and relating m^* with W is not strictly correct). In Fig. 18(b), a study of W for different cluster sizes using the Lanczos algorithm is reproduced from Poilblanc, Ziman, *et al.* (1993). Finite-size effects are small. W is approximately linear in the interval $0.1 \leq J/t \leq 0.5$ for all the clusters considered. On the other hand, in the Born approximation it was found that $W \sim 1.5J^{0.79}$ (Martinez and Horsch, 1991), and the difference may be due to the diagrams neglected in this approach.

An interesting feature of Fig. 18(a) is the degeneracy between momenta $\mathbf{p}=(\pi/2,\pi/2)$ and $\mathbf{p}=(0,\pi),(\pi,0)$. This is an artifact of the 4×4 cluster, which has a hidden symmetry making it isomorphic to a 2^4 hypercubic lattice (Dagotto, Joynt, *et al.*, 1990). However, it has been shown repeatedly that results obtained with this cluster size are usually qualitatively accurate when they are compared against predictions obtained on larger clusters or forecasted through other techniques (as will be discussed extensively in this review). Then, the 4×4 cluster results may be telling us that in the bulk limit the energies of those momenta are indeed very close to each other. Analyzed from the point of view of the Hubbard model, this is not surprising, since in the noninteracting limit $U/t=0$ both momenta belong to the Fermi surface; thus, at least at weak coupling, only a tiny splitting in energy is expected. Information about this feature can be obtained in the strong-coupling limit from the Born approximation results of Liu and Manousakis (1991, 1992) at $J/t=0.2$ on a 32^2 cluster. The results are shown in Fig. 19 (see also Marsiglio *et al.*, 1991, Fig. 6). Numerical results using a Green's-function Monte Carlo method on a 12×12 cluster are in good agreement with the Born approximation (Boninsegni, 1993; Dagotto, Nazarenko, and Boninsegni, 1994). A good fit to the numerical results at $J/t=0.4$ is given by

$$\epsilon(\mathbf{k}) = -1.255 + 0.34\cos k_x \cos k_y + 0.13(\cos 2k_x + \cos 2k_y) , \quad (3.15)$$

showing that holes prefer to move among sites belonging to the same sublattice to avoid distorting the antiferromagnetic background. This dispersion relation shows that the difference in energy Δ between $\mathbf{p}=(\pi/2,\pi/2)$ and $\mathbf{p}=(0,\pi),(\pi,0)$ is a small fraction of the total bandwidth. One of the implications of this result is that numerical studies that search for "pockets" of holes near $\mathbf{p}=(\pi/2,\pi/2)$ (Schrieffer, Wen, and Zhang, 1988) should be carried out at temperatures smaller than Δ, to avoid mixing with other states. This detail has been remarked upon recently by Dagotto, Nazarenko, and Boninsegni (1994), and it is the basis for a possible explanation of the behavior of the Hall coefficient with temperature in the cuprates (see also Trugman, 1990a). Quantum Monte Carlo results by Moreo and Duffy (1994) have confirmed these predictions.

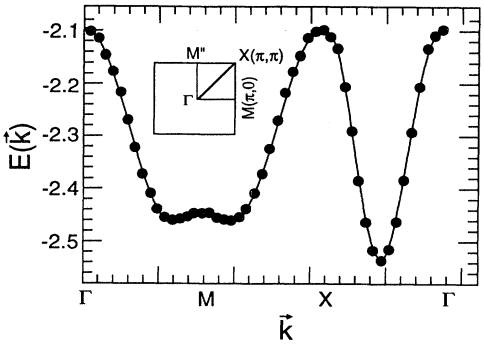

FIG. 19. Hole dispersion curve plotted along the direction $\Gamma MX\Gamma$ in the Brillouin zone (see inset), for a 32^2 lattice, for $J=0.2$ (taken from Liu and Manousakis, 1991, 1992).

4. Dynamical properties of one hole

One of the main advantages of exact diagonalization algorithms is that they provide information about *dynamical* properties of the model under consideration (as explained in Sec. II.A). This is very important, since most of the experimentally available information on superconductors is obtained from dynamical response measurements as a function of frequency ω. Thus Lanczos techniques provide theoretical results that can be compared directly with experiments. In the particular case of carriers in an antiferromagnetic background, the spectral function of one hole $A(\mathbf{p},\omega)$ can be evaluated. In the approximation where holes behave like independent particles in the normal state of the superconductors, this spectral function can be contrasted against photoemission spectroscopy (PES) experiments. Of particular importance is whether a quasiparticle-like excitation exists in the spectrum (i.e., a pole in the Green's function of the hole with a finite residue). This issue will be studied in more detail in Sec. III.B.6. It is fair to point out that there is an alternative picture to that of strings in the description of holes in antiferromagnets which we may call the polaron picture and which was elaborated by Su *et al.* (1989) and Chen and Schüttler (1990).

The spectral function of one hole in the t-J model is defined as

$$A(\mathbf{p},\omega) = \sum_n |\langle \phi_n | \bar{c}^\dagger_{\mathbf{p}\sigma} | \phi^{\text{g.s.}}_{0h} \rangle|^2 \delta(\omega - (E_n - E_0)) , \quad (3.16)$$

where the hole operator $\bar{c}^\dagger_{\mathbf{p}\sigma}$ creates a hole with momentum $\mathbf{p}$, and spin σ. $|\phi^{\text{g.s.}}_{0h}\rangle$ is the ground state of the undoped system, and $|\phi_n\rangle$ are eigenstates of the problem in the subspace of one hole with momentum $\mathbf{p}$ and spin σ.

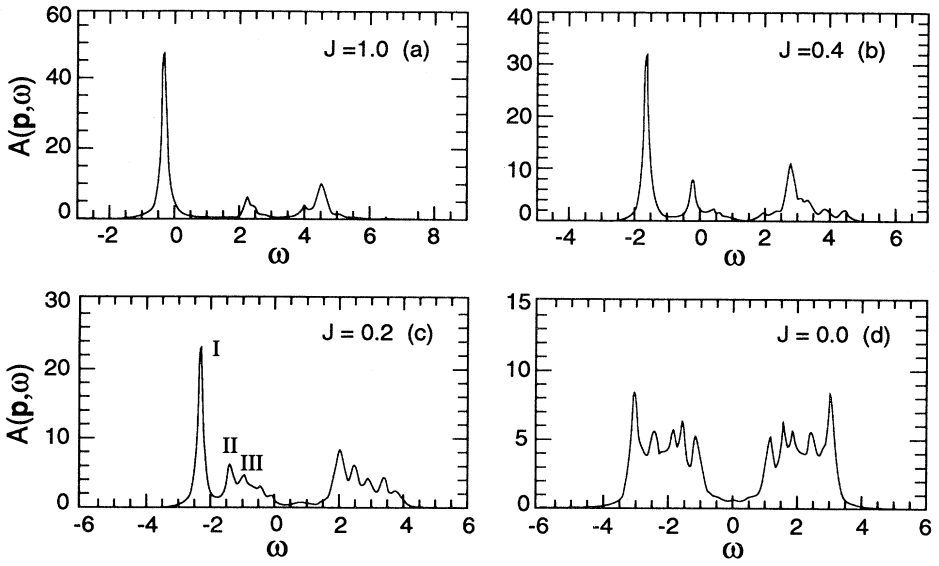

FIG. 20. Spectral function of one hole in the t-J model at $\mathbf{p}=(\pi/2,\pi/2)$: a, b, c, and d correspond to J/t equal to 1.0, 0.4, 0.2, and 0.0, respectively (from Dagotto, Joynt, Moreo, Bacci, and Gagliano, 1990).

Their energies are E_0 and E_n, respectively. The Lanczos approach can be used straightforwardly to calculate this spectral function (Sec. II.A). In Fig. 20, $A(\mathbf{p},\omega)$ is shown at momentum $\mathbf{p}=(\pi/2,\pi/2)$ on a 4×4 cluster at several couplings J/t (from Dagotto, Joynt, *et al.*, 1990; see also von Szczepanski *et al.*, 1990). The δ functions of Eq. (3.16) were plotted with a (arbitrary) width $\epsilon=0.1t$. The number of iterations in the continued fraction necessary to reach convergence is coupling dependent, but typically only ~100 iterations are enough to get results with high accuracy (this number is much smaller than the actual size of the one-hole Hilbert space).[3] Note that the energies are measured with respect to the ground-state energy of the undoped (no holes) system, with energies $\omega=E_n-E_0$ growing from left to right (this is not the standard way to plot a photoemission spectrum in the experimental literature, but in this case we shall simply follow the convention used in most of the papers on one-hole results).

At a relatively large coupling, like $J/t=1$, the spectral function has a simple structure; i.e., a dominant peak at the bottom of the spectrum is clearly observed, and a couple of spikes are present at higher energies. Extensive studies (Dagotto, Joynt, *et al.*, 1990) have shown that the dominant peak at $J/t>1$ corresponds to a hole almost localized at a given site with a large mass, while the higher energy excitations correspond to short string states of lengths 1 and 2, respectively. The momentum dependence of the energy of the lowest pole shows that the hole quasiparticle is mobile, but has a large mass. It is natural to relate this state to a "quasiparticle" state corresponding to a hole dressed by spin excitations. If the coupling is reduced to more realistic values, the amount of spectral weight at the bottom of the spectrum will also be reduced but remain finite. Reciprocally, more spectral weight will appear at higher energies. Let us consider the case of $J/t=0.2$, shown in Fig. 20(c). $A(\mathbf{p},\omega)$ still contains a large peak at the bottom of the spectrum (quasiparticle), but now it is followed by a lump of spectral weight with some internal structure. In turn, this is followed by a pseudogap and a second lump at higher energies. In this type of numerical study, it has been found empirically that low-energy structures are less affected by finite-size effects than the high-energy ones, and thus the pseudogap and second band may disappear as the lattice size is increased. However, the large quasiparticle peak and the low-energy satellite peaks may survive the bulk limit, as discussed below. Finally, at $J/t=0$, the spectrum at $\mathbf{p}=(\pi/2,\pi/2)$ becomes symmetric with respect to $\omega=0$, and it contains two bands separated by a pseudogap. As stressed before, the region of small coupling is the one where finite-size effects are more severe (since the hole wave-function size increases when J/t is reduced). Thus Fig. 20(d) may be strongly affected by size effects.

It has been shown that peaks denoted by I, II, and III in Fig. 20(c), corresponding to $J/t=0.2$, can be identified as the ground state and two next excited states of the string problem described in Sec. III.B.1 (Dagotto, Joynt, *et al.*, 1990). The main support for this statement is that the energies of the three states have a $(J/t)^{2/3}$ power-law dependence with the coupling similar to that predicted by the string picture. This result has been nicely confirmed by Liu and Manousakis (1991, 1992) in the self-consistent Born approximation discussed in Sec. III.B.2. These authors have shown that, for a 4×4 cluster, they can reproduce very well the numerical results,

[3]Results like those shown in Fig. 20 contain hundreds of poles, although to the eye only a few peaks can be observed. To observe the individual poles, Dagotto, Joynt, *et al.* (1990) provided an example in which the δ functions have a small width $\epsilon=0.01t$.

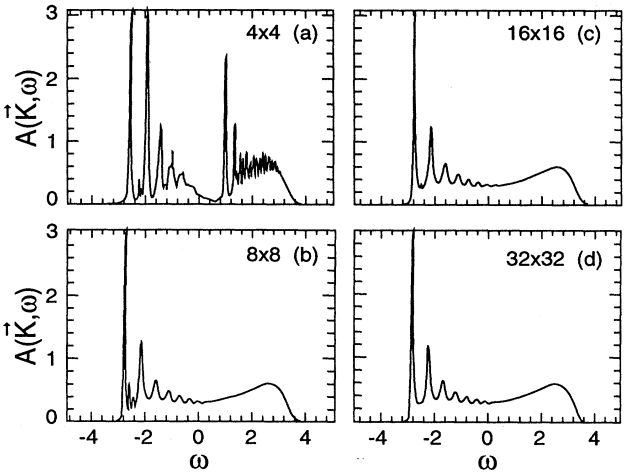

FIG. 21. $A(\mathbf{p},\omega)$ with $\mathbf{p}=(\pi/2,\pi/2)$ for $J=0.1$ and $\epsilon=0.01$ (width of the δ functions) and several lattice sizes (from Liu and Manousakis, 1991, 1992), using the rainbow approximation.

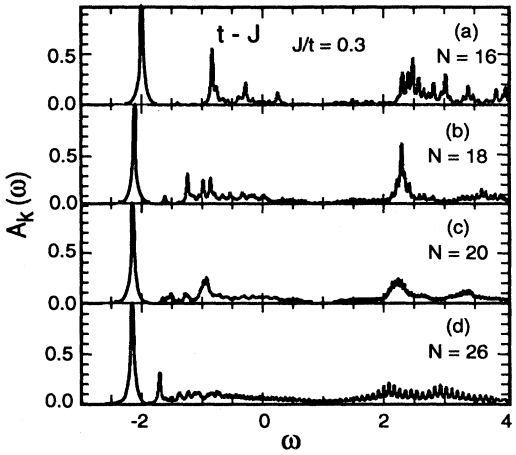

FIG. 22. Single-hole spectral function for the t-J model at the ground-state momentum, for various cluster sizes and $J/t=0.3$. The actual values of the momenta are $\mathbf{p}=(\pi/2,\pi/2)$ for the cluster of 16 sites; $\mathbf{p}=(\pi,\pi/3)$ for 18 sites; $\mathbf{p}=(4\pi/5,2\pi/5)$ for 20 sites; and $\mathbf{p}=(9\pi/13,7\pi/13)$ for 26 sites (from Poilblanc, Ziman, *et al.*, 1993).

at least for small J/t [see Fig. 21(a), obtained at $J/t=0.1$]. With this approximation it is possible to study larger clusters and check whether the string excitations survive the bulk limit. The results on a 32^2 cluster [Fig. 21(d)] have already converged to the bulk limit, and the main structure predicted by the string picture and the small cluster approach is still observed, namely, a large quasiparticle peak at the bottom of the spectrum (carrying a finite percentage of the total spectral weight), followed by satellite peaks at higher energies. The pseudogap of the small cluster is filled and becomes only a soft depression in the spectral weight. While both methods (exact diagonalization on small clusters and the rainbow technique on large clusters) are approximations to the thermodynamic problem, the good agreement in their predictions suggests that the results may indeed describe the bulk limit behavior of a hole in the t-J model. We then arrive at the conclusion that a quasiparticle exists in this model with ground-state and excited-state energies well described by the string picture. More on this issue will be discussed in Sec. III.B.6. It is also interesting to notice that lattice distortions can have an important effect over the physics of carriers in the cuprates. See, for example, Yonemitsu, Bishop, and Lorenzana (1992, 1993a, 1993b); Röder, Bishop, and Gammel (1993); Röder, Fehske, and Büttner (1993); Fehske *et al.* (1993); and by Dobry *et al.* (1994).

To check for finite-size effects in the results shown in Fig. 20, Poilblanc, Ziman, *et al.* (1993) recently carried out an exact diagonalization study on square clusters with up to $N=26$ sites.[4] Results are shown in Fig. 22 corresponding to $J/t=0.3$, i.e., in the physically realistic regime. The general trend observed in these results is that (i) the quasiparticle peak is robust and does not change much with the lattice size; and (ii) the structure at larger energies is more affected by the size of the clusters. However, care must be taken in this study, since the momentum at which the calculation has been performed is not the same for the four clusters. Actually, only the 4×4 cluster contains momentum $\mathbf{p}=(\pi/2,\pi/2)$, while the rest have momenta close to, but never at, this same value. Then, such a systematic error may distort the higher energy features of the spectrum. In spite of this problem, it is reassuring that the low-energy quasiparticle seems quite robust and may well survive the bulk limit.

An interesting issue to discuss is the momentum dependence of $A(\mathbf{p},\omega)$. In Fig. 23, the spectral functions at several momenta are shown at $J/t=0.2$ on the 4×4 cluster (Dagotto, Joynt, *et al.*, 1990). Unfortunately, the

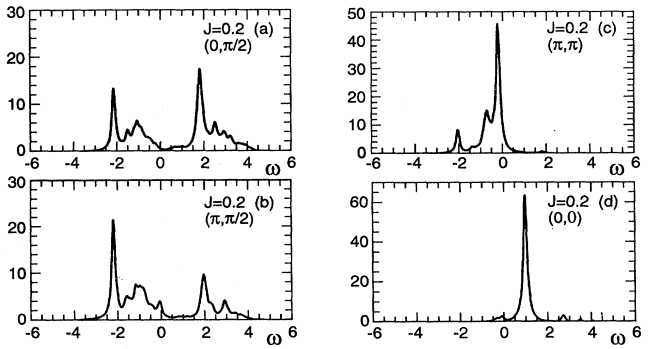

FIG. 23. Spectral function of one hole in the t-J model at $J=0.2$ for different values of $\mathbf{p}$ on a 4×4 cluster (Dagotto, Joynt, Moreo, Bacci, and Gagliano, 1990).

[4]Present-day supercomputers still do not allow an analysis of the next interesting clusters, which have $N=32$ and 36 sites, for the case of one hole in the t-J model.

small size of the cluster does not allow us to obtain a high-resolution result in **p** space. However, some qualitative conclusions can be made. For example, the shape of the spectrum for $\mathbf{p}=(0,\pi/2)$ and $(\pi,\pi/2)$ is qualitatively similar to $\mathbf{p}=(\pi/2,\pi/2)$, which corresponds to the actual hole ground state. On the other hand, at momenta $\mathbf{p}=(0,0)$ and (π,π), there are substantial qualitative changes, since most of the weight is concentrated at high energies. An analysis of different cluster sizes (Poilblanc, Ziman, *et al.*, 1993) showed that this is not a peculiarity of the 4×4 cluster; but, indeed, these two momenta seem to have a large spectral weight at high energies. The only effect of increasing the cluster size is to provide a finite width to the peaks, while the total amount of spectral weight in its vicinity remains approximately constant. This result is also in good agreement with the self-consistent rainbow approximation (Martinez and Horsch, 1991).

5. Binding of holes

The ground-state energy of two holes has been studied by several groups (Kaxiras and Manousakis, 1988; Bonča, Prelovšek, and Sega, 1989a; Hasegawa and Poilblanc, 1989; Riera and Young, 1989; Dagotto, Riera, and Young, 1990; Fehske *et al.*, 1991; Poilblanc, Riera, and Dagotto, 1993; and references therein). For clusters of different sizes, some of these authors found that the ground state belongs to the B_{1g} irreducible representation of the C_{4v} point group of the square lattice (i.e., $d_{x^2-y^2}$ symmetry). In Fig. 24(a), the average distance between the two holes, obtained from a study of hole-hole correlations in the exact ground-state wave functions, is plotted as a function of J/t for different cluster sizes (Barnes *et al.*, 1992; Poilblanc, Riera, and Dagotto, 1994). At least in the region $J/t \geq 0.5$, it is clear that the distance between holes is small (less than two lattice spacings), suggesting the formation of a bound state. Although such a bound state of two holes in an antiferromagnet is not sufficient evidence for the formation of a condensate, it is nevertheless suggestive that attractive effective forces are operative (at least in the *t-J* model). Thus it is important to carry out a detailed study of this two-hole problem, and in this section we review the status of this subject.

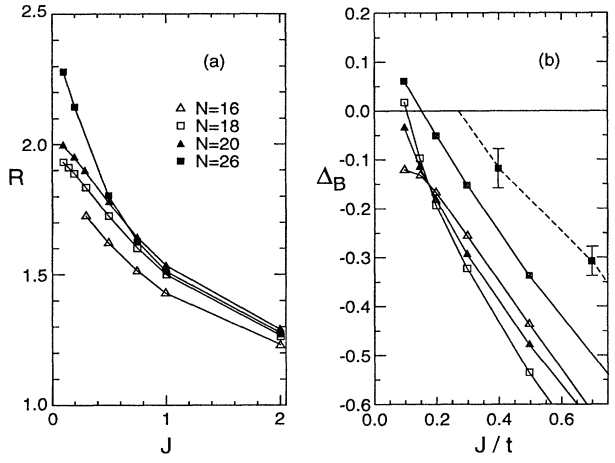

FIG. 24. (a) Average hole-hole distance in the ground state of two holes as a function of the coupling constant for several clusters (from Poilblanc, Riera, and Dagotto, 1994); (b) binding energy Δ_B of two holes in the *t-J* model as a function of the coupling. Open triangles denote results for 16 sites, open squares for 18 sites, solid triangles for 20 sites, and solid squares for 26 sites (taken from Poilblanc, Riera, and Dagotto, 1994). The points with the error bars joined by a dashed line are Green's-function Monte Carlo results from Boninsegni and Manousakis (1993).

Intuitively, it is clear that a bound state of two holes in an otherwise undoped antiferromagnet will be formed at large values of J/t. The reason is that each individual hole "breaks" four antiferromagnetic (AF) links, which costs an energy of the order of the superexchange coupling. At least in the small t limit (low mobility), two holes minimize the lost energy by sharing a common link. In this way they reduce the number of broken AF links from eight to seven. When the coupling J/t is reduced to more realistic values, this attraction may survive until some "critical" coupling is reached where holes unbind. Of course, the picture of "minimization of the number of broken AF links" as the origin of binding is very crude and probably wrong at small J/t, but no better intuitive picture is available. In Fig. 24(b) the "binding energy" of two holes is plotted based on results obtained using the Lanczos approach on clusters of $N=16$, 18, 20, and 26 sites (Poilblanc, Riera, and Dagotto, 1994). The binding energy is defined as $\Delta_B = e_2 - 2e_1$, where $e_n = E_n - E_0$, and E_n is the ground-state energy of the *t-J* model in the subspace of n holes. If two holes minimize their energy by producing a bound state, then Δ_B becomes negative. Note that in the bulk limit we expect Δ_B to vanish if the holes do not form a bound state, since $e_2 \approx 2e_1$ for two independent holes. However, on a finite cluster, it can be positive due to hole repulsion.

As shown in Fig. 24(b), our expectation of finding a bound state of holes is correct. Δ_B becomes negative (implying binding) very rapidly starting at small values of J/t. However, the convergence of the results increasing the lattice size is erratic. The reason is that Δ_B is considerably affected by finite-size effects, since it is defined as a difference between large numbers.[5] In addition, the energy of one hole enters in the definition of Δ_B and, as discussed before, this quantity carries an additional systematic error due to the absence of momentum $\mathbf{p}=(\pi/2,\pi/2)$ in the discrete set of momenta of the clusters with $N=18$, 20, and 26 sites. In spite of these problems, qualitative information can be obtained from Fig.

[5]In the continuum, Δ_B corresponds to the second derivative of the energy with respect to the number of particles.

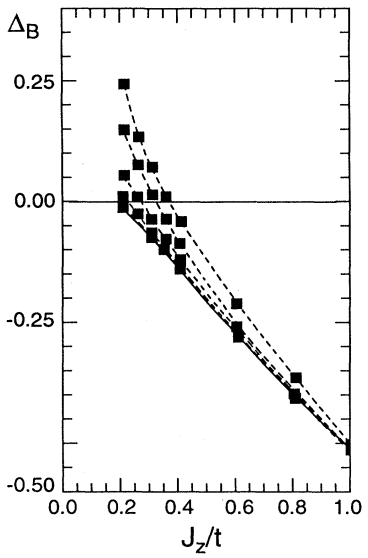

FIG. 25. Binding energy Δ_B as a function of J_z/t for the t-J_z model and several cluster sizes. Starting from above, the open squares denote results for $N=16$, 20, 26, 36, and 50 sites, respectively. The solid line is the binding energy extrapolated to the bulk limit, which is almost identical to the results in the 50-site cluster. These results were obtained with the "truncation" method described by Riera and Dagotto (1993a).

24(b) with some confidence. The "critical" coupling, $J/t|_c$, where two holes reduce their energy by forming a bound state, slowly grows with increasing lattice size, suggesting that it may converge to a finite value in the bulk limit, since we know that at large couplings there must be binding. In Fig. 24(b), Green's-function Monte Carlo results on 8×8 clusters obtained by Boninsegni and Manousakis (1992a, 1992b) are also shown. With this approach, supplemented by the use of appropriate variational guiding states obtained from the exact analysis of smaller clusters, it has been possible to study Δ_B for couplings J/t as small as 0.4, on large clusters. The dashed line in the figure shows an educated extrapolation suggesting that binding starts at $J/t|_c\sim0.3$, in qualitative agreement with the exact results on smaller clusters. Then, it seems quite possible that, indeed, a critical value of the coupling J/t exists beyond which two holes form a bound state in an antiferromagnetic background. Note that near the critical value the size of the pairs may well be very large, while for a larger J/t their size is small. If these pairs condense at zero temperature, the region of large-size pairs may resemble the BCS regime of the attractive Hubbard model, while the small-size-pairs region may behave like a Bose condensate of pairs.

Note that calculations on clusters of up to 50 sites in the t-J_z model, Eq. (3.8), where transverse spin fluctuations are switched off, have also shown that a critical coupling exists for hole pair formation (Fig. 25). The technique used to study such a large cluster is based on the selective truncation of the Hilbert space of the problem (Sec. II.A; Riera and Dagotto, 1993 and references therein; see also Inoue and Maekawa, 1992). In this model, the critical coupling is $J_z/t|_c\sim0.18$, in qualitative agreement with the results for the t-J model, since, in the absence of spin fluctuations, a stronger tendency to pairing would be expected.

The analysis of Δ_B for Hubbard-like models is more difficult. Studies of the three-band case have been restricted to very small systems, where the presence of hole binding has been reported (Balseiro *et al.*, 1988; Hirsch *et al.*, 1988, 1989). Unfortunately, a finite-size analysis of Δ_B is not possible in this model. With respect to the one-band Hubbard model, an analysis based on exact diagonalization and Monte Carlo simulations for 4×4 clusters shows that there is binding. However, Δ_B is considerably smaller than the binding energy reported for the t-J model, and thus finite-size effects may be more important (Dagotto, Moreo, Sugar, and Toussaint, 1990; Fano, Ortolani, and Parola, 1990). Actually, studies of one-dimensional Hubbard chains on finite clusters show also a negative Δ_B comparable in magnitude to that of the two-dimensional case. However, with an increase in the size of the chain, Δ_B seems to converge to zero in the bulk limit (Fye, Martins, and Scalettar, 1990). Similar negative conclusions for binding were found by Ding and Goddard (1993) in the one-dimensional three-band Hubbard model. Currently there is no convincing numerical evidence that the two-dimensional Hubbard model has hole binding near half-filling in the bulk limit. More work is necessary to clarify this issue.

6. Quasiparticles in models of correlated electrons

One of the most controversial issues in the context of models of correlated electrons proposed to describe the new superconductors is whether a hole injected in the undoped ground state behaves like a quasiparticle. While it is clear that spin-wave excitations will heavily dress the hole, increasing substantially its mass, the central point is whether this renormalization is so strong that the wave-function renormalization Z at the Fermi surface vanishes. This scenario has been proposed by Anderson (1990a) mainly based on results obtained in the one-dimensional Hubbard model where, indeed, Z vanishes in the bulk limit. However, this is a very particular situation caused by the dimensionality of the problem, and what occurs in two dimensions is unclear. In Fig. 26, we show a hole injected in an antiferromagnetic chain (e.g., large U/t Hubbard model) that propagates due to the hopping term in the Hamiltonian. As shown in the figure, the "ferromagnetic" link and the hole quickly become separated. The velocity corresponding to charge and spin degrees of freedom are different in this model; even if a wave packet is constructed at time $t=0$ with spin and charge localized near the same site, the time evolution of the packet will make charge and spin decouple (see, for example, Jagla, Hallberg, and Balseiro, 1993;

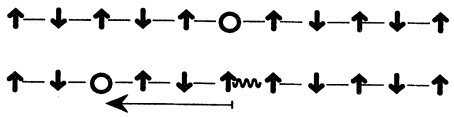

FIG. 26. Rough interpretation of the spin-charge separation in one-dimensional problems. The upper chain represents a hole injected in a staggered spin background. The lower chain is the state obtained after the hole hops three lattice spacings to the left. The ferromagnetic link is still at the original position of the hole, and thus the hole is not confined as in two-dimensional problems (contrast these results with Fig. 16).

see also Song and Annett, 1992). It is natural, then, that the overlap between the initial state and the ground state is zero in the bulk limit. Of course, there is no reason for this mechanism to work in two dimensions (2D). In 2D the hole propagation costs an energy proportional to the length of the walk, contrary to what occurs in 1D (remember the string excitations described in Sec. III.B.1). Spin-charge separation is not obvious in the dimension of interest.

Other more conservative approaches, like the spin-bag or string ideas, describe the hole as being surrounded by a region where the antiferromagnetic order parameter is reduced. The combination of charge plus the depleted antiferromagnetic background moves coherently and behaves like a particle with charge $Q=e$ and with spin $\frac{1}{2}$; i.e., Z is nonzero in this approach. Then, since different theories drastically disagree on the nature of quasiparticles in strongly correlated electrons, the important issue that needs to be clarified numerically is the following: Suppose we consider a large but finite cluster of N (even) sites, with $N-1$ spins and one hole. The ground state of the system has spin $\frac{1}{2}$ (unless ferromagnetism is favored, which occurs only in special cases). Where is this spin $\frac{1}{2}$ localized? Is it near the hole or spread over the entire lattice? In the first case, we are forming a spin polaron and the hole is a dressed quasiparticle with a finite Z weight. In the second case, this quasiparticle is unstable, and it basically decays into a holon and a spinon. Semiclassical calculations by Shraiman and Siggia (1988b) support the assumption that Z vanishes in the bulk limit in two dimensions. The main idea is that an infinite range $1/r$ distortion in the spin background occurs when a hole is injected in an antiferromagnet. However, these calculations have been reanalyzed recently by Reiter (1992), taking into account quantum fluctuations, and it was found that Z remains finite. Similar conclusions were reached by Auerbach and Larson (1991), suggesting that the hole is, in fact, a small polaron, as was found numerically.

The study of Z can be explicitly addressed using numerical techniques. In particular, Lanczos methods that provide the hole spectral function are especially suitable for this purpose. Z is simply given by the weight at the lowest pole in the spectrum, i.e.,

$$Z=\frac{|\langle\psi_{1h}^{\text{g.s.}}|\bar{c}_{\mathbf{p}\sigma}^{\dagger}|\psi_{0h}^{\text{g.s.}}\rangle|}{[\langle\psi_{0h}^{\text{g.s.}}|\bar{c}_{\mathbf{p}\sigma}\bar{c}_{\mathbf{p}\sigma}^{\dagger}|\psi_{0h}^{\text{g.s.}}\rangle]^{1/2}}\ , \tag{3.17}$$

where $|\psi_{nh}^{\text{g.s.}}\rangle$ is the ground state in the subspace of n holes, and the rest of the notation is standard. With the normalization used in Eq. (3.17), it can be shown that $0\le Z\le 1$. Results obtained for the t-J model using two-dimensional clusters of 16, 18, 20, and 26 sites are shown in Fig. 27(a). The behavior of Z suggests that the quasiparticle weight remains finite in the bulk limit for all the explored values of J/t, although work on larger lattices is necessary to confirm this result. A fit in the interval $0.1\le J/t\le 0.4$ suggests that $Z\sim J^{0.5}$, which vanishes only at $J/t=0$. However, care must be taken in the use of these clusters for calculations in the one-hole subspace, since, due to the geometry of the clusters, the momentum $\mathbf{p}=(\pi/2,\pi/2)$ exists only for $N=16$. In the other clusters the ground state has a momentum $\mathbf{p}=(\pi,\pi/3)$, $(4\pi/5,2\pi/5)$, and $(9\pi/13,7\pi/13)$ for the $N=18$, 20, and 26 sites, respectively. In spite of this difficulty, there are no major finite-size effects in Fig. 27(a). Nevertheless, it would be very important to study clusters slightly larger than those currently available (like $N=32$ sites) to carry out a finite-size scaling study with the proper momentum $\mathbf{p}=(\pi/2,\pi/2)$. It would also be important to study numerically the separation between spin and charge in two dimensions. In the spin $\frac{1}{2}$ of N-1 spins on an N-site lattice (N even) localized near the hole or

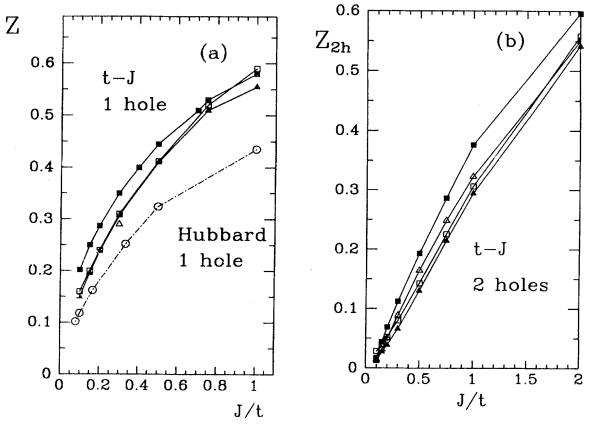

FIG. 27. (a) Wave-function renormalization Z of one hole in the t-J model [for the actual definition see Eq. (3.16)]. The solid squares denote results for a 16-site cluster (Dagotto and Schrieffer, 1991). Open squares are results for 18 sites, solid triangles are for 20 sites, and the open triangle corresponds to 26 sites (Poilblanc, Schulz, and Ziman, 1993). The open circles joined by the dot-dashed line correspond to results for the one-band Hubbard model using $J=4t^2/U$ and $t=1$ (from Fano, Ortolani, and Parola, 1992). The definition of Z by these authors is $Z=|\langle\psi_{1h}^{\text{g.s.}}|c_{\mathbf{p}\sigma}|\psi_{0h}^{\text{g.s.}}\rangle|^2$, i.e., different from that used in Eq. (3.16). With their definition, Z is restricted to the interval [0,1/2]. (b) Z_{2h} as defined in the text for the t-J model as a function of the coupling. The notation is the same as that in Fig. 27(a). From Poilblanc, Riera, and Dagotto (1994).

spread over the entire cluster? More work should be devoted to this issue.

The Born approximation to the spin-wave holon reformulation of the t-J model can also be used to calculate the quasiparticle weight (Martinez and Horsch, 1991; Liu and Manousakis, 1992). Within this approximation there is a well-defined quasiparticle peak in the spectrum carrying a finite percentage of the total weight, in good agreement with the Lanczos calculations. The Born approximation predicts $Z=0.63J^{0.667}$ in the interval $0.01\leq J\leq 0.5$, for $\mathbf{p}=(\pi/2,\pi/2)$ on a 16×16 cluster ($\sim$ bulk limit). The results are actually very close to those shown in Fig. 27(a), in spite of the different optimal power-law fit. This is an excellent example of how analytical and numerical techniques can complement each other efficiently in the study of a given problem. The results obtained in the Born approximation are appreciably closer to the numerical results than the dominant pole approximation, which instead predicts $Z\sim J$ (Kane, Lee, and Read, 1989). The remaining small discrepancy between numerics and the Born approximation may be due to higher-order corrections in the former, or to finite-size effects in the cluster results. We conclude, then that the evidence gathered in these studies favors a picture where, at a finite coupling J/t, Z is nonzero.

Similar issues have been addressed for the one-band Hubbard model, but the results are not as clear. The wave-function renormalization for one less particle than half-filling on a 4×4 cluster has been obtained by Fano, Ortolani, and Parola (1992). The results are also shown in Fig. 27(a), and they qualitatively resemble those obtained for the t-J model at large U/t, using the relation $J=4t^2/U$ [however, the definition of Z of these authors is different from that used in Eq. (3.17)]. Both in the t-J and in the Hubbard model, the weight of the quasiparticle decreases as the strong-coupling limit is approached, and seems to converge to zero only as $U/t\rightarrow\infty$. Unfortunately, clusters appreciably larger than those with $N=16$ sites are unreachable using exact diagonalization techniques, for the Hubbard model with one less particle than half-filling. Thus the finite-size study performed for the t-J model has not been carried out for this model. However, Z can also be obtained by studying $n(\mathbf{p})$. The "jump" in this quantity at the Fermi surface is proportional to Z. Moreo, Scalapino, *et al.* (1990) studied $n(\mathbf{p})$ using Monte Carlo techniques and found a finite jump at the Fermi surface (see Sec. IV.C.3). On the other hand, projector Monte Carlo calculations by Sorella (1992) seem to suggest the vanishing of Z as the cluster size is increased working at $U/t=4$. However, in the last calculation a small magnetic field was introduced to work with closed-shell configurations in order to alleviate the sign problem. How Z is influenced by this small magnetic field is unclear, and thus we believe that more work should be done in the one-band Hubbard model to clarify these issues.

It is also instructive to obtain the weight of the lowest energy peak in the spectral decomposition of the operator that creates a *pair* of holes over an undoped spin background. As we discussed in Sec. III.B.5, there is a wide region of parameter space in the t-J model where holes tend to bind in pairs, and thus isolated holes are unstable against pair formation. In other words, using a grand-canonical ensemble where the fermionic density $\langle n\rangle$ is regulated with a chemical potential μ, the state of one hole can never be reached in that binding region. Then, the actual "quasiparticles" in this regime are the hole pairs. They carry charge $Q=2e$, total spin 0 (if bound in a singlet), and internal quantum numbers related to the symmetry of the pair ($d_{x^2-y^2}$, according to the results discussed in Sec. III.B.5). These arguments are suggestive; however, to verify the picture that associates the bound state with a quasiparticle, it is necessary to show that the spectral decomposition of the pair operator that produces this state out of the undoped system contains a sharp δ function at the bottom of the spectrum. By complete analogy to the case of one hole, it is possible to define the spectral function of the operator Δ_α that creates a pair of holes from the "vacuum" (antiferromagnetic state) as

$$P(\omega)=\sum_n |\langle \psi_{2h}^n|\Delta_\alpha^\dagger|\psi_{0h}^{\text{g.s.}}\rangle|^2\delta(\omega-(E_{2h}^n-E_{0h}^{\text{g.s.}}))\ . \quad (3.18)$$

We have defined $\Delta_\alpha=\bar{c}_{i\uparrow}(\bar{c}_{i+x\downarrow}+\bar{c}_{i-x\downarrow}\pm\bar{c}_{i+y\downarrow}\pm\bar{c}_{i-y\downarrow})$, where $\alpha=s(d)$ corresponds to the $+$ $(-)$ signs and represents a pair with extended s-wave symmetry ($d_{x^2-y^2}$ symmetry). $\{|\psi_{2h}^n\rangle\}$ are states of the two-hole subspace with energy E_{2h}^n, and the rest of the notation is standard.[6] The results for a 4×4 cluster are shown in Fig. 28 for $J/t=0.4$ and both symmetries (Dagotto, Riera, and Young, 1990; see also Chernyshev, Dotsenko, and Sushkov, 1993 and Poilblanc, Riera, and Dagotto, 1994). Let us consider the first case: Clearly, for a d-wave operator, there is a sharp δ peak at the bottom of the spectrum containing an appreciable amount of the total spectral weight. The rest of the spectrum seems incoherent. This result supports the picture that the two holes form a d-wave bound state that behaves like a quasiparticle. On the other hand, the spectral function corresponding to an extended s-wave operator is drastically different. The weight at the bottom of the spectrum is negligible, and most of the spectral weight is concentrated at high energy. The s-wave spectrum clearly does not present a quasiparticle.

[6]The operator used to create the pair is not strictly a spin singlet, but a combination of singlet and triplet. Nevertheless, it is supposed to have an overlap with the ground state of two holes (which is a singlet) if the quantum numbers under rotations and reflexions are properly selected. Adding the pairing correlation functions over all distances removes the contribution of the triplets, and thus the superconducting susceptibility is a pure singlet.

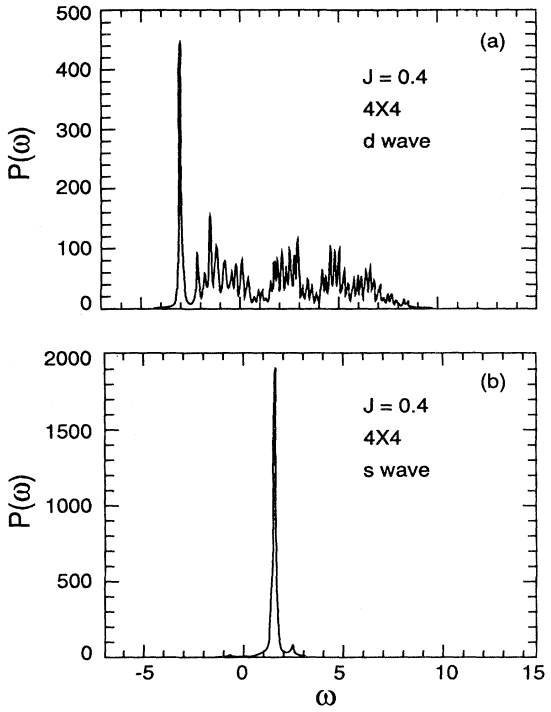

FIG. 28. Spectral decomposition of the operator that creates a pair of holes out of the undoped ground state (see text). Results are presented for $d_{x^2-y^2}$ symmetry (a), and extended s symmetry (b), on a 4×4 cluster at $J/t=0.4$ (from Dagotto, Riera, and Young, 1990). Similar results were obtained by Poilblanc, Riera, and Dagotto (1994), on larger clusters.

Poilblanc, Riera, and Dagotto (1994) recently studied the two-hole "quasiparticle weight" Z_{2h}, defined as

$$Z_{2h}=\frac{|\langle \psi_{2h}^{\text{g.s.}}|\Delta_\alpha^\dagger|\psi_{0h}^{\text{g.s.}}\rangle|}{[\langle \psi_{0h}^{\text{g.s.}}|\Delta_\alpha\Delta_\alpha^\dagger|\psi_{0h}^{\text{g.s.}}\rangle]^{1/2}}, \tag{3.19}$$

on several cluster sizes. Their results are shown in Fig. 27(b). In agreement with the one-hole study, no major differences are observed between the currently available clusters, suggesting that Z_{2h} remains finite in the bulk limit (unless J/t vanishes).[7] Note that this self-consistent picture of bound states behaving as quasiparticles can be wrong if a multibody condensate is formed when additional holes are added to the system. In other words, the formation of a superconducting condensate (through a possible Bose condensation of two-hole bound states), or the possibility of phase separation for small values of J/t, will break down the picture of independent pairs of holes at low temperatures. However, it may still correspond to a good approximation to the normal state of the problem above T_c.

Currently available numerical results for the t-J model suggest, then, that Z for one and two holes is finite for all finite values of J/t. A similar result was obtained using a self-consistent Born approximation. Results for the Hubbard model are more controversial.

IV. COMPARING EXPERIMENTS WITH COMPUTER SIMULATION RESULTS

A. Magnetic properties in the presence of carriers

In this section, the magnetic behavior of models of strongly correlated electrons (away from half-filling) is compared against experiments. The main conclusion of this analysis is that some of the "unusual" magnetic properties of the cuprate materials can be qualitatively reproduced by simple one-band electronic models. Raman scattering will not be reviewed in this paper, since not much computational work has been carried out at finite hole doping. The reader should consult Dagotto and Poilblanc (1990), Gagliano and Bacci (1990), and Haas *et al.* (1994) for an attempt to address this issue and for experimental references on this important subject.

1. Magnetic susceptibility

Here, we shall review experimental and theoretical results for the magnetic susceptibility χ_M of doped compounds. Figure 29 shows χ_M, as reported by Johnston and co-workers (Johnston *et al.*, 1988; Johnston, 1989), obtained in powder $La_{2-x}Sr_xCuO_4$ and $YBa_2Cu_3O_{6+x}$ (see also Lee, Klemm, and Johnston, 1989 and Torrance *et al.*, 1989). Common to both materials is the pronounced S-shaped curve for the samples close to or in the insulating regime. At half-filling, such a behavior is not surprising, since the appearance of a maximum in χ_M at temperatures of the order of the superexchange J ($\sim$1500 K for the cuprates) is known to occur in the two-dimensional spin-$\frac{1}{2}$ Heisenberg antiferromagnet on a square lattice (Gomez-Santos, Joannopoulos, and Negele, 1989; Gagliano, Bacci, and Dagotto, 1991; and references therein). Unfortunately, the temperature at which the maximum occurs is higher than the measurement limit, and thus this theoretical prediction has not been verified for the undoped cuprates. However, with increased doping, the results for $La_{2-x}Sr_xCuO_4$ show that this maximum becomes observable in the experimentally accessible temperature range, and it was found to shift towards lower temperatures with increasing Sr concentration. A qualitatively similar trend seems to occur in $YBa_2Cu_3O_{6+x}$ with increasing amounts of oxygen. In particular, for the samples with the highest T_c (i.e., having $O_{6.96}$), the susceptibility χ_M is almost flat. The same

[7]The ground state of two holes has zero momentum for all the clusters and couplings that Poilblanc, Riera, and Dagotto considered; thus the systematic problem found in the one-hole subspace related to the change in the ground-state momentum from cluster to cluster is absent in this subspace.

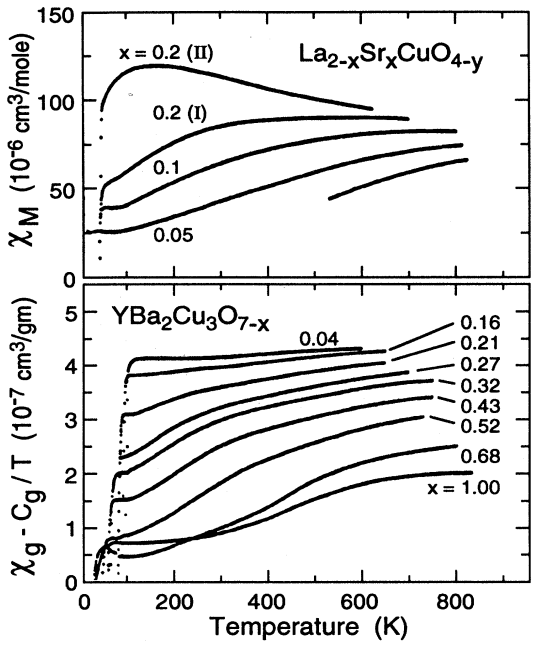

FIG. 29. Uniform magnetic susceptibility of $La_{2-x}Sr_xCuO_4$ and $YBa_2Cu_3O_{6+x}$ as a function of temperature (from Johnston *et al.*, 1988 and Johnston, 1989). In the upper figure, (I) and (II) refer to different oxygen compositions, namely, $y=0.0$ and 0.04, respectively.

figures show that working at fixed temperature but changing the amount of doping increases the magnetic susceptibility when the hole concentration is increased from the insulating regime.

These results can be qualitatively understood. When the antiferromagnetic parent compounds are doped, the effective Cu-Cu superexchange interaction J is reduced in average due to the presence of hole carriers. As a consequence, the temperature at which the maximum of the magnetic susceptibility is located should also decrease with increasing doping, as observed experimentally. To understand the doping dependence at a fixed and low temperature, simply remember that for an antiferromagnet the susceptibility at zero temperature is inversely proportional to the spin superexchange, i.e., $\chi_M \sim 1/J$. Thus, if J is reduced by doping, the zero-temperature susceptibility should increase as observed experimentally. Although the qualitative argument based on a smaller effective superexchange seems correct, in practice it is difficult to map χ_M to a universal curve by a rescaling of the energy scale, especially since χ_M is not known over a wide enough temperature range (Johnston *et al.*, 1988); thus this argument should only be considered as a first approximation to the problem.

Now, let us consider more elaborate theoretical predictions for magnetic properties of models of the cuprates. An analysis of χ_M using weak-coupling resummation methods [mainly random-phase approximation (RPA)] in the one-band Hubbard model has been carried out (Bulut *et al.*, 1990; Lu *et al.*, 1990). With this approach, the susceptibility is maximum at half-filling; i.e., it does *not* reproduce the experimental behavior of the cuprates. Is this a problem of the approximation or of the Hubbard model? To clarify this issue, the magnetic susceptibility of the one-band Hubbard model has recently been studied using quantum Monte Carlo techniques (Moreo, 1993a). The results are shown in Figs. 30(a) and 30(b). Since the sign problem is especially severe at large U/t and finite hole density, the temperature of this study is relatively high, $T=t/4$ (although smaller than J, at large couplings!). However, even at this high temperature a qualitatively different behavior is observed between $U/t=4$ and $U/t=10$. In weak coupling, χ_M is maximum at half-filling, as predicted by the RPA, while at large couplings the maximum is reached at $\langle n \rangle \sim 0.85$, in qualitative agreement with experiments. Similar results in the strong-coupling regime have been obtained using high-temperature expansions for the t-J model [Singh and Glenister, 1992a; Fig. 30(c)]. The series-expansion results are valid directly in the bulk limit, but are restricted to couplings $J/t>0.5$ and to temperatures $T>J/2\sim t/4$ due to uncertainties in the analytic continuations (involving Padé approximants) necessary to extrapolate the results from high to low temperatures

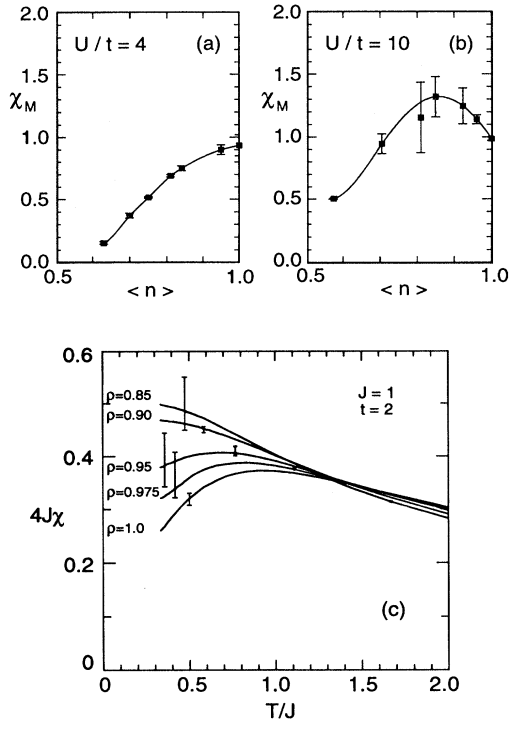

FIG. 30. (a) Uniform magnetic susceptibility as a function of density for the one-band Hubbard model on a 4×4 cluster obtained using quantum Monte Carlo techniques, at temperature $T=t/4$, and $U/t=4$ (from Moreo, 1993a); (b) same as (a), but obtained at $U/t=10$; (c) temperature dependence of the uniform susceptibility obtained with high-temperature expansions (Singh and Glenister, 1992a) using the t-J model at $J/t=0.5$ and several dopings.

(smaller couplings can be studied, but the results are reliable only for even larger temperatures). In spite of the limitations of the numerical and analytical results, it is reassuring to find a nice qualitative agreement among them, and also when they are compared with experiments.

In the regime of large U/t, the simple argument used to explain the behavior of χ_M based on a reduction of the effective J should be operative, and the numerical results of Moreo (1993a) confirm it. In the weak-coupling regime, the numerical simulation might not reach temperatures low enough to allow observation of the growth of the magnetic susceptibility away from half-filling, or a genuine qualitative difference might exist between strong and weak coupling. Nevertheless, it is interesting to observe that the regime of $U/t \sim 10$ of the one-band Hubbard model is able to reproduce qualitatively the behavior of the experimentally observed magnetic susceptibility. Later we shall explain that, for this same regime of coupling, infrared experiments for the optical conductivity, as well as photoemission results, are also qualitatively reproduced. The intermediate-to-large regime of U/t seems the most promising for describing the cuprate materials using one-band electronic models.

2. Antiferromagnetism at finite doping

One of the most distinctive features of the cuprate superconductors is the presence of antiferromagnetism in the undoped compounds. The experimental evidence for this behavior has been widely discussed in the literature, and it is not the purpose of the present review to further analyze this issue. Instead, we shall center our attention on the more interesting, and less understood, study of antiferromagnetism in *doped* materials. Figure 31(a) shows single-crystal neutron-scattering results for the antiferromagnetic spin-correlation length as a function of Sr concentration in $La_{2-x}Sr_xCuO_4$ at low temperatures (Birgeneau *et al.*, 1988). The solid line is the function $3.8/\sqrt{x}$ Å, which roughly reproduces the data. This function corresponds to the average separation distance between holes (assuming them to be static). Since the Cu-Cu distance in the plane is about 3.8 Å, Fig. 31(a) shows that, at the optimal concentration $x \sim 0.15$ for this compound, the spin correlation is approximately 2.6 times the Cu-Cu distance. Then, antiferromagnetism is still strong in this regime and for this compound (while, for $YBa_2Cu_3O_7$, it may be weaker). However, the presence of incommensurate correlations in these compounds (to be discussed below) somewhat alters the results of Fig. 31(a). Actually, the correlation length, with the spin incommensurability taken into account, is shown in Fig. 31(b) (from Aeppli, 1992b). This correlation is larger than what was previously found by Birgeneau *et al.* (1988).

Several theoretical works have studied the degree of suppression of antiferromagnetism by the addition of holes to the t-J or Hubbard models at half-filling. For example, consider the dynamical spin structure function $S(\mathbf{Q},\omega)$ calculated for the t-J model on a 4×4 cluster at $J/t=0.4$, and several dopings (see Fig. 32, which was taken from Dagotto, Moreo, Ortolani, Poilblanc, and Riera, 1992; see also Bonča *et al.*, 1989b). The momentum is $\mathbf{Q}=(\pi,\pi)$. The sharp peak at low frequencies and doping corresponds to the spin-wave excitation which, at half-filling and in the bulk limit, becomes massless. The finite size of the cluster, plus the effect of doping, opens a gap in the spectrum corresponding to this momentum. For doing $x=0.25$, a considerable amount of spectral weight is transferred to large energies. For the quarter-filled system, $\langle n \rangle = 0.50$, the spin-wave peak has virtually disappeared. Then, these rough numerical results obtained on a small cluster show that the rapid reduction of antiferromagnetism with doping can be mimicked by simple models of spins and holes; and it is not at all surprising. The same result is expected for most models of high-T_c superconductors.

To make this discussion more quantitative, let us consider the results shown in Fig. 33, which were obtained by Furukawa and Imada (1992) using the projector Monte Carlo technique. The inverse of the static structure factor $S(\mathbf{Q})$ at $\mathbf{Q}=(\pi,\pi)$ is shown as a function of the hole density (denoted by δ in the figure) for the one-band Hubbard model at $U/t=4$, on clusters with up to 10×10 sites. Let us assume that the mean value of the

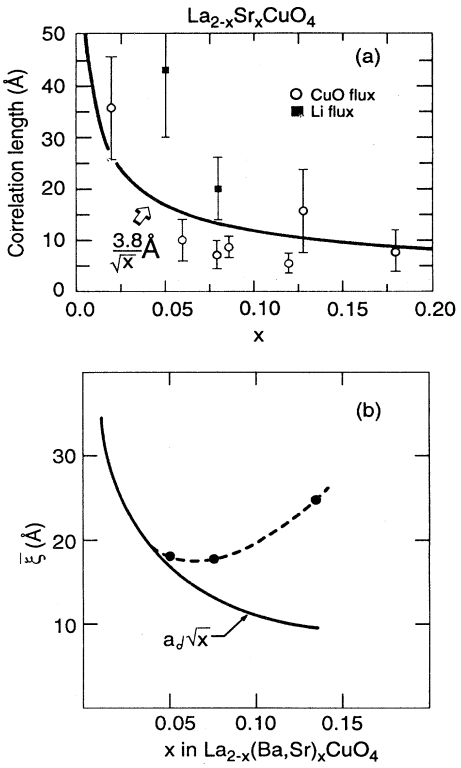

FIG. 31. (a) Antiferromagnetic correlation length vs temperature in $La_{2-x}Sr_xCuO_4$ (from Birgeneau *et al.*, 1988); (b) similar results with the presence of incommensurate correlations taken into account. The solid line is the fit, and the dashed line the experiments (Aeppli, 1992b).

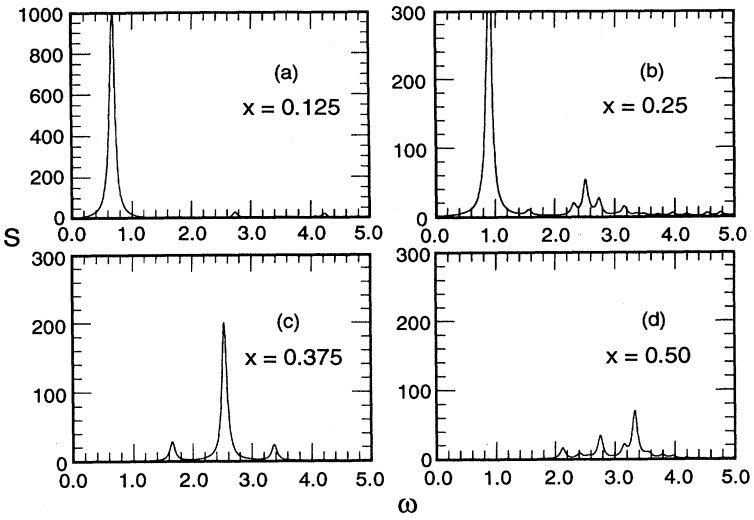

FIG. 32. $S=S(\mathbf{Q},\omega)$ [with $\mathbf{Q}=(\pi,\pi)$] as a function of frequency at $J/t=0.4$ for different doping fractions on a 4×4 cluster. The hole doping is (a) $x=0.125$; (b) $x=0.25$; (c) $x=0.375$; and (d) $x=0.50$. The units in the vertical axis are arbitrary. Results are taken from Dagotto, Moreo, Ortolani, Poilblanc, and Riera (1992).

spin correlation between spins located at the origin o and at site r is given by $\langle \mathbf{S}_o\cdot\mathbf{S}_r\rangle \sim e^{i\mathbf{Q}\cdot\mathbf{r}}e^{-r/\xi}$, where ξ is the spin-correlation length. Under this approximation, $S^{-1}(\mathbf{Q})$ should be roughly proportional to ξ^{-2} in two dimensions, and it should vanish in the bulk limit if there is long-range order. The Monte Carlo results of Fig. 33 suggest that as soon as doping is introduced, the long-range order disappears, and the spin-correlation length becomes finite. The approximate linear dependence observed in Fig. 33 implies that $\xi\sim1/\sqrt{x}$, in good agreement with experiments (Fig. 31). It would be interesting to verify these results using a larger value of the coupling U/t in order to work in a regime closer to that of the cuprate superconductors, namely, $U/t=8-10$. Unfortunately, Monte Carlo techniques at finite doping and on large clusters are not able to reach low temperatures, mainly due to the sign problem.

Finally, it is interesting to note that the influence of doping in the antiferromagnetic correlations is nonuniversal between hole- and electron-doped materials.

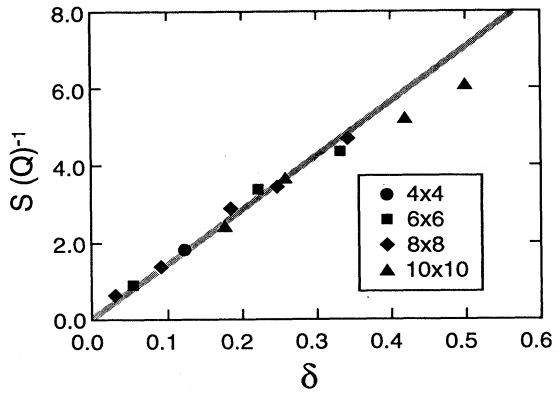

FIG. 33. Inverse of the static spin structure factor as a function of doping δ for a one-band Hubbard model at $U/t=4$ and several clusters. The technique used is the projector Monte Carlo. Results are taken from Furukawa and Imada (1992).

Single-crystal neutron-scattering measurements on $Nd_{2-x}Ce_xCuO_4$ by Thurston *et al.* (1990) have shown that the 3D antiferromagnetic order persists even with x as high as 0.14, while on $La_{2-x}Sr_xCuO_4$ a doping of $x\sim0.02$ is enough to destroy the long-range order. This difference can be attributed to several factors, but there is one that is very important: carriers in electron-doped materials seem to reside in Cu ions, while carriers in hole-doped materials reside on oxygen ions. As shown by Manousakis (1992), a study of the Heisenberg model with *static* randomly distributed holes shows a dependence of the antiferromagnetic spin-correlation function that reproduces better the results for $Nd_{2-x}Ce_xCuO_4$ than those for $La_{2-x}Sr_xCuO_4$, suggesting that the former loses antiferromagnetism through a dilution process (see also Gooding and Mailhot, 1991; Paul and Mattis, 1991).

3. Incommensurate spin order in doped materials

Neutron-scattering experiments have shown that $La_{2-x}Sr_xCuO_4$ with $x=0.075$ and $x=0.14$ presents incommensurate spin fluctuations. Figure 34 shows the results reported by Cheong *et al.* (1991) as a function of momentum for the two concentrations mentioned before (for a review, see Aeppli, 1992b). The splitting of the peak at (π,π) indicates the presence of incommensurability. It is important to note that the splitting was observed along the line joining momentum (π,π) with $(0,\pi),(\pi,0)$ in a notation corresponding to a two-dimensional square lattice. Cheong *et al.* (1991) also reported a *finite* (although large) spin-correlation length, suggesting that the incommensurate correlations in this material are of short range (while recent studies of the three-dimensional Mott-Hubbard system $V_{2-y}O_3$ show the presence of a static incommensurate order). Mason, Aeppli, and Mook (1992) showed that the incommensurate peaks in the cuprates are suppressed below T_c. Is the presence of these incommensurable correlations a

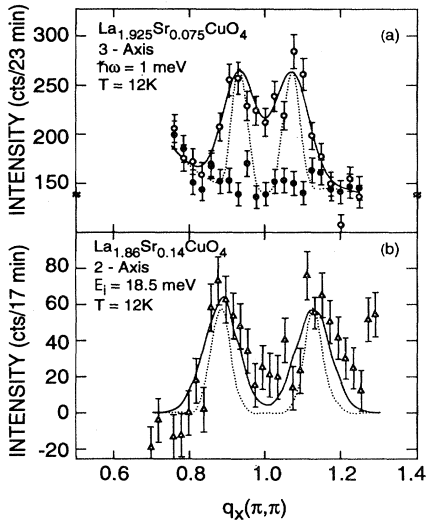

FIG. 34. Neutron-scattering experiment results for $La_{2-x}Sr_xCuO_4$ at two different Sr concentrations. For details, see Cheong *et al.* (1991).

universal feature of all high-T_c compounds? Tranquada *et al.* (1992) recently reported results for $YBa_2Cu_3O_{6+x}$. The claim is that separate peaks cannot be resolved, but the data are consistent with four unresolved incommensurate peaks similar to those reported in the lanthanum compounds. On the other hand, electron-doped materials $Nd_{2-x}Ce_xCuO_4$ analyzed by Thurston *et al.* (1990) showed *no* indications of incommensurability, adding more evidence against universality between hole- and electron-doped materials, at least with respect to their magnetic properties.

Can we understand the presence of these incommensurate correlations with simple electronic models? Hartree-Fock calculations have been presented for the one-band Hubbard model at large (Poilblanc and Rice, 1989) and small (Schulz, 1990a) coupling U/t. These studies predict the existence of locally stable solutions of the self-consistent equations consisting of line defects (solitons) in the antiferromagnetic order parameter. These solutions provide low-energy modes for the holes which are trapped in the solitons. For small U/t, the "charged" lines of defects are aligned along the crystal axes, while for large U/t they align along the diagonal (1,1) directions (contrary to experiments). Then, weak-coupling Hartree-Fock calculations seem in agreement with experiments. A "spiral" state has also been discussed by Shraiman and Siggia (1988b), which has incommensurate correlations produced by the movement of the holes (see also Frenkel *et al.*, 1990; Gooding, 1991; Gooding and Mailhot, 1993; Klee and Muramatsu, 1993; Kübert and Muramatsu, 1993). Furukawa and Imada (1992) argue that perturbation theory can explain the presence of incommensurability in the Hubbard model. Tanamoto, Kohno, and Fukuyama (1992, 1993a, 1993b) have developed a mean field for the t-J model that reproduces the experimental results. Psaltakis and Papanicolaou (1993) found a spiral phase in the t-J model using a $1/N$ expansion.

While Hartree-Fock results are suggestive, it is important to verify whether they correspond to the solution of minimum energy of the models under study using more powerful and unbiased techniques. In Fig. 35, results are shown for the one-band Hubbard model using quantum Monte Carlo as discussed by Moreo, Scalapino, *et al.* (1990). The static spin structure factor $S(\mathbf{Q})$ is presented for several fermionic densities (with $\langle n \rangle = 1$ corresponding to half-filling) on an 8×8 cluster, $U/t=4$ and $T=t/6$. The Monte Carlo results suggest that commensurate antiferromagnetism is suppressed when the fermionic density is reduced away from half-filling, and that weak short-range incommensurate correlations develop as the doping increases. Similar results were also obtained independently by Imada and Hatsugai (1989) and by Furukawa and Imada (1992) using a projector Monte Carlo method. Their results for $S(\mathbf{Q})$ are shown in Fig. 36(a), which was obtained at $U/t=4$ and

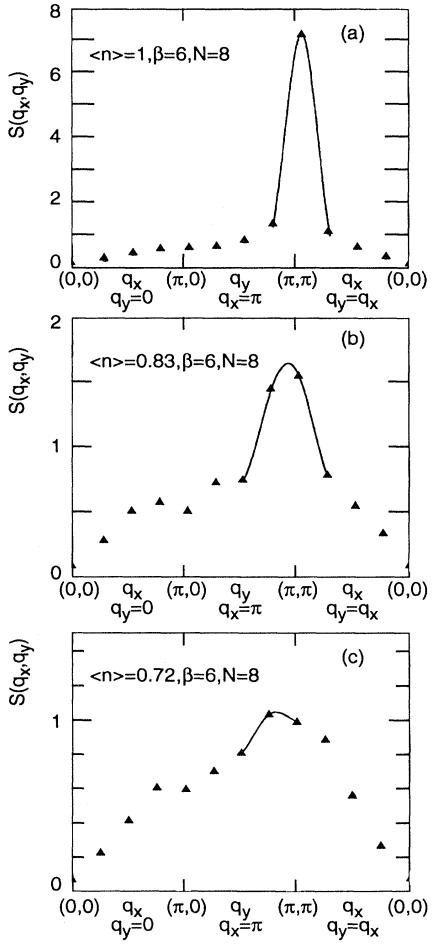

FIG. 35. Spin structure factor on an 8×8 cluster with $U/t=4$, $\beta=6/t$, and several densities. The solid line is there to guide the eyes. Results taken from Moreo, Scalapino *et al.* (1990).

$\langle n \rangle = 0.82$. The incommensurability is clearly observed in the figure. It would be desirable to obtain results at larger couplings U/t, but Monte Carlo methods have numerical instabilities in this regime. Unfortunately, t-J model calculations on large clusters are not available either, since a good Monte Carlo technique for this model has not been developed. However, the Lanczos algorithm can be applied to this model. Figure 36(b) shows $S(\mathbf{Q})$ calculated by Moreo, Dagotto, *et al.* (1990) on a 4×4 cluster at zero temperature and at a realistic value of the coupling $J/t = 0.2$. Again, a shift from momentum (π,π) is observed as a function of the number of holes. Then, we conclude that the presence of incommensurate (short-range) correlations seems a general feature of several models of correlated electrons, although we still do not have a clear, intuitive understanding of its origin.

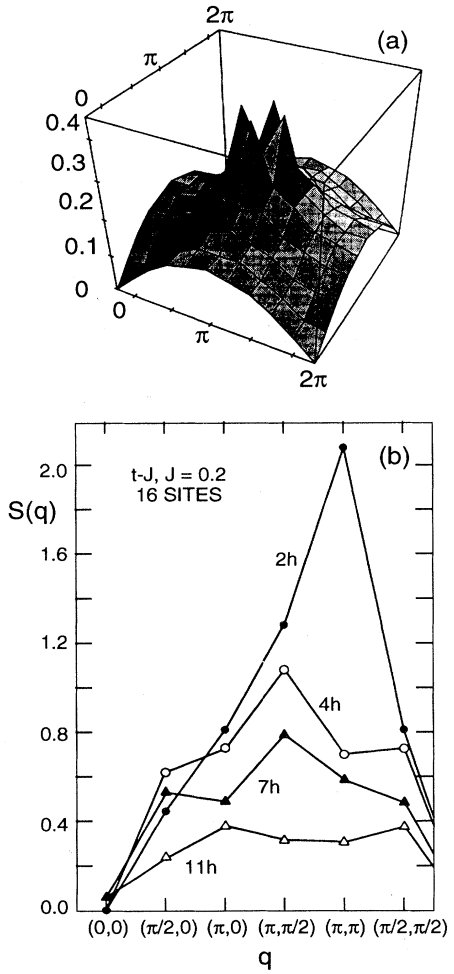

FIG. 36. (a) Equal-time spin correlation in momentum space on 10×10 lattices for 41 up- and down-spin fermions each (from Furukawa and Imada, 1992); (b) spin structure factor as a function of momentum for the 4×4 cluster and different numbers of holes (2, 4, 7, and 11; from Moreo, Dagotto, *et al.*, 1990).

B. Optical conductivity

Since the early days of high-T_c superconductors, attempts have been made to identify the superconducting gap and other special features responsible for the pairing mechanism, using the same infrared spectroscopy techniques that were successful in the analysis of classical low-temperature superconductors. However, it became clear, also from the beginning, that the infrared properties of the new superconductors were extremely complicated. Actually, it is not even clear if the superconducting gap has been properly identified using these techniques. This section consists of two parts. First, we shall attempt to summarize the vast experimental literature on infrared experiments closely following the excellent reviews on this subject by Timusk and Tanner (1989; Tanner and Timusk, 1992). Since different plots will be presented in different units, it is convenient to remember that

$$1\ \text{eV} = 8063\ \text{cm}^{-1} = 11\,600\ \text{K}\ . \tag{4.1}$$

The main conclusions of this first part will be the following: (i) Upon doping, weight appears inside the charge-transfer gap of the undoped compounds, defining the so-called midinfrared band; and (ii) the conductivity decays as $\sim 1/\omega$ at low energies instead of the behavior expected for free carriers, namely, $1/\omega^2$. The origin of the midinfrared band is still unclear. Some experimental authors attribute it in part to trapped holes near dopant atoms, while others claim that the Cu-O chains of the $YBa_2Cu_3O_{6+x}$ family originate most of this weight, at least for these particular compounds.

After the experimental results are summarized, we shall describe the present status of numerical studies of the optical conductivity in electronic models that may be of relevance for high-T_c materials. It is claimed that after a considerable effort by several groups, a consistent picture is emerging which suggests that the midinfrared band may be caused, at least in part, by the spin excitations that surround (i.e., renormalize) the hole carriers. The anomalous $1/\omega$ behavior can be mimicked by a perverse combination of the oscillator strength at the far-infrared $\omega\sim0$ and the spectral weight located at midinfrared energies, as some examples show. Finally, it is concluded that the unusual behavior of $\sigma(\omega)$ may not be correlated with the presence of superconductivity in a given material or model, and should be a general feature of strongly interacting electronic systems.

1. Experimental results

As described in Sec. I.A.1, $La_{2-x}Sr_xCuO_4$ is perhaps the simplest of the cuprate superconductors, since it has only one Cu-O plane per unit cell. Its carrier concentration can be varied over a wide range, $0 \le x < 0.3$, allowing a systematic study of the transitions from an antiferromagnetic insulator to a superconductor, and then, in-

creasing further the doping, to an "anomalous" metallic state. While the many early experimental studies of optical properties of this material were carried out on ceramic samples (Doll *et al.*, 1988, and references therein), good quality crystals (large and homogeneously doped) have recently been grown. In particular, Uchida *et al.* (1991) have measured the reflectance of $La_{2-x}Sr_xCuO_4$ for several dopings between $x=0$ and $x=0.34$, at room temperature (see also Shimada, Shimizu, *et al.*, 1992). The optical conductivity can be obtained after a Kramers-Kronig analysis of the reflectance. Their main result for the real part of the optical conductivity $\sigma_1(\omega)$ is shown in Fig. 37(a), which was obtained at 300 K. The undoped crystal in the figure ($x=0$) shows a negligible conductivity below 1 eV, in rough agreement with the expectation of a charge-transfer gap of about 2 eV for this insulating compound. With hole doping, the intensity above the gap is reduced and new features appear in the region around and below 1.5 eV; i.e., a transfer of weight from above the gap to lower energies seems to occur. In the lightly doped case (say, $x=0.02$), a clear feature centered about $\omega\sim 0.5$ eV appears. This is the famous midinfrared (MIR) band, which has been observed in several other cuprate superconductors and was discovered in the early days of high T_c in polycrystalline samples (Herr *et al.*, 1987; Orenstein *et al.*, 1987). At this doping, the

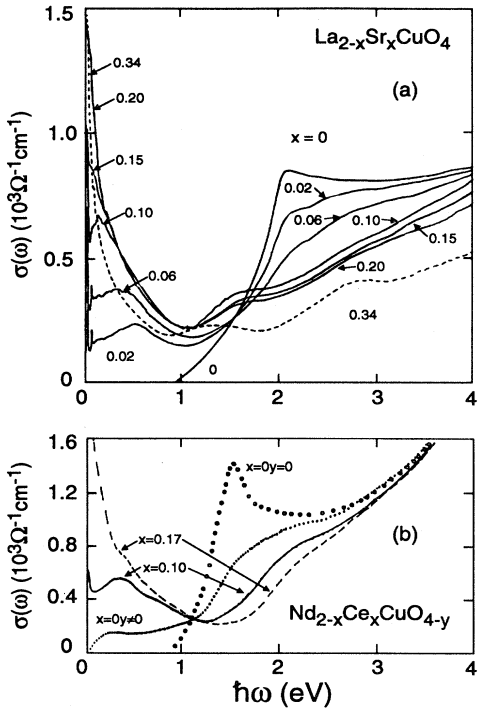

FIG. 37. (a) Optical conductivity of $La_{2-x}Sr_xCuO_4$ at 300 K vs energy. Data are shown parametric with the Sr concentration x, in the interval $0\le x\le 0.34$ (from Uchida *et al.*, 1991). (b) Optical conductivity of $Nd_{2-x}Ce_xCuO_{4-y}$ (at room temperature) vs energy, parametric with Ce concentrations between 0.0 and 0.20 (from Uchida *et al.*, 1991).

far-infrared signal near $\omega\sim 0$ is small and difficult to see in the graph, suggesting that the MIR and free-carrier absorptions are independent features in this material. With increased doping, the far infrared conductivity quickly grows, and at dopings larger than $x\sim 0.20$, it entirely masks the MIR band, which does not change as rapidly with doping.[8] At small frequencies the conductivity decays much more slowly than the Drude-type $1/\omega^2$ behavior expected for free carriers.

What happens in other materials? We have already discussed that electron-doped materials, like $Nd_{2-x}Ce_xCuO_4$, are structurally very similar to $La_{2-x}Sr_xCuO_4$. It has been found that their optical conductivities are also qualitatively similar [see Fig. 37(b), which is taken from Uchida *et al.*, 1991]. A MIR structure is clearly present near $\omega\sim 0.4$ eV for the $x=0.10$ sample. With increased doping, the MIR absorption merges with the low-frequency free-carrier absorption, as it occurs in the lanthanum compounds. Again, below 1 eV, the results for $\sigma_1(\omega)$ cannot be fit with a free-carrier law $1/\omega^2$. Other compounds of the same family can be obtained by replacing Nd with Pr. The optical properties of $Pr_{2-x}Ce_xCuO_4$ have been investigated (Cooper *et al.*, 1990) and the reported results are very similar to those of $Nd_{2-x}Ce_xCuO_4$.

Let us now consider $YBa_2Cu_3O_{6+x}$. This material has been widely analyzed experimentally, since good crystals with a very sharp superconducting transition at T_c can be prepared. However, it presents complications that are absent in simpler compounds like $La_{2-x}Sr_xCuO_4$. In particular, $YBa_2Cu_3O_{6+x}$ has Cu-O chains, which contribute substantially to $\sigma_1(\omega)$, and two Cu-O planes per unit cell. These features have to be taken into account when a theoretical description of this particular material is attempted. Figure 38(a) shows $\sigma_1(\omega)$ for the stoichiometric compound $YBa_2Cu_3O_7$ as measured by Kamarás *et al.* (1990) at several temperatures. The far infrared region depends strongly on temperature, especially below T_c, while the region above ~ 800 cm^{-1} is temperature independent. There is a clear minimum at $\sim 400-500$ cm^{-1} that can be easily seen at low temperatures but also exists above T_c. It has been argued that it may be caused by the coupling between the midinfrared carriers and phonons (Timusk and Tanner, 1989). Figure 38(b) shows the conductivity at a fixed temperature of 100 K for different oxygen compositions (and thus for samples with different values of T_c), taken from Orenstein *et al.* (1990). The 30-K material has a weak midinfrared and an onset of charge-transfer absorption at

[8]For theorists it is interesting to notice that the d.c. resistivity ρ_{dc} and the far-infrared resistivity $\rho_{fir}=\sigma^{-1}(\omega\to 0)$ obtained from the optical conductivity differ in this material by about a factor of 2, perhaps due to the experimental uncertainties of both methods. Care must then be taken when detailed quantitative comparisons between theory and experiment are attempted.

$\omega \sim 12\,000$ cm^{-1}. With an increase in the content of oxygen, the MIR absorption increases and shifts to lower energies. The minimum at ~ 400 cm^{-1} mentioned before can also be seen in these crystals.

What is the behavior of the optical conductivity in other cuprate superconductors? Let us now consider the so-called BISCCO family. $\sigma_1(\omega)$ for $Bi_2Sr_2CaCu_2O_8$ has been reported by Romero *et al.* (1992) using transmission measurements and a Kramers-Kronig analysis. This is a material of two Cu-O layers, similar to YBCO but without the one-dimensional chains. The results are shown in Fig. 39(a). In this material it was observed that (1) above ~ 300 cm^{-1} the decrease in the conductivity above T_c is closer to $1/\omega$ than the $1/\omega^2$ expected from free carriers, and (2) at high frequencies the temperature dependence is much weaker than at small frequencies. Then, this compound also seems to display the same non-Drude behavior as the other high-T_c materials.

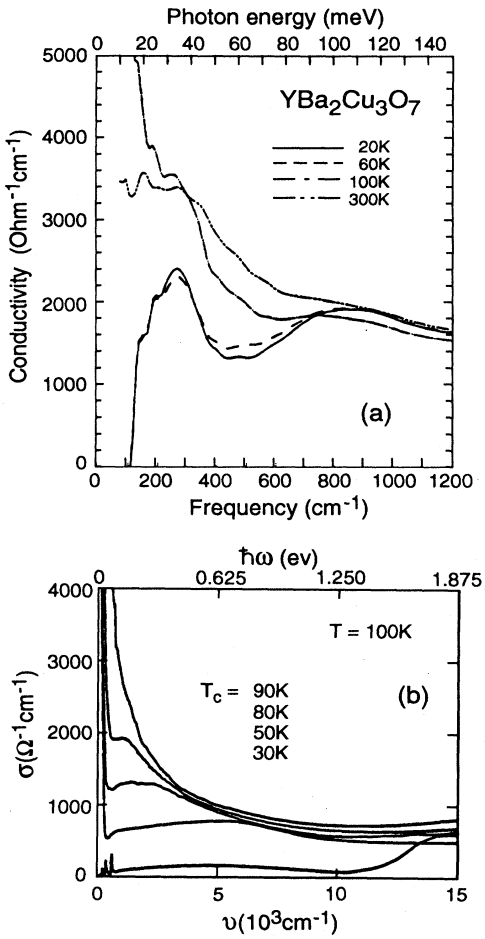

FIG. 38. (a) Optical conductivity as a function of frequency of a $Tc = 91$ K film of $YBa_2Cu_3O_{7-\delta}$ at several temperatures (from Kamarás *et al.*, 1990); (b) optical conductivity of four crystals of $YBa_2Cu_3O_{7-\delta}$ at 100 K. δ ranges from ~ 0.8 for the lowest curve to ~ 0 for the highest one (from Orenstein *et al.*, 1990; see also Thomas *et al.*, 1988).

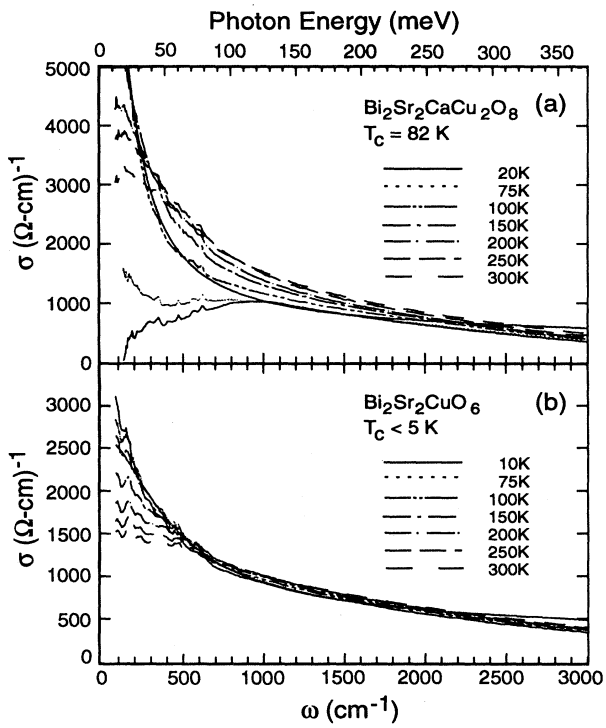

FIG. 39. (a) Optical conductivity of $Bi_2Sr_2CaCu_2O_8$ between 20 and 300 K (from Romero *et al.*, 1993); (b) frequency-dependent conductivity of $Bi_2Sr_2CuO_6$ between 10 and 300 K (from Romero *et al.*, 1993).

Compounds of the same Bi family, but which are *not* high-T_c superconductors, like $Bi_2Sr_2CuO_6$ (T_c less than 5 K), also present a behavior qualitatively similar to that of BISCCO above T_c [Fig. 39(b)]. From this study it can be inferred that the non-Drude optical behavior is mainly produced by holes in the CuO_2 planes, and it is not necessarily related to the appearance of a superconducting transition. Several other materials present an analogous behavior. For example, the compound $Tl_2Ba_2CaCu_2O_8$ has been analyzed (Foster *et al.*, 1990; Shimada, Mizuno, *et al.*, 1992), as well as $Pb_2Sr_2LCu_3O_8$, with L being a rare earth (Reedyk *et al.*, 1992). Both present a robust MIR band absorption.

Photoinduced absorption experiments have also shown the presence of a midinfrared band in the cuprate superconductors. Kim *et al.* (1987) reported results for $La_{2-x}Sr_xCuO_4$, while Nd_2CuO_4 was analyzed by Yu *et al.* (1992), and $YBa_2Cu_3O_{6+x}$ by Nieva *et al.* (1993). In all of them, the presence of spectral weight in the MIR region was observed. There is, then, a qualitative agreement between experiments carried out by adding holes chemically, or by photoexcitation.

How can we understand the presence of the MIR band in these compounds? A detailed study by Thomas (1991) and co-workers (Thomas *et al.*, 1992) on some insulating materials with vacancies suggests that this band may be caused in part by trapped holes near dopant sites [see Fig. 40(a)]. Let us concentrate on the electron-doped

Nd_2CuO_{4-y} compound. Since no Ce atoms have been added, there are no carriers and the system is insulating. However, the removal of oxygen induces vacancies which seem to produce an interesting structure in $\sigma_1(\omega)$. There are two clear, broad peaks in the experimental results. Thomas *et al.* (1992) argued that the lower energy peak E_J may be produced by the interaction with light of an electron captured in a bound state by the vacancy. Its movement costs energy because it disturbs the antiferromagnetic background of spins in a picture very similar to that of the "string" excitations described in Sec. III.B.1. Then, the peak E_J is associated with an excited state of a trapped hole. The second peak, E_I, may be produced by the ionization energy of this trapped electron (perhaps there are other bound states between E_J and E_I that are difficult to resolve). This analysis suggests that the midinfrared absorption can be partially accounted for by bound-state processes, and is not all due to free carriers (however, see Millis and Shraiman, 1992). Recent work by Cooper *et al.* (1993) supports these claims. However, it is not clear whether 100% of the MIR weight is caused by trapped holes. In the case of the $YBa_2Cu_3O_{6+x}$ compounds, it has been argued that chains produce a substantial contribution to the MIR band (Schlesinger *et al.*, 1990). Actually, Cooper *et al.* (1993) have recently shown that the MIR band can no longer be resolved in $YBa_2Cu_3O_{6+x}$ with $x=0.6$ and 1.0, once the chain contribution has been subtracted [see Fig. 40(b)]. Again, it is not clear that 100% of the MIR band is actually caused by the chains.

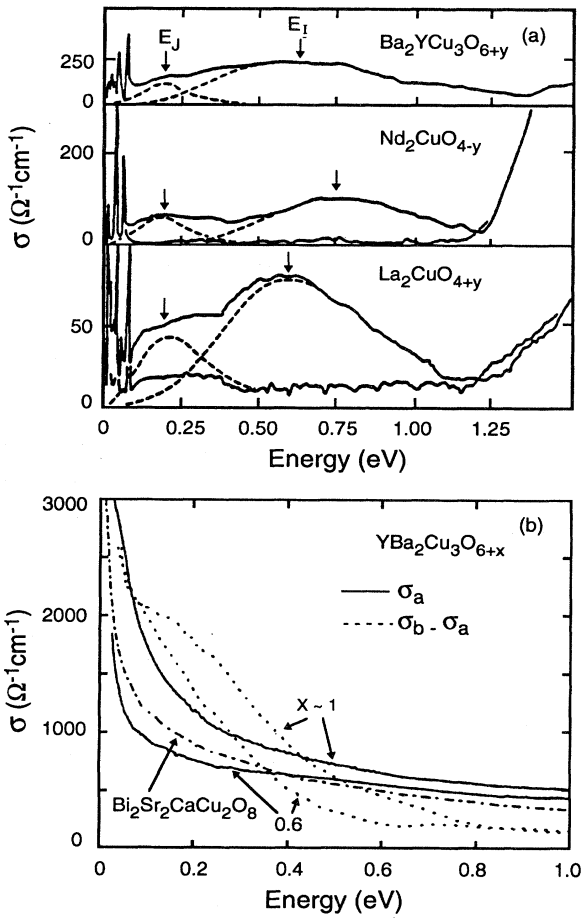

FIG. 40. (a) Optical conductivity in the midinfrared region of semi-insulating $YBa_2Cu_3O_{6+y}$ (upper panel), Nd_2CuO_{4-y} (center panel), and La_2CuO_{4+y} (lower panel). E_J and E_I are peaks discussed in the text (from Thomas *et al.*, 1991). (b) Real part of the optical conductivity below 1 eV in the CuO_2 planes [$=a$ axis] of single-domain $YBa_2Cu_3O_{6+x}$ (solid lines), compared with an estimate of the conductivity associated with the CuO chains [$=\sigma_b-\sigma_a$] (dotted lines). The dashed-dotted line is the conductivity of $Bi_2Sr_2CaCu_2O_8$ (from Cooper *et al.*, 1993).

Finally, in this short summary of experimental results for the optical conductivity of the cuprate materials, we shall *not* discuss the important issue of whether the superconducting gap has been observed using infrared techniques. The reason is that experimentally the answer is not clear. It is believed that, due to the small coherence length of the cuprates below T_c, the materials are in the extreme clean limit, and thus the gap feature in the conductivity should be difficult to observe. It has also been argued that the signal may be lost in the strong midinfrared conductivity region. Actually, the conductivity seems finite down to 150 cm^{-1}, and thus no definite answer to the presence of a superconducting gap in the high-T_c materials has been reported thus far (Tanner and Timusk, 1992).

2. Theoretical analysis of $\sigma(\omega)$

Here, we shall review the status of some theoretical studies of optical properties of models related to high-T_c superconductors. In particular, we shall concentrate on the response to an external field of an interacting system of electrons evaluated using numerical methods. A closed formula for the intensity of the Drude peak in $\sigma(\omega)$ will be derived as a special case of a more general equation. This derivation follows closely that given by Shastry and Sutherland (1990) and by Scalapino, White, and Zhang (1992).[9] Most of the results for $\sigma(\omega)$, discussed in Sec. IV.B.3, have been obtained using computational techniques, due to the difficulty in obtaining analytical information on models of correlated electrons when the interactions are strong.

As an example, we shall consider electrons described by the Hubbard model coupled to an external classical vector potential $A_l(\mathbf{r},t)$, where $\mathbf{r}$ denotes a site of the two-dimensional lattice, t is time, and l's are unit vectors in the lattice axes directions. The gauge-invariant way to couple particles on a lattice with a U(1) gauge field is by

[9]The help of Fabio Ortolani in some subtle parts of the calculation is acknowledged.

introducing phase factors in the kinetic-energy hopping term, i.e.,

$$\hat{H}=\hat{H}_0+\hat{V}$$
$$=-t\sum_{\mathbf{r},l,\sigma}[c^{\dagger}_{\mathbf{r}\sigma}c_{\mathbf{r}+l\sigma}e^{ieA_l(\mathbf{r},t)}+c^{\dagger}_{\mathbf{r}+l\sigma}c_{\mathbf{r}\sigma}e^{-ieA_l(\mathbf{r},t)}]$$
$$+U\sum_{\mathbf{r}}n_{\mathbf{r}\uparrow}n_{\mathbf{r}\downarrow}\ , \tag{4.2}$$

where we have set $\hbar=c=a=1$ (a is the lattice spacing) and the rest of the notation is standard. The phase factors "live" on the links of the lattice defined by sites $\mathbf{r}$ and $\mathbf{r}+l$. $\hat{H}_0$ is defined as the Hubbard Hamiltonian in the absence of a vector field but including the electron-electron interactions, while $\hat{V}$ contains the field dependence, and it vanishes when $A_l(\mathbf{r},t)=0$. Expanding in powers of the electric charge e, it can be easily shown that

$$\hat{V}=-e\sum_{\mathbf{r},l}\hat{j}_l(\mathbf{r})A_l(\mathbf{r},t)-\frac{e^2}{2}\sum_{\mathbf{r},l}\hat{K}_l(\mathbf{r})A_l^2(\mathbf{r},t)+\cdots\ , \tag{4.3}$$

where the "paramagnetic" current-density operator in the l direction is defined as $\hat{j}_l(\mathbf{r})=it\sum_{\sigma}(c^{\dagger}_{\mathbf{r}\sigma}c_{\mathbf{r}+l\sigma}-c^{\dagger}_{\mathbf{r}+l\sigma}c_{\mathbf{r}\sigma})$, and the operator $\hat{K}_l(\mathbf{r})$ is the kinetic-energy density also in the l direction, i.e., $\hat{K}_l(\mathbf{r})=-t\sum_{\sigma}(c^{\dagger}_{\mathbf{r}\sigma}c_{\mathbf{r}+l\sigma}+c^{\dagger}_{\mathbf{r}+l\sigma}c_{\mathbf{r}\sigma})$. The linear-response current is thus given by

$$\hat{J}_l(\mathbf{r},t)=-\frac{\partial\hat{H}}{\partial A_l(\mathbf{r},t)}=e\hat{j}_l(\mathbf{r})+e^2\hat{K}_l(\mathbf{r})A_l(\mathbf{r},t)+\cdots\ , \tag{4.4}$$

where the first term is the paramagnetic current density, and the second corresponds to the diamagnetic contribution.

The next step in the calculation of $\sigma(\omega)$ for the Hubbard model is to evaluate the mean value of the total current operator $\hat{J}_l(\mathbf{r},t)$ in the ground state of the Hamiltonian. As a starting point, let us derive the expectation value of an arbitrary time-dependent operator $\hat{O}(t)$ in the ground state of a given system. Following well-known steps described in several textbooks (see, for example, Fetter and Walecka, 1971) and working at first order in the external field contained in $\hat{V}$, it is possible to show that the following approximation holds,

$$\langle\psi(t)|\hat{O}(t)|\psi(t)\rangle=\langle\phi_0|\hat{O}|\phi_0\rangle+i\int_{-\infty}^{t}dt_1[e^{iE_0(t_1-t)}\langle\phi_0|\hat{V}e^{-i\hat{H}_0(t_1-t)}\hat{O}|\phi_0\rangle-e^{iE_0(t-t_1)}\langle\phi_0|\hat{O}e^{-i\hat{H}_0(t-t_1)}\hat{V}|\phi_0\rangle]+\cdots\ . \tag{4.5}$$

In the derivation of Eq. (4.5), we made explicit use of the definition of an operator in the interaction representation, i.e., $\hat{O}(t)=e^{i\hat{H}_0t}\hat{O}e^{-i\hat{H}_0t}$, and the time evolution of a state which is given by

$$|\psi(t)\rangle=\hat{T}\exp\left[-i\int_{-\infty}^{t}dt_1\hat{V}(t_1)\right]|\phi_0\rangle$$

(where $\hat{T}$ is the time-ordering operator, and $|\phi_0\rangle$ is the ground state of the fully interesting system in the *absence* of the external field, which has an energy E_0).

Let us now specialize Eq. (4.5) to our problem; i.e., consider $\hat{O}(t)=\hat{J}_l(\mathbf{r},t)$. Defining the Fourier transformation of the vector field as $A_l(\mathbf{r},t)=\int_{-\infty}^{+\infty}d\omega\,A_l(\mathbf{r},\omega)e^{-i\omega t}$ [with a similar definition for the transformation of the current $\langle\hat{J}_l(\mathbf{r},\omega)\rangle$], and after tedious but straightforward algebra, it can be shown that

$$\langle\hat{J}_x(\mathbf{r},\omega)\rangle=e^2\langle\hat{K}_x\rangle A_x(\mathbf{r},\omega)+ie^2\sum_{\mathbf{r}'}\int_0^{\infty}d\tau\langle\phi_0|[\hat{j}_x(\mathbf{r})e^{-i(\hat{H}_0-E_0-\omega)\tau}\hat{j}_x(\mathbf{r}')-\hat{j}_x(\mathbf{r}')e^{i(\hat{H}_0-E_0+\omega)\tau}\hat{j}_x(\mathbf{r})]|\phi_0\rangle A_x(\mathbf{r}',\omega)\ , \tag{4.6}$$

where (1) the gauge field has been specialized to the x direction [$A_l(\mathbf{r},t)=\delta_{l,x}A_x(\mathbf{r},t)$]; (2) the paramagnetic current in the ground state without external fields is assumed to vanish ($\langle\phi_0|\hat{j}_l(\mathbf{r})|\phi_0\rangle=0$); (3) the change of variables $t-t_1\rightarrow-\tau, t\rightarrow t$ was carried out; and (4) the notation $\langle\hat{K}_x\rangle=\langle\phi_0|\hat{K}_x(\mathbf{r})|\phi_0\rangle$ was introduced, since this mean value is site independent in the ground state of the Hubbard model defined on a cluster with periodic boundary conditions. Equation (4.6) can be further simplified by working in momentum space. Defining the spatial Fourier transformed as

$$A_x(\mathbf{r},\omega)=\frac{1}{N}\sum_{\mathbf{q}}A_x(\mathbf{q},\omega)e^{i\mathbf{q}\cdot\mathbf{r}}$$

and applying the operatorial identity $\int_0^{\infty}dx\,e^{i\hat{a}x-\epsilon x}=i/(\hat{a}+i\epsilon)$ (where ϵ is a constant, and $\hat{a}$ an arbitrary operator), we arrive at a *general* equation for the response of the total current to an arbitrary, but small, vector field in the x direction,

$$\langle \hat{J}_x(\mathbf{q},\omega)\rangle = e^2\langle \hat{K}_x\rangle A_x(\mathbf{q},\omega) + e^2\left[\frac{1}{N}\langle\phi_0|\hat{j}_x(-\mathbf{q})\frac{1}{\hat{H}_0-E_0+\omega+i\epsilon}\hat{j}_x(\mathbf{q})|\phi_0\rangle + \frac{1}{N}\langle\phi_0|\hat{j}_x(\mathbf{q})\frac{1}{\hat{H}_0-E_0-\omega-i\epsilon}\hat{j}_x(-\mathbf{q})|\phi_0\rangle\right] A_x(\mathbf{q},\omega)\ . \tag{4.7}$$

ϵ is a small parameter introduced to regularize the poles that will appear at particular values of the frequency.

Now, let us study the special case of the response to an electric field defined by $A_x(\mathbf{q}=0,\omega)=E_x(\mathbf{q}=0,\omega)/(i\omega-\delta)$, where δ is a small number. We consider zero momentum, since we are interested in a *uniform* electric field (a pure magnetic field will be analyzed in Sec. IV.E.4 when superfluidity is discussed). In linear-response theory the conductivity is defined through the relation $\langle \hat{J}_x(\mathbf{q}=0,\omega)\rangle = \sigma_{xx}(\omega)E_x(\mathbf{q}=0,\omega)$. It can be shown by using Eq. (4.7) that the *real* part of the conductivity for $\omega>0$ is equal to

$$\sigma_1(\omega)=\mathrm{Re}\sigma_{xx}(\omega)=D\delta(\omega)+\frac{e^2\pi}{N}\sum_{n\neq 0}\frac{|\langle\phi_0|\hat{j}_x|\phi_n\rangle|^2}{E_n-E_0}\delta(\omega-(E_n-E_0))\ , \tag{4.8}$$

where the so-called Drude weight D is given by

$$\frac{D}{2\pi e^2}=\frac{\langle -\hat{T}\rangle}{4N}-\frac{1}{N}\sum_{n\neq 0}\frac{|\langle\phi_0|\hat{j}_x(q_x=0,q_y=0)|\phi_n\rangle|^2}{E_n-E_0}\ , \tag{4.9}$$

and $\langle \hat{T}\rangle$ $(=2N\langle \hat{K}_x\rangle)$ is the total kinetic energy of the problem in two dimensions. To derive Eq. (4.8), we introduced a complete basis $I=\sum_n |\phi_n\rangle\langle\phi_n|$, and we also used the well-known identity $1/(u+i\epsilon)=P(1/u)-i\pi\delta(u)$, valid in the limit of small ϵ, where P denotes the principal part, and u is a real number. Note the important detail that the real part of the conductivity contains a delta function at zero frequency, which is produced by the "free" acceleration of the quasiparticles. For a system with periodic boundary conditions, Kohn (1964) showed that D can be used as an order parameter for metal-insulator transitions. Actually, it can be shown that for an insulator, D converges exponentially to zero with increasing lattice size, while for a metal it converges to a nonzero constant, which implies *zero* resistance in the ground state. This is not surprising, since in the Hubbard model there is no dissipative mechanism (unless disorder is introduced). A model where $D\neq 0$ can correspond to a perfect metal or a superconductor, showing that the vanishing of the resistivity in the ground state is only a necessary condition for achieving superconductivity, but is not sufficient. This point will be discussed in more detail in Sec. IV.E.4. It is also interesting to note that only *interacting* fermions on a *lattice* can have a metal-insulator transition, signaled by the vanishing of the Drude weight. In the continuum or for lattice free fermions, $[\hat{j}_x,\hat{H}]=0$, and thus all the weight of the conductivity is concentrated at zero frequency. Actually, for noninteracting carriers in the continuum, the well-known Drude formula is recovered from Eq. (4.9), namely,

$$\sigma_1(\omega)=\frac{ne^2\pi}{m}\delta(\omega)\ , \tag{4.10}$$

where $n=N_e/N$ is the density of carriers, N_e is the number of particles, and $m=1/(2t)$ their mass. In deriving Eq. (4.10), we have assumed a *low* density of particles, each carrying an energy approximately given by $(-4t)$ as it occurs in the noninteracting Hubbard model at the bottom of the band.

By integrating in ω both terms of Eq. (4.8), we can easily arrive at the well-known sum rule (Maldague, 1977) relating the total weight of $\sigma_1(\omega)$ with the mean value of the kinetic energy in the ground state,[10]

$$\int_0^\infty d\omega\,\sigma_1(\omega)=\frac{\pi e^2}{4N}\langle -\hat{T}\rangle\ . \tag{4.11}$$

At a given coupling, $\langle -\hat{T}\rangle$ is in principle a function of the fermionic density, but near half-filling it changes smoothly with $\langle n\rangle$. Then, in several cases it is a good approximation to assume that the spectral weight in $\sigma(\omega)$ is conserved upon doping, and thus it can only be redistributed [however, the larger the coupling U/t, the worse is this approximation, as shown below in Fig. 44(a)].

3. Numerical results

After setting up the formalism to calculate $\sigma(\omega)$ in models of correlated electrons, it is necessary to find a reliable technique to evaluate the complicated matrix elements appearing in Eq. (4.8). In this review we shall mainly describe calculations performed with the help of computers, since they can provide unbiased and fairly accurate estimates of several physical quantities. Unfortunately, the computational analysis of $\sigma_1(\omega)$ is by no means simple. Quantum Monte Carlo methods cannot handle the evaluation of dynamical ω-dependent quantities, since in this technique calculations are performed in imaginary time. Analytic continuations from imaginary to real time have been attempted, but this approach, while promising, is not yet fully developed for two-dimensional problems (see Silver *et al.*, 1990; Jarrell

[10] In deriving Eq. (4.11), remember that $\int_0^\infty d\omega\delta(\omega)=1/2$.

et al., 1991). The Lanczos method applied to small clusters is then one of the few available tools for calculating the optical conductivity of correlated electrons. Several groups around the world have actively worked on $\sigma(\omega)$ using this technique. To apply the Lanczos formalism to the evaluation of dynamical quantities as discussed in Sec. II.A.2, it is convenient to rewrite Eq. (4.8) as

$$\mathrm{Re}\sigma_{xx}(\omega)=D\delta(\omega)+\frac{e^2}{\omega N}\mathrm{Im}\left[\langle\phi_0|\hat{j}_x\frac{1}{\hat{H}_0-E_0-\omega-i\epsilon}\hat{j}_x|\phi_0\rangle\right], \tag{4.12}$$

which is precisely the form of Eq. (2.6). The second term on the right-hand side (sometimes called the incoherent or regular part of the conductivity) can be obtained using the Lanczos formalism of Sec. II.A.2. Typically, a couple hundred Lanczos iterations provide the incoherent part with high accuracy. Thus it is not necessary to explicitly obtain all the excited states to calculate the regular part of Eq. (4.8), as would have been naively required. The Drude contribution is calculated using Eq. (4.9), since with the Lanczos approach it is also possible to obtain the mean value of the kinetic-energy operator very accurately. The effects of electronic interactions are fully taken into account with this technique, and the approach works equally well for any coupling and doping fraction. Of course, the intrinsic problem of this method is the constraint to working on relatively small clusters, since, in the calculations, vectors of the size of the dimension of the Hilbert space of the cluster need to be used. However, in recent years the availability of supercomputers with large amounts of memory, like the Cray-2, have allowed calculations in cluster sizes that are expected to capture at least qualitatively the physics of models of correlated electrons.

In Fig. 41, $\sigma_1(\omega)$ is shown for the one-band Hubbard model at $U/t=10$, evaluated on a 4×4 cluster. The results are parametric with the hole-doping fraction in the interval $0.0\le x\le0.375$. The results of Fig. 41 have recently been discussed in the literature (Dagotto, Moreo, Ortolani, Riera, and Scalapino, 1992), but in this reference they were presented with a very high resolution, $\epsilon=0.01t$, to distinguish between the individual δ functions in the spectrum. On the contrary, here in Fig. 41, we give to the δ functions a *large* width $\epsilon=t$ to simulate the several effects not considered in our idealized Hamiltonian that contribute to the broadening of the peaks. The results are very interesting (Fig. 41). Selecting appropriately the coupling constant in the Hubbard Hamiltonian, and without providing additional information, a $\sigma_1(\omega)$ that resembles the experimental results for hole- and electron-doped materials is obtained [compare Fig. 41 against Figs. 37(a), 37(b)]. At half-filling ($x=0$), the weight is accumulated above a gap which is about $6t$ for this coupling. If t takes the value suggested in some calculations (Hybertsen *et al.*, 1990; Bacci, Gagliano, Martin, and Annett, 1991), i.e., $t\sim0.3$–0.4 eV, then the gap

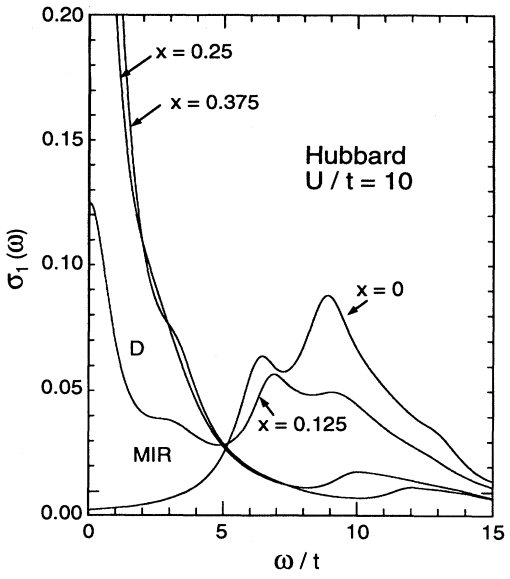

FIG. 41. Real part of the optical conductivity of the one band Hubbard model at $U/t=10$ on a 4×4 cluster. The results are parametric with hole doping x. D denotes the Drude peak at zero frequency, while MIR indicates the midinfrared band that is observed for doping $x=0.125$. The δ functions appearing in the continued fraction expansion have been given a large width $\epsilon=t$.

is similar to that observed in the high-T_c materials, namely, about 2 eV. As explained earlier, with the Hubbard model we can *mimic* the charge-transfer gap of the real materials by means of the Hubbard gap. The weight in $\sigma_1(\omega)$ above the gap is produced by charge excitations, and it is basically related to the upper Hubbard band of the model. The small weight below the gap at $x=0$ is produced by the "tails" of the smeared δ functions above the gap.

The more interesting results occur upon doping, since a redistribution of the spectral weight takes place. Since the kinetic energy in sum rule (4.11) is not strongly doping dependent, this basically amounts to a transfer of weight from the charge excitations band down to lower energies. Consider $x=0.125$, which corresponds to two holes on the 4×4 cluster. Figure 41 shows, in the infrared region below the gap, two main features dominating: (i) a sharp peak at $\omega=0$, which is precisely the Drude peak with damping, and (ii) considerable weight centered near the middle of the gap, which hereinafter we shall call the midinfrared (MIR) band in analogy with the weight observed experimentally located inside the charge-transfer gap upon doping. Increasing the hole doping, we observe that the Drude peak grows rapidly with x, while the weight at the midinfrared band is only weakly doping dependent. In the scale of the plot, results for $x=0.25$ and 0.375 are virtually identical. Even the appearance of what Uchida *et al.* (1991) called an "isosbestic" point (the point around $\omega\sim5t$ where conductivities for different densities cross) is neatly reproduced!

Results such as these shown in Fig. 41 can be obtained if U/t is selected in the intermediate region of couplings, namely, when U is of the order of the bare bandwidth $8t$. If the coupling U/t is larger, then it can be shown that between the MIR region and the charge excitations there is an empty region with no spectral weight. On the other hand, if U/t is too small, then, upon doping, the MIR band and charge excitations merge; they are difficult to distinguish. The same "optimal" region in parameter space necessary to mimic experiments on cuprates also appears in studies of photoemission (see Sec. IV.C) and for the magnetic susceptibility (Sec. IV.A.1).

What is the origin of the MIR band in these numerical studies? We know that this band also appears in the t-J model, and thus it is not related to charge excitations. It is tempting to associate the MIR band with the considerable amount of spectral weight found above the quasiparticle peak in the study of the spectral function of a hole $A(\mathbf{p},\omega)$ (Secs. III.B.4 and IV.C), since both appear at similar energies. That weight was caused by spin fluctuations around the hole; i.e., the hole is a dressed quasiparticle that carries a "bag" of reduced antiferromagnetism in its neighborhood. At large U/t, the properties of this spin polaron are dominated by the string excitations (Sec. III.B.1). These claims are supported in part by the fact that the presence of the MIR band is a two-dimensional effect. Actually, $\sigma_1(\omega)$ has also been calculated on a 16-site t-J model chain (Stephan and Horsch, 1990). $\sigma_1(\omega)$ has a robust Drude peak but, contrary to its two-dimensional counterpart, negligible weight at finite frequencies. This result supports the previous interpretation that the dressing of the hole by spin excitations is a key ingredient in the explanation of the origin of the MIR band. In 1D, spin and charge separation takes place (there are no "string" excitations in one dimension), while in two dimensions the cloud of distorted antiferromagnetic background seems to follow the holes. This example also shows that it is dangerous to naively relate 1D and 2D results.

To complete the analysis of the numerical results, $\sigma_1(\omega)$ of Fig. 41 with $x=0.25$ and 0.375 in the range $1t \le \omega \le 5t$ was fit with a power law, $\sigma_1(\omega) \sim A/\omega^{\alpha}$. It is remarkable that the best fit was obtained for $\alpha \sim (1.00 \pm 0.05)$, again in excellent agreement with experiments that consistently suggest a $1/\omega$ decay of the conductivity at intermediate energies. However, for this finite cluster, we know *exactly* that there is a Drude peak that has to decay as $1/\omega^2$ at small enough frequencies (in practice, $\omega < 0.1$ eV or less). This peak carries a considerable amount of the total spectral weight at $x=0.25$, and it has been given the same large damping $\epsilon = t$ as the rest of the δ functions. Then, the observed $1/\omega$ decay of the numerical results is caused by a perverse combination of the oscillator strength of the free carriers, and that of the MIR band. This may be a possible explanation for the puzzling experimental results observed in the cuprates.

At this point, it is convenient to clarify that the purpose of this theoretical exercise of analyzing in detail $\sigma(\omega)$ of Fig. 41 is *not* to claim that the Hubbard model contains all the key ingredients to describe the superconductors. We only want to remark that once a calculation can be performed under some controlled approximations (in this case with the help of computational techniques), and if enough damping is provided to the otherwise sharp δ functions, then some of the intriguing "anomalous" features of the experimentally observed optical conductivity can be qualitatively reproduced using models of strongly correlated electrons. To produce a band at mid-infrared energies with electronic models, we only seem to need strongly dressed quasiparticles, and thus its presence may well be a generic feature of several theories. Of course, other processes may substantially contribute to the MIR band observed experimentally. As mentioned before, studies by several groups have shown that holes trapped near dopant atoms, as well as chain contributions in the YBCO family, can account for a large percentage of this weight. Thus we expect that these effects plus that created by the heavily dressed quasiparticles

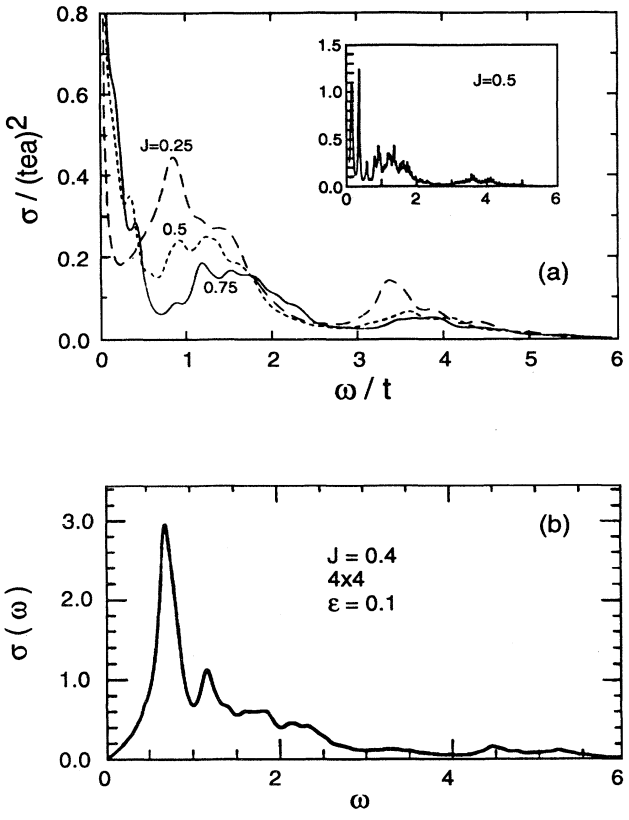

FIG. 42. (a) Optical conductivity of the t-J model on a 4×4 cluster evaluated by Stephan and Horsch (1990), for the case of one hole, open boundary conditions, and several couplings J/t. The width of the deltas is $\epsilon = 0.1t$. The inset shows results for $J=0.5$ with a higher resolution $\epsilon = 0.02t$. (b) Same as (a), but using periodic boundary conditions. These results were obtained by Moreo and Dagotto (1990). The Drude peak is not shown, only the "incoherent" part of the conductivity.

will be operative in the cuprates. It would be quite difficult to distinguish among them experimentally. Note also that the relation between these unusual features and the superconducting mechanism remains obscure, since measurements of pairing correlations in the same cluster that presents a robust MIR band do not show signals of superconductivity (as will be discussed in more detail in Sec. IV.E).

The MIR band in $\sigma_1(\omega)$ was first observed numerically in the *t-J* model independently by Sega and Prelovšek (1990); Moreo and Dagotto (1990); Stephan and Horsch (1990); and Chen and Schüttler (1991). For additional information, see Rice and Zhang (1989). Figure 42 shows some of those results which were obtained on 4×4 clusters with one hole. In both cases considerable weight is observed at intermediate energies. It is interesting to note that the results of Fig. 42(a) were obtained using *open* boundary conditions (OBC). What happens with the Drude peak for a perfect metal if the numerical study is carried out on a finite cluster with OBC? In this case we do not expect to find a Drude peak at zero frequency, since no current can propagate with OBC. However, in the thermodynamic limit, open and periodic conditions should give the same result. The way in which this "paradox" is resolved is by the appearance of a Drude precursor peak at very small frequencies when open boundary conditions are used as shown in the inset of Fig. 42(a). The position of this peak converges to zero, increasing the size of the cluster, as was discussed by Moreo and Dagotto (1990) and Fye *et al.* (1991). Figure 42(b) shows $\sigma_1(\omega)$, obtained using periodic boundary conditions instead. The Drude peak is not shown, and the large weight between $0.5t$ and $2.0t$ is the MIR band.[11]

Studies of $\sigma_1(\omega)$ using the three-band Hubbard model have also been carried out. Wagner, Hanke, and Scalapino (1991) obtained the result shown in Fig. 43(a), using a cluster with four copper atoms and ten oxygen atoms with periodic boundary conditions. The structure at *A* indicates charge-transfer excitations. Note the appearance of the spectral weight *B* at intermediate energies upon doping. In this lot the Drude peak is not shown explicitly. Results for the three-band model have also been reported by Tohyama and Maekawa (1991). Finally, on Fig. 43(b), results are presented for the so-called Kondo-Heisenberg model with the particular values of parameters shown in the caption (Chen and Schüttler, 1991). The Drude peak is not shown, and the large peak near $\omega \sim 2$ should be considered part of the MIR band. Then,

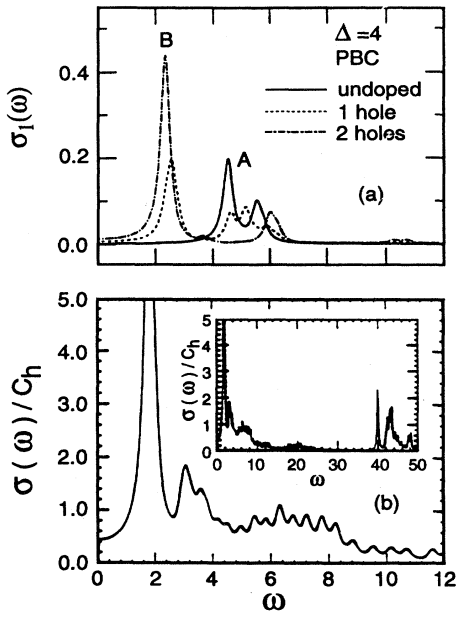

FIG. 43. (a) $\sigma_1(\omega)$ vs frequency for the three-band Hubbard model on a 2×2 copper cluster (14 atoms total) with different numbers of holes. The parameters in the Hamiltonian are $\Delta=4$, $U_d=6$, $U_p=3$, and $t=1$. Periodic boundary conditions were used. The Drude peak is not shown (from Wagner, Hanke, and Scalapino, 1991). (b) Optical conductivity of the Kondo-Heisenberg model on a 4×4 cluster with one hole. The Kondo spin-exchange coupling is $W=8$, and the nearest-neighbor oxygen-oxygen hole transfer $t_{pp}=4$. c_h is 1/16, and the width of the delta functions is $0.2t$ (for more details, see Chen and Schüttler, 1991).

all the models of correlated electrons that have been studied in two dimensions present spectral weight inside the insulator gap of the undoped system. The existence of the "electronic" MIR band seems a generic feature of these models.

To complete this study, in Figs. 44 and 45 we show the expectation value of the kinetic-energy operator, as well as the Drude weight *D*, as a function of doping obtained on a 4×4 cluster at several coupling, for the one-band Hubbard and *t-J* models (Dagotto, Moreo, Ortolani, Poilblanc, and Riera, 1992). In both cases the Drude weight seems to increase with the number of holes at small hole doping (with the only exception of the noninteracting $U/t=0$ limit in the Hubbard model). The doping dependence is approximately linear, and thus the finite-cluster approach roughly predicts $D \sim x$. In the other limit of small electronic density, $D \sim 1-x = \langle n \rangle$, as in the case of a gas of weakly interacting electrons. Similar results were obtained in the one-dimensional Hubbard model by Schulz, 1990b; Zotos, Prelovšek, and Sega, 1990; Fye *et al.*, 1991, 1992; and Kawakami and Yang, 1991. Although the behavior of both models is roughly similar, it is surprising that in the *t-J* model the results are almost *J* independent. This effect can be traced back to the three-

[11]In the first studies of $\sigma(\omega)$ with periodic boundary conditions (Moreo and Dagotto, 1990; and others), it was claimed that sum rule (4.11) was not satisfied. This is not correct, and the reason for this confusion is that the Drude peak does not come out automatically from the numerical calculations, which only provide the incoherent part. The weight at zero frequency needs to be calculated separately from Eq. (4.9), as it is currently done in the literature.

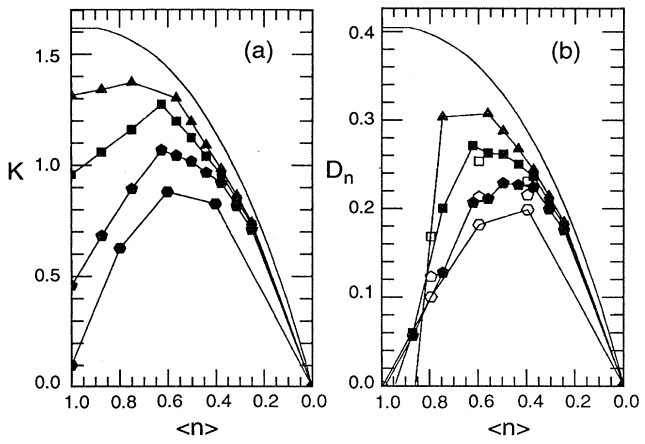

FIG. 44. (a) Kinetic energy per site of the Hubbard model $K=\langle\phi_0|(-\hat{T})|\phi_0\rangle/N$ on a 4×4 cluster as a function of density $\langle n\rangle$ for $U/t=4$ (solid triangles), $U/t=8$ (solid squares), and $U/t=20$ (solid pentagons). We also show results for a 10-site cluster at $U/t=100$ (solid hexagons). The solid line without points corresponds to results for $U/t=0$ in the bulk limit (from Dagotto, Moreo, Ortolani, Poilblanc, and Riera, 1992). (b) $D_n=D/(2\pi e^2)$ vs density for various couplings U/t. Solid triangles, squares, and pentagons denote results for $U/t=4$, 8, and 20, respectively, on a 4×4 cluster. Open squares, pentagons, and hexagons indicate results for a 10-site cluster at $U/t=8$, 20, and 100, respectively. The solid lines are exact results at $U/t=0$ in the bulk limit.

site terms left aside in the derivation of the t-J model from the Hubbard model, as recently discussed by Stephan and Horsch (1992). The approximate J independence of the t-J model results has also been addressed recently by Poilblanc, Ziman, *et al.* (1993) in a finite-size scaling analysis of the optical conductivity using clusters

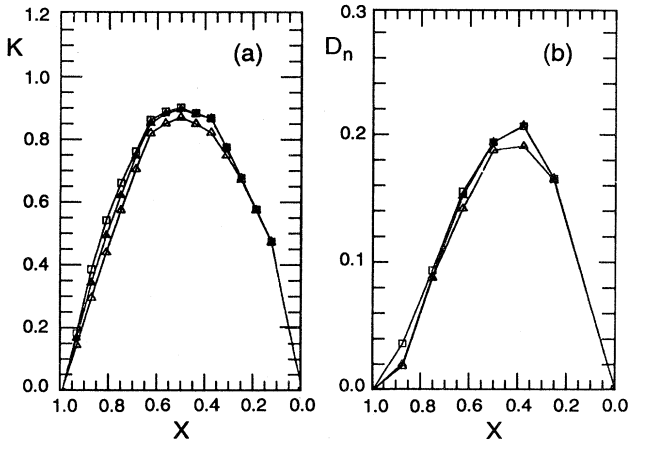

FIG. 45. (a) Kinetic energy per site of the t-J model $K=\langle\phi_0|(-\hat{T})|\phi_0\rangle/N$ on a 4×4 cluster as a function of hole density x for $J/t=0.1$ (open squares), $J/t=0.4$ (solid triangles), and $J/t=1$ (open triangles). From Dagotto, Moreo, Ortolani, Poilblanc, and Riera (1992). (b) $D_n=D/(2\pi e^2)$ vs density for various couplings J/t. The notation is the same as that used in (a).

of up to 26 sites.

The Drude weight D has a maximum located near quarter-filling for both the t-J and large-U/t models. The maximum slowly moves towards half-filling when the interaction strength U/t is decreased in the one-band case. Its position may be used as a rough estimator of the doping fraction at which the carriers turn from hole-like to electronlike (Dagotto, Moreo, Ortolani, Poilblanc, and Riera, 1992). Figure 44(a) also shows some of the weaknesses of the calculation. The Drude weight of the Hubbard model at half-filling obtained using Eq. (4.9) can actually become negative on a finite system (Moreo, 1990; Fye *et al.*, 1991; Stafford, Millis, and Shastry, 1991). This unphysical result is a finite-size effect that has been studied extensively in one-dimensional rings, where it was shown that $|D|$ converges to zero at half-filling, as expected for an insulator, but with alternating signs depending on the number of sites of the chain (for more details about one-dimensional calculations of the optical conductivity, see Giamarchi and Millis, 1992 and Stafford and Millis, 1993). A comparison between variational Monte Carlo techniques and exact diagonalization was presented by Millis and Coppersmith (1990). Their conclusion was that finite-size effects were important. However, considerably better numerical results have been produced since the publication of that paper (see, for example, Dagotto, Moreo, Ortolani, Poilblanc, and Riera, 1992), and thus their conclusions need revision. An attempt to study numerically the optical conductivity of the Hubbard model in a three-dimensional cubic lattice was presented by Tan and Callaway (1992).

Some recent developments in the context of studies of $\sigma(\omega)$ are worth mentioning.

(1) Poilblanc and Dagotto (1991; see also Poilblanc, 1991) have claimed that by introducing different boundary conditions on the clusters (through a phase factor) and averaging over them, results closer to the bulk limit can be obtained. They have also studied the dependence of the energy levels with an external flux in two dimensions. The Drude weight can be obtained as the second derivative of the ground-state energy with respect to that flux.

(2) The Drude weight can be evaluated by quantum Monte Carlo techniques (Scalapino, White, and Zhang, 1992) for the Hubbard model at those densities where the sign problem allows calculations at low temperatures. The Drude weight obtained by quantum Monte Carlo is approximately 0.3 on an 8×8 cluster at quarter-filling $\langle n\rangle=\frac{1}{2}$, and $U/t=4$, in good agreement with the Lanczos result shown in Fig. 44(b) for the same parameters. Finite-size effects seem to affect only weakly the Drude weight, at least at that density.

(3) Recently, interesting results were obtained by Tikofsky, Laughlin, and Zou (1992). These authors used the anyon superconductivity formalism to calculate the optical conductivity and total kinetic energy of the t-J model. They observed an excellent quantitative agreement with the exact diagonalization results discussed in

this review.

The following are the main conclusions in the study of the optical conductivity.

Experiments: All materials with CuO_2 planes, regardless of their T_c, seem to have MIR bands. In several of them (especially those at its "optimal" compositions) a $\sim 1/\omega$ decay of the optical conductivity is observed beyond some threshold in energy and doping. Possible explanations include the presence of trapped holes near dopant atoms, and the important contributions of the chains in $YBa_2Cu_3O_{6+x}$.

Computational Studies: All proposed purely electronic models of Cu-O planes studied numerically predict a $\sigma_1(\omega)$ qualitatively similar to that observed experimentally (see Fig. 41). The weight in the MIR region is created by the dressing of the hole quasiparticles with spin excitations, and it corresponds with the substantial spectral weight observed in the hole spectral function $A(\mathbf{p},\omega)$ at similar energies. Although in these studies there is a Drude peak in the spectrum, the conductivity can decay as $1/\omega$ if enough damping is provided, due to the combination of the free-carrier contribution with the MIR band. These results are observed in a regime where superconductivity was not numerically detected in the ground state, suggesting that the MIR feature and superconductivity may not be related processes.

C. Electron spectroscopy

In a typical photoemission spectroscopy (PES) experiment, photons of a known energy are directed to a sample of the material being analyzed. An electron with initial energy E_i in the sample is ejected with a kinetic energy E_f. These electrons are collected, and their energy analyzed. Using energy conservation, the initial energy is given by $E_i = E_f + \phi - h\nu$, where $h\nu$ is the photon energy, and ϕ the work function of the material. If the photon energies used are about 1 keV, the technique is called x-ray photoemission spectroscopy (XPS); if these energies are below 100 eV, the method is called ultraviolet photoemission spectroscopy (UPS); and for the "inverse" experiment, where electrons are added to the system, we use the name "inverse photoemission spectroscopy" (IPES). In the simplest approximation, the photoelectron spectrum provides the occupied density of states of the system. However, one of the main problems of this technique lies in its surface sensitivity, since photoelectrons mostly come from a narrow region near the surface of about one unit cell deep (deeper electrons are strongly scattered and absorbed in the sample). Then, care must be taken to carry out the experiment on an ultrahigh vacuum with clean crystal surfaces. In Fig. 46, we compare an XPS experimental result obtained by Ghijsen *et al.* (1988) for the charge-transfer insulator CuO, which is considered to have many similarities with the high-T_c compounds, with numerical exact-diagonalization results for a Cu_2O_7 cluster using a multiband Hubbard-like Hamiltonian (Eskes and Sawatzky, 1991). The agreement

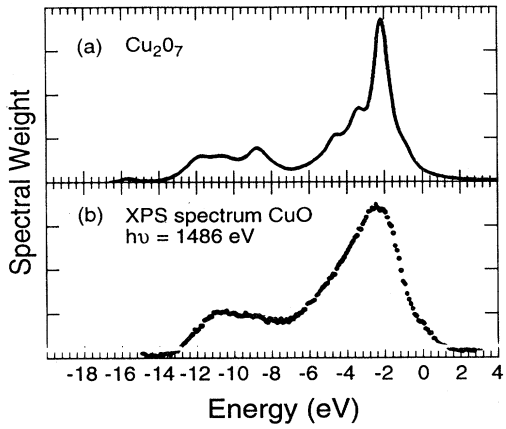

FIG. 46. Photoemission spectra calculated by Eskes and Sawatzky (1991) using a Cu_2O_7 cluster and several Cu and O orbitals in the undoped limit (a), compared with experimental XPS results (b) for CuO (Ghijsen *et al.*, 1988).

at the scale of eV's is excellent, showing that both the experimental method and the study of small clusters provide interesting information about real materials [band-structure calculations applied to the same compound do not predict the insulator gap, nor some of the satellite peaks, although work by Svane (1992) has shown that the self-interaction-corrected local-spin-density approximation is able to reproduce the presence of antiferromagnetism in the undoped compounds]. However, the relevant scale of physics we expect for superconductivity in the cuprates is of order meV. Thus considerably more work is needed to show that both the experimental technique and the theoretical approach are able to provide useful information in this subtle regime. Another important technique that complements the PES results is the x-ray absorption spectroscopy (XAS). In this method, an electron in an occupied core level (like the oxygen 1*s* level) is excited by the x ray to an empty state above the Fermi level, and thus there the unoccupied states of the system can be analyzed. Of course, removing a deep core electron may induce strong local distortions of the electronic density that may affect the final results; thus, as in PES, care must be taken in the analysis of the data.

What PES and XAS results should we expect to observe in the high-T_c materials? In Fig. 47 a rough scheme of the electronic band structure of a charge-transfer insulator is shown. *Assuming* that the bands do not change with doping (rigid-band approximation), then upon hole doping we should observe in a PES experiment that the Fermi energy is smaller than for the insulator, and thus it will be located below the top of the valence band. On the other hand, for an electron-doped material, the Fermi energy is above the bottom of the conduction band; thus PES should give a two-peak structure. For XAS experiments that test the *unoccupied* states, the situation is basically reversed compared with PES; i.e., for hole-doped samples, a double-peak structure should be

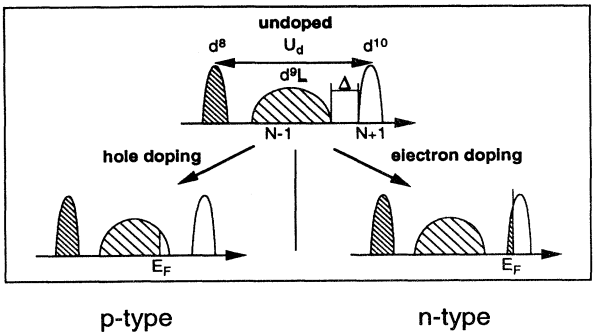

FIG. 47. Schematic effect of doping for a charge transfer CuO_2 plane. Hole doping is expected to move the Fermi level into the charge-transfer band, while electron doping is expected to move it into the upper Hubbard band. This would give an energy difference of the Fermi levels of approximately 2 eV (from Dessau, 1992).

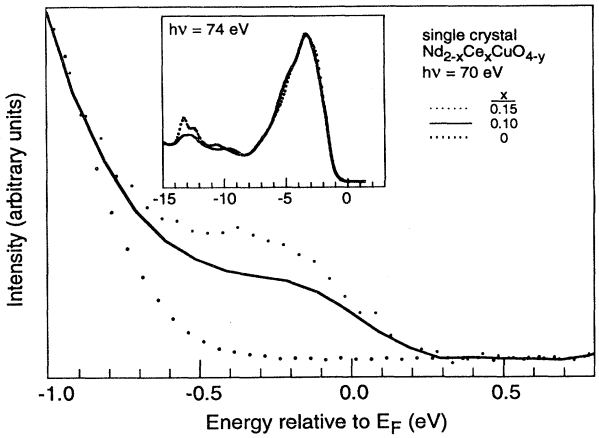

FIG. 48. Photoemission spectra of $Nd_{2-x}Ce_xCuO_4$ single crystals at three different dopings. The position of E_F is about 0.5 eV above the top of the valence band, which implies that the spectral weight induced by doping lies in the insulating gap (from Anderson *et al.*, 1993).

observed, while for electron doping, only one peak is expected.

In this section, experimental and theoretical results will be discussed. They systematically show that the naive rigid-band picture is not correct for the high-T_c cuprates. An apparent disagreement between PES and XAS experiments that were supposed to probe the same electronic density of states will be discussed. The experimental summary given in this section closely follows review articles by Allen (1991a, 1991b) and Dessau (1992). See also Fink *et al.* (1993) for a review on electron energy loss and XAS spectroscopy.

1. Density of states (experiments)

Photoemission spectroscopy experiments on single crystals and ceramic samples for $La_{2-x}Sr_xCuO_{4+\delta}$ have produced interesting, and somewhat surprising, results (Shen *et al.*, 1987; Matsuyama *et al.*, 1989; Allen *et al.*, 1990; Takahashi *et al.*, 1990). We would have expected, based on the rigid-band picture, that the Fermi energy E_F would move into the insulator valence band as x increases. However, metallic samples with $x=0.15$ produce (weak) PES intensity in the region of the gap of the insulator; i.e., E_F lies in *new* states inside the insulator gap. On the other hand, XAS experiments on ceramic samples suggest a different picture for the density of states of this material (Romberg *et al.*, 1990; Chen *et al.*, 1991). By exciting core electrons into unoccupied states near the Fermi energy, XAS provides information about the empty multibody states of the problem. X-ray absorption spectroscopy experiments on $La_{2-x}Sr_xCuO_{4+\delta}$ show the presence of states in the gap, as in PES, but also two peaks: one with weak intensity at low energies which is associated with empty states at the top of the valence band for the Sr-doped system, and a peak at higher energies with a larger intensity which is associated with the upper Hubbard band. Then, XAS results seem approximately in agreement with the naive rigid-band picture described before, and in disagreement with PES experiments.

A similar discrepancy was observed in electron-doped compounds. The naive rigid-band picture discussed above would predict that PES experiments in these materials should show a two-peak structure, one corresponding to the electrons added to the system at the bottom of the conduction band, and a larger structure related to the $O2p$ band (or the lower Hubbard band in a one-band description of the material). However, actual PES studies of $Nd_{2-x}Ce_xCuO_4$ consistently show that there is a steady growth of spectral weight at energies *inside* the insulator gap (Fukuda *et al.*, 1989; Allen *et al.*, 1990; Namatame *et al.*, 1990; Suzuki *et al.*, 1990), as if electrons added to the system would occupy new states created in the gap. For example, consider the recent experimental results obtained by Anderson *et al.* (1993), which are shown in Fig. 48 for single crystals with $x=0.0$, 0.10, and 0.15. The $x=0$ insulator spectrum has been positioned on the energy axis relative to those for nonzero x, by aligning the higher energy main band and satellite features. These results suggest that the Fermi energy E_F does not appear to change appreciably with Ce concentration, and in doped metals it lies in states that fill in the gap of the insulator.[12] In other words, E_F does *not* move into states present in the insulator and does *not*

[12]However, recent results by King *et al.* (1993) on $Nd_{2-x}Ce_xCuO_4$ show a shift of the chemical potential with electron doping, as expected by band-filling scenarios, and no double-peak structure in the results. Then, the experimental situation is not quite clear.

jump across the gap if the doping is changed from holes to electrons, but has roughly the same position relative to the valence-band maximum for both holes and electrons. Such results are indeed unexpected. In contrast to PES data, the XAS experiments for electron-doped materials seem to suggest that E_F lies near the bottom of the upper Hubbard band upon electron doping (Alexander *et al.*, 1991). In these experiments, only one peak is observed, which is assigned to the upper Hubbard band. This result is consistent with the naive rigid-band picture and inconsistent with PES experiments. The fact that μ is observed directly in photoemission but must be inferred after data interpretation in XAS favors the PES result on this question. However, the greater surface sensitivity of photoemission relative to XAS can be mentioned as a reason against PES data.

What occurs in other materials? Results for $Bi_2Sr_2CaCu_2O_8$ (Olson *et al.*, 1989, 1990; Shen *et al.*, 1991; Dessau, 1992) and $YBa_2Cu_3O_{6+x}$ (Liu, Veal, *et al.*, 1992; Liu *et al.*, 1992) studied with angle-resolved photoemission suggest that in these compounds the hole doping causes a shift of E_F together with a non-rigid-band variation in the intensity of the emission. Inverse-photoemission studies of $Bi_2Sr_2CaCu_2O_8$ also support these claims (Takahashi *et al.*, 1991; Watanabe *et al.*, 1991). Dessau (1992) claims that $Bi_2Sr_2CaCu_2O_8$ samples may be in a doping regime where some aspects of the Fermi-liquid description are recovered (while the previously described materials $La_{2-x}Sr_xCuO_4$ and $Nd_{2-x}Ce_xCuO_4$ may lie much closer to the insulating regime, disturbing their regular behavior). Thus Bi2212 and YBCO do not now seem to be as paradoxical as the single plane compounds.

Summarizing, there is an important feature in the experimental PES and XAS results for several high-T_c compounds that is novel and puzzling. A discrepancy seems to exist between PES and XAS experiments regarding the behavior of the chemical potential as a function of doping: the potential does not seem to move in PES results, while XAS data suggest that μ crosses the insulator gap when changing from hole to electron doping. Actually, recent results by Anderson *et al.* (1993) have shown that PES and XAS data obtained from the *same* sample of $Nd_{2-x}Ce_xCuO_4$ at the same time still show the same discrepancy. An interesting feature that is not controversial is the appearance of weight in the insulator gap upon doping. This result is also in agreement with the theoretical analysis of models of strongly correlated electrons (shown below), and in disagreement with a rigid-band picture of the problem. However, as recently remarked by Fujimori *et al.* (1992; see also Fujimori, 1992a, 1992b), the formation of these gap states is a very general phenomenon that appears in several strongly correlated (but non-high-T_c) compounds, and thus it might not be essential in understanding the mechanism of superconductivity in the cuprates. A very interesting example is presented in Fig. 49, where the inverse PES spectra of $La_{2-x}Sr_xNiO_4$ is shown. This material is a

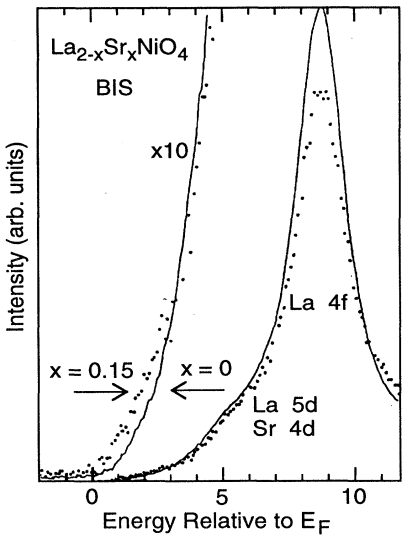

FIG. 49. BIS spectrum (inverse photoemission) of $La_{2-x}Sr_xNiO_4$ (from Fujimori, 1992 and Eisaki *et al.*, 1992).

hole-doped charge-transfer insulator. As seen in the figure, upon doping, new states appear in the gap. This material is not even metallic for small x, and the holes may be localized. Then, gap states may not be crucial for superconductivity; nevertheless, it is a poorly understood general phenomenon of strongly correlated materials that should be carefully analyzed.

2. Density of states (theory)

Can the experimental results for the cuprates be understood using models of strongly correlated electrons? As shown below, the answer is that the presence of gap states is very natural in these models, at least in some region of parameter space. On the other hand, the chemical potential μ moves across the gap when hole doping is changed into electron doping in *all* the purely electronic models of high T_c considered in the literature (of course, without explicit impurities). Thus the paradoxical behavior of μ still needs a theoretical explanation.

Let us consider the PES results in more detail. In order to analyze the presence of gap states in the one-band Hubbard model, it is necessary to perform a reliable calculation of the density of states $N(\omega)$. This quantity can be evaluated using Lanczos methods following the same approach that was described in detail in Sec. II.A.2. We use the definition of the density of states as $N(\omega)=\sum_{\mathbf{p}} A(\mathbf{p},\omega)$, where the spectral function corresponding to a given momentum $\mathbf{p}$ and energies ω is given by

$$A(\mathbf{p},\omega)=\sum_n |\langle \phi_n^{N+1}|c^{\dagger}_{\mathbf{p},s}|\phi_0\rangle|^2\delta(\omega-E_n^{N+1}+E_0^N) \quad (\omega>\mu)\,, \tag{4.13}$$

$$A(\mathbf{p},\omega)=\sum_n |\langle \phi_n^{N-1}|c_{\mathbf{p},s}|\phi_0\rangle|^2\delta(\omega-E_n^{N-1}+E_0^N) \quad (\omega<\mu)\,.$$

$|\phi_0\rangle$ is the ground state in the subspace of N particles (with energy E_0^N). $|\phi_n^{N\pm1}\rangle$ are eigenstates in the subspace of $N\pm1$ particles with energy $E_n^{N\pm1}$. The fermionic operator $c_{\mathbf{p},s}$ destroys a fermion with a given momentum $\mathbf{p}$ and spin s. The results for $\omega>\mu$ correspond to IPES, while $\omega<\mu$ with energy equal to $|\omega-\mu|$ determines the PES spectrum, when integrated over all momenta. The results for $N(\omega)$ are shown in Fig. 50. They were obtained on 4×4 cluster at $U/t=8$ and for different fermionic densities $\langle n\rangle$. The δ functions in the figure have been given an (arbitrary) width $\epsilon=0.2t$ to plot the results. Figure 50(a) corresponds to half-filling. A clear gap exists in $N(\omega)$ which is caused by the antiferromagnetic order (or, equivalently, by the spin-density-wave order) in the ground state. The large dominant structures at energy $|\omega|\sim2-3t$ correspond to the "quasiparticle" band produced when one electron is added ($\omega>0$) or removed ($\omega<0$) from half-filling. μ is located at $\omega=0$, and the symmetry under a reflection $\omega\rightarrow-\omega$ is caused by the particle-hole symmetry of the one-band problem at half-filling. The rest of the structure in $N(\omega)$ at larger $|\omega|$ has the same origin as the "incoherent" part of the hole spectral function discussed in Sec. III.B.4; namely, the state $c_{\mathbf{p},\sigma}|\phi_0\rangle$ obtained by the sudden annihilation of an electron is not an exact eigenstate of the interacting problem. Decomposed in a complete basis of eigenstates, it has a projection in virtually all of the states with the same quantum numbers, and thus only a *fraction* of the total weight resides on the quasiparticle peak. The rest of the weight is distributed at higher energies.

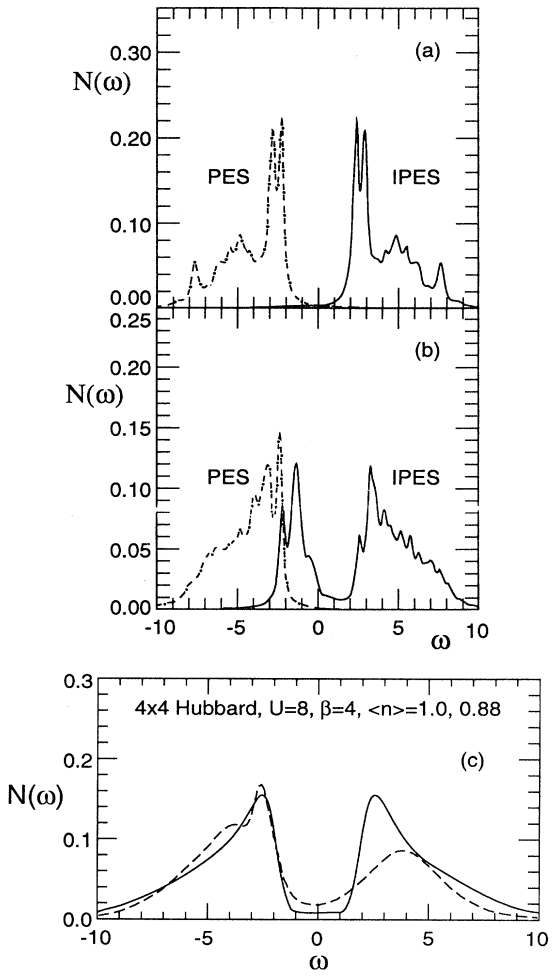

FIG. 50. (a) Density of states $N(\omega)$ obtained using the one-band Hubbard model on a 4×4 cluster at density $\langle n\rangle=1$ (i.e., half-filling) and $U/t=8$. The technique used is the Lanczos method. (b) Same as (a), but at density $\langle n\rangle=0.875$. Both figures taken from Dagotto, Ortolani, and Scalapino (1992). The solid lines are the IPES spectrum, while the dot-dashed lines denote PES results. (c) Density of states obtained with a recently developed technique to produce real-frequency results from the quantum Monte Carlo data using a 4×4 cluster, $U/t=8$, densities $\langle n\rangle\approx0.88$ (dashed line) and $\langle n\rangle=1$ (solid line), and temperature $T=t/4$ (from Bulut, Scalapino, and White, 1994; see also Scalapino, 1991).

What occurs at finite doping? For example, consider $\langle n\rangle=0.875$, which corresponds to two holes on the 16-site cluster [Fig. 50(b)]. The PES spectrum (dashed line) resembles that obtained at half-filling, but it is shifted towards smaller energies. Naturally, its total weight is reduced, since the integral of the density of states up to the chemical potential (or E_F) has to be equal to the number of particles. μ is now near $\omega\sim-2.4t$, as shown in the figure. We now consider the IPES spectrum. At an energy $\omega\sim4t$ or larger, a considerable amount of weight is located, which corresponds to the upper Hubbard band (that also exists in the IPES spectrum at half-filling). The interesting new feature is that, immediately after μ, a considerable amount of weight is observed which peaks near the chemical potential and then slowly decreases, covering the whole original antiferromagnetic gap of the half-filled case and extending into the upper Hubbard band. In this respect, the result is qualitatively similar to that found experimentally, namely, that states appear in the gap upon doping. However, contrary to PES experiments, the chemical potential moves to the top of the valence band upon hole doping. Reciprocally, for electron doping, it moves to the bottom of the conduction band. This last result is obvious from the particle-hole symmetry of this model, and thus an explicit calculation is not needed. As with the optical conductivity $\sigma(\omega)$ (Sec. IV.B), it is important to remark that other nonelectronic processes may well be contributing substantially to the spectral weight in the gap. For example, impurities can produce localized gap states. Then, the numerical study of purely electronic models without impurities only *suggests* that *part* of the weight may have electronic origin, but does not claim to explain entirely the experimentally observed spectrum. Finally, and for completeness, it is useful to compare the results obtained using the exact Lanczos approach [Figs. 50(a) and 50(b)] with those obtained using a recently developed technique to produce real-frequency results from the quantum Monte Carlo data (Silver *et al.*, 1990; White, 1990; Jarrell *et al.*, 1991) using the same cluster, coupling and density, and temper-

ature $T=t/4$ (which cannot be lowered further due to the sign problem). Results are shown in Fig. 50(c) (from Bulut, Scalapino, and White, 1994; see also Scalapino, 1991). $N(\omega)$ at half-filling is qualitatively correct; i.e., the gap appears in the spectrum with a magnitude similar to that of Fig. 50(a). The structure of the lower and upper Hubbard bands is washed out, showing that this technique cannot reproduce the fine details of $N(\omega)$, but the main physics of the problem has been captured by the approximation. Similar conclusions are reached at finite doping. In the opinion of the author, the analytic continuation technique applied in combination with Lanczos diagonalization on small clusters is a promising algorithm.

In the numerical result shown in Fig. 50(b), the origin of the states in the gap is easy to understand (Dagotto *et al.*, 1991; Eskes, Meinders, and Sawatzky, 1991). Consider a "snapshot" of the doped ground state at large U/t, as shown in Fig. 51(a). Double occupancy is strongly suppressed. The PES spectral weight is obtained by destroying one electron, and that process does not require much energy. On the other hand, the IPES spectrum must necessarily consist of two parts. The new electron added to the system can either occupy an already occupied state (with opposite spin), and thus expend a large energy U/t, or be created in an empty site, which requires less energy. The former corresponds to the upper Hubbard band structure, while the latter is the origin of the gap states. Adding suddenly a new electron to an empty site does not correspond to an eigenstate of the problem. Decomposed into a complete basis, it has a projection over several other states in the subspace without double occupancy; thus its spectral function has a typical finite width of order $W\sim 8t$, as has the spectral function of one added hole in the t-J model (Sec. III.B.4). This width is enough to fill the entire gap at $U/t=8$. Needless to say, this behavior cannot be reproduced by a rigid-band approximation.

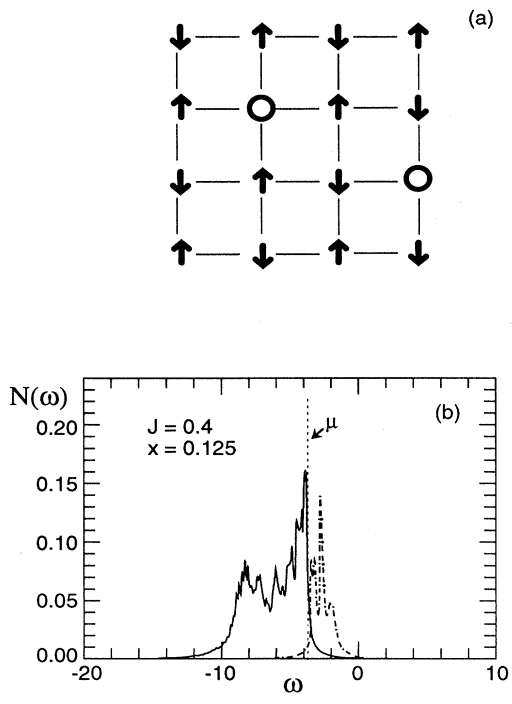

FIG. 51. (a) Snapshot of the ground state of Hubbard-like models on a square lattice at large U/t and low hole doping. (b) Density of states of the t-J model at $J/t=0.4$ and density $\langle n\rangle=0.875$ (i.e., two holes on a 4×4 cluster). Results taken from Dagotto, Moreo, Ortolani, Poilblanc, and Riera (1992). See also Stephan and Horsch (1991).

The explanation, then, for the presence of weight in the antiferromagnetic gap is fairly simple in electronic models. Note that such reasoning also predicts that at large values of U/t, where the gap is larger than the typical total width of the spectrum of one added particle (of order t), the gap cannot then be filled completely. This prediction can be easily verified by studying the results obtained at $U/t=20$. Effectively it was found that the gap is not filled in this case (Dagotto *et al.*, 1991; Dagotto, Moreo, Ortolani, Poilblanc, and Riera, 1992). In the other limit of small U/t, where the antiferromagnetic gap is much smaller than $8t$, a small doping fraction will wash out the details of the gap entirely. This result has also been verified numerically. Then, there is a window in parameter space, roughly centered near $U\sim 8t$ in two dimensions, where the experimental results are qualitatively reproduced by a one-band Hubbard model; i.e., the gap is filled entirely, but a "pseudogap" remains (here defined as a region with small spectral weight). In previous sections of this review, we also found that a coupling U in the neighborhood of $8t$ to $10t$ systematically reproduces several features of the experiments (see Secs. IV.A.1 and IV.B.3). For completeness, in Fig. 51(b) the density of states of the t-J model is shown at $x=0.125$ and $J=0.4t$ obtained on a 4×4 cluster (Dagotto, Moreo, Ortolani, Poilblanc, and Riera, 1992). Note the similarity between this figure and the spectrum of the one-band Hubbard model at the same doping for energies below the pseudogap. Also note that results for the attractive Hubbard model have been presented by Dagotto *et al.* (1991; see also Dagotto, Moreo, Ortolani, Riera, and Scalapino, 1992). In this case the chemical potential remains inside the superconducting gap upon doping.

Thus far we have observed the appearance of spectral weight in the insulator gap using *one*-band models. What happens with the more realistic (and complicated) three-band Hamiltonian defined in Sec. I.C.1? To gain some intuitive understanding of this problem, it is convenient to study first the limit of zero hybridization (i.e., all hopping amplitudes equal to zero). Consider the Hamiltonian of the model written in this limit as

$$H=(\epsilon_d-\mu)\sum_i n_i^d+(\epsilon_p-\mu)\sum_j n_j^p + U_d\sum_i n_{i\uparrow}^d n_{i\downarrow}^d+U_p\sum_j n_{j\uparrow}^p n_{j\downarrow}^p\ , \tag{4.14}$$

where p and d denote oxygen and copper sites, respectively, and the rest of the notation was introduced in Eq. (1.1) (we use hole operators; the special case where the nearest-neighbor density-density interaction U_{dp} is zero is studied). Assume that $\epsilon_p > \epsilon_d$. Then the ground-state energy of one hole is $E = \epsilon_d - \mu$; and in the large U_d limit the ground-state energy of two holes corresponds to having one hole in a copper and another in an oxygen, and it has an energy $E = \epsilon_d + \epsilon_p - 2\mu$. Then, in order to make stable the state of one hole, we need to tune the chemical potential such that it lies in the interval $\epsilon_d \leq \mu \leq \epsilon_p$. As an example, let us consider one of the extremes of the interval, i.e., $\mu = \epsilon_d$. In this case the energy of zero and one hole are zero; the energy of two holes (one in copper and one in oxygen) is $\Delta = \epsilon_p - \epsilon_d$; and two holes on a copper (oxygen) ion have an energy U_d ($U_p + 2\Delta$).

Then, in the PES and IPES spectrum of a CuO_2 Hamiltonian in the atomic limit and in the case of one hole in the ground state, we expect to observe weight at the energies mentioned before, namely, 0, Δ, U_d, and $U_p + 2\Delta$, all referred to the chemical potential. When the hopping amplitudes are turned on, each of these sharp energies will acquire a width that grows with t_{pd}. The results of a numerical exact-diagonalization study carried out by Tohyama and Maekawa (1992) on a cluster with four copper atoms and 13 oxygen atoms are shown in Fig. 52, for both hole and electron doping (see also Horsch *et al.*, 1989 and Ohta *et al.*, 1992). As parameters these authors considered $U_d = 8.5$ eV, $U_p = 4.1$ eV, $t_{pd} = 0.966$ eV, and $\Delta = 3.255$ eV. A direct oxygen-oxygen hopping was also included, $t_{pp} = 0.395$ eV. Let us concentrate on the results at the top of the figure. The inverse photoemission structure (BIS) corresponds to the states with no holes (in the electronlike language, this is the upper Hubbard band corresponding to the copper atoms; i.e., it is obtained by adding one more electron to the system). Reciprocally, at large and positive energy, we can observe the lower Hubbard band that corresponds to two holes (four electrons) distributed such that two holes are on the same copper site ($d^9 \rightarrow d^8$). Near E_F a gap of charge-transfer origin exists (but it is difficult to see in Fig. 52, since the δ functions have been given a finite width to present the results). The arrow indicates the position of Δ, i.e., the place where weight related to the case of two independent holes located one in copper and the other in oxygen should start. We clearly see a considerable spectral weight in that regime, in nice agreement with the atomic limit.

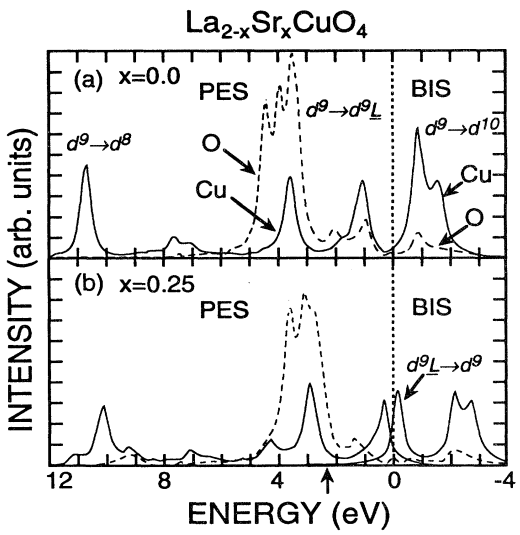

FIG. 52. One-particle excitation spectra for Cu and O orbitals in the middle of a Cu_4O_{13} cluster. (a) corresponds to $x = 0.0$, and (b) to $x = 0.25$ for $La_{2-x}Sr_xCuO_4$. The solid and dashed lines denote results for Cu and O, respectively. The broadening of the Lorentzians is 0.4 eV. The results were obtained using exact-diagonalization techniques by Tohyama and Maekawa (1992).

However, note that in addition to these features an appreciable amount of spectral weight exists at much lower energies, making the actual gap at half-filling considerably smaller than Δ. These states are the Zhang and Rice singlets (Zhang and Rice, 1988), which correspond to a spin singlet combination between the hole at the copper with a hole at the surrounding oxygen ions (thus Fig. 47 is actually incomplete!). The energy of this correlated state is reduced by the formation of such a singlet, and, according to Zhang and Rice, in the strong-coupling limit this energy becomes $E_{\text{singlet}} = \Delta - 8t_{pd}^2[1/\Delta + 1/(U_d - \Delta)]$. For the same reason there is a triplet in the spectrum whose energy is equal to Δ in this limit. Upon doping, the chemical potential shifts into the Zhang-Rice band, and states fill the insulator gap, in a manner very similar to that observed in the one-band Hubbard model (see also Sá de Melo and Doniach, 1990; Wagner, Hanke, and Scalapino, 1991; and Dickinson and Doniach, 1993).

We have seen that one of the unconventional features of $N(\omega)$, i.e., the presence of the states in the gap, has a possible explanation in the context of simple electronic models of the superconductors. However, the second paradoxical feature, namely, the behavior of the chemical potential with doping, cannot be explained using these models. This conclusion can be inferred from the results for $N(\omega)$ discussed earlier, or in more detail by considering the behavior of the electronic density $\langle n \rangle$, of the one-band Hubbard model as a function of the chemical potential μ, as reported by Moreo, Dagotto, and Scalapino (1991). In the regime of small and intermediate U/t, quantum Monte Carlo techniques are able to study large clusters, and the results are shown in Fig. 53(a), where Lanczos results on a smaller cluster are also shown. It is clear that in order to change the density from hole doped ($\langle n \rangle < 1$) to electron doped ($\langle n \rangle > 1$), the chemical potential has to cross a gap that corresponds to the "antiferromagnetic" gap observed in the density of states. Similar conclusions were reached by Furukawa and Imada (1992). A quantum Monte Carlo study of the three-band Hubbard model by Dopf, Muramatsu, and Hanke

(1990) on a 4×4 Cu-O cluster (16 cells) at the particular couplings shown in Fig. 53(b) (i.e., in the proper charge-transfer regime) arrived at similar conclusions, i.e., the chemical potential needs to cross a gap to change the density from hole to electron doping (see also Scalettar, 1989 and Scalettar *et al.*, 1991). Thus it is clear that purely electronic models of strongly correlated electrons *cannot* explain the strange pinning of the chemical potential observed in PES experiments. We do not think that this qualitative conclusion would change as a function of the couplings of the model as long as we have an antiferromagnetic gap in the one-band Hubbard model (or charge-transfer gap in the three-band model). No work has been carried out including phonons and disorder to explore their influence on μ.

Summarizing, we have seen that the study of $N(\omega)$ and $\langle n \rangle$ vs μ shows that models of strongly correlated electrons predict the presence of new states in the insulator gap when doping is added to the half-filled ground state. This is in agreement with several experimental results for the cuprate superconductors and other nonsuperconducting materials. On the other hand, the behavior of the chemical potential with doping observed experimentally using PES techniques remains a mystery, since all theoretical models consistently support the notion that μ needs to cross the insulator gap when hole doping is changed into electron doping. The presence of phase separation in the Sr- and Ce-doped compounds may be an explanation for this problem (Moreo, 1994). The solution of this paradox may well be very important for our understanding of correlated electrons and high-T_c superconductors.

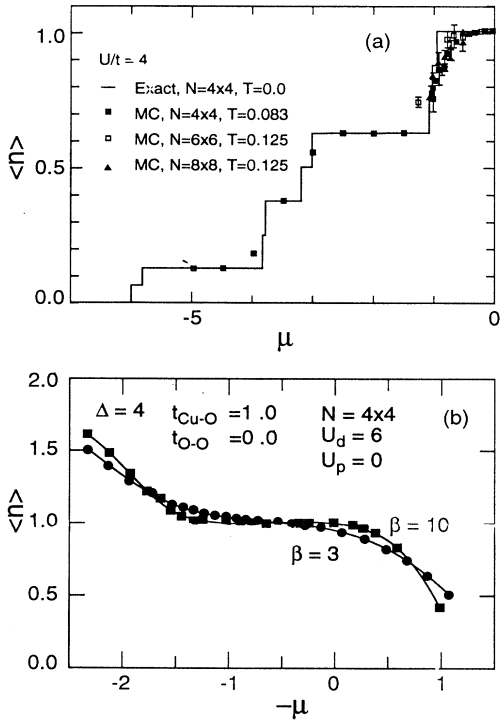

FIG. 53. (a) Density $\langle n \rangle$ vs μ for the one-band Hubbard model at $U/t = 4$ using quantum Monte Carlo on clusters of different sizes (dots), and exact Lanczos results for the 4×4 cluster (solid line). T denotes temperature. Results taken from Moreo, Dagotto, and Scalapino (1991). See also Dagotto, Moreo, Ortolani, Poilblanc, and Riera (1992). (b) Total hole occupation number per elementary cell as a function of the chemical potential μ, for the parameters of the three-band Hamiltonian shown in the figure. Sixteen CuO_2 cells are considered at two temperatures (β=3 and 10). The charge-transfer gap is clearly observed. Taken from Dopf, Muramatsu, and Hanke (1990). See also Scalettar *et al.* (1991).

3. Angle-resolved photoemission

The photoemission data discussed in the previous section provide information about the integral over all momenta $\mathbf{p}$ of the spectral function $A(\mathbf{p},\omega)$ of electrons ejected from the materials in the photoemission process. However, it is experimentally possible to obtain explicitly $A(\mathbf{p},\omega)$ as a function of $\mathbf{p}$. This technique is called angle-resolved photoemission spectroscopy (ARPES). For example, ARPES results have been obtained for single crystals of $YBa_2Cu_3O_{6+x}$ at several different dopings in the interval $0.2 \leq x \leq 0.9$. According to Campuzano *et al.* (1990, 1991), Liu *et al.* (1992; see also Liu, Veal, *et al.*, 1992), and Veal *et al.* (1993), several features of the fermiology of this material have been established using this method. In particular, band dispersions and a Fermi surface have been observed. These authors claim that predictions of band theory appear to be quite reliable near the Fermi energy E_F, at least in the oxygen range $x \geq 0.5$, where the material shows metallic behavior. They also interpret their results as giving support to a Fermi-liquid picture of this particular compound, although they clarify that no general agreement has been reached on what theoretical framework provides the best description of their results. Recently King *et al.* (1993) studied the electronic structure of $Nd_{2-x}Ce_xCuO_{4-\delta}$ using ARPES techniques, with $x = 0.15$ and 0.22. They concluded that a Fermi surface is observed that agrees very well with band-structure calculations and appears to shift with electron doping, as expected by a band-filling scenario.

$Bi_2Sr_2CaCu_2O_{8+\delta}$ has also been carefully studied using ARPES techniques. Olson *et al.* (1990; see also Dessau, 1992) concluded that a Fermi surface exists in this material. Actually, a band along the $\Gamma - Y$ direction in the Bi2212 notation was observed to cross the Fermi surface, in rough agreement with predictions from band theory calculations (see Fig. 54). These authors also found that the spectra show correlation effects in the form of an increased effective mass, but the essence of the single-particle band structure is retained. It may be convenient at this point to remind the reader that the standard notation for $\mathbf{p}$ points of the Brillouin zone of a Cu-O plane is that the Γ point is at the center, the M point is at the corner, and the $X(Y)$ points are midway along the edges. However, Bi2212 has a different notation with the map-

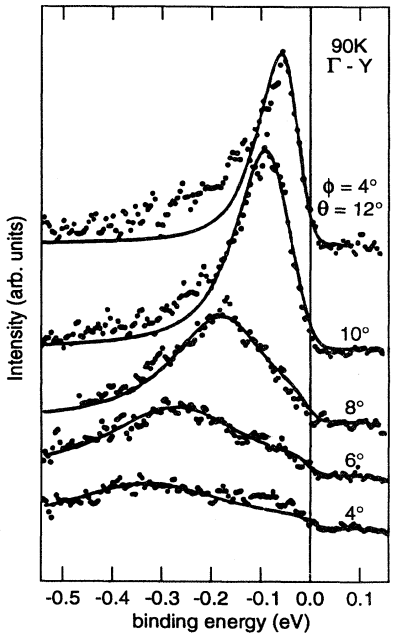

FIG. 54. ARPES obtained by Olson *et al.* (1990) in the normal state of Bi2212 along the $\Gamma - Y$ edge [equivalent to scanning between $\mathbf{p}=(0,0)$ and (π,π) in the notation of the square lattice]. The solid lines are fits assuming a marginal Fermi-liquid behavior, i.e., inverse hole lifetimes proportional to $|E-E_F|$. However, note the large background in the figures.

ping $\Gamma \rightarrow \Gamma$, $M \rightarrow X(Y)$, and $X(Y) \rightarrow \bar{M}$. Figure 55(a) clarifies this relation. In Fig. 55(b), the experimentally observed band structure along various high-symmetry directions is shown (taken from Dessau, 1992).

Olson *et al.* (1990) claimed that a good fit of their Bi2212 results can be obtained using a quasiparticle lifetime linear in $|E-E_F|$ as predicted in the marginal Fermi-liquid (MFL) theory of Varma *et al.* (1989), instead of being proportional to $(E-E_F)^2$ as in a Fermi-liquid (FL) theory. Additional support for the MFL hypothesis came from neutron-scattering measurements by Hayden *et al.* (Hayden, Aeppli, Mook *et al.*, 1991; see also Aeppli, 1992a and Bénard, Chen, and Tremblay, 1993). However, Liu, Anderson, and Allen (1991) have recently shown that once the difficult issue of the background in the ARPES spectra is handled carefully, MFL and FL fits will be equally good. Systematic studies of ARPES experiments in materials with a well-known many-body ground state are necessary before extracting conclusions from these experiments for the high-T_c superconductors (see, for example, Claessen *et al.*, 1992). Current ARPES experiments have *not* been able to solve the important issue of whether there are quasiparticles in he cuprates (i.e., whether the quasiparticle weight Z is a finite number). Actually, different theorists extract quite different conclusions from exactly the same ARPES data! More work remains to be done on the experimental side to reach a consensus about the correct description of the normal-state line shape of the cuprates.

On the theoretical side, the study of $A(\mathbf{p},\omega)$ has been carried out only for simple one- and three-band models of correlated electrons. A comparison between theory and experiments is difficult, even at a qualitative level, because Bi2212 and YBCO have a complicated structure with two CuO_2 planes close to each other plus other bands produced by charge reservoir ions. Then, only rough qualitative details can be theoretically addressed, such as the presence of dispersive bands in the spectrum and the existence of a Fermi surface in the models under consideration. These two issues will be briefly discussed in this section. Let us first consider the undoped case. In the study of spin-density waves at half-filling in the one-band Hubbard model, we found in Sec. III.A that a simple mean-field approximation was enough to describe qualitatively the physics of the model. By using this approximation, it can be easily shown (Dagotto, Ortolani, and Scalapino, 1992) that the spectral weight is given by

$$A(\mathbf{p},\omega)_{\mathrm{MF}}=\frac{1}{2}\left[1+\frac{\epsilon_{\mathbf{p}}}{E_{\mathbf{p}}}\right]\delta(\omega-E_{\mathbf{p}}) + \frac{1}{2}\left[1-\frac{\epsilon_{\mathbf{p}}}{E_{\mathbf{p}}}\right]\delta(\omega+E_{\mathbf{p}}) , \tag{4.15}$$

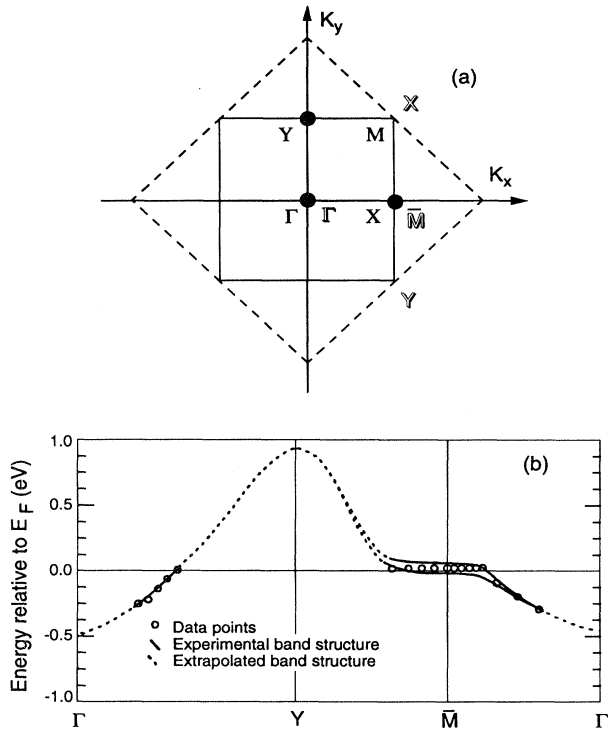

FIG. 55. (a) Momentum notation used for Bi2212. The solid lines denote the standard convention for the square lattice with $\Gamma=(0,0)$, $M=(\pi,\pi)$, $X=(\pi,0)$, and so on. The dashed line and the characters in open letters denote the convention followed in Bi2212, caused by the presence of the BiO planes. (b) The ARPES experimental band structure along various high-symmetry directions in Bi2212 (from Dessau, 1992). The momentum notation is that of Bi2212; i.e., the Y ($\bar{M}$) point in the figure corresponds to $\mathbf{p}=(\pi,\pi)$ [$\mathbf{p}=(\pi,0)$] in the notation of the square lattice.

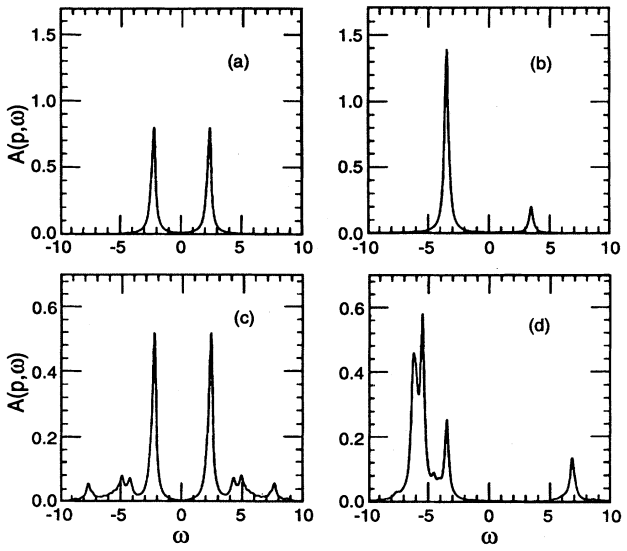

FIG. 56. Mean-field spectral weight vs ω in units of t. (a) corresponds to momentum $(\pi,0)$, while (b) is (0,0). Lanczos calculations of $A(\mathbf{p},\omega)$ at $\langle n\rangle=1$, using a 4×4 cluster and $U/t=8$. (c) has momentum $(\pi,0)$; and (d), (0,0).

where $E_{\mathbf{p}}=(\epsilon_{\mathbf{p}}^2+\Delta_{\mathrm{SDW}}^2)^{1/2}$, $\epsilon_{\mathbf{p}}=-2t(\cos p_x+\cos p_y)$, and the spin-density-wave gap Δ_{SDW} is given by the solution of the equation

$$1=\frac{U}{N}\sum_{\mathbf{p}}\frac{1}{2E_{\mathbf{p}}}\ .$$

The mean-field results are shown in Fig. 56 for two different momenta and at a coupling $U/t=8$. At $\mathbf{p}=(0,\pi)$ or $(\pi/2,\pi/2)$, the spectral function has sharp peaks with a gap in between,[13] and it is symmetric around $\omega=0$ [Fig. 56(a)]. On the other hand, Fig. 56(b) corresponds to zero momentum; i.e., in the PES spectrum an electron well below the Fermi surface is destroyed. As expected, considerable spectral weight is observed in the PES spectrum, while that corresponding to the IPES is small. The situation is reversed if a momentum $\mathbf{p}=(\pi,\pi)$ is used (not shown in the figure). These mean-field results are in good agreement with numerical results obtained on 4×4 clusters using exact-diagonalization methods, which are shown in Figs. 56(c) and 56(d) (taken from Dagotto, Ortolani, and Scalapino, 1992; see also Feng and White, 1992 and Leung *et al.*, 1992). They are also in good agreement with QMC-maximum entropy calculations (White, 1991). The structure away from the dominant peaks in the numerical results shows that an important percentage of the spectral weight is not in the quasiparticle peak, as explained in Sec. III.B.4 (in other words, in these models, $Z<1$ as discussed earlier). The density of states $N(\omega)$ can be obtained by summing over $\mathbf{p}$.

Away from half-filling, there is no universally accepted mean-field approximation to describe models of correlated electrons. In that case, we turn to computational studies for some guidance. In Fig. 57, $A(\mathbf{p},\omega)$ is shown for the one-band Hubbard model at $U/t=8$ and $\langle n\rangle=0.875$. The chemical potential is located approximately at $\mu=-2.4t$. Note the presence of a dominant peak for $\mathbf{p}=(\pi,0)$ located right after the chemical potential on the IPES side of the spectrum [Fig. 57(a)]. This peak is followed by spectral weight that fills the original antiferromagnetic (AF) gap. At higher energies the remnants of the upper Hubbard band can be observed. The effect of doping is to remove weight from the lower and upper Hubbard bands and to create states in the gap, as we discussed in the previous section. Moving in momentum space away from the noninteracting Fermi surface, in the direction of the Γ point, the PES weight increases, while IPES weight decreases. On the contrary, increasing the momentum towards the (π,π) point, the situation is reversed. For momentum $\mathbf{p}=(\pi/2,\pi/2)$, the dom-

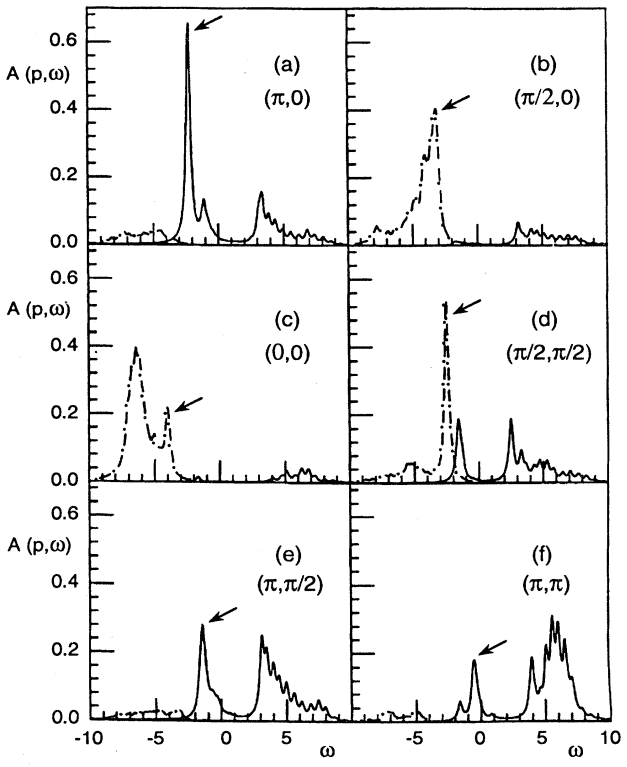

FIG. 57. $A(\mathbf{p},\omega)$ obtained on a 4×4 cluster with $U/t=8$ and $\langle n\rangle=0.875$. The chemical potential is at $\mu\sim-2.4t$. The IPES weight is shown as a solid line, and the PES as dot-dashed. (a) corresponds to momentum $(\pi,0)$; (b), to $(\pi/2,0)$; (c), to (0,0); (d), to $(\pi/2,\pi/2)$; (e), to $(\pi,\pi/2)$; and, finally, (f) is (π,π). The arrows mark the peaks that can be labeled as "quasiparticles" (results taken from Dagotto, Ortolani, and Scalapino, 1992).

[13]The small weight inside the gap is caused by the tail of the Lorentzians of width $\epsilon=0.2t$ used to plot the δ functions in Fig. 56.

inant peak seems split, and thus this momentum may be close to the new Fermi surface of the doped system [Fig. 57(d)]. Coming back to the comparison between theory and experiment, we can conclude that the existence of dispersive features is observed both in ARPES results and in studies of simple models of correlated electrons. Similar conclusions have been obtained in the *t-J* model (Stephan and Horsch, 1991; Dagotto, Moreo, Ortolani, Poilblanc, and Riera, 1992) and in the three-band Hubbard model (Dopf *et al.*, 1992). A more quantitative comparison would be very difficult with the numerical methods currently available for studying these models.

4. Fermi surface in models of correlated electrons

The study of $\langle n_p \rangle$ in the one-band Hubbard model using quantum Monte Carlo techniques (Moreo, Scalapino, *et al.*, 1990) shows that, working on a 16×16 cluster at doping $\langle n \rangle = 0.87$ and coupling $U/t = 4$, the locus of points where $\langle n_p \rangle = 0.5$ is close to that of a noninteracting system at the same filling. These results are shown in Fig. 58(a). Although this simulation was carried out at a finite temperature (due to sign problems), the conclusions are similar to those reached by exact-diagonalization studies on 4×4 clusters (Dagotto, Ortolani, and Scalapino, 1992) at zero temperature [schematically shown in Fig. 58(b), based on the results shown in Fig. 57]. The

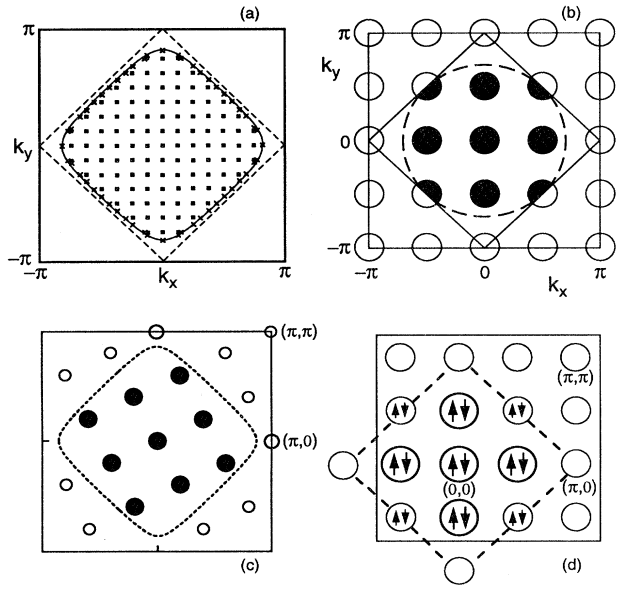

FIG. 58. Fermi surface of models of correlated electrons according to different studies: (a) corresponds to the one-band Hubbard model on a 16×16 cluster using quantum Monte Carlo (from Moreo, Scalapino, *et al.*, 1990); (b) results of Dagotto, Ortolani, and Scalapino (1992) on a 4×4 cluster using exact diagonalization (one-band Hubbard model); (c) results obtained by Stephan and Horsch (1991) using Lanczos techniques applied to the *t-J* model on a 20-site cluster; (d) results by Ding (1993) for the *t-J* model based on $\langle n_p \rangle$. The Fermi surfaces are sketched in all of the plots.

$\mathbf{p}=(\pi,0),(0,\pi)$ states do not seem populated, while $\mathbf{p}=(\pm\pi/2,\pm\pi/2)$ are close to the Fermi surface. Studies of the *t-J* model using exact-diagonalization techniques at a doping of approximately $\sim10\%$ holes on a 20-site lattice are consistent with a large electronic Fermi surface [see Fig. 58(c), taken from Stephan and Horsch, 1991]. High-temperature expansion calculations reached similar conclusions (Singh and Glenister, 1992b), i.e., the presence of a Fermi surface in these models (note that a Fermi surface does not inevitably imply a Fermi liquid as remarked by Anderson, 1990a). A Lanczos study of $\langle n_p \rangle$ (Ding, 1992) has produced a Fermi surface very similar to that observed in Hubbard model calculations, showing that holes doped into an antiferromagnet may actually prefer to be located in the vicinity of momenta $\mathbf{p}=(0,\pi),(\pi,0)$ rather than at the $\mathbf{p}=(\pm\pi/2,\pm\pi/2)$ [Fig. 58(d)]. A similar "nonstandard" result was discussed by Poilblanc and Dagotto (1990). The claim is based on the following argument: If, indeed, two holes in an antiferromagnet form a *d*-wave state (as argued earlier in this review), then the contribution of hole states at $\mathbf{p}=(\pm\pi/2,\pm\pi/2)$ cancels, since $f(k)=\cos k_x-\cos k_y$ vanishes, while $\mathbf{p}=(\pm0,\pm\pi)$ makes $f(k)=2$ maximum. Note that all these results seem in contradiction with the picture that would have emerged from studies of single holes in antiferromagnets. In this case, holes have momentum $\mathbf{p}=(\pm\pi/2,\pm\pi/2)$ in the ground state, and thus, assuming a rigid-band picture, hole *pockets* should appear in the neighborhood of these points in momentum space. Then, once interactions have been taken into account, the rigid-band approach naively does not seem a good approximation to the present problem (for a different point of view, see Eder and Wróbel, 1992; Eder and Ohta, 1994). Unfortunately, with currently available numerical techniques, it is difficult to study very low density of holes and temperatures to search for indications of hole pockets (for recent results on this issue predicting the presence of hole pockets at very low temperature, see Dagotto, Nazarenko, and Boninsegni, 1994). Indications of hole pockets using QMC have been recently reported (Moreo and Duffy, 1994). Thus, hole pockets may be there after all!

D. Phase separation

1. Experimental results

There is considerable experimental evidence that $La_2CuO_{4+\delta}$ has a regime in which phase separation occurs (Jorgensen *et al.*, 1988; see also Harshman *et al.*, 1989). Using La NMR, Hammel *et al.* (1992) have shown that the temperature at which phase separation takes place is $T_{ps}\sim250$ K (see also Hammel, Reyes, *et al.*, 1990; Hammel, Ahrens, *et al.*, 1991; and references therein). The separation occurs between a phase with a stoichiometry very close to La_2CuO_4 and a phase rich in oxygen that becomes superconducting at about 40

K. In Fig. 59 the phase diagram temperature δ is shown (Hammel *et al.*, 1992; Reyes *et al.*, 1993). The regime of doping fractions between $\delta \sim 0.01$ and ~ 0.06 is not thermodynamically stable; i.e., if a sample is prepared with this nominal composition, it will spontaneously separate into two regions with the densities shown in the figure. The oxygen-poor phase exhibits long-range antiferromagnetic order, which is reasonable since δ is very small in this phase, and we know La_2CuO_4 is an antiferromagnet. Then, phase separation may well be driven by the energy gained by forming a magnetically ordered phase (Hammel *et al.*, 1992). The more widely analyzed $La_{2-x}Sr_xCuO_4$ compound does not seem to phase separate, although a more careful work should be carried out for this compound.

Given these experimental results, we may try to blame oxygen "chemistry" for the existence of phase separation. The dopant oxygen atoms may cluster together for reasons that are unrelated to the physics of electrons in the CuO_2 planes. If this be the case, then phase separation would just become one more curiosity of the cuprate superconductors. However, it has been claimed that the mobility of the oxygens is exceptionally large at T_{ps} (Hammel *et al.*, 1992). In addition, it is quite remarkable that T_{ps} is very close to the Néel temperature of the material where 3D antiferromagnetism develops. These features open the possibility, recently addressed by Emery and Kivelson (1993), that the effect is actually produced by the physics of electrons in the planes and is due to phase separation into hole-rich and hole-poor regions. In this scenario, the excess oxygens would simply follow the holes of the plane in their search for the minimum-energy configuration. The important physics would be contained in the planes. Recently, other challenging concepts have been introduced (Cho *et al.*, 1992, 1993). In a study of $La_{2-x}Sr_xCuO_{4+\delta}$, with both x and δ changed, it has been claimed that the oxygen-poor phase has a novel segregation of doped holes into walls of hole-rich material separating undoped domains. This implies that the so-called spin-glass phase of the [214] material may actually be formed by walls of holes that disrupt the long-range AF order, constraining the spin-correlation length to a maximum value given by the distance between walls. In short, the presence of phase separation may be an important issue in understanding the physics of the cuprates, and it certainly deserves a careful theoretical analysis.

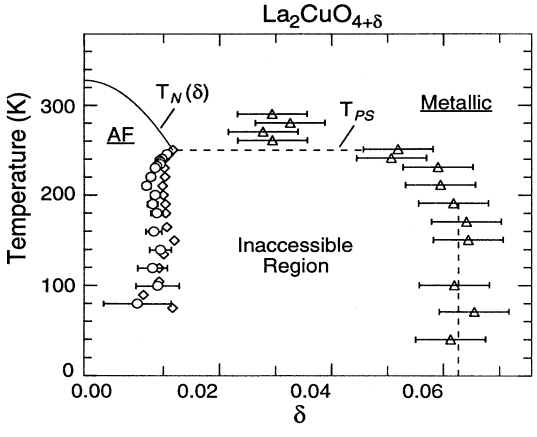

FIG. 59. Phase diagram of $La_2CuO_{4+\delta}$. The oxygen-poor phase is described by the left set of data. Circles and diamonds are results from two samples. The second phase having higher doping is metallic and, at low temperatures, superconducting (not shown in the plot). The region bounded by the two curves and below T_{ps} is inaccessible (from Reyes *et al.*, 1993; see also Hammel *et al.*, 1992).

2. Theoretical results

Initially, the study of phase separation in models of strongly correlated electrons did not receive as much attention as the search for superconductivity. However, after some effort, it was clear that even the mere existence of a superconducting phase in these models was a subject considerably more subtle than expected. Then, to gain more insight about the behavior of correlated electrons, it became important to understand the full phase diagram of some popular models of the cuprates, including regimes where the phenomenon of phase separation takes place.

In the *t-J* model, it was rapidly realized that at large J/t the model phase separated (Riera and Young, 1989; Emery, Kivelson, and Lin, 1990; Marder, Papanicolaou, and Psaltakis, 1990; Nori, Abrahams, and Zimanyi, 1990; and references therein). As explained in Sec. III.B.5, adding a low mobility hole to the undoped system amounts to removing four antiferromagnetic links, thus increasing the energy of the system. Then, in order to minimize the number of "broken" AF links, an additional hole added to the system will prefer to be located at a distance of one lattice spacing from the first one. In this way, the number of broken AF links is minimized. When more (low mobility) holes are added to the system, the configuration that minimizes the energy is the one where they form a compact cluster. Then, at large J/t the ground state of the *t-J* model clearly separates into hole-rich and hole-poor regions. Of course, the regime of large J/t is not physically realized in the high-T_c compounds (Sec. I.C.2), and this problem seems only of academic interest. However, phase separation may survive a reduction of J/t. Then, it becomes important to study whether the regime of phase separation at large J/t exists also for small values of this coupling near half-filling, i.e., in the physically interesting regime.

Unfortunately, the answer to this problem is still controversial. Emery, Kivelson, and Lin (1990) claimed that the boundary of phase separation in the *t-J* model is schematically given by the diamonds shown in Fig. 60(a). Their result is based on variational arguments and exact-diagonalization studies of the 4×4 cluster. Note that their phase-separation boundary seems to converge to $J/t=0$ as the undoped limit $\langle n \rangle = 1$ is approached.

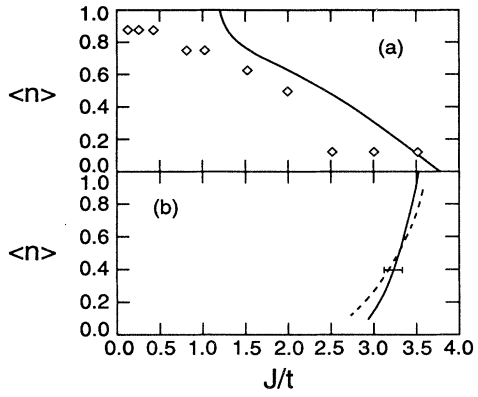

FIG. 60. (a) Line of phase separation in the two-dimensional t-J model based on the high-temperature expansions (Putikka, Luchini, and Rice (1992; solid line) and on the analysis of Emery, Kivelson, and Lin (1990; points). The major difference between these authors occurs near half-filling. (b) For completeness, here we also show the results for the same model in one dimension. The solid line denotes the high-temperature-series result, while the dashed one shows finite cluster exact-diagonalization results by Ogata *et al.* (1991). Note the nice agreement between the two techniques for the 1D chain.

However, precisely this behavior near half-filling is the subject of controversy between different groups. The boundary of phase separation in the same model has been studied by Putikka, Luchini, and Rice (1992), using a high-temperature series expansion up to tenth order in $\beta=1/T$. The series has a finite radius of convergence, and, in order to get results at small temperatures, an analytic continuation based on Padé and integrals approximants is needed. At $J/t\sim 0.3$ and density $\langle n\rangle\sim 0.9$, temperatures $T\sim t/5$ were reached by this procedure. The result of the high-temperature expansion method is also shown in Fig. 60(a) with a solid line. Note that the phase boundary touches the half-filled axis at a finite coupling $J/t\sim 1.2$, contrary to the results of Emery, Kivelson, and Lin (1990). Other numerical studies have also addressed this issue. For example, Dagotto, Moreo, Ortolani, Poilblanc, and Riera (1992) carried out an analysis similar to that discussed by Emery, Kivelson, and Lin, i.e., exact diagonalization on 4×4 clusters. Dagotto *et al.* arrived at different conclusions, since they interpreted the diamonds of Fig. 60(a) as indicating the region where *binding* of holes takes place, i.e., where individual holes are unstable towards pair formation, but not necessarily towards phase separation which starts at a larger coupling similar to that given by the high-temperature expansions (and it is roughly signaled by the tendency of four holes to form a bound state which roughly starts at $J/t\sim 1$). Similar conclusions based on the use of larger clusters were obtained by Fehske *et al.* (1991), Röder *et al.* (1991), and Prelovšek and Zotos (1993; in the last reference it is argued that a "striped phase," namely, holes forming domain walls, exists before the onset of hole clustering). If phase separation would indeed start at a coupling $J/t>1$, then it may only be of academic interest. Different would be the situation if, in the realistic regime of $J/t\sim 0.2$–0.4, phase separation exists near half-filling. In short, the gist of the disagreement between numerical studies and the results of Emery *et al.* is whether small J/t and large J/t physics are related. While Emery *et al.* claim that the simplest assumption is phase separation for all values of the coupling near half-filling, the numerical results suggest that phase separation starts at a coupling J/t of order one, and that an intermediate regime (approximately $0.3\leq J/t\leq 1.0$) exists where binding of holes prevails without phase separation. In this region, a superfluid may be formed if these pairs condense at zero temperature (Dagotto, Moreo, Ortolani, Poilblanc, and Riera, 1992). See Sec. IV.E for more details.

What occurs in the one-band Hubbard model? At large U/t this model should be qualitatively equivalent to the t-J model at small J/t. Then, it is worth studying the issue of phase separation directly in the Hubbard model, where quantum Monte Carlo techniques are available for its analysis. Unfortunately, with this method it is difficult to study large couplings; thus results at low temperature have been obtained only in the intermediate region $U/t=4$. In Fig. 53(a), results given by Moreo, Dagotto, and Scalapino (1991) were discussed in order to compare theoretical results with those observed experimentally in PES experiments. But the same data can be used to address the issue of phase separation in these models. The results of Fig. 53(a) show a study of the density $\langle n\rangle$ as a function of the chemical potential μ. This criterion is based on the following idea: *if* a discontinuity is observed in $\langle n\rangle$ vs μ, then the densities inside the gap are unstable; i.e., if a system is initially prepared with such nominal densities, it will evolve in time into a phase-separated state, with the two regions having the densities corresponding to the extremes of the gap. However, the results of Fig. 53(a) do not show signs of discontinuity. The simulations have been carried out on clusters with up to 8×8 sites, and thus finite-size effects are not expected to change the results drastically. However, it is possible that the finite temperature at which the simulations have been carried out may have some influence on the results (due to the sign problem, it is not possible to work at temperatures as low as those obtained at half-filling). The temperatures reached by quantum Monte Carlo at finite density are approximately similar to those reached by the high-temperature expansions. However, Lanczos (Dagotto, Moreo, Ortolani, Poilblanc, and Riera, 1992) and perturbative results (Galan and Vergés, 1991) support the results of Moreo, Dagotto, and Scalapino (1991).

The conclusions of Moreo *et al.* are also in agreement with a projector Monte Carlo simulation carried out by Furukawa and Imada (1992). With the use of this algorithm there is no finite temperature contamination.

However, the method is based on applying the operator $e^{-\tau H}$ to an initial ansatz for the ground state. To obtain ground-state properties, it is necessary to study the limit $\tau \to \infty$, which can be obtained numerically only up to some accuracy. Then, finite temperature errors are traded for finite τ errors in this method. The dependence of the chemical potential with hole doping in their simulation is shown in Fig. 61, where $U/t=4$ and clusters of up to 12×12 have been used. After the chemical potential crosses the antiferromagnetic gap at half-filling, Furukawa and Imada (1992) concluded, the electronic density will vary continuously as $\langle n \rangle \sim \sqrt{\mu_c - \mu}$. This result is in agreement with the conclusions of Moreo *et al.* and with the behavior of the one-dimensional Hubbard model. Then, Monte Carlo studies suggest that the Hubbard model at intermediate couplings does not phase separate. The behavior at larger couplings is unknown.

The numerical results described in this section are considered by Emery and Kivelson (1993) to be inconclusive. They argue that the high-temperature series are not reliable for temperatures much below J, since they are based on a Padé analysis, which is difficult to control. Actually Singh and Glenister (1992) claim that various Padé approximants diverge from each other for temperatures below $J/2$, and the uncertainty increases with decreasing J/t [however, the analytic continuation techniques used by Putikka, Luchini, and Rice (1992) based on integral approximants allowed them to reach temperatures $\sim t/5$ for the free energy. These approximants have more analytical information incorporated than Padé extrapolations]. The Monte Carlo simulations have also been criticized, since they are carried out at a finite temperature $T \sim t/8$; while the Lanczos calculations on small clusters can only work at a finite number of densities, and they may miss small discontinuities in the $\langle n \rangle$ versus μ curve. Then, more work is necessary to further clarify the presence of phase separation near half-filling at small J/t.

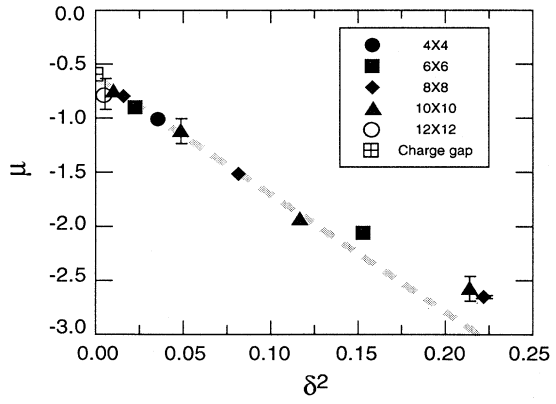

FIG. 61. Projector Monte Carlo results for the two-dimensional one-band Hubbard model at $U/t=4$, obtained by Furukawa and Imada (1992). $\delta=1-\langle n \rangle$, and μ is the chemical potential. Results are obtained for clusters of different sizes. They show that there are no apparent discontinuities in the curve, and thus no phase separation, in agreement with the previous results by Moreo, Dagotto, and Scalapino (1991).

The effect of the long-range Coulomb interactions that tend to destroy phase separation also deserves more theoretical work [for preliminary work in this direction, see Troyer *et al.* (1993); Riera and Dagotto (1994)]. Recently, Haas *et al.* (1994) observed that $1/r$ interactions induce a competition between superconductivity and charge-density-wave states.

E. Superconductivity in models of strongly correlated electrons

1. Superconductivity in the one- and three-band Hubbard models

After our long journey through the several physical quantities that characterize the normal state of the cuprates, we have finally arrived at the study of the superconducting phase. Leaving this subject to the end of the review is not an accident. In spite of the considerable effort that has been devoted to the search for superconducting long-range correlations in models of strongly interacting electrons, no clear indications of their existence have been found in the realistic regime of parameter space. What became clear over the years is that the presence of superconductivity in Hubbard-like models is a subtle issue, much more than originally believed. Nevertheless, recent results discussed below still leave open the possibility for the existence of a superconducting phase in these models.

Early results by White, Scalapino, Sugar, Bickers, and Scalettar (1989) suggested that in the $d_{x^2-y^2}$ mode, the pair-field susceptibility of the one-band Hubbard model was enhanced at low temperatures with respect to the uncorrelated pair-field susceptibility (Fig. 62). Small finite-size effects were observed in these studies between clusters with 4×4 and 8×8 sites. These results were consistent with the attractive $d_{x^2-y^2}$ channel observed in the strong-coupling limit (t-J model) for the case of two holes in an antiferromagnetic background (as was shown in Sec. III.B.5) and led to considerable excitement. However, we know that in a superconducting state in the bulk limit, the expectation value of the pair operator $\langle \Delta \rangle$ should be nonzero. Although for any *finite* system $\langle \Delta \rangle$ is identically zero, the pair-pair correlation functions should indicate the presence of superconductivity (if it exists in the ground state) by converging to a finite number when the separation of the pairs is sent to infinity. Do we see this effect in the one-band Hubbard model? Unfortunately, studies carried out by several groups showed that at the temperatures and lattice sizes currently accessible to Monte Carlo simulations, there are no signals of superconductivity in the ground state, as we shall see below.

In Fig. 63 the dependence with distance of the equal-time pair-pair correlation function is shown for the $d_{x^2-y^2}$ and extended-s waves (Moreo, 1992b). The operator that destroys a pair is defined as $c_{i\uparrow}(c_{i+x\downarrow}+c_{i-x\downarrow}\pm c_{i+y\downarrow}$

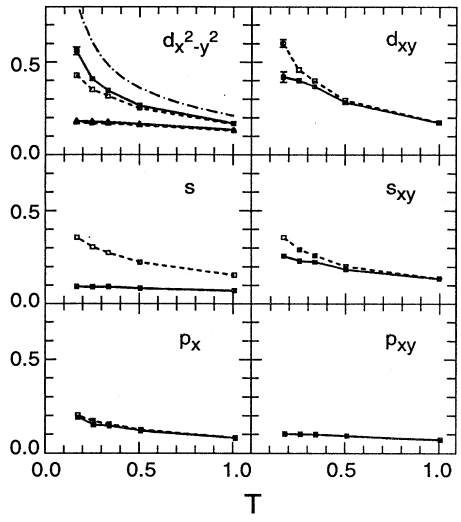

FIG. 62. Pair-field susceptibility (solid lines) and the uncorrelated pair-field susceptibility (dashed lines) vs temperature for $\langle n \rangle = 0.875$, and different channels. The noninteracting ($U/t=0$) $d_{x^2-y^2}$ susceptibility is also in the upper right box for comparison (from White, Scalapino, Sugar, Bickers, and Scalettar, 1989).

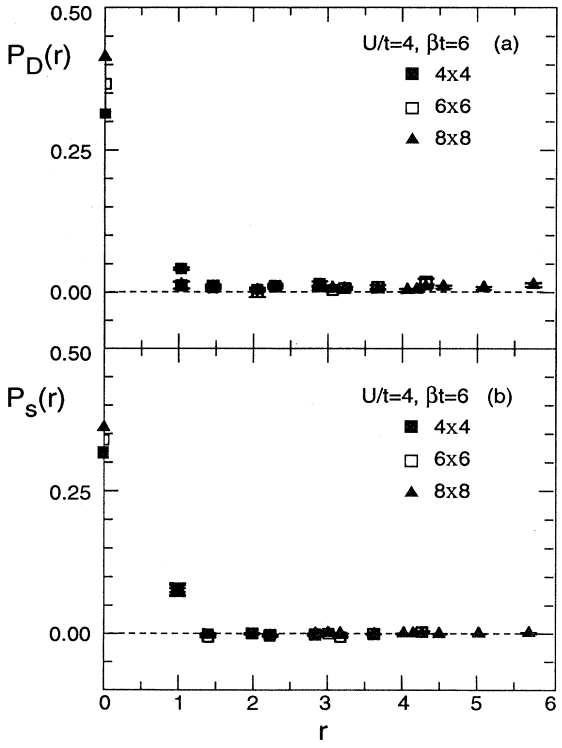

FIG. 63. Pair-pair correlation function for the one-band Hubbard model as a function of distance $r(=\sqrt{r_x^2+r_y^2})$, obtained using quantum Monte Carlo (Moreo, 1992b). The density is $\langle n \rangle = 0.85$. (a) corresponds to $d_{x^2-y^2}$ symmetry, and (b) is extended s. The temperature and lattice sizes are shown in the figure.

$\pm c_{i-y\downarrow}$), where the (+) sign corresponds to extended s-wave, and the (−) to $d_{x^2-y^2}$ wave (see footnote 6). The pair-pair correlation is defined as $P(\mathbf{r}) = \langle \Delta^\dagger(\mathbf{0})\Delta(\mathbf{r}) \rangle$, where $\mathbf{0}$ and $\mathbf{r}$ are sites of the lattice, and the susceptibility is given by $\chi_{\rm sup} = \sum_{\mathbf{r}} P(\mathbf{r})$. For both waves, the sign problem prevents the simulation from being carried out at temperatures smaller than $T = t/6$; but this is the same temperature at which enhancement in the pair-field susceptibility was observed by White, Scalapino, Sugar, Bickers, and Scalettar (1989), and thus indications of superconductivity should be observed if they exist in the ground state. Unfortunately, Fig. 63 clearly shows that already at distances of two lattice spacings or larger, the pairs are not correlated in any of the two channels, with a minimal finite-size effect. Similar conclusions have been formed by Imada and Hatsugai (1989; see also Imada, 1991b). Actually, Hirsch (1993) has claimed for some time that the Hubbard does not superconduct. The reason for the apparent contradiction between the results of Figs. 62 and 63 is simple. A pair-field susceptibility contains information about the pair-pair correlations at *all* distances. Thus a susceptibility may be robust and actually increase with decreasing temperatures, if the short-distance correlations are enhanced as the temperature is reduced. Such an enhancement is *not* related to long-range order, and, if that occurs, the susceptibility should not increase like the number of sites when the cluster size is increased. For the one-band Hubbard model, it has been shown (Scalapino, 1993) that the on-site $d_{x^2-y^2}$ pair correlation (i.e., $r=0$) can be written exactly as a linear function of the spin-spin correlations at a distance of one lattice spacing. With a decrease in temperature, the presence of antiferromagnetic correlations induces an enhancement in this spin correlation, and thus the pair susceptibility is also enhanced; but this effect is unfortunately unrelated to superconductivity. In the one-band Hubbard model, then, there are currently no indications of strong pairing correlations for the clusters and temperatures available to numerical studies. This result has to be contrasted with those obtained for the *attractive* Hubbard model. Using the same cluster sizes, temperatures, and algorithm, clear numerical indications of superconductivity were observed in this model. There is no doubt then that numerical methods can indeed detect this type of long-range order if present in the ground state (Scalettar *et al.*, 1989; Moreo and Scalapino, 1991; Randeria, Trivedi, Moreo, and Scalettar, 1992). Another important issue is how we can know when a cluster is large enough to rule out the presence of superconductivity in a given model. The only way is to compare the lattice size with a typical correlation length ξ in the problem as predicted by other studies (typically based on self-consistent approximations), at the temperature at which the simulation was carried out. Unfortunately, this is a difficult task in many of the proposed theories of the cuprates, and thus such a comparison is difficult. Some recent calculations by Monthoux (1993) show that, using self-consistent diagrammatic techniques, the criti-

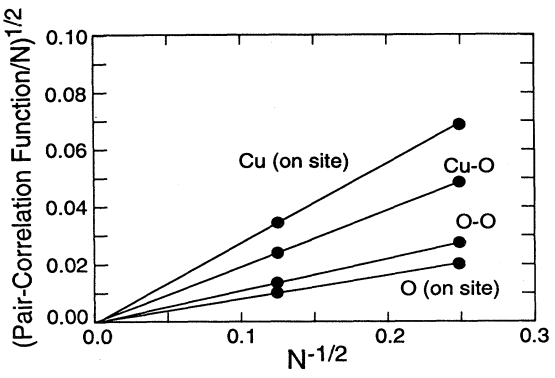

FIG. 64. Scaling of the *s*-wave pair-correlation functions with the system size N for the three-band Hubbard model using $\Delta=3t$, $U_d=5t$, $\beta=8$, and 1.25 holes per unit cell. The four lines correspond to different pair operators. All of them converge to zero in the bulk limit. For more details see Frick *et al.* (1990).

cal temperature of the one-band Hubbard model is $T_c \sim 0.02t$, i.e., not reachable by Monte Carlo simulations. Then, it may be that the one-band Hubbard model superconducts, although at very small temperatures. This remains an issue.

Results similar to those observed for the one-band case have been obtained for the three-band Hubbard model. In Fig. 64, the equal-time pair-correlation function is shown for several channels as described in the caption (Frick *et al.*, 1990). The correlation is normalized such that superconductivity is signaled by the convergence of this quantity to a nonzero value in the bulk limit. Since the pair-correlation function actually converges to zero as N increases, no indications of superconductivity in this model were detected in the parameter region analyzed by Frick *et al.* (1990; for a similar study, see Dopf, Muramatsu, and Hanke, 1990). Scalettar (1989) found that in the three-band model the pairing susceptibility indicated that the extended *s*-wave channel was competitive with the *d*-wave, and, indeed, Scalettar *et al.* (1991) showed that the addition of an intersite copper-oxygen Coulomb repulsion stabilized the *s*-pairing further. However, as in studies of the single-band model, the equal-time correlations do not show long-range order.

2. Superconductivity in the *t-J* model

The results shown in the previous section suggest that the one- and three-band Hubbard models do not superconduct, at least in the range of temperatures and cluster sizes that are accessible to present-day numerical studies. Then, the natural question is, do any of the models of correlated electrons that are currently widely studied present a superconducting phase in some region of parameter space? In trying to answer this question, let us consider the *t-J* model in more detail. Lanczos studies of this model near half-filling and $J/t<1$ by several groups do not show enhancement of the pairing correlations. This is not surprising, since, e.g., a hole density of $x=0.125$ corresponds to only one hole pair on a 16-site lattice, and just one pair cannot produce long-range order. However, the Monte Carlo results for the Hubbard model shown in the previous section on larger clusters (and thus with more holes) also do not show indications of long-range pairing correlations, and we would expect some qualitative relation between the Hubbard model and the *t-J* model at small J/t. Then, the tentative conclusion is that the *t-J* model does not superconduct at small J/t and hole density.

However, we know that the *t-J* model presents hole binding near half-filling approximately in the region $J/t>0.3$ (as was observed in Sec. III.B.5). In addition, at large J/t, it is well established that there is phase separation (Sec. IV.D), and thus it is clear that effective attractive forces are operative in this model. The pairs formed near half-filling at $J/t \geq 0.3$ may actually condense at low temperatures or, in other words, it can be argued that the attraction that leads to phase separation may create mobile *pairs*, before that regime is reached. Actually, this phenomenon explicitly occurs in the opposite regime of low *electronic* density (rather than hole density). Emery, Kivelson, and Lin (1990) have shown that a pair of electrons in an otherwise empty lattice are bound in a spin singlet in the region $J/t>2$, while phase separation seems to occur at larger couplings. It is expected that these pairs will condense at low temperature into a superfluid phase. If the pairs are small in size compared with the mean distance between pairs, then a Bose condensation will occur (i.e., in the "normal" state above T_c, preformed pairs will exist). The appearance of superconductivity near phase separation was also addressed using large-N techniques by Grilli *et al.* (1991). These authors found an instability in the A_{1g} and B_{2g} channels. Di Castro and Grilli (1992) studied the relation between phase separation and superconductivity using slave bosons. A study of the spectrum of the *t-J* model by Moreo (1992a) also suggested that superconductivity may exist near phase separation.

Then, according to these arguments, a numerical analysis of the two-dimensional *t-J* model near phase separation may finally show the elusive indications of superconductivity that we are looking for. What doping fraction is the most favorable? As explained earlier, near half-filling (and also in the other extreme of small electronic density) very few pairs are available to contribute to the pairing correlations. Then, $\langle n \rangle = \frac{1}{2}$ seems optimal, since in this regime the maximum number of pairs that can be formed grows like $N/4$, where N is the number of sites of the cluster. An analysis in this region of parameter space has been carried out recently by Dagotto and Riera (1992, 1993) and Dagotto *et al.* (1993). Indications of superconductivity in the ground state have been observed by these authors. To discuss their results, we introduce the pairing correlation function $C(\mathbf{m})=(1/N)\sum_i \langle \Delta_i^\dagger \Delta_{i+\mathbf{m}} \rangle$ (where the operator Δ was defined in the previous section) and the pairing "suscepti-

bility" $\chi_{sup}=\sum_{\mathbf{m}} C(\mathbf{m})$, as indicators of the presence of long-range superconductivity in the model. Results obtained on a 4×4 cluster at density $\langle n \rangle = 1/2$ are shown in Fig. 65(a). The susceptibility has a large peak in the vicinity of $J/t=3$, suggesting strong pairing correlations. The sharp decay for larger values of the coupling is caused by the transition to the phase-separation regime as explained by Dagotto and Riera (1993). However, from our discussion for the one-band Hubbard model, it is important to study the explicit distance dependence of the pair correlations where the susceptibility is enhanced. In Fig. 65(b) the correlations are shown for the extended s-wave and $d_{x^2-y^2}$ symmetries. The $d_{x^2-y^2}$ channel seems enhanced and appreciably large at the largest distance available on this small cluster. Finally, Fig. 65(c) shows the coupling dependence of the results. The pairing correlations have maximum strength at $J/t \sim 3$, as suggested by Fig. 65(a). Of course, these results are not final, since a proper finite-size study of these correlations has not been carried out thus far. However, they are very suggestive that, indeed, the argument expressed above relating phase separation and superconductivity may be operative (see also Dagotto *et al.*, 1994).

To gain further insight into the superconducting region detected in the t-J model, it is convenient to enlarge the Hamiltonian to include a repulsive density-density interaction $V\sum_{\langle ij \rangle} n_i n_j$. This t-J-V model was studied near the atomic limit, $t \sim 0$, by Kivelson, Emery, and Lin (1990). In the intermediate regime where $J \sim V$, a "liquid of spin dimers" was reported, and the possibility of s-wave superconductivity through a condensate of these spin dimers was discussed. Recently, their results were confirmed by Dagotto and Riera (1992) using exact-diagonalization techniques on a 4×4 cluster at large J and V couplings and for a density $\langle n \rangle = 1/2$. These numerical results are shown in Fig. 66. Three regimes were detected: (i) At small superexchange, the system forms a charge-density wave; (ii) at intermediate couplings, spin singlets are formed in a regular array [shown in Fig. 66(a)]; and (iii) at large J/V there is phase separation. These results can be obtained either by a simple minimization of the energy at $t=0$, or by the use of numerical techniques on a finite cluster in the large-couplings regime. At strictly $t=0$, the spin singlets of the intermediate phase are not mobile; but, including corrections in powers of t, Kivelson, Emery, and Lin (1990) argued that the system would become superfluid. Similar conclusions were reached in the numerical study by Dagotto and Riera (1992), where, in addition, it was observed that the pairing correlations are maximized at *intermediate* values of the new coupling V/t, as it is shown in Fig. 66(b). The regions of superconductivity observed at large V/t and for the pure t-J model ($V=0$) seem analytically connected, and speculations linking their properties with those of the attractive Hubbard model have been presented (Dagotto and Riera, 1992). An interesting feature of the t-J-V model is that a spin gap appears in the spectrum. This is natural, since in the large V,J limit the ground state is formed by short-range dimers, and thus an energy as large as J/t is needed to create a triplet. (However, note that the presence of the spin gap suggests that superconductivity should appear in the s-wave channel at finite V, contrary to the previously described claims at $V=0$ that the $d_{x^2-y^2}$ channel is dominant. An interesting crossover may exist between the two regimes in the superconducting phase.) Recent studies by Troyer *et al.* (1993) in the one-dimensional version of this model have shown that the spin gap opens very rapidly when V/t is increased, starting from the t-J limit (Fig. 67). Actually, the physics of the one-dimensional chain t-J-V is very

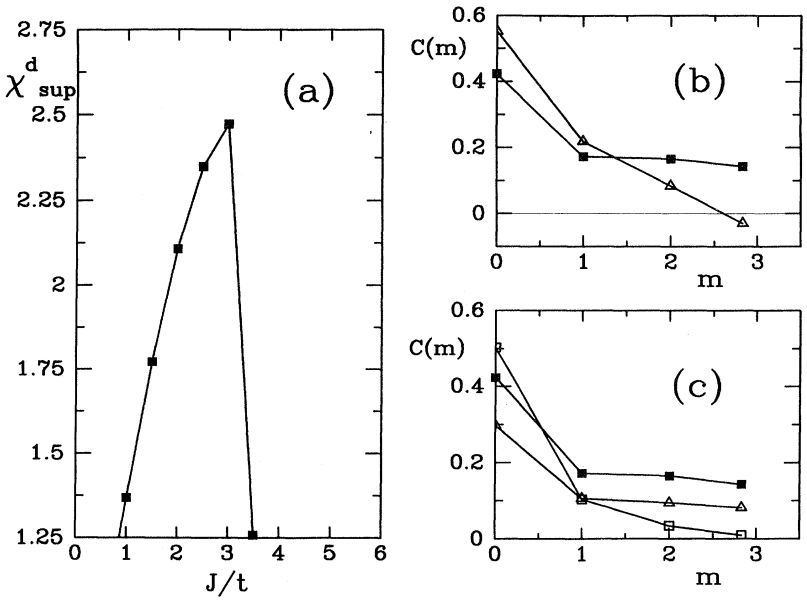

FIG. 65. (a) $d_{x^2-y^2}$ superconducting susceptibility as a function of J/t, at density $\langle n \rangle = 0.5$. (b) Pairing correlation function $C(\mathbf{m})$ as a function of distance, at $\langle n \rangle = 0.5$, and $J/t=3$. The solid squares denote $d_{x^2-y^2}$ correlations, while the open triangles are extended s correlations. (c) Pairing-pairing correlation function $C(\mathbf{m})$ vs distance at density $\langle n \rangle = 0.5$. The open triangles, solid squares, and open squares denote results for $J/t=1.0$, 3.0, and 4.0, respectively. All the results were obtained on a 4×4 cluster using exact-diagonalization techniques (Dagotto and Riera, 1993).

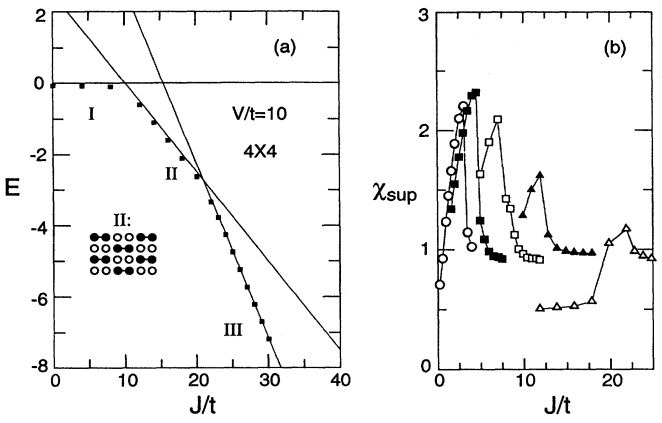

FIG. 66. (a) Ground-state energy of the t-J-V model on a 4×4 cluster at $V/t=10$ and $\langle n\rangle=0.5$, as a function of J/t. The results clearly show three different regimes. The intermediate one (II) presents electron pair formations. The solid lines are variational results in the bulk limit discussed in Dagotto and Riera (1992). (b) Superconducting susceptibility of the t-J-V model as a function of J/t, obtained at $\langle n\rangle=0.5$ on a 4×4 cluster. From the left, the results correspond to $V/t=0.0$, 1.0, 3.0, 5.0, and 10.0. Note the presence of a sharp peak for all values of V/t (results taken from Dagotto and Riera, 1992).

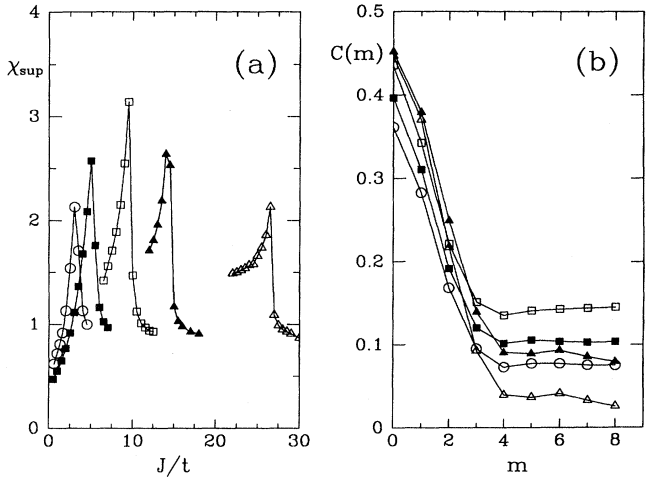

FIG. 68. (a) Superconducting susceptibility of the one-dimensional t-J-V model as a function of J/t for various values of V/t. Open circles, solid squares, open squares, solid triangles, and open triangles denote results for $V/t=0.0$, 1.0, 3.0, 5.0, and 10.0, respectively. The peaks are located immediately before the region of phase separation is reached. (b) Pairing correlation function $C(\mathbf{m})$ vs distance for various values of V/t [same convention as in (a)], and at the value of J/t corresponding to the maximum in the susceptibility.

similar to that of its two-dimensional counterpart, with analogous behavior of the pairing correlations and superconducting susceptibilities [see Figs. 68(a) and 68(b)]. Troyer *et al.* (1993) also studied the influence of long-range interactions, noticing that the superconducting region is not enhanced by suppressing phase separation. Instead it seems to follow phase separation, forming a narrow strip in its neighborhood. A charge-density-wave state may compete with superconductivity in the region where phase separation becomes unstable due to the long-range forces. For other studies including $1/r$ interactions, see Barnes and Kovarik (1990); Riera and Dagotto (1993); and Haas *et al.* (1994).

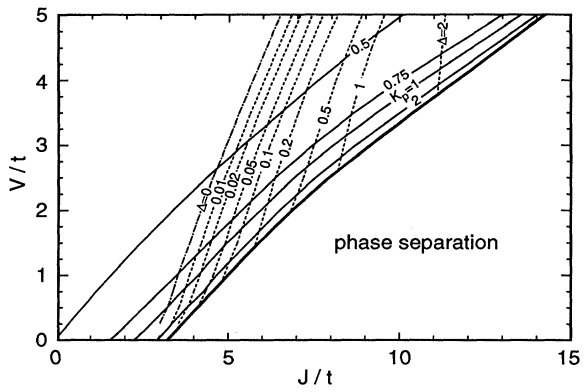

FIG. 67. Phase diagram of the one-dimensional t-J-V model obtained by exact-diagonalization techniques at $\langle n\rangle=0.5$. Contour lines of constant K_ρ and constant spin gap Δ are shown. $K_\rho>1$ implies that the superconducting correlations dominate in the ground state, although they cannot develop long-range order in this dimension (taken from Troyer *et al.*, 1993).

Before addressing other issues related to superconductivity, we note that some of the usual models of correlated electrons defined on particular geometries are also candidates to show superconductivity. In particular, it is interesting to study "ladders" (i.e., two coupled chains) and two coupled planes. The former have been explored to address questions concerning the stability of Luttinger liquids (Anderson, 1990a; Schulz, 1991), the existence of a spin gap (Dagotto and Moreo, 1988; Hida, 1991, 1992; Barnes *et al.*, 1993; Bose and Gayen, 1993), and superconductivity (Emery, 1986; Dagotto, Riera, and Scalapino, 1992). Barnes *et al.* (1993) showed that at half-filling a spin gap appears in the spectrum as soon as an exchange coupling along the rungs is turned on. In this respect, the physics at half-filling resembles a dimerization process. There are real materials such as $(VO)_2P_2O_7$ that consist of weakly coupled arrays of one-dimensional metal oxide ladders (Johnston, 1987). Rice, Gopalan, and Sigrist (1993; see also Gopalan, Rice, and Sigrist, 1993) also remarked recently on the importance of studying ladder systems for a possible description of $Sr_{n-1}Cu_{n+1}O_{2n}$ compounds. The study of coupled planes is also interesting, since the structures of some of the high-T_c superconductors, like YBCO and Bi2212, have Cu-O planes at short distance in the unit cell (Dagotto, 1992; Dagotto, Riera, and Scalapino, 1992; Millis and Monien, 1993. See also Morgenstern *et al.*, 1993). Numerical studies of superconductivity have been

carried out in both the *ladder t-J* and Hubbard models. In the former, there is a simple argument that guarantees the presence of superconductivity in a particular region of parameter space. Consider the limit of large superexchange coupling along the *rungs*. In this limit, the undoped ground state is formed by spin singlets along these rungs. If two holes are added to the system, energetically it is favorable to break only one spin singlet, and thus they will share the same rung, leading to short-range pairing. It can be shown that residual interactions will favor a superconducting state in this limit, as was effectively observed in a numerical study by Dagotto, Riera, and Scalapino (1992). Actually, this mechanism is very similar to that proposed earlier by Imada (1991a) in a dimerized *t-J* model. Unfortunately, for the realistic regime where $J/t < 1$ and where there is no asymmetry between the couplings along the chains and rungs, there are no numerical indications of superconductivity (Dagotto, Riera, and Scalapino, 1992). The Hubbard model has also been studied numerically on a ladder geometry. Some (weak) indications of long-range superconducting order have been detected in the ground state (Bulut, Scalapino, and Scalettar, 1992; Noack *et al.*, 1992). The analysis of these models deserves further study.

3. Phase diagram of the two-dimensional *t-J* model

Based on several calculations reviewed in the previous section and others, it is possible to make an educated guess for the phase diagram of the two-dimensional *t-J* model. The result is shown in Fig. 69(a). At large J/t, there is a well-established region of phase separation. At low electronic density ($x \sim 1$ in the figure), phase separation starts near $J/t \sim 4$ (Kivelson, Emery, and Lin, 1990; Putikka, Luchini, and Rice, 1992). In the other limit, i.e., near half-filling, computational and high-temperature expansion results suggest that phase separation starts at a finite coupling $J/t \sim 1$ (see Sec. IV.D). However, since these results are still controversial (Emery, Kivelson, and Lin, 1990), we prefer to leave that region undefined in Fig. 69(a). Near half-filling, strong antiferromagnetic correlations (AF) are present, perhaps with some slight modulation into an incommensurate state (Sec. IV.A.3). For very small J/t and close to half-filling, ferromagnetism (FM) exists. We have not discussed this phase in detail in the present review, since it is not of obvious relevance to the understanding of the cuprates. For more details, see the vast literature on this subject (of which a small sample is Kanamori, 1963; Mattis, 1981; Doucot and Wen, 1989; Fang *et al.*, 1989; Barbieri, Riera, and Young, 1990; Trugman, 1990c; Putikka, Luchini, and Ogata, 1992; Long and Zotos, 1993). At small electronic densities and couplings, the system numerically looks like a weakly interacting gas of electrons (PM). It is likely that this regime can be described by a Fermi liquid, but this issue is still under study. In the low electronic density region, it is well established that electrons form bound states starting at $J/2=2$, but phase separation occurs at a larger coupling (Kivelson, Emery, and Lin, 1990). It is natural to assume that these pairs may condense into a superconducting regime at low temperatures. Actually, variational calculations performed at $\langle n \rangle \ll 1$ support this idea (Dagotto *et al.*, 1993). In this case the symmetry of the condensate is *s* wave, as shown in Fig. 69(a). With an increase in the density towards quarter-filling, the *d*-wave region discussed in the previous section appears (Dagotto and Riera, 1994). More work is necessary to quantitatively find the boundaries of these phases.

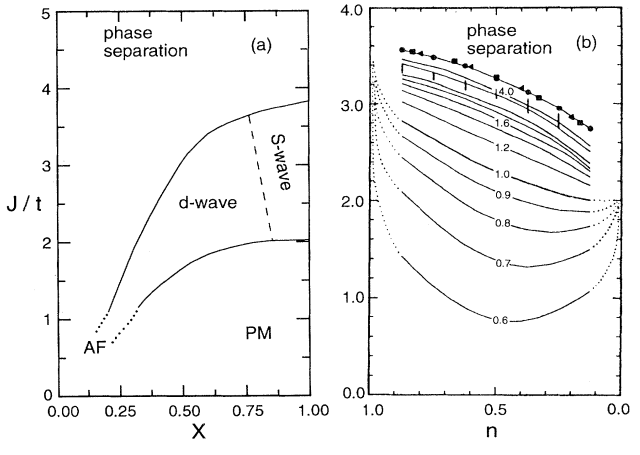

FIG. 69. (a) Schematic phase diagram of the two-dimensional *t-J* model at zero temperature. $x = 1 - \langle n \rangle$ is the hole density. The meaning of the different phases is explained in the text (from Dagotto *et al.*, 1993). (b) Phase diagram of the one-dimensional *t-J* model, taken from Ogata *et al.* (1991). n is the electronic density, and the contours correspond to lines of constant K_ρ. In the region $K_\rho > 1$, superconductivity dominates.

Of particular importance is the study of the superconducting regime away from $\langle n \rangle \sim \frac{1}{2}$ and closer to half-filling. Does this phase follow the phase-separation regime all the way to small hole density? In the one-dimensional *t-J* model, Ogata *et al.* (1991) have shown that indeed there is a region where superconducting correlations are dominant near phase separation, and for densities as close to half-filling as $\langle n \rangle = 0.87$ (for results at low electronic density, see Chen and Lee, 1993; Hellberg and Mele, 1993; and Waas, Fehske, and Büttner, 1993). Actually, in Fig. 69(b) the regime where the parameter K_ρ is larger than 1 indicates that the superconducting correlations decay the slowest in the ground state (for details about the definition of this parameter, see Ogata *et al.*, 1991; Troyer *et al.*, 1993; and references therein). For additional information about the one-dimensional case, see Assaad and Würtz (1991); Imada and Hatsugai (1989); Imada (1990); Bonča *et al.* (1992); and Prelovšek *et al.* (1993). Then, the one-dimensional results support the idea that superconductivity appears in electronic models near the regime of phase separation even close to half-filling. If these results can be extended to two dimensions, then the *t-J* model

would superconduct in the realistic regime of couplings and densities, becoming a strong candidate to describe the cuprates. It may simply occur that in two-dimensional numerical studies near half-filling we would not have a strong signal of superconductivity due to the small number of pairs in the system. Then, we may still have a chance of describing high-T_c superconductors with purely electronic models! However, thus far these are speculations that clearly need (and deserve) more work and thinking.

4. Meissner effect and flux quantization

In addition to the pairing correlation functions, it would be important to develop a formalism to explore numerically the Meissner effect and the superfluid density. This issue can be addressed following steps similar to those that led us to Eq. (4.9) for the Drude weight. In other words, it is possible to express the "superfluid weight" D_s in terms of suitable current-current correlations. First, let us recall the well-known basic ideas of London's theory. In this approach the superfluid current is proportional to the transverse gauge field,

$$\mathbf{J}_s = -\frac{e^2 n_s}{m}\mathbf{A} , \tag{4.16}$$

where n_s is the carrier density of the superfluid, e the unit of charge, and m the mass of the particles. This equation can be derived from the assumption that the carriers in the superfluid do not collide: Let us define the supercurrent as $\mathbf{J}_s = -en_s\mathbf{v}_s$, where $\mathbf{v}_s$ is the velocity of the carriers in the superfluid. Taking time derivatives on both sides and replacing the acceleration by $\mathbf{a}=\mathbf{F}/m = -e\mathbf{E}/m$ (where $\mathbf{E}$ is an external electric field), we arrive at

$$\frac{d\mathbf{J}_s}{dt} = \frac{e^2 n_s}{m}\mathbf{E} . \tag{4.17}$$

In the absence of external scalar potentials ϕ, we can derive Eq. (4.16) by a time integration of Eq. (4.17). Now, we define D_s through the proportionality constant between the superfluid current and the gauge field, i.e.,

$$\mathbf{J}_s = -e^2 D_s \mathbf{A} , \tag{4.18}$$

and thus $D_s = n_s/m$. It can also be shown easily that $D_s = 1/(e^2\lambda^2)$, where λ is the London's penetration depth, defined by the exponential decay of the magnetic field inside a superconductor [$B(x)=B(0)e^{-x/\lambda}$, where x is perpendicular to the surface. For details see Schrieffer, 1988].

Having set up these simple ideas and definitions, we now need to evaluate the expectation value of the current operator in the ground state of the many-body problem under consideration in order to get D_s (Scalapino, White, and Zhang, 1992). Using linear-response theory in Sec. IV.B.2, we arrived at a general relation between the current in the many-body interacting ground state and an external gauge field in the x direction; i.e., we showed that $\langle \hat{J}_x(\mathbf{q},\omega)\rangle = K(\mathbf{q},\omega)A_x(\mathbf{q},\omega)$, where the function $K(\mathbf{q},\omega)$ is given by

$$K(\mathbf{q},\omega) = e^2\langle \hat{K}_x\rangle + e^2\left[\frac{1}{N}\langle\phi_0|\hat{j}_x(-\mathbf{q})\frac{1}{\hat{H}_0 - E_0 + \omega + i\epsilon}\hat{j}_x(\mathbf{q})|\phi_0\rangle + \frac{1}{N}\langle\phi_0|\hat{j}_x(\mathbf{q})\frac{1}{\hat{H}_0 - E_0 - \omega - i\epsilon}\hat{j}_x(-\mathbf{q})|\phi_0\rangle\right] , \tag{4.19}$$

and the notation was explained in Sec. IV.B.2. To study the particular case of the Meissner effect, let us consider the limit of a uniform static transverse gauge potential that produces a magnetic field. Then, we need to work at $\omega=0$ and with $\mathbf{q}\to 0$. This is nontrivial, and care must be taken in the way in which the uniform limit is approached. To understand how subtle this limit is, note that the condition of transversality tells us that $K(\mathbf{q},0) = (1-q_x^2/\mathbf{q}^2)K(\mathbf{q}^2)$ where $K(\mathbf{q}^2)$ depends only on $\mathbf{q}^2$ [Schrieffer (1988), Sec. 8.3]. Then, if the uniform limit is obtained following the path $q_y=0, q_x\to 0$, the kernel $K(\mathbf{q},0)$ cancels even though $K(\mathbf{q}^2)$ may be nonzero. Then, it is clearly more convenient to take first $q_x=0$ and then $q_y\to 0$ as the limiting process. With this approach, and following the same steps that allowed us to derive Eq. (4.9) for the Drude weight, we can express the superfluid weight as

$$\frac{D_s}{2\pi e^2} = \frac{\langle -\hat{T}\rangle}{4N} - \frac{1}{N}\sum_{n\neq 0}\frac{|\langle\phi_0|\hat{j}_x(q_x=0,q_y\to 0)|\phi_n\rangle|^2}{E_n - E_0} , \tag{4.20}$$

where the notation is the same as that used in Sec. IV.B.2. Then, in order to study D_s, or, equivalently, the presence of a Meissner effect in the problem, we need to analyze numerically the correlation between currents at a nonzero (but vanishingly small) momentum (while for the Drude weight it was necessary to study the particular case where $\mathbf{q}$ was strictly zero). In practice, the computational effort to get both quantities is basically the same. This approach, introduced by Scalapino, White, and Zhang (1992), has recently been applied to numerical studies of both the one-band Hubbard and the t-J models. In the case of the t-J model, the superfluid weight has

been evaluated in the region where indications of superconductivity were found (Figs. 65 and 66), i.e., density $\langle n \rangle \sim 1/2$, and close to phase separation. A large peak was observed in D_s on a 4×4 cluster (Dagotto and Riera, 1993), in the same region where the pairing correlation functions suggested the presence of superconductivity in the ground state. Unfortunately, the minimum nonzero value of the momentum in the y direction on this small cluster is $q_y=\pi/2$, and thus the limit of $\mathbf{q}\to0$ is difficult to approach smoothly.[14]

Both the Drude and the superfluid weights can also be evaluated using quantum Monte Carlo methods. Although this algorithm does not allow the calculation of ω-dependent quantities, the particular case of $\omega=0$ can be studied in the imaginary time formalism using a Matsubara frequency $\omega_m=2\pi T$. Then, the main limitation of the method comes from the standard sign problem and finite temperature effects. In Fig. 70, results are shown for an 8×8 cluster, working at $U/t=4$, density $\langle n \rangle=0.72$, and temperature $T=t/6$. The result indicates that the Drude weight is nonzero, in good agreement with the exact-diagonalization predictions of Sec. IV.B.3 [Fig. 44(b)]. Actually, there is even quantitative agreement between the results obtained with both methods. Figure 44(b), corresponding to a 4×4 cluster at zero temperature, predicted that $D/(2\pi e^2)\sim0.28$ at $U/t=4$, while from Fig. 70(b) we found $\Lambda_{xx}(\mathbf{q}=0,\omega_m)$ between 0.0 and 0.10, which, in combination with the kinetic energy, makes a Monte Carlo prediction of $D/(2\pi e^2)\sim0.26$–0.31. Thus the Drude weight is only weakly affected by finite-size effects (see also Denteneer, 1994). Finally, Fig. 70(b) shows that the superfluid density seems to vanish in this model. This result is in agreement with the negative conclusions about superconductivity obtained studying pairing correlation functions in Sec. IV.E.1.

Another criterion to search for superconducting phases is the "flux quantization." In a normal state, the ground-state energy is a periodic function of the flux ϕ with period $\phi_0=hc/e$, and it is minimized at $\phi/\phi_0=0,\pm1,\pm2,\ldots$. In a superconducting phase, new stable states appear at $\phi/\phi_0=\pm\frac{1}{2},\pm\frac{3}{2},\ldots$. The new unit of flux is $\phi_0/2$, due to the presence of pairs in the ground state ("anomalous" flux quantization). The actual flux dependence of the energy can be studied on finite clusters using exact-diagonalization and quantum Monte Carlo methods. The t-J model near phase separation shows anomalous flux quantization, in agreement with the conclusions based on pairing correlations and a study of D_s (Dagotto and Riera, 1993). The one-dimensional two-band Cu-O model near phase separation also shows flux quantization on a ring (Sudbo *et al.*, 1993; see also Fig. 71). The Hubbard model has also been studied (Assaad and Hanke, 1992; Ferretti *et al.*, 1992). However, care must be taken with this type of analysis, since some *nonsuperconducting* systems also show the presence of minima at $\phi/\phi_0=\pm\frac{1}{2},\pm\frac{3}{2},\ldots$. Consider, for example, two holes in the t-J model (Poilblanc, 1991) and CDW states on rings (Bogachek *et al.*, 1990).

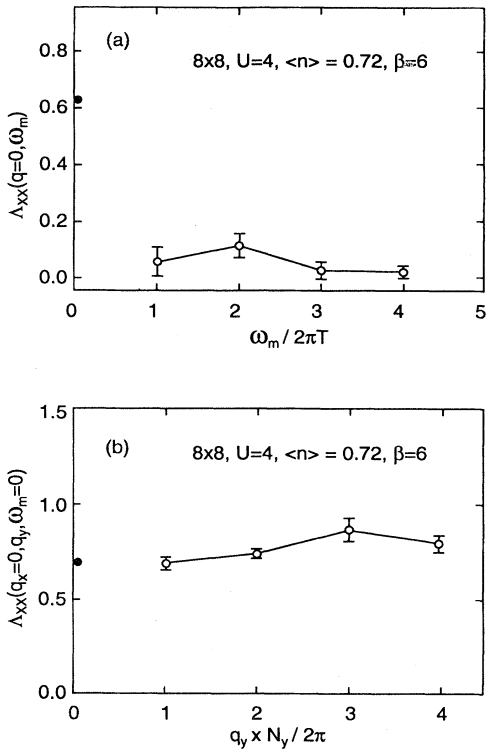

FIG. 70. (a) Quantum Monte Carlo results for the one-band Hubbard model obtained at the parameters in the figure. The solid circle denotes $-\langle k_x \rangle$, which is the mean value of the kinetic energy per site divided by the dimension. Δ_{xx} is the current-current correlation function in the notation of Scalapino, White, and Zhang, 1993. The Drude peak is obtained from these results as $D/(\pi e^2)=\langle -k_x \rangle-\Delta_{xx}(\mathbf{q}=0,\omega_m\to0)$. (b) Quantum Monte Carlo results at the same parameters as (a), but now measuring the superfluid weight D_s, which is obtained as $D_s/(\pi e^2)=\langle -k_x \rangle-\Delta_{xx}(q_x=0,q_y\to0,\omega=0)$ (also from Scalapino, White, and Zhang, 1993). The near cancellation of D_s suggests that the one-band Hubbard model does not superconduct for these parameters.

5. $d_{x^2-y^2}$ superconductivity

We close this review of properties of strongly correlated electrons by describing recent ideas that have induced considerable excitement among experimentalists and theorists working on high-T_c superconductors. It has been proposed, and supported by several calculations, that the superconducting state of the cuprates has $d_{x^2-y^2}$ symmetry, instead of the standard s-wave of the BCS theory (see Bulut and Scalapino, 1991; Monthoux, Balat-

[14]In the same region of parameter space the Drude peak was very large, suggesting that the resistivity in the ground state near phase separation is zero for the t-J model.

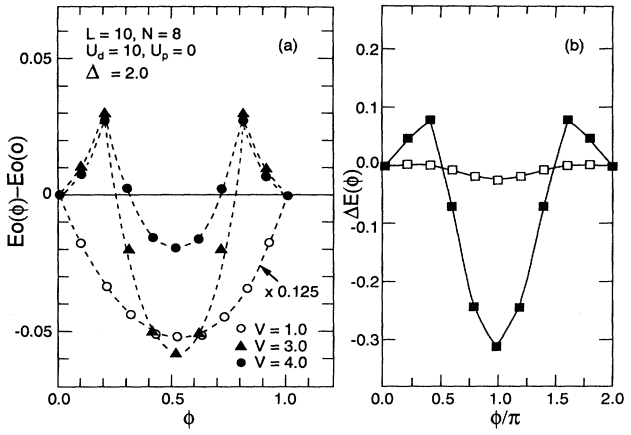

FIG. 71. Energy as a function of an external flux: (a) For the two-band Hubbard model in one dimension at different values of the density-density interaction V. For more details see Sudbo *et al.* (1993). (b) Energy of the ground state as a function of an external magnetic flux ϕ, for the two-dimensional t-J model on a 4×4 cluster at density $\langle n \rangle = 0.5$. Results are presented with respect to the energy at zero flux. The solid squares are results for $J/t = 3.0$, while the open squares denote results for $J/t = 4.0$, i.e., inside the phase-separation region (Dagotto and Riera, 1993).

sky, and Pines, 1991; and references therein). The calculations are based on pairing mechanisms that involve antiferromagnetic spin fluctuations. Although early experiments seemed consistent with s-wave pairing, recent results suggest that the pairing state is indeed highly anisotropic, giving support to these theoretical ideas. The evidence comes from several sources, in particular from NMR studies, penetration depth measurements, and ARPES experiments [in addition, recent experiments by Wollman *et al.* (1993) measuring the phase coherence of YBCO-Pb dc SQUIDs have also reported evidence in favor of d-wave superconductivity]:

(i) NMR experiments probe the local magnetic fields around an atom and allow measurements of the copper relaxation rates. Recent results by Martindale *et al.* (1993) observed that this relaxation rate varies as T^3 below the critical temperature, in agreement with the predictions of some $d_{x^2-y^2}$ models.

(ii) In an s-wave superconductor the penetration depth λ (Sec. IV.E.4) varies exponentially with temperature at small temperatures. This is a direct consequence of the presence of a gap in the spectrum. However, when nodes are present in the energy gap, and thus pairs can be broken more easily, λ is expected to change linearly with temperature if the symmetry of the superconducting state is $d_{x^2-y^2}$. Hardy *et al.* (1994) have recently reported such a linear variation in experiments carried out on clean $YBa_2Cu_3O_{6.95}$ crystals in support of d-wave pairing. However, note that previous experiments in Bi2212 and thin films of YBCO found a T^2 dependence of the penetration depth (see Beasley, 1993), and thus more work is needed to clarify these experimental results. Lee (1993) claimed that this behavior is compatible with a dirty d-wave superconductor. Note also that Wu *et al.* (1993) reported that, for $Nd_{2-x}Ce_xCuO_4$, λ follows an exponential temperature behavior as in an s-wave superconductor. This is in agreement with some remarks made in this review about the differences between electron- and hole-doped materials in the behavior of the resistivity ρ with temperature (Sec. I.B), and the spin correlations (Sec. IV.A). In spite of what the one-band Hubbard model may suggest, electron- and hole-doped compounds seem to behave differently from the experimental point of view.

(iii) Shen *et al.* (1993) recently reported the presence of a strong anisotropy in the superconducting gap of $Bi_2Sr_2CaCu_2O_{8+\delta}$ crystals measured with ARPES techniques. In some directions the gap is zero (within the experimental accuracy of about 4 meV), compatible with $d_{x^2-y^2}$ superconductivity.

However, note that there are neutron-scattering experiments (Mason *et al.*, 1993) that urge caution about the existence of a d-wave condensate in the cuprates. These authors observed that superconductivity does not induce anisotropy in the magnetic scattering of $La_{2-x}Sr_xCuO_4$, as would be expected from such a condensate [although, in a recent preprint, Bulut and Scalapino (1993) claim that the neutron-scattering experiments are not inconsistent with d-wave symmetry].

Before these recent developments, the presence of an attractive interaction in the $d_{x^2-y^2}$ channel appeared frequently in the theoretical analysis of holes in antiferromagnetic backgrounds (Miyake, Schmitt-Rink, and Varma, 1986; Scalapino, Loh, and Hirsch, 1987; Gros, 1988; Chen *et al.*, 1990). In previous sections of this review, we have also found the presence of hole attraction in the $d_{x^2-y^2}$ channel, both close to half-filling (Poilblanc, Riera, and Dagotto, 1994, and references therein) and at density $\langle n \rangle = 1/2$ (Dagotto and Riera, 1993). Although the calculations used to obtain these results are approximate (finite clusters and self-consistent equations), their common conclusions suggest that, indeed, $d_{x^2-y^2}$ is a concrete possibility in models of correlated electrons presumed to describe the actual high-T_c materials. In spite of these experimental and theoretical results, some theorists remain skeptical. It is believed that impurities can easily reduce the critical temperature of a $d_{x^2-y^2}$ superconductor. However, in the high-T_c cuprates such a sensitivity has not been observed. Actually, the materials can be easily prepared even by nonexperts, under considerably less than perfect conditions. Thus the study of the role of impurities in a d-wave superconductor is an important issue to be addressed (Hirschfeld and Goldenfeld, 1993; Lee, 1993). Needless to say, the physical properties of $d_{x^2-y^2}$ superconducting condensates are currently being investigated by several experimental and theoretical groups around the world, and a more detailed comparison with experiments will clarify whether the high-T_c

superconductors are indeed $d_{x^2-y^2}$ superconductors. Surely, we shall hear more about these interesting ideas in the near future!

V. CONCLUSIONS

In this review, we have attempted to summarize some of the results obtained in the rapidly growing field of computational techniques applied to models of strongly correlated electrons. Some purely analytical methods and their predictions have also been addressed. In addition, we presented an overview of the current experimental situation in high-T_c superconductors to provide a summary of the main results, and its comparison with computational calculations. In the last few years, a remarkable level of maturity has been reached in the computational studies of interacting electrons, with several groups independently arriving at similar conclusions, as was shown in several sections of this review. It is becoming common practice to study models from as many points of view as possible, including computational techniques, perturbative or self-consistent calculations, mean-field, and variational approaches. It is clear that the complexity of the problems requires as much help as we can get, and thus the use of numerical techniques is likely to keep on growing fast in all areas of condensed-matter theory. The computational results are widely used as benchmarks to test analytical approximations, especially in the very difficult regime of strong correlations where there are no obvious small parameters in the problem (for a good example, see Sec. III.B.3). One cannot help but think of this branch of theoretical physics as having common features with experimental physics. It naturally provides a link between abstract theoretical ideas and the actual properties of a given model.

The main conclusions of this review are the following.

(a) Regarding normal-state properties, a qualitative comparison between computational results and experiments for the high-temperature superconducting materials was carried out. Remarkable agreements between theory and experiments have been observed, showing that some of the "anomalous" properties of the copper oxides may have a simple explanation through purely electronic models. In particular, the magnetic susceptibility in the t-J model and in the real cuprates behave similarly, both showing deviations from a canonical Fermi-liquid behavior which is caused by the presence of antiferromagnetic correlations. The presence of a mid-infrared band in the optical conductivity $\sigma(\omega)$ in Hubbard-like models is quite natural and related to the presence of an incoherent part in the hole spectral function (although it is likely that holes trapped near Sr, or the chains in the YBCO materials, also appreciably contribute to this feature in the experiments). In the density of states $N(\omega)$, new states are observed in the gap upon doping in the models of correlated electrons that have been analyzed, in agreement with experiments (again, other possibilities, like the presence of impurity bands, may also contribute to the spectral weight in the gap). In general, one gets the feeling that the standard pairing theory (perhaps in an unusual non-s-wave channel) and Fermi-liquid descriptions of the normal state may explain the features of the cuprates, once the presence of antiferromagnetic correlations is taken into account, as well as the two dimensionality of the problem. We are simply not used to working with a material having competing orders. The analytical tools are not well developed for this purpose; thus the help of computational techniques is crucial to obtaining qualitative information about the properties of a given model, and to checking the accuracy of the various mean-field and perturbative approaches described in the literature,[15] saving resources and time to the condensed-matter-theory community.

(b) New, exciting ideas about the possible description of the cuprates as $d_{x^2-y^2}$ superconductors were briefly reviewed. It is reassuring that the existence of hole attraction in this same channel has been computationally observed since the early numerical studies of the t-J and Hubbard models, providing a nice first-principles confirmation of the recently proposed ideas based on self-consistent approximations. Precisely, one of the main advantages of numerical methods is that they allow a comparison between abstract "theories" and the actual properties of the model under consideration.

(c) Thus far numerical studies are consistent with a quasiparticle (Fermi-liquid) description of holes in antiferromagnetic backgrounds, in the sense that the wave-function renormalization Z is nonzero. Then, the use of one-dimensional problems (where $Z=0$) as paradigms of their two-dimensional counterparts seems questionable. Unfortunately, for this particular problem, numerical techniques have not yet reached a high enough level of accuracy to completely rule out non-Fermi-liquid scenarios. More work is necessary to clarify this important issue.

(d) The development of better algorithms is crucial to improve the accuracy of the numerical predictions for models of correlated electrons. In the context of Lanczos or exact-diagonalization techniques, where the main constraints come from the rapid growth of the Hilbert space with lattice size, the use of reduced basis sets, as in quantum chemistry problems, is a possible direction for exploring large clusters, keeping the advantages of this method, especially the possibility of studying response functions in real time. With Monte Carlo algorithms, efforts should be concentrated on the alleviation of the sign problem and the development of reliable algorithms to study real-time dynamics. The development of a Monte Carlo algorithm for the two-dimensional t-J model is also highly desirable.

---

[15] In this respect computer studies of correlated electrons play a role similar to that of lattice gauge theory in the study of quantum chromodynamics (which is a theory of strongly interacting quarks).

(e) It is important to explore other "unusual" properties of the cuprates, like the behavior of the Hall coefficient, and the resistivity as a function of temperature. Not much work has been done on this front. Also, the paradoxical behavior of the chemical potential with doping (Sec. IV.C.1) does not seem to have an explanation within two-dimensional models of correlated electrons. It is important to devote some effort to analyze the strange behavior of μ in the cuprates.

The author strongly believes that in the near future the use of computational techniques to study the behavior of correlated electrons will become common practice in several areas of condensed-matter physics, not only in high-T_c superconductors. These methods provide unbiased information and can accelerate the process of acceptance or rejection of models of a given material saving a huge amount of time for the physics community. It is encouraging that the new generations of physicists know how to deal with computers, and they are realizing that numerical information about a given model is crucial in problems where perturbative calculations following the traditional RPA or ladder-summing diagrams are not reliable. With the rapid development of supercomputers and algorithms, the analysis of 3D systems will also be possible soon. Perhaps some day materials could be designed and tested in a computer environment before they are actually synthesized in the laboratory. The future of computational studies of models of materials is indeed bright.

ACKNOWLEDGEMENTS

The author specially thanks Frank Marsiglio, Adriana Moreo, Franco Nori, Bill Putikka, and Richard Scalettar for a careful reading of this manuscript and for useful suggestions. He also thanks G. Aeppli, J. W. Allen, K. Bedell, N. Bonesteel, S. L. Cooper, D. Dessau, H. Q. Ding, G. Fano, A. Fujimori, H. Fukuyama, P. Fulde, R. J. Gooding, P. C. Hammel, P. Horsch, M. Imada, T. Jolicoeur, T. Kaplan, S. Maekawa, D. C. Mattis, A. Muramatsu, A. Nazarenko, F. Ortolani, P. Prelovšek, G. C. Psaltakis, J. Riera, Z.-X. Shen, S. Sorella, and D. Tanner for many useful comments about a preliminary draft of this review. The help of Linda Burns, Ken Ford, and Kim Voigt in the preparation of the figures of this review and its distribution is acknowledged. This work was supported by the Office of Naval Research through grant ONR-N00014-93-1-0495. Partial support by the donors of the Petroleum Research Fund administered by the American Chemical Society is also acknowledged.

APPENDIX A: CLUSTER SHAPES

In Sec. II.A the Lanczos method was described and a general rule was given to construct "tilted" squares that cover the bulk lattice. In Fig. 72 we explicitly provide the actual shape of some of these clusters, which may be useful for the implementation of the Lanczos technique in 2D systems. Each of these clusters can be circumscribed by a square. Note that some of these clusters do *not* have all the symmetry properties of the bulk (reflections with respect to the axis are particularly subtle). But the reader should not be confused by the exotic shapes of these clusters. For example, rotations in 90 degrees exist in the $N=32$ sites cluster and in many others, although it may not seem obvious.

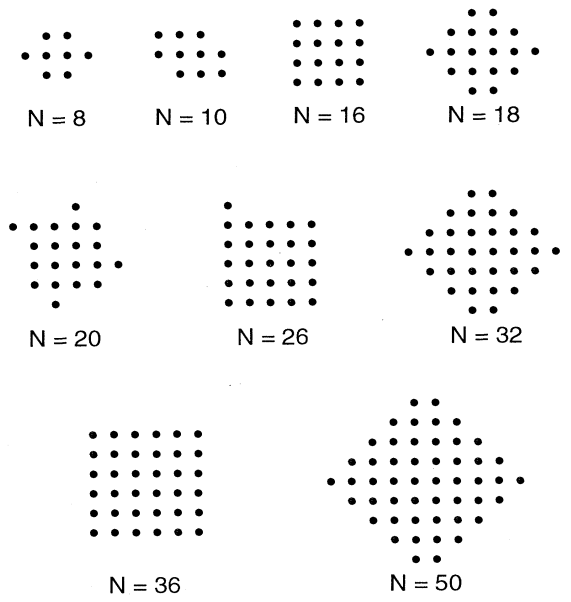

FIG. 72. Shapes of some popular tilted clusters used in the Lanczos literature. N is the total number of sites.

APPENDIX B: FLAT QUASIPARTICLE BANDS

Recent ARPES experiments by the Argonne (Abrikosov, Campuzano, and Gofron, 1993; Gofron *et al.*, 1993) and Stanford groups (Dessau *et al.*, 1993) have shown the presence of "flat bands" in the hole-doped cuprates. As a typical example, consider the results of Fig. 73 which were obtained by Dessau *et al.* (1993) for Bi2212. Using the notation of the 2D square lattice, the ARPES results show that near the X point [i.e., $\mathbf{p}=(\pi,0)$] the quasiparticle dispersion observed in photoemission is momentum independent (i.e., "flat"). The Fermi energy is only slightly above this flat region. It is difficult to explain this effect using band-structure calculations, because it would require that all hole-doped high-T_c compounds present the same abnormal flat region near the Fermi level. An alternative explanation was recently provided by Dagotto, Nazarenko, and Boninsegni (1994) and by Bulut, Scalapino, and White (1994), who proposed that the flat bands have a many-body origin. Consider, for example, the 2D t-J model for a realistic coupling $J/t=0.4$. If one hole is studied in an antiferromagnetic

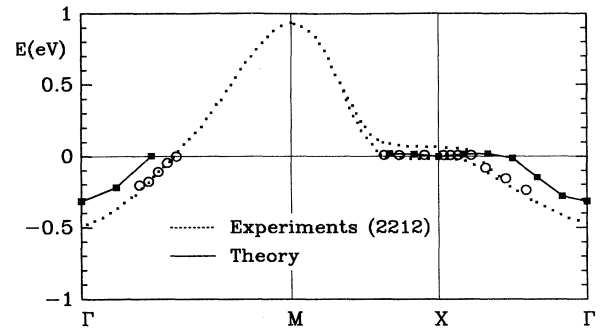

FIG. 73. Quasiparticle dispersion for Bi2212 (open circles) obtained using ARPES techniques by Dessau *et al.* (1993). The solid squares are results obtained in the context of the 2D *t-J* model by Dagotto, Nazarenko, and Boninsegni (1994). The dots are a fit of the data produced by Dessau *et al.* (1993). The momentum notation is the standard for a 2D square lattice.

background, its energy vs momentum may represent a good approximation to the quasiparticle dispersion observed experimentally, as long as antiferromagnetism is robust in the normal state of the cuprates. In other words, the normal state was approximated by Dagotto, Nazarenko, and Boninsegni (1994) by a noninteracting gas of dressed quasiparticles. In Fig. 73 the dispersion calculated numerically on a 12×12 cluster is shown and compared with the ARPES experiments. There is a good agreement with experiments.

Why is this region flat? It was observed numerically that the hole-energy difference Δ between $\mathbf{p}=(\pi,0)$ and $\mathbf{p}=(\pi/2,\pi/2)$ is small compared to the total bandwidth (itself drastically reduced compared with the noninteracting $U/t=0$ Hubbard limit as discussed in Sec. III.B.3). This small energy difference is natural, since in the Hubbard model, from which the *t-J* model can be considered to be derived, at small and very large coupling the one-hole states become degenerate. Thus, for intermediate couplings, they are similar in energy. In addition, the saddle point of the dispersion was found close to the X point, adding to the flatness of the region. For more details, see Dagotto, Nazarenko, and Boninsegni (1994). Bulut, Scalapino, and White (1994) arrived at similar numerical conclusions using a Monte Carlo simulation.

This additional small scale Δ in the problem has interesting consequences at room temperature, especially regarding the shape of the Fermi surface and the Hall coefficient (Trugman, 1990a; Dagotto, Nazarenko, and Boninsegni, 1994). The actual shape of the quasiparticle dispersion can be fit using $\epsilon_{\mathbf{p}}/t = -1.255 + 0.34\cos p_x \cos p_y + 0.13(\cos 2p_x + \cos 2p_y)$. This dispersion allows quasiparticles to move within the same sublattice, since they have an effective up- or down-spin (remember that the background is assumed to be antiferromagnetic). Thus the normal state may be modeled by a simple Hamiltonian of quasiparticles roughly distributed as half in one sublattice (spin up) and the other half in the other (spin down), moving according to the dispersion $\epsilon_{\mathbf{p}}/t$ given above.

APPENDIX C: IS THERE SUPERCONDUCTIVITY IN THE HUBBARD AND *t-J* MODELS IN THE REALISTIC REGIME?

Our study of Sec. IV.E may have led one to the conclusion that the Hubbard model in 2D is not superconducting, at least according to Monte Carlo simulations at presently accessible temperatures. As described in that section, the analysis by Dagotto and Riera (1993) suggested a more optimistic scenario. These authors found superconductivity at large J/t in the 2D *t-J* model, and this presents the possibility that pair formation *may* exist in the realistic regime of the cuprates, i.e., small J/t (large U/t) and densities close to half-filling. The reason why numerically it is difficult to observe superconductivity may be either that the number of pairs in the small clusters that can be diagonalized exactly are not enough to provide a large signal, or that temperatures are still too high in the Monte Carlo simulations. While these arguments are, of course, only speculative, it is gratifying that recent results support this point of view. The purpose of this appendix is to discuss these new results.

Some time ago, in the context of the Hubbard model, Bickers, Scalapino, and White (1989) suggested that the critical temperature of this model is $T_c \approx 0.015t - 0.020t$ at $U/t=4$ and densities close to half-filling (this temperature is too small to be reached by Monte Carlo simulations). This result was obtained in the so-called fluctuation exchange approximation. Recently, Pao and Bickers (1994) and Monthoux and Scalapino (1994) improved this approximation in a self-consistent treatment of the Hubbard model. For example, with the aid of a renormalization-group approach, Pao and Bickers (1994) found a $d_{x^2-y^2}$ instability at temperatures between $0.020t$ and $0.030t$, with a small U/t dependence at density $\langle n\rangle=0.875$ as shown in Fig. 74(a). Pao and Bickers observed that clusters of 16×16 sites in momentum space are enough to obtain accurate results. The maximum value of the gap as a function of temperature, as well as the results of Monthoux and Scalapino (1994), is shown in Fig. 75. Both techniques provide similar information. Note the surprisingly large ratio $2\Delta/kT_c$ at zero temperature, obtained in this approximation. Actually, the mere fact that there is a phase transition with a nonzero-order parameter is surprising, since in two dimensions the Mermin-Wagner theorem forbids such transitions (only Kosterlitz-Thouless transitions are allowed as those found in the attractive Hubbard model by Scalettar *et al.*, 1989). Nevertheless, it is expected that the transition described by Pao and Bickers and by Monthoux and Scalapino can be stabilized by a coupling between planes, like that in the actual high-T_c cuprates.

More recently, a very similar critical temperature was found in an approximate treatment of the 2D *t-J* model by Dagotto, Nazarenko, and Moreo (1994). The approach of these authors is based on the quasiparticle dispersion discussed in Appendix B, supplemented by information of the two-holes problem in an antiferromagnet. In particular, the simple and rough argument dis-

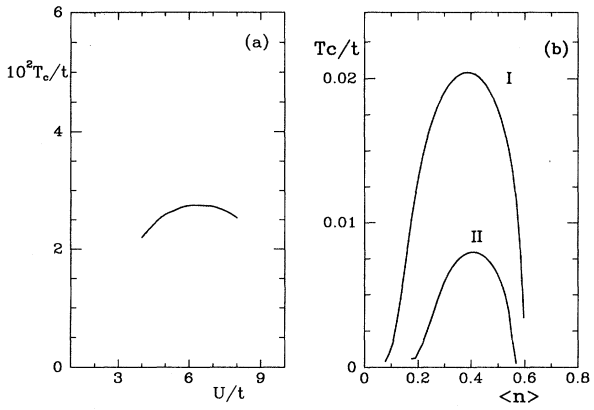

FIG. 74. (a) T_c vs U/t at $\langle n \rangle = 0.875$ (from Pao and Bickers, 1994); (b) T_c vs density of holes using the formalism described in Appendix C for the 2D t-J model (Dagotto, Nazarenko, and Moreo, 1994). "I" corresponds to $|V| = 0.2t$, while "II" is at $|V| = 0.1t$. $J/t = 0.4$ is assumed.

cussed in Sec. III.B.5 (i.e., presence of pairing caused by the minimization of the number of antiferromagnetic broken links) suggests that as a starting point the quasiparticles can be allowed to interact through a nearest-neighbor attractive term in the Hamiltonian which is proportional to J. This interaction links particles in sublattice A (spin up) and sublattice B (spin down) as described in Appendix B. While formally of the density-density form, it can be considered also as a spin-spin interaction, since it couples different sublattices. Thus the Hamiltonian considered by Dagotto, Nazarenko, and Moreo (1994) is

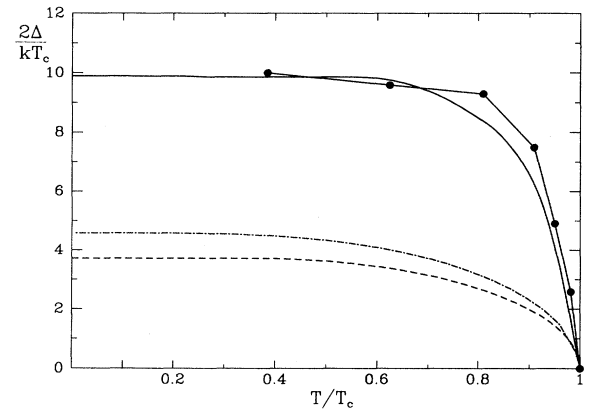

FIG. 75. $2\Delta/kTc$, where Δ is the maximum value of the gap, as a function of temperature T/T_c. The solid line was obtained by Pao and Bickers (1994) at $U/t = 4$ and density 0.875; the solid circles, by Monthoux and Scalapino (1994) at the same coupling and density; the dot-dashed line by Dagotto, Nazarenko, and Moreo (1994) using the 2D t-J model at the density where the saddle point in the dispersion is reached; and the dashed line corresponds to BCS (as described by Monthoux and Scalapino, 1994).

$$H = \sum_{\mathbf{p}} \epsilon_{\mathbf{p}} a_{\mathbf{p}}^{\dagger} a_{\mathbf{p}} + \sum_{\mathbf{p}} \epsilon_{\mathbf{p}} b_{\mathbf{p}}^{\dagger} b_{\mathbf{p}} - |V| \sum_{\langle \mathbf{im} \rangle} n_{\mathbf{i}} n_{\mathbf{m}} , \qquad \text{(C1)}$$

where the $a_{\mathbf{p}}$ ($b_{\mathbf{p}}$) operators destroy fermions with momentum $\mathbf{p}$ belonging to sublattice A (B), and $n_{\mathbf{i}}$ and $n_{\mathbf{m}}$ are number operators belonging to nearest-neighbor sites in sublattices A and B, respectively. The naive argument of minimization of broken antiferromagnetic links leads to a rough value of the interaction $|V| = 0.6J$; i.e., the effective Hamiltonian (C1) does not have free parameters, since its form is entirely deduced from the t-J model. Dagotto, Nazarenko, and Moreo (1994) studied Hamiltonian (C1) using the standard BCS gap equation (neglecting retardation effects, which are not believed to be crucial in a d-wave superconductor). The results for the critical temperature as a function of doping are shown in Fig. 74(b). The symmetry of the superconducting order parameter that leads to the lowest energy (or highest T_c) is $d_{x^2-y^2}$. It is remarkable that T_c, at the density where it is the highest, is of the same order of magnitude as that found by Pao and Bickers and by Monthoux and Scalapino (1994). In addition, a nontrivial density dependence is found, with T_c having a maximum at a particular doping concentration that basically corresponds to the density where the saddle point contained in the quasiparticle dispersion is reached. Thus this simple model seems to reproduce some of the results of the sophisticated self-consistent calculation, providing as a bonus a natural tentative explanation for the "optimal hole concentration" observed experimentally in all the cuprates. Thus this approach (where antiferromagnetism instead of band-structure effects provides the saddle point in the quasiparticle dispersion) is promising and can be considered as a combination of the Van Hove and antiferromagnetic ideas used to describe the cuprates. In Fig. 75 the gap as a function of temperature is obtained. By using Eq. (C1), a ratio $2\Delta/(kT_c) \sim 5$ is obtained at zero temperature.

In short, the main point of this appendix is that recent calculations suggest that the Hubbard and t-J models may indeed superconduct in the realistic regime of couplings and densities at small temperatures of the order of those observed in the cuprates. Certainly more work is needed to confirm these results.

REFERENCES

Abrikosov, A. A., J. C. Campuzano, and K. Gofron, 1993, Physica C **214**, 73.

Aeppli, G., 1992a, J. Magn. Magn. Mater. **104-107**, 507.

Aeppli, G., 1992b, Lectures Notes for E. Fermi Summer School, Varenna, Italy.

Aeppli, G., S. M. Hayden, H. A. Mook, Z. Fisk, S.-W. Cheong, D. Rytz, J. P. Remeika, G. P. Espinosa, and A. S. Cooper, 1989, Phys. Rev. Lett. **62**, 2052.

Alexander, M., *et al.*, 1991, Phys. Rev. B **43**, 333.

Allen, J. W., 1991a, Physica B **171**, 175.

Allen, J. W., 1991b, Proceedings of the Adriatico Research Conference, Trieste.

Allen, J. W., *et al.*, 1990, Phys. Rev. Lett. **64**, 595.
Almasan, C., and M. B. Maple, 1991, in *Chemistry of High-Temperature Superconductors,* edited by C. N. R. Rao (World Scientific, Singapore).
Anderson, P. W., 1987, Science **235**, 1196.
Anderson, P. W., 1990a, Phys. Rev. Lett. **64**, 1839.
Anderson, P. W., 1990b, Phys. Rev. B **42**, 2624.
Anderson, P. W., and J. R. Schrieffer, 1991, Phys. Today **44**, 55.
Anderson, R. O., *et al.*, 1993, Phys. Rev. Lett. **70**, 3163.
Ashcroft, N., and N. D. Mermin, 1976, *Solid State Physics* (Saunders, Philadelphia).
Assaad, F. F., and P. De Forcrand, 1990, in *Quantum Simulations of Condensed Matter Phenomena,* edited by J. D. Doll and J. E. Gubernatis (World Scientific, Singapore), p. 1.
Assaad, F. F., and W. Hanke, 1992, Würzburg preprint.
Assaad, F. F., and D. Würtz, 1991, Phys. Rev. B **44**, 2681.
Auerbach, A., and B. Larson, 1991, Phys. Rev. Lett. **66**, 2262.
Bacci, S., E. Gagliano, R. Martin, and J. Annett, 1991, Phys. Rev. B **44**, 7504.
Bacci, S., E. Gagliano, and F. Nori, 1991, Int. J. Mod. Phys. B **5**, 325.
Balseiro, C. A., A. G. Rojo, E. R. Gagliano, and B. Alascio, 1988, Phys. Rev. B **38**, 9315.
Barbieri, A., J. Riera, and A. P. Young, 1990, Phys. Rev. B **41**, 11 697.
Barbour, Ian, N.-E. Behilil, E. Dagotto, F. Karsch, A. Moreo, M. Stone, and H. W. Wyld, 1986, Nucl. Phys. B **275**, 296.
Bardeen, J., L. N. Cooper, and J. R. Schrieffer, 1957, Phys. Rev. **108**, 1175.
Barnes, T., 1991, Int. J. Mod. Phys. C **2**, 659.
Barnes, T., E. Dagotto, A. Moreo, and E. S. Swanson, 1989, Phys. Rev. B **40**, 10 977.
Barnes, T., E. Dagotto, J. Riera, and E. S. Swanson, 1993, Phys. Rev. B **47**, 3196.
Barnes, T., and G. J. Daniell, 1988, Phys. Rev. B **37**, 3637.
Barnes, T., A. E. Jacobs, M. D. Kovarik, and W. G. Macready, 1992, Phys. Rev. B **45**, 256.
Barnes, T., and M. Kovarik, 1990, Phys. Rev. B **42**, 6159.
Barnes, T., and M. Kovarik, 1993, Phys. Rev. B **47**, 11 247.
Batlogg, B., 1990, in *High-Temperature Superconductivity: The Los Alamos Symposium,* edited by K. Bedell, D. Coffey, D. Meltzer, D. Pines, and J. R. Schrieffer (Addison-Wesley, Reading, MA).
Batlogg, B., 1991, Phys. Today **44**, No. 6, p. 44.
Batlogg, B., H. Takagi, H. L. Kao, and J. Kwo, 1992, in *Electronic Properties of High-T_c Superconductors, The Normal and the Superconducting State,* edited by Kuzmany *et al.* (Springer-Verlag, Berlin/Vienna/New York).
Batrouni, G. G., and R. T. Scalettar, 1990, Phys. Rev. B **42**, 2282.
Beasley, M. R., 1993, in *Proceedings of the 2nd International Conference on High-Temperature Superconductivity,* Israel.
Bednorz, J. G., and K. A. Müller, 1986, Z. Phys. B **64**, 189.
Bednorz, J. G., and K. A. Müller, 1988, Rev. Mod. Phys. **60**, 585.
Belinicher, V. I., and A. L. Chernyshev, 1993, Phys. Rev. B **47**, 390.
Bénard, P., Liang Chen, and A.-M. S. Tremblay, 1993, Phys. Rev. B **47**, 589.
Bickers, N. E., D. J. Scalapino, and R. T. Scalettar, 1987, Int. J. Mod. Phys. B **1**, 687.
Bickers, N. E., D. J. Scalapino, and S. R. White, 1989, Phys. Rev. Lett. **62**, 961.
Binder, K., and D. W. Heermann, 1992, *Monte Carlo Simulations in Statistical Physics,* Springer Series in Solid-State Sciences Vol. 80 (Springer-Verlag, Berlin/Heidelberg/New York).
Birgeneau, R., 1990, Am. J. Phys. **58**, 28.
Birgeneau, R., *et al.*, 1988, Phys. Rev. B **38**, 6614.
Blankenbecler, R., D. J. Scalapino, and R. L. Sugar, 1981, Phys. Rev. D **24**, 2278.
Bogachek, E. N., I. V. Krive, I. O. Kulik, and A. S. Rozhavsky, 1990, Phys. Rev. B **42**, 7614.
Bonča, J., P. Prelovšek, and I. Sega, 1989a, Phys. Rev. B **39**, 7074.
Bonča, J., P. Prelovšek, and I. Sega, 1989b, Europhys. Lett. **10**, 87.
Bonča, J., P. Prelovšek, I. Sega, H. Q. Lin, and D. K. Campbell, 1992, Phys. Rev. Lett. **69**, 526.
Bonesteel, N., and J. Wilkins, Phys. Rev. Lett. **66**, 2684 (1991).
Boninsegni, M., 1994, Phys. Lett. A **188**, 330.
Boninsegni, M., and E. Manousakis, 1991, Phys. Rev. B **43**, 10 353.
Boninsegni, M., and E. Manousakis, 1992a, Phys. Rev. B **45**, 4877.
Boninsegni, M., and E. Manousakis, 1992b, Phys. Rev. B **46**, 560.
Boninsegni, M., and E. Manousakis, 1993, Phys. Rev. B **47**, 11 897.
Bose, I., and S. Gayen, 1993, Phys. Rev. B **48**, 10 653.
Brinkman, W., and T. M. Rice, 1970, Phys. Rev. B **39**, 6880.
Bucher, B., P. Steiner, J. Karpinski, E. Kaldis, and P. Wachter, 1993, Phys. Rev. Lett. **70**, 2012.
Bulut, N., D. W. Hone, D. J. Scalapino, and N. E. Bickers, 1990, Phys. Rev. B **41**, 1797.
Bulut, N., and D. Scalapino, 1991, Phys. Rev. Lett. **67**, 2898.
Bulut, N., and D. J. Scalapino, 1993, University of California at Santa Barbara preprint.
Bulut, N., D. J. Scalapino, and R. T. Scalettar, 1992, Phys. Rev. B **45**, 5577.
Bulut, N., D. J. Scalapino, and S. R. White, 1994a, University of Illinois preprint.
Bulut, N., D. J. Scalapino, and S. R. White, 1994b, preprint.
Burns, G., 1992, *High-Temperature Superconductivity* (Academic, New York).
Campuzano, J. C., L. C. Smedskjaer, R. Benedek, G. Jennings, and A. Bansil, 1991, Phys. Rev. B **43**, 2788.
Campuzano, J. C., *et al.*, 1990, Phys. Rev. Lett. **64**, 2308.
Chakravarty, S., 1990, in *High-Temperature Superconductivity,* edited by K. Bedell, D. Coffey, D. Meltzer, D. Pines, and J. R. Schrieffer (Addison-Wesley, Reading, MA), p. 136.
Chen, C. T., *et al.*, 1991, Phys. Rev. Lett. **66**, 104.
Chen, C.-X., and H.-B. Schüttler, 1990, Phys. Rev. B **41**, 8702.
Chen, C.-X., and H.-B. Schüttler, 1991, Phys. Rev. B **43**, 3771.
Chen, C.-X., H.-B. Schüttler, and A. J. Fedro, 1990, Phys. Rev. B **41**, 2581.
Chen, G. J., R. Joynt, F. C. Zhang, and C. Gros, 1990, Phys. Rev. B **42**, 2662.
Chen, Y. C., and T. K. Lee, 1993, Phys. Rev. B **47**, 11 548.
Chen, Y.-H., F. Wilczek, E. Witten, and B. I. Halperin, 1989, Int. J. Mod. Phys. B **3**, 1001.
Cheong, S-W., G. Aeppli, T. E. Mason, H. Mook, S. M. Hayden, P. C. Canfield, Z. Fisk, K. N. Clausen, and J. L. Martinez, 1991, Phys. Rev. Lett. **67**, 1791.
Chernyshev, A., A. V. Dotsenko, and O. P. Sushkov, 1993, preprint.
Cho, J. H., F. Borsa, D. C. Johnston, and D. R. Torgeson, 1992, Phys. Rev. B **46**, 3179.

Cho, J. H., F. C. Chou, and D. C. Johnston, 1993, Phys. Rev. Lett. **70**, 222.
Claessen, R., R. O. Anderson, J. W. Allen, C. G. Olson, C. Janowitz, W. P. Ellis, S. Harm, M. Kalning, R. Manzke, and M. Skibowski, 1992, Phys. Rev. Lett. **69**, 808.
Cooper, S. L., D. Reznik, A. Kotz, M. Karlow, R. Liu, M. Klein, W. Lee, J. Giapintzakis, and D. M. Ginsberg, 1993, Phys. Rev. B **47**, 8233.
Cooper, S. L., G. A. Thomas, J. Orenstein, D. Rapkine, A. Millis, S.-W. Cheong, A. S. Cooper, and Z. Fisk, 1990, Phys. Rev. B **41**, 11 605.
Dagotto, E., 1991, Int. J. Mod. Phys. B **5**, 907.
Dagotto, E., 1992, in *Computational Approaches in Condensed-Matter Physics,* Springer Proceedings in Physics Vol. 70, edited by S. Miyashita, M. Imada, and H. Takayama (Springer-Verlag, Berlin), p. 84.
Dagotto, E., R. Joynt, A. Moreo, S. Bacci, and E. Gagliano, 1990, Phys. Rev. B **41**, 9049.
Dagotto, E., and A. Moreo, 1985, Phys. Rev. D **21**, 865.
Dagotto, E., and A. Moreo, 1988, Phys. Rev. B **38**, 5087; **44**, 5396(E).
Dagotto, E., A. Moreo, and T. Barnes, 1989, Phys. Rev. B **40**, 6721.
Dagotto, E., A. Moreo, R. Joynt, S. Bacci, and E. Gagliano, 1990, Phys. Rev. B **41**, 2585.
Dagotto, E., A. Moreo, F. Ortolani, D. Poilblanc, and J. Riera, 1992, Phys. Rev. B **45**, 10 741.
Dagotto, E., A. Moreo, F. Ortolani, J. Riera, and D. J. Scalapino, 1991, Phys. Rev. Lett. **67**, 1918.
Dagotto, E., A. Moreo, F. Ortolani, J. Riera, and D. Scalapino, 1992, Phys. Rev. B **45**, 10 107.
Dagotto, E., A. Moreo, R. L. Sugar, and D. Toussaint, 1990, Phys. Rev. B **41**, 811.
Dagotto, E., A. Nazarenko, and M. Boninsegni, 1994, Phys. Rev. Lett. **73**, 728.
Dagotto, E., A. Nazarenko, and A. Moreo, 1994, "Antiferromagnetic and van Hove scenarios for the cuprates: taking the best of both worlds," National High Magnetic Field Lab preprint.
Dagotto, E., F. Ortolani, and D. Scalapino, 1992, Phys. Rev. B **46**, 3183.
Dagotto, E., and D. Poilblanc, 1990, Phys. Rev. B **42**, 7940.
Dagotto, E., and J. Riera, 1992, Phys. Rev. B **46**, 12 084.
Dagotto, E., and J. Riera, 1993, Phys. Rev. Lett. **70**, 682.
Dagotto, E., J. Riera, Y. C. Chen, A. Moreo, A. Nazarenko, F. Alcaraz, and F. Ortolani, 1994, Phys. Rev. B **49**, 3548.
Dagotto, E., J. Riera, and D. Scalapino, 1992, Phys. Rev. B **45**, 5744.
Dagotto, E., J. Riera, and A. P. Young, 1990, Phys. Rev. B **42**, 2347.
Dagotto, E., and J. R. Schrieffer, 1991, Phys. Rev. B **43**, 8705.
Denteneer, P. J. H., 1994, Phys. Rev. B **49**, 6364.
De Raedt, H., and M. Frick, 1993, Phys. Rep. **231**, 107.
De Raedt, H., and W. von der Linden, 1992, Phys. Rev. B **45**, 8787.
Dessau, D., 1992, Ph.D. thesis (Stanford University).
Dessau, D., *et al.*, 1993, Phys. Rev. Lett. **71**, 2781.
Di Castro, C., and M. Grilli, 1992, Phys. Scr. **T45**, 81.
Dickinson, P. H., and S. Doniach, 1993, Phys. Rev. B **47**, 11 447.
Ding, H.-Q., 1992, Physica C **203**, 91.
Ding, H.-Q., and W. Goddard, III, 1993, Phys. Rev. B **47**, 1149.
Ding, H.-Q., G. Lang, and W. Goddard, III, 1992, Phys. Rev. B **46**, 14 317.
Dobry, A., A. Greco, J. Lorenzana, and J. Riera, 1994, Phys. Rev. B **49**, 505.
Doll, G., J. Nicholls, M. Dresselhaus, A. Rao, J. Zhang, G. Lehman, P. Eklund, G. Dresselhaus, and A. Strauss, 1988, Phys. Rev. B **38**, 8850, and references therein.
Dopf, G., A. Muramatsu, and W. Hanke, 1990, Phys. Rev. B **41**, 9264.
Dopf, G., J. Wagner, P. Dieterich, A. Muramatsu, and W. Hanke, 1992, Phys. Rev. Lett. **68**, 2082.
Doucot, B., and X. G. Wen, 1989, Phys. Rev. B **40**, 2719.
Eder, R., 1992, Phys. Rev. B **45**, 319.
Eder, R., K. W. Becker, and W. H. Stephan, 1990, Z. Phys. B **81**, 33.
Eder, R., and P. Wróber, 1992, Max-Planck (Stuttgart) preprint.
Eder, R., and Y. Ohta, 1994, Phys. Rev. Lett. **72**, 2816.
Eisaki, H., S. Uchida, T. Mizokawa, H. Namatame, A. Fujimori, J. van Elp, P. Kuiper, G. A. Sawatzky, S. Hosoya, and H. Katayama-Yoshida, 1992, Phys. Rev. B **45**, 12 513.
Emery, V. J., 1986, Synth. Met. **13**, 21.
Emery, V. J., 1987, Phys. Rev. Lett. **58**, 2794.
Emery, V. J., and S. A. Kivelson, 1993, Physica C **209**, 597.
Emery, V. J., S. A. Kivelson, and H. Q. Lin, 1990, Phys. Rev. Lett. **64**, 475.
Emery, V. J., and G. Reiter, 1988a, Phys. Rev. B **38**, 4547.
Emery, V. J., and G. Reiter, 1988b, Phys. Rev. B **38**, 11 938.
Emery, V. J., and G. Reiter, 1990, Phys. Rev. B **41**, 7247.
Eskes, H., M. Meinders, and G. A. Sawatzky, 1991, Phys. Rev. Lett. **67**, 1035.
Eskes, H., and G. A. Sawatzky, 1988, Phys. Rev. Lett. **61**, 1415.
Eskes, H., and G. A. Sawatzky, 1991, Phys. Rev. B **43**, 119.
Fahy, S. B., and D. R. Hamann, 1990, Phys. Rev. Lett. **65**, 3437.
Fahy, S. B., and D. R. Hamann, 1991, Phys. Rev. B **43**, 765.
Fang, Y., A. Ruckenstein, E. Dagotto, and S. Schmitt-Rink, 1989, Phys. Rev. B **40**, 7406.
Fano, G., F. Ortolani, and A. Parola, 1990, Phys. Rev. B **42**, 6877.
Fano, G., F. Ortolani, and A. Parola, 1992, Phys. Rev. B **46**, 1048.
Fano, G., F. Ortolani, and F. Semeria, 1990, Int. J. Mod. Phys. B **3**, 1845.
Fehske, H., H. Röder, A. Mistriotis, and H. Büttner, 1993, J. Phys. Condens. Matter **5**, 3565.
Fehske, H., V. Waas, H. Röder, and H. Büttner, 1991, Phys. Rev. B **44**, 8473.
Feng, G., and S. R. White, 1992, Phys. Rev. B **46**, 8691.
Ferretti, A., I. O. Kulik, and A. Lami, 1992, Phys. Rev. B **45**, 5486.
Fetter, A., and J. Walecka, 1971, *Quantum Theory of Many-Particle Systems* (McGraw-Hill, New York).
Fink, J., *et al.*, 1993, High Temperature Superconductivity special issue of the Journal of Electron Spectroscopy, in print.
Foster, C. M., K. F. Voss, T. W. Hagler, D. Mihailović, A. J. Heeger, M. M. Eddy, W. L. Olson, and E. J. Smith, 1990, Solid State Commun. **76**, 651.
Frenkel, D. M., R. J. Gooding, B. I. Shraiman, and E. D. Siggia, 1990, Phys. Rev. B **41**, 350.
Frick, M., P. Pattnaik, I. Morgenstern, D. Newns, and W. von der Linden, 1990, Phys. Rev. B **42**, 2665.
Fujimori, A., 1992a, in *Mechanisms of Superconductivity,* Japanese Journal of Applied Physics, Series 7, p. 125.
Fujimori, A., 1992b, J. Phys. Chem. Solids **53**, 1595.
Fujimori, A., *et al.*, 1992, Phys. Rev. B **46**, 9841.
Fukuda, Y., T. Suzuki, M. Nagoshi, Y. Syono, K. Oh-ishi, and M. Tachiki, 1989, Solid State Commun. **72**, 1183.

Fukuyama, H., 1991, Physica C **185–189**.
Fukuyama, H., S. Maekawa, and A. P. Malozemoff, 1989, Eds., *Strong Correlation and Superconductivity,* Springer Series in Solid-State Sciences Vol. 89 (Springer-Verlag, Berlin/Heidelberg/New York).
Fulde, P., 1991, *Electron Correlations in Molecules and Solids,* Springer Series in Solid-State Sciences Vol. 100 (Springer-Verlag, Berlin/Heidelberg/New York).
Fulde, P., and P. Horsch, 1993, Europhys. News **24**, 73.
Fulde, P., and P. Unger, 1993, Phys. Rev. B **47**, 8947.
Furukawa, N., and M. Imada, 1991a, J. Phys. Soc. Jpn. **60**, 810.
Furukawa, N., and M. Imada, 1991b, J. Phys. Soc. Jpn. **60**, 3669.
Furukawa, N., and M. Imada, 1992, J. Phys. Soc. Jpn. **61**, 3331.
Fye, R., M. Martins, D. Scalapino, J. Wagner, and W. Hanke, 1991, Phys. Rev. B **44**, 6909.
Fye, R., M. Martins, D. Scalapino, J. Wagner, and W. Hanke, 1992, Phys. Rev. B **45**, 7311.
Fye, R., M. Martins, and R. T. Scalettar, 1990, Phys. Rev. B **42**, 6809.
Gagliano, E., and S. Bacci, 1990, Phys. Rev. B **42**, 8772.
Gagliano, E., S. Bacci, and E. Dagotto, 1990, Phys. Rev. B **42**, 6222.
Gagliano, E., S. Bacci, and E. Dagotto, 1991, Phys. Rev. B **44**, 285.
Gagliano, E., and C. Balseiro, 1987, Phys. Rev. Lett. **59**, 2999.
Gagliano, E., E. Dagotto, A. Moreo, and F. Alcaraz, 1986, Phys. Rev. B **34**, 1677; **35**, 5297(E).
Galan, J., and J. Vergés, 1991, Phys. Rev. B **44**, 10 093.
Ghijsen, J., L. H. Tjeng, J. van Elp, H. Eskes, J. Westerink, G. A. Sawatzky, and M. T. Czyzyk, 1988, Phys. Rev. B **38**, 11 322.
Giamarchi, T., and A. Millis, 1992, Phys. Rev. B **46**, 9325.
Gofron, K., J. C. Campuzano, H. Ding, C. Gu, R. Liu, B. Dabrowski, B. W. Veal, W. Cramer, and G. Jennings, 1993, J. Phys. Chem. Solids **54**, 1193.
Gomez-Santos, G., J. D. Joannopoulos, and J. W. Negele, 1989, Phys. Rev. B **39**, 4435.
Gooding, R. J., 1991, Phys. Rev. Lett. **66**, 2266.
Gooding, R. J., and A. Mailhot, 1991, Phys. Rev. B **44**, 11 852.
Gooding, R. J., and A. Mailhot, 1993, Phys. Rev. B **48**, 6132.
Gopalan, S., T. M. Rice, and M. Sigrist, 1993, Zürich preprint.
Grilli, M., R. Raimondi, C. Castellani, C. Di Castro, and G. Kotliar, 1991, Phys. Rev. Lett. **67**, 259.
Gros, C., 1988, Phys. Rev. B **38**, 931.
Gros, C., 1989, Ann. Phys. (N.Y.) **189**, 53.
Gubernatis, J. E., D. J. Scalapino, R. L. Sugar, and W. D. Toussaint, 1985, Phys. Rev. B **32**, 103.
Haas, S., E. Dagotto, A. Nazarenko, and J. Riera, 1994, "On the liaison between superconductivity and phase separation," Florida State preprint.
Haas, S., *et al.*, 1994, J. Appl. Phys. **75**, 6340.
Hamann, D. R., and S. B. Fahy, 1990, Phys. Rev. B **41**, 11 352.
Hammel, P. C., E. T. Ahrens, A. P. Reyes, R. H. Heffner, P. C. Canfield, S-W. Cheong, Z. Fisk, and J. E. Schirber, 1991, Physica C **185**, 1095.
Hammel, P. C., E. Ahrens, A. Reyes, J. Thompson, Z. Fisk, P. Canfield, J. Schirber, and D. MacLaughlin, 1992, in *Phase Separation in Cuprate Superconductors,* Workshop Held in Erice, Italy.
Hammel, P. C., A. P. Reyes, Z. Fisk, M. Takigawa, J. D. Thompson, R. H. Heffner, S-W. Cheong, and J. E. Schirber, 1990, Phys. Rev. B **42**, 6781.
Hardy, W. N., D. A. Bonn, D. C. Morgan, R. Liang, and K. Zhang, 1994, Phys. Rev. Lett. **70**, 3999.
Harris, J. M., Y. F. Yan, and N. P. Ong, 1992, Phys. Rev. B **46**, 14 293.
Harshman, D. R., G. Aeppli, B. Batlogg, G. P. Espinosa, R. J. Cava, A. S. Cooper, L. W. Rupp, E. J. Ansaldo, and D. Ll. Williams, 1989, Phys. Rev. Lett. **63**, 1187.
Harshman, D. R., and A. P. Mills, Jr., 1992, Phys. Rev. B **45**, 10 684.
Harshman, D. R., *et al.*, 1988, Phys. Rev. B **38**, 852.
Hasegawa, Y., and D. Poilblanc, 1989, Phys. Rev. B **40**, 9035.
Hayden, S. M., G. Aeppli, H. Mook, D. Rytz, M. F. Hundley, and Z. Fisk, 1991, Phys. Rev. Lett. **66**, 821.
Hayden, S. M., G. Aeppli, R. Osborn, A. D. Taylor, T. G. Perring, S-W. Cheong, and Z. Fisk, 1991, Phys. Rev. Lett. **67**, 3622.
Haydock, R., V. Heine, and M. J. Kelly, 1972, J. Phys. C **5**, 2845.
Haydock, R., V. Heine, and M. J. Kelly, 1975, J. Phys. C **8**, 2591.
Heeb, E. S., and T. M. Rice, 1993, Z. Phys. B **90**, 73.
Hellberg, C. S., and E. J. Mele, 1993, University of Pennsylvania preprint.
Herr, S., K. Kamarás, C. Porter, M. Doss, D. Tanner, D. Bonn, J. Greedan, C. Stager, and T. Timusk, 1987, Phys. Rev. B **36**, 733.
Hida, K., 1991, J. Phys. Soc. Jpn. **60**, 1347.
Hida, K., 1992, J. Phys. Soc. Jpn. **61**, 1013.
Hidaka, Y., and M. Suzuki, 1989, Nature **338**, 635.
Hirsch, J. E., 1985, Phys. Rev. B **31**, 4403.
Hirsch, J. E., in *Proceedings of the International Conference on Strongly Correlated Electron Systems,* San Diego, August 1993, in press.
Hirsch, J. E., E. Loh, Jr., D. J. Scalapino, and S. Tang, 1989, Phys. Rev. B **39**, 243.
Hirsch, J. E., and F. Marsiglio, 1989, Phys. Rev. B **39**, 11 515.
Hirsch, J. E., and S. Tang, 1989, Phys. Rev. Lett. **62**, 591.
Hirsch, J. E., S. Tang, E. Loh, Jr., and D. J. Scalapino, 1988, Phys. Rev. Lett. **60**, 1668.
Hirschfeld, P., and N. Goldenfeld, 1993, preprint.
Horsch, P., W. Stephan, K. von Szczepanski, M. Ziegler, and W. von der Linden, 1989, Physica C **162–164**, 783.
Hubbard, J., 1963, Proc. R. Soc. London, Ser. A **276**, 238.
Hubbard, J., 1964, Proc. R. Soc. London, Ser. A **281**, 401.
Hybertsen, M. S., M. Schlüter, and N. E. Christensen, 1989, Phys. Rev. B **39**, 9028.
Hybertsen, M. S., E. B. Stechel, M. Schlüter, and D. R. Jennison, 1990, Phys. Rev. B **41**, 11 068.
Imada, M., 1990, J. Phys. Soc. Jpn. **59**, 4121.
Imada, M., 1991a, J. Phys. Soc. Jpn. **60**, 1877.
Imada, M., 1991b, J. Phys. Soc. Jpn. **60**, 2740.
Imada, M., and Y. Hatsugai, 1989, J. Phys. Soc. Jpn. **58**, 3752.
Inoue, J., and S. Maekawa, 1992, Prog. Theor. Phys. Suppl. **108**, 313.
Inui, M., S. Doniach, and M. Gabay, 1988, Phys. Rev. B **38**, 6631.
Ito, T., K. Takenaka, and S. Uchida, 1993, Phys. Rev. Lett. **70**, 3995.
Jagla, E., K. Hallberg, and C. Balseiro, 1993, Centro Atomico Bariloche preprint.
Jarrell, M., J. Gubernatis, R. N. Silver, and D. S. Sivia, 1991, Phys. Rev. B **43**, 1206.
Johnston, D. C., 1987, Phys. Rev. B **35**, 219.
Johnston, D. C., 1989, Phys. Rev. Lett. **62**, 957.
Johnston, D. C., S. K. Sinha, A. J. Jacobson, and J. M. Newsam, 1988, Physica C **153–155**, 572.

Jorgensen, J. D., 1991, Phys. Today **44**, June, 34.
Jorgensen, J. D., B. Dabrowski, Shiyou Pei, D. G. Hinks, L. Soderholm, B. Morosin, J. E. Schirber, E. L. Venturini, and D. S. Ginley, 1988, Phys. Rev. B **38**, 11 337.
Kamarás, K., *et al.*, 1990, Phys. Rev. Lett. **64**, 84.
Kampf, A., and J. R. Schrieffer, 1990, Phys. Rev. B **42**, 7967.
Kanamori, J., 1963, Prog. Theor. Phys. **30**, 275.
Kane, C., P. Lee, and N. Read, 1989, Phys. Rev. Lett. **39**, 6880.
Kaplan, T. A., S. D. Mahanti, and H. Chang, 1992, Phys. Rev. B **45**, 2565.
Kawakami, N., and S.-K. Yang, 1991, Phys. Rev. B **44**, 7844.
Kaxiras, E., and E. Manousakis, 1988, Phys. Rev. B **38**, 866.
Keimer, B., *et al.*, 1992, Phys. Rev. B **46**, 14 034.
Kim, Y., A. Heeger, L. Acedo, G. Stucky, and F. Wudl, 1987, Phys. Rev. B **36**, 7252.
King, D. M., *et al.*, 1993, Phys. Rev. Lett. **70**, 3159.
Kivelson, S., V. Emery, and H. Q. Lin, 1990, Phys. Rev. B **42**, 6523.
Klee, S., and A. Muramatsu, 1993, Z. Phys. B **91**, 407.
Knowles, P., and N. Handy, 1989, J. Chem. Phys. **91**, 2396.
Kogut, John B., 1979, Rev. Mod. Phys. **51**, 659.
Kogut, John B., 1983, Rev. Mod. Phys. **55**, 775.
Kohn, W., 1964, Phys. Rev. **133**, A171.
Koike, Yoji, Y. Iwabuchi, S. Hosoya, N. Kobayashi, and T. Fukase, 1989, Physica C **159**, 105.
Kovarik, M., 1990, Phys. Rev. B **41**, 6889.
Kübert, C., and A. Muramatsu, 1993, Phys. Rev. B **47**, 787.
Lanczos, C., 1950, J. Res. Nat. Bur. Stand. **45**, 255.
Larbalestier, D., 1991, Phys. Today **44**, No. 6, 74.
Laughlin, R. B., 1988a, Science **242**, 525.
Laughlin, R. B., 1988b, Phys. Rev. Lett. **60**, 2677.
Lee, P. A., 1993, Phys. Rev. Lett. (in press).
Lee, W. C., R. A. Klemm, and D. C. Johnston, 1989, Phys. Rev. Lett. **63**, 1012.
Leung, P. W., Z. Liu, E. Manousakis, M. A. Novotny, and P. E. Oppenheimer, 1992, Phys. Rev. B **46**, 11 779.
Levin, K., Ju H. Kim, J. P. Lu, and Q. Si, 1992, University of Chicago preprint.
Littlewood, P. B., C. M. Varma, and E. Abrahams, 1987, Phys. Rev. Lett. **60**, 379.
Liu, L. Z., R. O. Anderson, and J. W. Allen, 1991, in *Proceedings of Workshop on Fermiology of High Tc,* Argonne National Lab, March 25–27.
Liu, Rong, B. W. Veal, A. P. Paulikas, J. W. Downey, H. Shi, C. G. Olson, C. Gu, A. J. Arko, and J. J. Joyce, 1992, Phys. Rev. B **45**, 5614.
Liu, Rong, *et al.*, 1992, Phys. Rev. B **46**, 11 056.
Liu, Z., and E. Manousakis, 1991, Phys. Rev. B **44**, 2414.
Liu, Z., and E. Manousakis, 1992, Phys. Rev. B **45**, 2425.
Loh, E. Y., Jr., J. E. Gubernatis, R. T. Scalettar, S. R. White, D. J. Scalapino, and R. L. Sugar, 1990, Phys. Rev. B **41**, 9301.
Long, M. W., and X. Zotos, 1993, Phys. Rev. B **48**, 317.
Lorenzana, J., M. D. Grynberg, L. Yu, K. Yonemitsu, and A. R. Bishop, 1993, Phys. Rev. B **47**, 13 156.
Lu, Jian Ping, Qimiao Si, Ju H. Kim, and K. Levin, 1990, Phys. Rev. Lett. **65**, 2466.
Lu, Yu, Su Zhao-Bin, and Li Yan-Min, 1993, Trieste preprint.
Maekawa, S., and M. Sato, 1991, Eds., *Physics of High-Temperature Superconductors,* Springer Series in Solid-State Sciences Vol. 106 (Springer-Verlag, Berlin/Heidelberg/New York).
Mahanti, S. D., T. A. Kaplan, H. Chang, and J. F. Harrison, 1993, J. Appl. Phys. **73**, 6105.
Maldague, P., 1977, Phys. Rev. **16**, 2437.
Manousakis, E., 1991, Rev. Mod. Phys. **63**, 1.
Manousakis, E., 1992, Phys. Rev. B **45**, 7570.
Marder, M., N. Papanicolaou, and G. C. Psaltakis, 1990, Phys. Rev. B **41**, 6920.
Markiewicz, R. S., 1991, Int. J. Mod. Phys. B **5**, 2037.
Marsiglio, F., A. E. Ruckenstein, S. Schmitt-Rink, and C. Varma, 1991, Phys. Rev. B **43**, 10 882.
Martindale, J. A., S. E. Barrett, K. E. O'Hara, C. P. Slichter, W. C. Lee, and D. M. Ginsberg, 1993, Phys. Rev. B **47**, 9155.
Martinez, G., and P. Horsch, 1991, Phys. Rev. B **44**, 317.
Mason, T. E., G. Aeppli, S. M. Hayden, A. P. Ramirez, and H. A. Mook, 1993, Phys. Rev. Lett. **71**, 919.
Mason, T. E., G. Aeppli, and H. A. Mook, 1992, Phys. Rev. Lett. **68**, 1414.
Matsuyama, H., *et al.*, 1989, Physica C **160**, 567.
Mattis, D. C., 1981, *The Theory of Magnetism I. Statistics and Dynamics,* Springer Series in Solid-State Sciences Vol. 17 (Springer-Verlag, Berlin/Heidelberg/New York).
Mattis, D. C., and H. Chen, 1991, Int. J. Mod. Phys. B **5**, 1401.
Mattis, D. C., M. Dzierzawa, and X. Zotos, 1990, Phys. Rev. B **42**, 6787.
Mila, F., 1988, Phys. Rev. B **38**, 11 358.
Millis, A. J., and S. N. Coppersmith, 1990, Phys. Rev. B **42**, 10 807.
Millis, A. J., and H. Monien, 1993, Phys. Rev. Lett. **70**, 2810.
Millis, A. J., H. Monien, and D. Pines, 1990, Phys. Rev. B **42**, 167.
Millis, A. J., and B. I. Shraiman, 1992, Phys. Rev. B **46**, 14 834.
Miyake, K., S. Schmitt-Rink, and C. M. Varma, 1986, Phys. Rev. B **34**, 6554.
Monthoux, P., 1993, private communication.
Monthoux, P., A. Balatsky, and D. Pines, 1991, Phys. Rev. Lett. **67**, 3448.
Monthoux, P., and D. Pines, 1993, Phys. Rev. B **47**, 6069.
Monthoux, P., and D. J. Scalapino, 1994, Phys. Rev. Lett. **72**, 1874.
Moreo, A., 1990, private communication.
Moreo, A., 1992a, Phys. Rev. B **45**, 4907.
Moreo, A., 1992b, Phys. Rev. B **45**, 5059.
Moreo, A., 1993, Phys. Rev. B **48**, 3380.
Moreo, A., 1993b, unpublished.
Moreo, A., 1994, Phys. Rev. B **49**, 13 172.
Moreo, A., and E. Dagotto, 1990, Phys. Rev. B **42**, 4786.
Moreo, A., E. Dagotto, T. Jolicoeur, and J. Riera, 1990, Phys. Rev. B **42**, 6283.
Moreo, A., E. Dagotto, and D. Scalapino, 1991, Phys. Rev. B **43**, 11 442.
Moreo, A., and D. Duffy, 1994, "Hole pockets in the doped 2D Hubbard model," Florida State preprint.
Moreo, A., and D. J. Scalapino, 1991, Phys. Rev. Lett. **66**, 946.
Moreo, A., D. J. Scalapino, R. Sugar, S. White, and N. Bickers, 1990, Phys. Rev. B **41**, 2313.
Morgenstern, I., Th. Husslein, J. M. Singer, and H.-G. Matuttis, 1993, J. Phys. I (Paris) **3**, 1043.
Mori, H., 1965a, Prog. Theor. Phys. **33**, 423.
Mori, H., 1965b, Prog. Theor. Phys. **34**, 399.
Muramatsu, A., G. Zumbach, and X. Zotos, 1993, Int. J. Mod. Phys. C, in press.
Nagaoka, Y., 1966, Phys. Rev. **147**, 392.
Nagaosa, N., and P. A. Lee, 1990, Phys. Rev. Lett. **64**, 2450.
Namatame, H., *et al.*, 1990, Phys. Rev. B **41**, 7205.
Nazarenko, A., 1993, unpublished.
Newns, D. M., P. C. Pattnaik, and C. C. Tsuei, 1991, Phys. Rev. B **43**, 3075.

Nieva, G., E. Osquiguil, J. Guimpel, M. Maenhoudt, B. Wuyts, Y. Bruynseraede, M. Maple, and I. Schuller, 1993, University of California at San Diego preprint.
Noack, R. M., R. T. Scalettar, N. Bulut, and D. J. Scalapino, 1992, UCSB preprint.
Nori, F., E. Abrahams, and G. T. Zimanyi, 1990, Phys. Rev. B **41**, 7277.
Nori, F., E. Gagliano, and S. Bacci, 1992, Phys. Rev. Lett. **68**, 240.
Nori, F., and G. T. Zimanyi, 1991, Europhys. Lett. **16**, 397.
Nori, F., G. T. Zimanyi, and E. Abrahams, 1991, Int. J. Mod. Phys. B **5**, 119.
Nücker, N., J. Fink, B. Renker, D. Ewert, C. Politis, P. J. W. Weijs, and J. C. Fuggle, 1987, Z. Phys. B **67**, 9.
Ogata, M., M. Luchini, S. Sorella, and F. Assaad, 1991, Phys. Rev. Lett. **66**, 2388.
Ohta, Y., K. Tsutsui, W. Koshibae, T. Shimozato, and S. Maekawa, 1992, Phys. Rev. B **46**, 14 022.
Oitmaa, J., and D. D. Betts, 1978, Can. J. Phys. **56**, 897.
Olson, C. G., R. Liu, D. W. Lynch, R. S. List, A. J. Arko, B. W. Veal, Y. C. Chang, P. Z. Jiang, and A. P. Paulikas, 1990, Phys. Rev. B **42**, 381.
Olson, C. G., A. Liu, A.-B. Yang, D. W. Lynch, A. J. Arko, R. S. List, B. W. Veal, Y. C. Chang, P. Z. Jiang, and A. P. Paulikas, 1989, Science **245**, 731.
Orenstein, J., G. A. Thomas, A. Millis, S. L. Cooper, D. Rapkine, T. Timusk, L. Schneemeyer, and J. Waszczak, 1990, Phys. Rev. B **42**, 6342.
Orenstein, J., G. A. Thomas, D. Rapkine, C. Bethea, B. Levine, R. Cava, E. Reitman, and D. Johnson, Jr., 1987, Phys. Rev. B **36**, 733.
Pao, C.-H., and N. E. Bickers, 1994, Phys. Rev. Lett. **72**, 1870.
Pattnaik, P. C., C. L. Kane, D. M. Newns, and C. C. Tsuei, 1992, Phys. Rev. B **45**, 5714.
Paul, P., and D. C. Mattis, 1991, Phys. Rev. B **44**, 2384.
Pettifor, D. G., and D. L. Weaire, 1985, Eds., *The Recursion Method and Its Applications,* Springer Series in Solid-State Sciences Vol. 58 (Springer, Berlin/Heidelberg).
Poilblanc, D., 1991, Phys. Rev. B **44**, 9562.
Poilblanc, D., and E. Dagotto, 1990, Phys. Rev. B **42**, 4861.
Poilblanc, D., and E. Dagotto, 1991, Phys. Rev. B **44**, 466.
Poilblanc, D., E. Gagliano, S. Bacci, and E. Dagotto, 1991, Phys. Rev. B **43**, 10 970.
Poilblanc, D., and T. M. Rice, 1989, Phys. Rev. B **39**, 9749.
Poilblanc, D., J. Riera, and E. Dagotto, 1994, Phys. Rev. B **49**, 12 318.
Poilblanc, D., H. J. Schulz, and T. Ziman, 1992, Phys. Rev. B **46**, 6435.
Poilblanc, D., H. J. Schulz, and T. Ziman, 1993, Phys. Rev. B **47**, 3268.
Poilblanc, D., T. Ziman, H. J. Schulz, and E. Dagotto, 1993, Phys. Rev. B **47**, 14 267.
Prelovšek, P., I. Sega, and J. Bonča, 1990, Phys. Rev. B **42**, 10 706.
Prelovšek, P., I. Sega, J. Bonča, H. Q. Lin, and D. K. Campbell, 1993, Phys. Rev. B **47**, 12 224.
Prelovšek, P., and X. Zotos, 1993, Phys. Rev. B **47**, 5984.
Psaltakis, G. C., and N. Papanicolaou, 1993, Phys. Rev. B **48**, 456.
Putikka, W. O., M. U. Luchini, and M. Ogata, 1992, Phys. Rev. Lett. **69**, 2288.
Putikka, W. O., M. U. Luchini, and T. M. Rice, 1992, Phys. Rev. Lett. **68**, 538.
Putilin, S. N., E. V. Antipov, O. Chmaissem, and M. Marezio, 1993, Nature **362**, 226.
Ramsak, A., and P. Prelovšek, 1989, Phys. Rev. B **40**, 2239.
Randeria, M., N. Trivedi, A. Moreo, and R. T. Scalettar, 1992, Phys. Rev. Lett. **69**, 2001.
Reedyk, M., T. Timusk, J. Xue, and J. Greedan, 1992, Phys. Rev. B **45**, 7406.
Reger, J. D., and A. P. Young, 1988, Phys. Rev. B **37**, 5024.
Reiter, G. F., 1992, preprint.
Reyes, A. P., P. C. Hammel, E. T. Ahrens, J. D. Thompson, P. C. Canfield, Z. Fisk, and J. E. Schirber, 1993, in *Conference on Spectroscopies in Novel Superconductors,* Proceedings, Santa Fe.
Rice, T. M., S. Gopalan, and M. Sigrist, 1993, Europhys. Lett. **23**, 445.
Rice, T. M., and F. C. Zhang, 1989, Phys. Rev. B **39**, 815.
Riera, J., and E. Dagotto, 1993a, Phys. Rev. B **47**, 15 346.
Riera, J., and E. Dagotto, 1993b, Phys. Rev. B **48**, 9515.
Riera, J., and E. Dagotto, 1994, Phys. Rev. B **50**, 452.
Riera, J., and A. P. Young, 1989, Phys. Rev. B **39**, 9697.
Röder, H., A. R. Bishop, and J. Tinka Gammel, 1993, Phys. Rev. Lett. **70**, 3498.
Röder, H., H. Fehske, and H. Büttner, 1993, Phys. Rev. B **47**, 12 420.
Röder, H., V. Waas, H. Fehske, and H. Büttner, 1991, Phys. Rev. B **43**, 6284.
Romberg, H., M. Alexander, N. Nücker, P. Adelmann, and J. Fink, 1990, Phys. Rev. B **42**, 8768.
Romero, D., C. Porter, D. Tanner, L. Forro, D. Mandrus, L. Mihaly, G. Carr, and G. Williams, 1992, Solid State Commun. (in press).
Sachdev, S., 1989, Phys. Rev. B **39**, 12 232.
Sá de Melo, C., and S. Doniach, 1990, Phys. Rev. B **41**, 6633.
Scalapino, D. J., 1991, Physica C **185–189**, 104.
Scalapino, D. J., 1993, UCSB preprint.
Scalapino, D. J., E. Loh, and J. E. Hirsch, 1986, Phys. Rev. B **34**, 8190.
Scalapino, D. J., E. Loh, and J. E. Hirsch, 1987, Phys. Rev. B **35**, 6694.
Scalapino, D. J., S. R. White, and S. C. Zhang, 1992, Phys. Rev. Lett. **68**, 2830.
Scalapino, D. J., S. R. White, and S. C. Zhang, 1993, UCSB preprint.
Scalettar, R. T., 1989, Physica C **162–164**, 313.
Scalettar, R. T., N. E. Bickers, and D. J. Scalapino, 1989, Phys. Rev. B **40**, 197.
Scalettar, R. T., S. R. White, D. J. Scalapino, and R. L. Sugar, 1991, Phys. Rev. B **44**, 770.
Schilling, A., M. Cantoni, J. D. Guo, and H. R. Ott, 1993, Nature **363**, 56.
Schlesinger, Z., R. T. Collins, F. Holtzberg, C. Feild, S. H. Blanton, U. Welp, G. W. Crabtree, Y. Fang, and J. Z. Liu, 1990, Phys. Rev. Lett. **65**, 801.
Schmitt-Rink, S., C. M. Varma, and A. E. Ruckenstein, 1988, Phys. Rev. Lett. **60**, 2793.
Schrieffer, J. R., 1988, *Theory of Superconductivity* (Addison-Wesley, Reading, MA), fourth printing.
Schrieffer, J. R., X-G. Wen, and S.-C. Zhang, 1988, Phys. Rev. Lett. **60**, 944.
Schrieffer, J. R., X.-G. Wen, and S.-C. Zhang, 1989, Phys. Rev. B **39**, 11 663.
Schulz, H., 1990a, Phys. Rev. Lett. **64**, 1445.
Schulz, H., 1990b, Phys. Rev. Lett. **64**, 2831.
Schulz, H., 1991, Int. J. Mod. Phys. B **5**, 57.
Schüttler, H.-B., and A. J. Fedro, 1989, J. Less-Common Met.

149, 385.
Schüttler, H.-B., and A. J. Fedro, 1992, Phys. Rev. B **45**, 7588.
Sega, I., and P. Prelovšek, 1990, Phys. Rev. B **42**, 892.
Serene, J. W., and D. W. Hess, 1991, Phys. Rev. B **44**, 3391.
Shastry, B., and B. Sutherland, 1990, Phys. Rev. Lett. **65**, 243.
Shen, Z.-X., D. S. Dessau, B. O. Wells, C. G. Olson, D. B. Mitzi, Lou Lombado, R. S. List, and A. J. Arko, 1991, Phys. Rev. B **44**, 12 098.
Shen, Z.-X., *et al.*, 1987, Phys. Rev. Lett. **36**, 8414.
Shen, Z.-X., *et al.*, 1993, Phys. Rev. Lett. **70**, 1553.
Shimada, M., K. Mizuno, S. Miyamoto, M. Shimizu, and J. Tanaka, 1992, Physica C **193**, 353.
Shimada, M., M. Shimizu, J. Tanaka, I. Tanaka, and H. Kojima, 1992, Physica C **193**, 277.
Shraiman, B., and E. Siggia, 1988a, Phys. Rev. Lett. **61**, 467.
Shraiman, B., and E. Siggia, 1988b, Phys. Rev. Lett. **61**, 740.
Shraiman, B., and E. Siggia, 1989a, Phys. Rev. Lett. **62**, 1564.
Shraiman, B., and E. Siggia, 1989b, Phys. Rev. B **40**, 9162.
Silver, R. N., J. E. Gubernatis, D. S. Sivia, and M. Jarrell, 1990, Phys. Rev. Lett. **65**, 496.
Simon, R., 1991, Phys. Today **44**, No. 6, p. 64.
Singh, R. R. P., and R. L. Glenister, 1992a, Phys. Rev. B **46**, 11 871.
Singh, R. R. P., and R. L. Glenister, 1992b, Phys. Rev. B **46**, 14 313.
Song, J., and J. F. Annett, 1992, Europhys. Lett. **18**, 549.
Sorella, S., 1991, Int. J. Mod. Phys. B **5**, 937.
Sorella, S., 1992, Phys. Rev. B **46**, 11 670.
Sorella, S., S. Baroni, R. Car, and M. Parrinello, 1989, Europhys. Lett. **8**, 663.
Sorella, S., E. Tosatti, S. Baroni, R. Car, and M. Parrinello, 1988, Int. J. Mod. Phys. B **2**, 993S.
Stafford, C. A., and A. Millis, 1993, Phys. Rev. B **48**, 1409.
Stafford, C. A., A. Millis, and B. Shastry, 1991, Phys. Rev. B **43**, 13 660.
Stechel, E. B., and D. R. Jennison, 1988, Phys. Rev. B **38**, 4632.
Stephan, W., and P. Horsch, 1990, Phys. Rev. B **42**, 8736.
Stephan, W., and P. Horsch, 1991, Phys. Rev. Lett. **66**, 2258.
Stephan, W., and P. Horsch, 1992, Int. J. Mod. Phys. B **6**, 589.
Su, W. P., 1988, Phys. Rev. B **37**, 9904.
Su, Z. B., Y. M. Li, W. Y. Lai, and L. Yu, 1989, Phys. Rev. Lett. **63**, 1318.
Sudbo, A., C. M. Varma, T. Giamarchi, E. B. Stechel, and R. T. Scalettar, 1993, Phys. Rev. Lett. **70**, 978.
Suzuki, T., M. Nagoshi, Y. Fukuda, K. Oh-ishi, Y. Syono, and M. Tachiki, 1990, Phys. Rev. B **42**, 4263.
Svane, A., 1992, Phys. Rev. Lett. **68**, 1900.
Takagi, H., S. Uchida, K. Kitazawa, and S. Tanaka, 1987, Jpn. J. Appl. Phys. (Lett.) **26**, L123.
Takagi, H., *et al.*, 1992, AT&T preprint.
Takahashi, T., H. Matsuyama, H. Katayama-Yoshida, K. Seki, K. Kamiya, and H. Inokuchi, 1990, Physica C **170**, 416.
Takahashi, T., *et al.*, 1991, in *Proceedings of Workshop on Fermiology of High-T_c Superconductors,* Argonne.
Tan, L., and J. Callaway, 1992, Phys. Rev. B **46**, 5499.
Tanamoto, T., H. Kohno, and H. Fukuyama, 1992, J. Phys. Soc. Jpn. **61**, 1886.
Tanamoto, T., H. Kohno, and H. Fukuyama, 1993a, J. Phys. Soc. Jpn. **62**, 717.
Tanamoto, T., H. Kohno, and H. Fukuyama, 1993b, J. Phys. Soc. Jpn. **62**, 1455.
Tanner, D. B., and T. Timusk, 1992, "Optical Properties of High-Temperature Superconductors," in *Physical Properties of High-Temperature Superconductors III,* edited by Donald M. Ginsberg (World Scientific, Singapore), p. 363.
Testardi, L. R., J. H. Wernick, and W. A. Roger, 1974, Solid State Commun. **15**, 1.
Thomas, G. A., 1991, in *Proceedings of the Thirty-Ninth Scottish Universities Summer School in Physics,* St. Andrews.
Thomas, G. A., J. Orenstein, D. Rapkine, M. Capizzi, A. Millis, R. Bhatt, L. Schneemeyer, and J. Waszczak, 1988, Phys. Rev. Lett. **61**, 1313.
Thomas, G. A., D. Rapkine, S. Cooper, S-W. Cheong, A. Cooper, L. Schneemeyer, and J. Waszczak, 1992, Phys. Rev. B **45**, 2474.
Thurston, T. R., *et al.*, 1990, Phys. Rev. Lett. **65**, 263.
Tikofsky, A. M., R. B. Laughlin, and Z. Zou, 1992, Phys. Rev. Lett. **69**, 3670.
Timusk, T., and D. B. Tanner, 1989, "Infrared Properties of High-T_c Superconductors," in *Physical Properties of High-Temperature Superconductors I,* edited by Donald M. Ginsberg (World Scientific, Singapore), pp. 339–407.
Tohyama, T., and S. Maekawa, 1991, J. Phys. Soc. Jpn. **60**, 53.
Tohyama, T., and S. Maekawa, 1992, Physica C **191**, 193.
Torrance, J. B., A. Bezinge, A. I. Nazzal, T. C. Huang, S. S. P. Parkin, D. T. Keane, S. J. LaPlaca, P. M. Horn, and G. A. Held, 1989, Phys. Rev. B **40**, 8872.
Tranquada, J. M., P. M. Gehring, G. Shirane, S. Shamoto, and M. Sato, 1992, Phys. Rev. B **46**, 5561.
Troyer, M., H. Tsunetsugu, T. M. Rice, J. Riera, and E. Dagotto, 1993, Phys. Rev. B **48**, 4002.
Trugman, S., 1988, Phys. Rev. B **37**, 1597.
Trugman, S., 1990a, Phys. Rev. Lett. **65**, 500.
Trugman, S., 1990b, Phys. Rev. B **41**, 892.
Trugman, S., 1990c, Phys. Rev. B **42**, 6612.
Tsuei, C. C., A. Gupta, and G. Koren, 1989, Physica C **161**, 415.
Uchida, S., T. Ido, H. Takagi, T. Arima, Y. Tokura, and S. Tajima, 1991, Phys. Rev. B **43**, 7942.
Varma, C. M., P. B. Littlewood, S. Schmitt-Rink, E. Abrahams, and A. Ruckenstein, 1989, Phys. Rev. Lett. **63**, 1996.
Varma, C. M., S. Schmit-Rink, and E. Abrahams, 1987, Solid State Commun. **62**, 681.
Veal, B. W., *et al.*, 1993, Argonne preprint.
Vekic, M., and S. R. White, 1993, Phys. Rev. B **47**, 16 131.
Virosztek, A., and J. Ruvalds, 1990, Phys. Rev. B **42**, 4064.
Viswanath, V. S., and G. Müller, 1990, J. Appl. Phys. **67**, 5486.
Viswanath, V. S., and G. Müller, 1991, J. Appl. Phys. **70**, 6178.
von der Linden, W., 1992, Phys. Rep. **220**, 53.
von Szczepanski, K. J., P. Horsch, W. Stephan, and M. Ziegler, 1990, Phys. Rev. B **41**, 2017.
Waas, V., H. Fehske, and H. Büttner, 1993, Phys. Rev. B **48**, 9106.
Wagner, J., W. Hanke, and D. Scalapino, 1991, Phys. Rev. B **43**, 10 517.
Watanabe, T., T. Takahashi, S. Suzuki, S. Sato, and H. Katayama-Yoshida, 1991, Phys. Rev. B **44**, 5316.
Welp, U., W. K. Kwok, G. W. Crabtree, K. G. Vandervoort, and J. Z. Liu, 1989, Phys. Rev. Lett. **62**, 1908.
Wen, X.-G., F. Wilczek, and A. Zee, 1989, Phys. Rev. B **39**, 11 413.
Wenzel, W., and K. G. Wilson, 1992, Phys. Rev. Lett. **69**, 800.
White, S. R., 1991, Phys. Rev. B **44**, 4670.
White, S. R., D. J. Scalapino, R. L. Sugar, N. Bickers, and R. Scalettar, 1989, Phys. Rev. B **39**, 839.
White, S. R., D. J. Scalapino, R. L. Sugar, E. Y. Loh, J. E. Gubernatis, and R. T. Scalettar, 1989, Phys. Rev. B **40**, 506.
Wollman, D. A., D. J. van Harlingen, W. C. Lee, D. M.

Ginsberg, and A. J. Leggett, 1993, Phys. Rev. Lett. **71**, 2134.
Wu, Dong Ho, Jian Mao, S. N. Mao, J. L. Peng, X. X. Xi, T. Venkatesan, R. L. Greene, and Steven M. Anlage, 1993, Phys. Rev. Lett. **70**, 85.
Wu, M. K., J. R. Ashburn, C. J. Torng, P. H. Hor, R. L. Meng, L. Gao, Z. J. Huang, Y. Q. Wang, and C. W. Chu, 1987, Phys. Rev. Lett. **58**, 908.
Yokoyama, H., and H. Shiba, 1988, J. Phys. Soc. Jpn. **57**, 2482.
Yonemitsu, K., A. R. Bishop, and J. Lorenzana, 1992, Phys. Rev. Lett. **69**, 965.
Yonemistu, K., A. R. Bishop, and J. Lorenzana, 1993a, Phys. Rev. B **47**, 8065.
Yonemistu, K., A. R. Bishop, and J. Lorenzana, 1993b, Phys. Rev. B **47**, 12 059.
Yu, G., C. Lee, A. Heeger, and S.-W. Cheong, 1992, Physica C **203**, 419.
Zaanen, J., and A. M. Oles, 1988, Phys. Rev. B **37**, 9433.
Zaanen, J., G. A. Sawatzky, and J. W. Allen, 1985, Phys. Rev. Lett. **55**, 418.
Zhang, F. C., and T. M. Rice, 1988, Phys. Rev. B **37**, 3759.
Zhang, F. C., and T. M. Rice, 1990, Phys. Rev. B **41**, 7243.
Zhang, S., and M. H. Kalos, 1991, Phys. Rev. Lett. **67**, 3074.
Zotos, Z., P. Prelovšek, and I. Sega, 1990, Phys. Rev. B **42**, 8445.

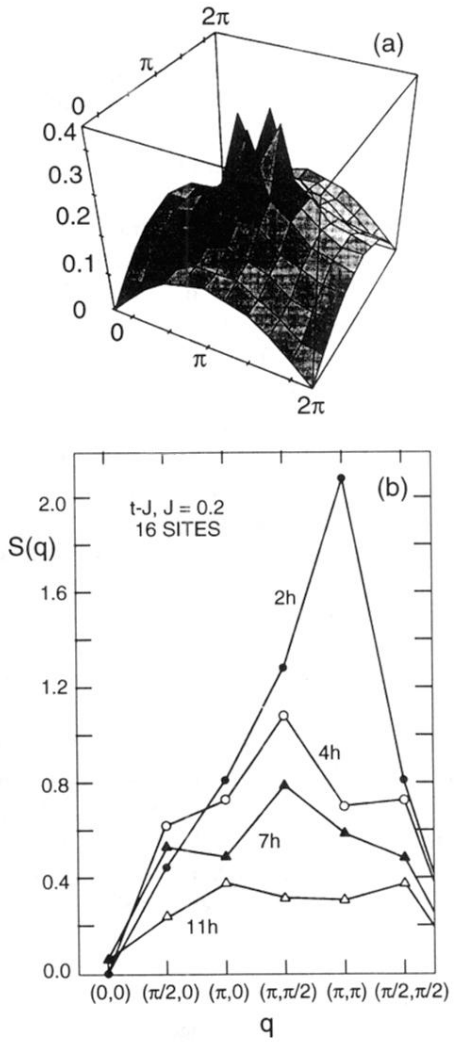

FIG. 36. (a) Equal-time spin correlation in momentum space on 10×10 lattices for 41 up- and down-spin fermions each (from Furukawa and Imada, 1992); (b) spin structure factor as a function of momentum for the 4×4 cluster and different numbers of holes (2, 4, 7, and 11; from Moreo, Dagotto, *et al.*, 1990).